Identification of *in vivo* Protein Targets of Nitric Oxide in *Drosophila melanogaster*

A thesis submitted to the University of Sussex for the degree of
Master of Philosophy
Jully 2010
By
Shreya Saha
School of Life Sciences
The University of Sussex

Declaration

I hereby declare that this thesis has not been and will not be, submitted in whole or in part to this or any other University for the award of any other degree.

Shreya Saha

Jully 2010

Acknowledgements

I can not begin with anyone other than my supervisor, Dr. Ian J.H Roberts. Apart from sparing his lab for me, it is his patience, all-round guidance, support and encouragement during my lab work and write up, that enabled me to work successfully.

I extend my gratitude to my co supervisor Dr. Roger Guy Phillips, who had equipped me with the rudimentary knowledge of confocal microscopy and would like to thank him for all his valuable suggestions during my lab work.

I would like to convey my thanks to Dr. Alexander Brehm and his group for sharing the anti-Mi-2 antibody with me. I would like to thank Dr. Fumiko Hirose and his group for sending me the ani-Dref antibody.

I am thankful to my lab mate and friend Miss Anna Scott, for her tremendous help and suggestions during this project.

I can not forget to thank some very supportive friends of mine, Mrs Vidisha Krishnan, Mr Awoyemi Awofala, Dr. Sharada Ramasubramanyan**,** Mr Pavel Roy, Mr. G.V.N. Srikanth and Miss Nithya Palaniappan for their continuous encouragements.

I would like to convey my heartfelt regards to my parents and love to my sister for supporting me constantly, in spite of several problems.

Contents

Identification of *in vivo* Protein Targets of Nitric Oxide in *Drosophila melanogaster*

A thesis submitted to the University of Sussex for the degree of Master of Philosophy

By Shreya Saha

School of Life Sciences

May 2010

Nitric Oxide (NO) is known to alter cell proliferation and growth. This project investigated the molecular targets of NO, using the salivary glands of *Drosophila melanogaster* third instar larvae.

A screen of 75 transgenic *Drosophila* lines expressing Yellow Fluorescent Protein tagged proteins, for those that showed a rapid alteration in sub-cellular localization after organ culture with an NO donor was undertaken. This screen revealed Mi-2 as a target of NO action. This was confirmed *in vivo* as localization of Mi-2-YFP was altered in whole salivary glands expressing Nitric Oxide Synthase (*NOS2*). The localization of the endogenous Mi-2 protein was similarly altered in *NOS2* expressing single cells. A quantitative analysis using the image analysis software "Velocity" demonstrated an increase in the nuclear concentration of Mi-2 protein in these cells. Targeted expression of RNAi-Mi-2 as well as analysis of *Mi-2* transheterozygous mutant larvae revealed that NO can impart its reduced growth phenotype independently of Mi-2.

Dref can associate with Mi-2 and can control cell proliferation and growth. Localisation of Dref did not show any noticeable change in single cells expressing NOS. However when these cells were double labelled both with anti-Dref and anti-Mi-2 antibodies, the anti-Dref staining was altered. This indicates that NO can alter the availability of the Dref antigen by reorganising the Mi-2/Dref complex.

Mi-2 is a component of the NuRD complex. The effect of NO in altering the Mi-2/Dref complex was exploited to investigate the effect of *simj* (a regulatory component of NuRD), on either of the proteins after potential disassociation of the complex. The data demonstrated an independent effect of *simj* on the localization of each protein.

NO and FOXO regulate the expression of a common set of genes and FOXO is required for the anti growth properties of NO. Thus the effect of FOXO expression on Mi-2 and Dref protein distribution was determined. Although no consistent alteration of Mi-2 localization was observed, a quantitative analysis showed a large increase of Dref protein concentration in FOXO expressing cells. Double antibody staining of these cells with both anti-Dref and anti-Mi-2 antibodies showed a novel nuclear localization of the proteins imparted by FOXO. Thus this study has identified the regulation of the Mi-2/Dref protein complex as a possible growth control mechanism by NO and FOXO.

Abbreviations

ACh	Acetylcholine
ADP	Adenosine diphosphate
ADMA	Asymmetric dimethylarginine
ANOVA	Analysis of variance
ATP	Adenosine triphosphate
BrdU	5-bromo-deoxyuridine
BSA	Bovine serum albumin
cGMP	cyclic GMP
CO_2	Carbon dioxide
CPTI	Cambridge Protein Trap Insertion project
DAPI	4',6-diamidino-2-phenylindole, dihydrochloride
DMSO	Dimethyl sulfoxide
DNA	Deoxyribonucleic Acid
EDRF	Endothelium Derived Relaxing Factor
FAD	Flavin adenine dinucleotide
FLP	Flippase
FRT	Flippase recognition target site
FMN	Flavin mononucleotide
FOXO	Forkhead-related transcription factors
GAL4	Yeast protein that binds DNA
GFP	Green fluorescent protein
GSNO	S-nitrosoglutathione
H_4bioprotein	(6R)-5,6,7,8-tetrahydro-lbiopterin

L-NAME	Nω-nitro-L-arginine methyl ester
L-NMMA	L-monomethylarginine
LTP	Long term potentiation
MAC	Macrophage
NADPH	Nicotinamide adenine dinucleotide phosphate
NGF	Nerve growth factor
NO	Nitric Oxide
NOH-ARG	N-hydroxy-L-arginine
NOS	Nitric Oxide Synthase
NMMA	N^G-monomethyl-L-arginine
PBS	Phosphate buffered saline
PBT	Phosphate Buffered plus Triton
RNA	Ribonucleic Acid
RNAi	RNA interference
SD	Standard Deviation
SDMA	Symmetric dimethylarginine
SG	Salivary gland
siRISC	siRNA-induced silencing complex
siRNA	Small interfering RNAs
SNAP	S-nitroso-N-acetyl-penicillamine
SNP	Sodium nitroprusside
UAS	Upstream activator sequence
VSMC	Vascular smooth muscle cells
wt	Wild type
YFP	Yellow fluorescent protein

CHAPTER 1: General Introduction

1.1. Brief introduction to cell signalling: NO as signalling molecule

Cell signalling is essential for the physiological functions, growth and biochemistry of cells. Cell signalling can be achieved by molecules which are expressed on the surface or secreted from one cell and interact with the receptors on or in other cells. These signalling molecules mediate a series of intracellular reactions which can regulate cell proliferation, differentiation, survival and metabolism (Alberts et al., 2002). There are two different types of cell signalling, one is contact dependent signalling, which is also referred as direct cell to cell signalling and occurs by the direct interaction with the neighbouring cells. The other is through the action of secreted signalling molecules (Alberts et al., 2002). Signalling, mediated by secreted signalling molecules can be of three different types, endocrine signalling, paracrine signalling and autocrine signalling (Hancock, 1997). In case of endocrine signalling, cells secrete signalling molecules into the circulatory system, which can carry the signal to target cells, distributed throughout the body. The main class of molecules in endocrine signalling are hormones, which, after release, diffuse and travel a long distance to impart their effect on a distantly placed second cell. In the case of paracrine signalling, the signalling molecules act as local mediators and affect the neighbouring cells present in the immediate environment. Neurotransmitters released from neurons, imparting their effect on neighbouring neurons, are good examples of paracrine signalling molecules. Cells involved in autocrine signalling release molecules which can bind back to their own receptors. Production of growth hormones by tumour cells, stimulating their own growth, is an example of autocrine signalling (Hancock, 1997). Signalling molecules range from cell surface receptor proteins, intracellular signalling proteins to simple gases. Hydrogen peroxide and carbon monoxide are simple gases acting as signalling molecules. Nitric Oxide (NO) is a vital and highly studied example of a gas acting as a signalling molecule (Hancock, 1997). By acting as a paracrine signalling molecule NO can regulate guanylyl cyclase activity, control neurotransmitter release and itself acts as a neurotransmitter. NO performs several physiological roles on the nervous and cardiovascular systems. Moreover, it plays a major role in the variety of physiological processes such as immune defence, regulation of cell death (apoptosis), cell motility and

as a physiological modulator of cell proliferation (Villalobo, 2006). Due to all these vital roles NO was declared to be the molecule of the year (Culotta and Jr., 1992).

1.2. Synthesis and Mode of action of NO

Acetylcholine, which is released from axons, when activated neurons send an electrical impulses along their axon, plays an important role in cell signalling as a neurotransmitter (Hancock, 1997). It has been observed that acetylcholine acts on the muscarinic receptors of the cells of rabbit thorasic aorta and other blood vessels in the presence of endothelial cells, to trigger the synthesis of a substance which causes relaxation of vascular smooth muscles (Furchgott and Zawadzki, 1980). By using "sandwich mount method" it has been shown that, when the endothelial cells of rabbit aortic strips are stimulated by acetylecholine, a relaxing factor is released, termed Endothelium Derived Relaxing Factor or EDRF (Furchgott, 1983). A detailed comparative study between the biological and chemical properties of EDRF and NO revealed that the EDRF is NO (Ignarro LJ et al., 1987). The preliminary step of Nitric Oxide synthesis is triggered by the release of neurotransmitters like acetylcholine from the activated nerve terminus to the walls of blood vessels during several physiological processes such as dilation of the blood vessels, regulation of the contraction of smooth muscles. Acetylecholine acts on the endothelial cells and activates NOS (Nitric Oxide Synthase), catalysing the formation of NO from L-arginine. The guanidine group of L-arginine is oxidized by using five electrons resulting in the synthesis of citruline and NO along with two molecules of water passing through an intermediary step in which hydroxyarginine (N^{ω}~-hydroxy-L-arginine) is formed. Formation of the intermediate, N^{ω}~-hydroxy-L-arginine (NOH-ARG) from L-Arginine, catalysed by NOS requires 1 equivalent of NADPH. The primary role of NADPH in the reaction is to contribute two electrons required for the oxidation of guanidino nitrogen of L-arginine. NOH-ARG undergoes three-electron-oxidation, with the electrons contributed by 0.5 equivalents of NADPH leading to the formation of NO and citruline (Griffith OW and DJ., 1995).

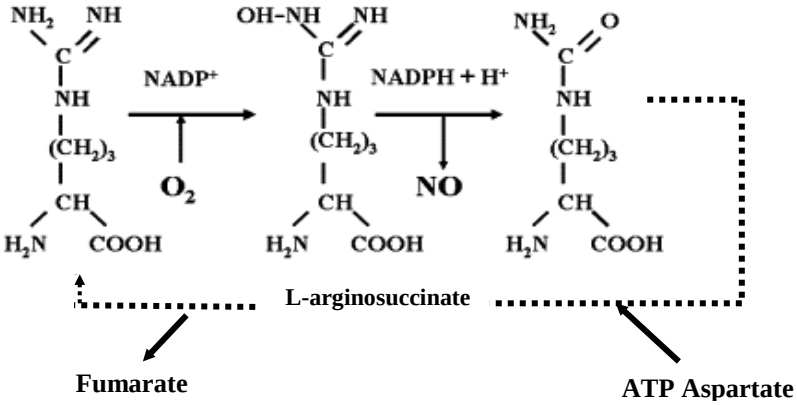

Figure 1.1. NO biosynthesis from L-arginine. The intermediate in the formation of NO, the enzyme bound N-hydroxy-L-arginine is shown. The dotted line shows recycling of L-citrulline back to L-arginine. Figure adapted from (Bruckdorfer, 2005).

After synthesis, NO diffuses rapidly across the plasma membrane and can enter neighbouring cells. Within neighbouring cells NO can react with iron bound to the active site of the enzyme guanylyl cyclase resulting in the increase of its enzymatic activity and in the production of the second messenger molecule cyclic GMP. cGMP induces muscle cell relaxation and dilation of blood vessels. It has been reported that the accumulation of cGMP is elicited by nitric oxide (CA Gruetter et al., 1981). A study of the biochemical interaction between guanylyl cyclase and NO demonstrated that 1 mol of NO-heme complex is bound to 1 mol of holoenzyme (heme containing guanylate cyclase) followed by a 50 fold increases in the specific activity of the heme bound guanylate cyclase (Ignarro et al., 1986).

However, there are many other effector molecules that NO has been shown to activate and much of the signalling from NO has been shown to be guanylate cyclase independent. NO is reported to activate delayed rectifier potassium channel (I_{ks}) independent of soluble guanylate cyclase (Asada et al., 2009). A Study of NOS2 (Section 1.3) knockout macrophages of mammalian cells revealed that NOS2 mediates regulation of several genes by interferon gamma and the process is cGMP independent as reviewed in (Stamler et al., 2001).

NO is a free radical denoted as $NO^{\cdot}$, which means that it contains an unpaired electron. Because of the presence of the unpaired electron, NO is always in an unfavoured

electronic state which makes it highly reactive. Being a highly reactive molecule NO is extremely unstable and thus has a very short half life of 3-6 seconds in tissue and 1-2 seconds in blood (Malinski) and thus its mode of action is restricted within local regions.

1.3. Nitric Oxide Synthases

The enzyme which catalyses the synthesis of NO is NOS (Nitric Oxide Synthase), is a family of protein isoforms in vertebrates. A soluble, native, monomeric enzyme was purified from rat cerebellum by utilizing 2', 5' – ADP affinity column eluted with NADPH and showed a single 150-kDa band on SDS/PAGE (Bredt and Snyder, 1990). Three different isoforms of NOS have been purified from mammalian system: bNOS (brain NOS, now known as NOS1) (Schmidt et al., 1991), eNOS (epithelial NOS, now known as NOS3) (Pollock et al., 1991) and macNOS (macrophage NOS now known as NOS2) (Yui et al., 1991). Unlike the *Drosophila NOS* (dNOS) gene, the *NOS2* gene used in this study, is not regulated by calcium (Regulski and Tully, 1995). As this mouse *NOS2* gene is not regulated by Ca^{2+}, it was decided to use this in the present study instead of using the *dNOS* gene. This mouse *NOS2* cDNA has been previously expressed in *Drosophila* under the control of a heat shock promoter (Kuzin et al., 1996). The same *NOS2* cDNA was cloned into pUAST (Brand and Perrimon, 1993) and four transformants were generated. These transformants were mapped to the X chromosome, two on the second chromosome and one on the third chromosome (Kimber, 2005). The transformant which was used for this particular study was UAS-NOS2, located on the X chromosome, as it showed the highest levels of expression.

Although NOS isoforms differ from each other in their sensitivity to react with various agrinine analogue, (Bredt DS and SH., 1994) in size, in expression levels and in regulation, they show a 30-40% amino acid homology at their C-terminal end and function as homodimers (Griffith OW and DJ., 1995). A structural study of cytokine-inducible mouse NOS isoform (NOS2) revealed that, two N-terminal catalytic oxygenase domains of each subunit interact with each other and form a dimmer in a head to head manner whereas the C-terminal reductase domains are extended from the end of each subunit. The oxygenase domain contains heme (iron protoporphyrin IX) and (6R)-5,6,7,8-tetrahydro-lbiopterin (H_4bioprotein) whereas the reductase domain contains two flavin molecules (one FMN and one FAD) all of which function as bound prosthetic groups or cofactors (Stuehr and Ikeda-Saito, 1992).

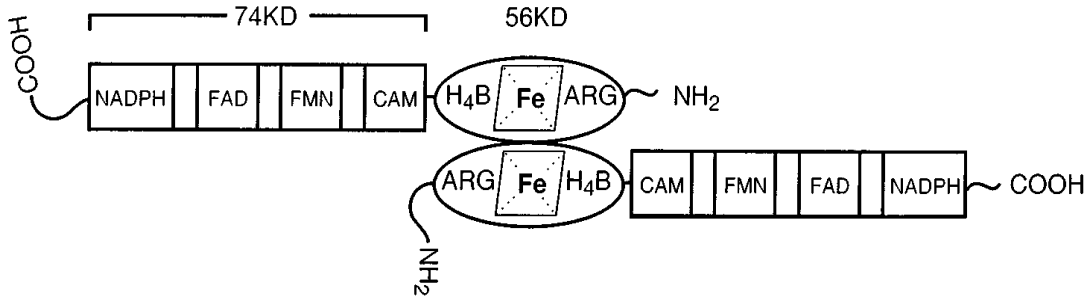

Figure 1.2. Biochemical structure of NOS2: Figure showing the head to head alignment of 56kDa of NOS oxygenase subunits and the 74kDa reductase subunits as extensions (Stuehr, 1997).

In addition to the prosthetic groups, the oxygenase domain has a binding site for L-arginine and the reductase domain has a binding site for NADPH (Essam A. Sheta et al., 1994). The transfer of reducing equivalents from NADPH to the heme group by the FAD and FMN molecules facilitates the binding of oxygen with the oxygenase domain resulting in the step-wise oxidation of L-arginine (Stuehr, 1997). By performing steady state and stopped flow kinetic studies on a nNOS, Miller *et al* reported that resembling the cytochrome P450 reductase (CPR) the oxygenase domain of NOS receives the electrons required for the L-arginine oxidation from the reductase domain (R. Timothy Miller et al., 1999).

There are several inhibitors of NOS present in blood which prevent the synthesis of NO by NOS. Arginine methyl-transferases are the enzymes which catalyse the formation of several arginine analogues such as L-monomethylarginine (L-NMMA), asymmetric dimethylarginine (ADMA), symmetric dimethylarginine (SDMA) by methylating the guanidino nitrogen group of arginine residues within proteins leading to their post translational modification (Leiper et al., 1999). Proteolysis of proteins containing these arginine analogues causes the release of the methylarginines. These methylarginines [L-NMMA and ADMA but not SDMA] (Leiper et al., 1999) compete with L-arginine binding with NOS and result in the loss of the catalytic activity of NOS and hence synthesis of NO is prevented (Bruckdorfer, 2005).

1.4. Physiological Roles of NO

1.4.1. Nitric Oxide signalling in smooth muscle

NO plays a vital role in the lowering of blood pressure by allowing relaxation and dilation of smooth muscle. NO opposes the effect of vasoconstrictors and increases the smooth flow of blood, limiting the chances of hypertension (Naseem, 2005). In case of several diseases such as atherosclerosis, the process of endothelium regulated vasorelaxation is prevented indicating the loss of NO activity (Naseem, 2005). It has been reported that coronary arteries, obtained from the hearts of cardiac transplantation patients having atherosclerosis, show impairment of cardiac muscle relaxation mediated by EDRF/NO (Forstermann et al., 1988) (Louis J. IGNARRO et al., 1987).

1.4.2. Nitric Oxide signalling in platelets

A simultaneous study of platelet aggregation and NO production by activated platelets was performed by using NO-selective microelectrode in a standard platelet aggregometer which revealed that a NOS inhibitor, Nω-nitro-L-arginine methyl ester (L-NAME), reduced NO production (92%) and cyclic GMP production (33%) along with an increase of platelet aggregation (35%) (Freedman et al., 1997). Another study reported that aggregating platelets from patients suffering from acute coronary syndrome produces less NO as compared to controls (Freedman et al., 1998).

1.4.3. Nitric Oxide signalling in nervous system

NO displays many of the properties of a neurotransmitter. Neurons, whose transmission function is brought about with the release of NO are termed as Nitrergic Nerves (Salvador Moncada et al., 1997). In the central nervous system, NO plays a vital role as a principal non-adrenergic, non-cholinergic (NANC) neurotransmitter by regulating relaxation of smooth muscles in the cerebral circulations and also regulates aspects of learning and memory (Bredt, 1999). It has been reported that the deletion of both endothelial and the neuronal NOS isoforms, expressed in neurons, reduced the rate of induction of long term potentiation (LTP) which is a form of synaptic plasticity associated with learning and memory (Duncan and Heales, 2005). A detailed study has shown that the inhibitors of NOS can cause the destruction of spatial learning (Holscher,

1997). Smith et al reported the involvement of the powerful oxidant, peroxynitrile, in Alzeimer's disease, by measuring the immunoreactivity index of nitrotyrosine produced during the nitration of tyrosine residue by peroxynitrile, which is formed as a result of the reactions between NO and superoxides (Mark A. Smith et al., 1997).

1.4.4. Nitric Oxide and cell proliferation

Endogenous NO synthesized by NOS acts as an antiproliferative agent to down-regulate the proliferation of a variety of cells (Villalobo, 2006). The inhibition of proliferation of lymphocytes is mediated by the presence of exogenous L-Arginine and increasing the number of macrophages and is suppressed by the presence of N^G-monomethyl-L-arginine (NMMA), a specific inhibitor of nitric oxide synthesis (Denham and Rowland, 1992). The soluble cytokine, interferon-gamma, shows anti-proliferative activity on rat vascular smooth muscle cells with an increase in the level of cyclic GMP (cGMP) concentration by Nitric Oxide generation and this anti-proliferative activity of NO is repressed by N^G-nitro-L-arginine, a Nitric Oxide (NO) synthase inhibitor (Nunokawa and Tanaka, 1992). NO induces the cytostatic effect of nerve growth factor (NGF) followed by growth arrest and changes the program of cell proliferation towards cell differentiation. Inhibition of NOS causes interruption in the cytostatic effect of NGF thus preventing cell differentiation (Natalia and Grigori, 1995). Another study reveals that vascular endothelial growth factor (VEGF) induced proliferation of BeWo cells is up regulated by the NOS inhibitor, L-NAME, but is repressed by the NO donor, sodium nitroprusside (Cha et al., 2001). An important role of NO is in growth arrest and cell cycle regulation of cancer and tumour cells as there is a negative relationship between proliferation of tumour cells and NOS activity in them. A study reported that in the neuroblastoma cell line (SK-N-BE) and in primary cerebellar granule cells, NO represses cell proliferation leading to cell differentiation along with a simultaneous decrease in the expression level of the proto-oncogene, N-Myc (Ciani et al., 2004). Measurements of cell growth, as determined by the rates of protein and DNA synthesis, has revealed that a concentration of 1-30 µM of NOHA (the principle intermediate formed during NO production) and NO (in the form of DETA/NO) inhibit proliferation of human Caco-2 tumor cells by 30-85% (Buga et al., 1998). Partially purified ribonucleotide reductase (RR) from L1210 mouse lymphoma cells, which is a rate limiting enzyme of DNA synthesis, has been inhibited leading to the inhibition of DNA

synthesis by NO produced by activated macrophages (Kwon et al., 1991). Therefore NO can impart its antiproliferative action by negatively regulating DNA synthesis.

1.5. NO donor molecules

NO is poorly soluble in water (only 2-3mM) and being a free radical gas, having a lone unpaired electron, NO is unstable in the existence of numerous oxidants (Tingwei Bill Cai). This chemical nature makes the introduction of NO to a biological system complex. Consequently several chemical agents, which can act as NO donors and can release NO in biological systems have been utilised to study the biochemical effects of NO. Hence the practical aspect of study of the antiproliferative effect of NO on normal cells requires extensive use of chemical NO donors. With the advancement of chemistry, numerous NO donors have been developed which have made possible the spontaneous discharge of NO and thus the controlled donation of NO in biological systems. Diverse NO donors differ in their chemical reactivity and also in NO release mechanisms as they have variation in their chemical structures. There are three different types of mechanisms of release NO by NO donors. The first way is to liberate NO spontaneously through thermal or photochemical self-decomposition which is performed by S-nitrosothiols, diazeniumdiolates, oximes. The second way is liberating NO by reacting with acid, alkali, metal and thiols which is accomplished by several NO donors such as organic nitrates, nitrites and syndnonimines and the third mode is oxidation, catalyzed by some enzymes such as NO synthases or oxidases which metabolically activate NO release from N-hydroxyguanidines. Being capable to release NO under specific conditions, numerous NO donors are found to be of great importance to treat diseases like hypertension and atherosclerosis which are caused by scarcity of NO production in biological systems. The NO donor Glyceryl trinitrate has been used as a vasodialator drug since 1879 and is also used to relieve acute attacks of angina pectoris (Tingwei Bill Cai). Besides being used as medicines, several chemical NO donors have already proved to be efficient tools for research into the treatment of diseases resulting from extreme proliferation and uncontrolled cell growth. By incorporating [^{3}H] thymidine, performing flow cytometry and calculating cell numbers it has been established that Sodium nitroprusside (SNP) represses epidermal growth factor regulated development of vascular smooth muscle cells (VSMC) at G1/S phase of cell cycle, and also restrains EGF induced DNA synthesis along with an up-regulation of the level of cGMP. The

mechanism of antiproliferative activity of SNP mimics that of endothelium released NO which also participates in the regulation of vascular smooth muscle cells (VSMC) proliferation via a cGMP regulated mechanism (Yu et al., 1997). Another investigation reported evidence of cell cycle arrest during G_0/G_1 phase when p53 deficient SW620 colon cancer cells were exposed to the NO donor S-nitrosoglutathione (GSNO) (Jeon et al., 2005). A study examining the antiproliferative effect of another NO donor, Glyco-2 SNAP, on the development and proliferation of MDA-MB-231 breast cancer cell lines discovered that 100μM concentration of this NO donor inhibited DNA synthesis of these cells. (Laudanski et al., 2001). The antiproliferative action of NO in fibroblasts requires p53 signaling as it has been shown that p53 lacking cell lines do not exhibit growth arrest when given a 30mins exposure to the NO donor SNAP (Nakaya N et al., 2000).

1.6. Study of NO by using *Drosophila melanogaster* as a model organism

The role of NO in halting cell growth and directing the cell cycle towards cell differentiation has been extensively studied by in *Drosophila.* The *Drosophila* NOS gene (*dNOS*) synthesises a 152kDa protein which shows 43% amino acid sequence similarity with the NOS isolated from rat neuronal cells (Regulski and Tully, 1995). NO acts as an antiproliferative agent allowing cell differentiation to occur at late larval stages, in transgenic *Drosophila* carrying the mouse *NOS2* cDNA gene under the control of heat shock promoter (Kuzin et al., 1996). The action of NO on the suppression of DNA Synthesis was shown by analysing BrdU (5-bromo-deoxyuridine) incorporation during S phase of imaginal disc growth of third instar larvae (Kuzin et al., 1996). Kuzin et al reported that imaginal tissues from larvae of transgenic flies carrying nitric oxide synthase gene (dNOS1) induced by the heat shock promoter showed fewer BrdU-labeled cells as compared to flies in which NOS expression is inhibited (Kuzin et al., 2000).

1.7. Technologies For Gene Manipulation In *Drosophila melanogaster*

Drosophila has long been a favourite organism for genetics and developmental research, but it was primarily through the use of several ingenious gene transformation technologies that the powerful tools of molecular biology were fully exploited.

1.7.1. Transposon associated gene manipulation

Among the foremost genetic tools for introducing transgenic DNA into flies are transposons such as P elements (Spradling and Rubin, 1982). The P element is 2.9 kb long transposon and contains 31 bp terminal inverted repeat sequences. It generates direct repeats of target DNA of 8 bp at the site of insertion upon integration. The P element has 4 open reading frames and encodes a protein called transposase, an enzyme required for transposition of the P element. Because of the expressional specificity of transposase in germ line cells transposition, mobilization of P element occurs only in the germ line. P elements can be engineered to carry a marker gene to identify transformants. Both selectable and visible markers can be used but the transformation efficiency is often higher if a visible marker (eye colour gene) is used instead of a selectable marker (neomycin resistance gene) (Spradling and Rubin, 1982). P elements can carry an insert up to 40kb (Haenlin et al., 1985). The most important use of P element is generation of transgenic flies. The drawback of using P element is their insertional specificity (Venken and Bellen, 2005). P element insertion often occurs within 400bp of the transcriptional start site of genes. Approximately two thirds of all P-element insertions occur in disproportionately few genomic locations termed hot or medium hot spots. To overcome this problem, use of the Piggy Bac vector has been employed which has no obvious insertional preference as reviewed in (Venken and Bellen, 2005). Unlike the P-element, Piggy Bac inserts do not frequently produce mutant alleles of the tagged gene. As a result, Piggy Bac insertions are not useful in generating new mutant alleles of genes. As remedy of this drawback a hybrid transposable element has been constructed by carrying a Piggy Bac backbone with P element inserted inside. Use of this hybrid vector, has increased the probability of random insertion (due to the presence of Piggy Bac backbone) along with mutagenesis (through imprecise excisions of the P-element) (Venken and Bellen, 2005).

1.7.2. Enhancer Trapping

In this technique a reporter *LacZ* is fused to a weak promoter and is controlled by the activity of a nearby enhancer. The reporter gene used in this enhancer trap constructs was originally the *LacZ* gene from *Escherichia coli*, which codes for *β*-galactosidase (O'Kane and Gehring, 1987). The *LacZ* promoter fusion is mobilised within a P element and inserted in *Drosophila* (O'Kane and Gehring, 1987). LacZ fusions act as an efficient cell marker, which facilitate genetic and developmental studies. This strategy of gene manipulation made possible the visualization of tissue and cell specific expression of Lac-Z (O'Kane and Gehring, 1987). Enhancer trap strategies allow a thorough study of expression patterns of trapped genes, but are not informative at the protein level, particularly the subcellular localisations of proteins (Xavier Morin et al., 2001). A technique which establishes a correspondence between gene and protein and also facilitates the study of the gene product was necessary (Jarvik et al., 1996). A more recent strategy of "Protein Trapping" has been developed (Discussed in Section 3.1.1).

1.8. Previous research in laboratory

As the present investigation is a continuation of the previous research which was on going in our laboratory, a brief description of the previous findings will be given. Microarray analysis of tissue culture cells treated with 200μM of the NO donor S-nitroso-N-acetyl-penicillamine (SNAP), identified *Thor* as one of seven transcripts up-regulated after 4hrs of NO treatment which was also up-regulated at 8 and 12hrs post NO exposure (Kimber, 2005). Further analysis, and comparison to other data sets, showed that expression of a common set of genes are regulated both by NO and the transcription factor FOXO (Kimber, 2005). Subsequently *Drosophila* FOXO was confirmed to be a target of NO (Scott, 2009).

Previous work attempted to identify other targets of NO. For this purpose YFP tagged CPTI (transgenic *Drosophila*) lines were used. Previously, salivary glands from more than 35 YFP tagged CPTI lines were examined after exposure to the NO donor S-Nitroso-N-acetylpenicillamine (SNAP). Among these, the Mi-2 tagged line CPTI-000232, showed consistent changes after SNAP exposure for 24hrs, 20hrs, 16hrs, 12hrs, 8hrs and 4 hrs respectively (Lasala, 2007). It was observed that the expression of the YFP tagged Mi-2 protein was higher after NO treatment compared to untreated control salivary glands. Up regulation of the expression of YFP tagged Mi-2 in CPTI-000232

established Mi-2 as another probable target of NO. It is possible that the up-regulation of the expression of Mi-2 after SNAP treatment may be controlled by FOXO.

1.9. Why use the salivary gland?

The growth of larval salivary glands is achieved by endoreplication where there no cytokinesis after DNA replication resulting in an increase in cell size instead of cell number (Demerec, 1950) (Andrew et al., 2000). After determination of the salivary gland primordia (8hrs AEL) there is an increase in polytenization until the end of the third larval instar (Demerec, 1950). Hence, the individual cells of the mature third instar larval salivary glands are large (Demerec, 1950). This large cell and nuclear size makes the study of subcellular localization of proteins easier. Previous work has demonstrated that the salivary glands cells respond to NO expressed from within those cells with reduced growth and increased expression of NO dependent genes (Scott, 2009, Kimber, 2005). Exogenously provided NO has also been demonstrated to alter the localisation of some tagged proteins in a small scale pilot study (Lasala, 2007). I therefore decided to use larval salivary glands to study the subcellular accumulation of proteins in response to NO.

1.10. A Brief introduction about Mi-2 and associated proteins

1.10.1. Mi-2 - A brief description

Immunofluorescence study with anti-Mi-2 positive sera of dermatomyositis patients recognized the 218 kDa nuclear human Mi-2 protein, encoded on chromosome 12 (Hans Peter Seelig et al., 1995). *Drosophila* Mi-2 is reported to contain a HMG box, two PHD fingers, two chromodomains and a ATPase domain (Bouazoune et al., 2002).

1.10.2. Mi-2 is a component of NuRD complex

Immunoprecipitation experiments performed with human Hela cells have demonstrated that Mi-2 is a component of multiprotein Nucleosome Remodelling Deacetylating (NuRD) complex (Ahringer, 2000) (Tong et al., 1998). The 2MDa NuRD complex (Ahringer, 2000) consists of eight polypeptides: MTA1/2, HDAC1, HDAC2, RbAp46, RbAp48, MBD3, p66 and Mi-2 (Ng and Bird, 2000) (Ahringer, 2000). The nucleosome remodelling activity of NuRD is provided by its Mi-2/CHD protein complex which contains helicase/ATPase domains (Ahringer, 2000). The histone deacetylases (HDAC 1/2) present in NuRD provides the histone deacetylation activity (Yi Zhang et al., 1998).

Therefore, NuRD contributes to both ATP dependent nucleosome disruption and also histone deacetylase activity (Yi Zhang et al., 1998) (Xue et al., 1998, Tong JK et al., 1998).

1.10.3. Functional roles of Mi-2/NuRD

Transcriptional activators are commonly associated with histone acetyltransferases (HATs), whereas transcriptional repressors have a functional connection with histone deacetylases (HDACs) (Ng and Bird, 2000, Struhl, 1998). The functional link between histone deacetylation and transcriptional suppression became evident when a mammalian histone deacetylase, HDAC1, purified via its affinity for the histone deacetylase inhibitor trapoxin, was shown to be related to the yeast transcriptional repressor, RPD3 (Taunton et al., 1996). The exact mechanism through which the SIN3-RPD3 associated transcriptional repressor Ume6 decaetylates histone H4, leading to a transcriptional suppression of Ume6 binding site containing genes, has been demonstrated in *Saccharomyces cerevisiae* (Stephen E. Rundlett et al., 1998). Therefore, this evidence suggests that HDACs in NuRD play a vital role in transcriptional repression. The structural similarity of NuRD with the Sin3 complex suggests that, like Sin3, NuRD also takes part in transcriptional repression (Ayer, 1999). Further data linking NuRD with transcriptional repression is that one subunit of NuRD is the metastasis associated protein MTA1 (Toh et al., 1994). MTA1 has a high degree of similarity with the nuclear receptor corepressor, N-CoR (Xue et al., 1998). N-CoR, is an associated factor of the transcriptional repressor complex Sin3 and facilitates Mxi1/Sin3 regulated transcription of Myc family transcriptional repressors leading to overall growth arrest and tumour suppression. (Alland et al., 1997)

Mi-2, a core component of the NuRD complex, facilitates chromatin and nucleosome remodelling through ATP hydrolysis leading to a transcriptional activation (Wade et al., 1998). Mi-2 is a member of SWI2/SNF2 family proteins which show a DNA stimulated ATPase activity required to destabilise histone-DNA interactions in nucleosomes leading to binding of transcription factors to histone associated DNA (Pazin and Kadonaga, 1997). The two chromodomains present in Mi-2 are essential for the binding of nucleosomes to Mi-2 through protein-DNA binding during the preliminary stage of nucleosome remodelling (Bouazoune et al., 2002). It has been revealed that, the nucleosome structure is destabilized to permit the binding to DNA of sequence specific transcription factors and other transcriptional machinery (Tsukiyama and Wu, 1997). In

Drosophila, *Mi-2* mutant germ cells do not develop to produce embryos and this can be rescued by expressing a *Mi-2* transgene. This indicates that the Mi-2 protein is essential for germline development in *Drosophila.* (Kehle et al., 1998).

A sequence specific DNA binding protein Hunchback (Hb) initiates *Hox* gene repression whereas Polycomb group, PcG, proteins, maintain the suppression activity in *Drosophila* (Pirrotta, 1997). *Drosophila* Mi-2 has been assumed to take part in HoX gene repression. Hb requires NuRD in this repression activity via interactions with Mi-2 which in turn modifies the chromatin structure, facilitating the binding of PcG and DNA resulting in HoX gene repression (Kehle et al., 1998). The methylation of DNA at the dinucletide CpG is performed by the methyl CpG binding protein MeCp2, which in turn brings about transcriptional regulation. It has been reported that MeCp2 protein recruits the transcriptional repressor and decaetylase complex Mi-2/NuRD for gene regulation by DNA methylation in mouse (Nan et al., 1998) . Therefore, the process of gene regulation by transcriptional silencing is achieved by a relationship between DNA methylation and histone decaetylation established by MeCp2 and Mi-2/NuRD. This regulation has also been shown in *Xenopus laevis* (Wade et al., 1999).

In addition, the Mi-2α associated proteins, Ikaros and Aiolos, are associated with the NuRD complex (Kim et al., 1999) These proteins act as sequence specific DNA binding factors required for the development of the mouse haemopoietic system (Cortes et al., 1999). Ikaros is reported to be necessary in the regulation of mouse B and T cell differentiation (Georgopoulos et al., 1997).

In summary ATP hydrolysis dependent changes in chromatin structure such as acetylation, deacetylation and methylation of core histones, which regulate the contact of several transcription factors with DNA, are achieved by three core components of NuRD: Mi-2, HDAC1/2, and MBD3, resulting in the regulation of gene expression.

1.10.4. P66 the regulatory component of NuRD

In *Drosophila,* the p66 component of NuRD is localised in the nucleus and represses wingless target genes and performs vital roles in development through the regulation of ecdysone-responsive genes (Kon et al., 2005). Purified MeCP1 contains methyl-CpG-binding protein, MBD2 along with all the components of Mi-2/NuRD complex including p66 (Feng and Zhang, 2001). A confocal microscopic study revealed the direct association between p66 protein family members and the MBD2/3 proteins, which are the components of MeCP1 protein complex in DNA methylation mediated

transcriptional repression (Brackertz et al., 2002). Analysis and characterization of the MeCP1 complex revealed two p66 homologues p66 and p68. These homologues, isolated from different organisms showed two highly conserved regions, CR1 and CR2. CR1 is involved in the attachment of p66 with the other MeCP1 components whereas CR2 functions in localisation of p66 and MBD2/3 to specific loci during DNA methylation mediated transcriptional repression (Feng et al., 2002). Another report suggests that the DNA demethylase, MBD2, which is a component of MeCP1 complex, interacts with Mi-2/NuRD and directs it to methylated DNA (Zhang et al., 1999). p66 is reported to interact with MBD2 and MBD3 (Kon et al., 2005) and over expression of p66 alters the localisation of MBD3 (Feng and Zhang, 2001). All these reports support the hypothesis that p66 involves NuRD in methylation mediated gene silencing through MBD2, and hence functions as a regulatory component of Mi-2/NuRD (Kon et al., 2005).

Some parts of this study will focus to determine the effect of NO on p66 in *Drosophila*. According to the gene naming in Flybase, p66 will be referred to as Simj in the rest of this thesis.

1.10.5. Dref - An associated protein of Mi-2

Antibodies raised against Dref (DNA replication related element factor) can co-immunoprecipitate Mi-2 in *Drosophila* which confirms the *in vivo* presence of Dref/Mi-2 complex (Hirose et al., 2002). Mi-2 genetically interacts with Dref. Mi-2 and Dref are found to negatively regulate each other's function. Binding of Mi-2 and Dref to polytene chromosome is mutually exclusive (Hirose et al., 2002). Active Dref is a 86kDa homodimeric polypeptide. BLAST searches revealed that the human homologue of Dref has 22% sequence homology with *Drosophila* Dref (Ohshima et al., 2003). DNAase I foot-printing analysis indicates that *Drosophila* Dref binds with the DRE (DNA replication related element) (Fumiko Hirose et al., 1993). DRE is the transcription regulatory region which contains an 8 bp palindromic sequences (5'-TATCGATA) and stimulates the promoter activity of DNA replication related genes (Fumiko Hirose et al., 1993). Dref contains 701 amino acids (Hirose et al., 1996). Proliferating cell nuclear antigen (PCNA) interacts with DNA polymerase during DNA synthesis. The DNA binding region of PCNA probably functions to increase the processivity of DNA polymerase (Yamaguchi et al., 1990). The presence of the 8 base pair DRE sequence was identified in both the DNA polymerase α and PCNA genes

(Hirose et al., 1991). The DRE sequence can effect within 1.4 kb from the transcription initiation site and its presence in the DNA polymerase α and PCNA gene promoters suggests that expression of both the genes is regulated by Dref (Fumiko Hirose et al., 1993). More than 150 genes which are involved in several physiological reactions related to cell proliferation carry DRE sequences. This indicates that expression of these genes is likely to be controlled by Dref (Matsukage et al., 2008). A gradual decrease in the expression of Dref is mediated by several differentiation related transcription factors and suggests differentiation-coupled suppression of cell proliferation by DRE/Dref (Matsukage et al., 2008). Parts of this study will concentrate on the effect of NO on the Mi-2 associated protein Dref.

1.11. Aims of the project

The primary aim of this study was to identify the *in vivo* protein targets of Nitric Oxide signalling in *Drosophila melanogaster* particularly from the perspective of cell proliferation, growth and development. As previous work in the laboratory had identified Mi-2 as a target of NO, the present study was focused on the confirmation and extension of these previous results. This study extended the understanding of the effects of NO on Mi-2 and its associated proteins.

Previous data in the laboratory also identified FOXO as a probable target of NO (Scott, 2009) and revealed that a common set of genes are regulated by both NO and FOXO signalling (Kimber, 2005).

Therefore, this research also focused on the analysis of whether the effect of NO on Mi-2 is regulated by FOXO. Moreover, the dependency of NO on Mi-2 for growth regulation was also determined.

Although the core area of the present research is focused on the study of the effect of NO on Mi-2 and associated proteins, another aspect of the project covers the annotation and analysis of several YFP tagged transgenic *Drosophila* lines generated by Cambridge Protein Trap Insertion project (CPTI). Records of this can be obtained from CPTI created *Drosophila* database "The Flannotator". In addition, a screen for other targets of NO was also performed by exploiting YFP tagged CPTI transgenic *Drosophila* lines.

Chapter 2: Material and Methods

2.1. General

2.1.1. Fly Husbandry

Drosophila stocks and crosses were grown on D+ food, in 8cm x 2.5cm plastic vials, sealed with either cotton wool or rayon balls. Flies were raised at either 25^{o}C or 18^{o}C on a 12 hour light-dark cycle. Adult flies were observed using CO_2. Dissection of third instar larvae was performed using microscope with a Microtec MFO-90 light source.

D+ Glucose Food Media

Agar 40g
D+ Glucose anhydrous 551g (Fisher Scientific)
Yeast 143g
Sucrose 185g
Maize meal 236g
Propionic acid 25mls
Nipagen 10%w/v 82mls
Water 5500mls

Method

Yeast and anhydrous D+ Glucose were mixed to prepare a paste by using a small amount of water. The agar and maize were mixed with the rest of the water and were boiled together to dissolve. The paste was then added and the mixture was brought to the boil again. Lastly the mixture was allowed to cool before pouring into plastic vials or glass bottles.

2.1.2. Over expression using the Gal4-UAS system

The Gal4-UAS system as described in (Greenspan, 1997) and in (Ornitz et al., 1991) was utilized for over expression of specific genes. The gene to be over expressed was linked to an element containing multiple UAS (upstream activator sequence) sequences (Brand and Perrimon, 1993, Tuan Rocky. S and Lo W Cecillia, 2000). The transcription factor GAL4 binds to UAS and drives the transcription of the desired gene subcloned downstream of UAS. Flies carrying the gene to be expressed linked to UAS sequence,

were crossed to flies that carrying the Gal4 coding sequence fused to a tissue specific promoter or enhancer. Offspring carrying both the UAS and Gal4 inserts were observed.

2.1.3. Generating single cell clones

Single cell clones were generated by using a combination of UAS-GAL4 and FLP/FRT technique (Tuan Rocky. S and Lo W Cecillia, 2000). FLP is a site-specific recombinase encoded by the *S. cerevisiae* 2μm plasmid. The expression of FLP is regulated by a heat shock promoter, so the recombinase is also referred as hsFLP. FLP efficiently catalyzes recombination between two copies of its specific 34 bp recognition site (called the Flp recognition target (FRT). A heat shock FLP construct was used to remove a segment of DNA flanked by FRT sites, which lies in between the Actin5C promoter and the Gal4 driver, preventing the expression of the later. After the excision of the FRT cassette ubiquitous expression of the GAL4 driver occurs under the control of Actin 5C promoter followed by expression of the UAS tagged gene of interest (Duffy, 2002) (Tuan Rocky. S and Lo W Cecillia, 2000). Recombination was induced at a low level, 24-48 hours after egg laying (AEL), (Demerec, 1950) by heat shocking the larvae for between 4 to 5 and half minutes. This system produced single cells expressing UAS-GFP/UAS-mRFP as a marker or simultaneously expressing the marker and UAS-NOS (or any other gene of interest). The single cells expressing *NOS2* produced by this experimental design could then be used to study the molecular and cellular consequences of high levels of NO production as compared to surrounding wild type cells which are not affected by Flp mediated recombination thus do not over express the gene of interest.

2.1.4. Visualisation of protein expression in YFP tagged CPTI transgenic *Drosophila* lines

Materials:

1xPBS (10xPBS: 1.37M NaCl, 0.1M Na_2HPO_4, 0.01M NaH_2PO_4; pH7.4).

Method:

The coordinating team of Department of Genetics, University of Cambridge, have generated CPTI-YFP transgenic *Drosophila* lines. In each transgenic *Drosophila melanogaster* line a particular gene is tagged by utilizing a fluorescent tagging method,

where YFP is used as a reporter gene to study the expression of the tagged gene (Section 3.1.2). 150 CPTI transgenic *Drosophila* lines were examined to study the expression of YFP tagged genes in different tissues. Third instar larvae were used as sources of three sample tissues (the brain, the imaginal discs, and the salivary gland) to study the expression of the genes tagged with. Larvae were dissected in 1X PBS and sample tissues were mounted on clean glass slides. Images of the tissues were collected using a Zeiss LSM 510 Meta Laser scanning Confocal microscope at 488nm, and modifying the excitation to avoid fluorescence saturation.

2.1.5. *Ex vivo* culture and NO donor treatment

Materials

1xPBS (10xPBS: 1.37M NaCl, 0.1M Na_2HPO_4, 0.01M NaH_2PO_4; pH7.4).
SNAP (S-Nitroso-N-acetylpenicillamine) (Sigma Aldrich, N 3398, original stock 20mM dissolved in DMSO)
DMSO (Sigma Aldrich).
Schneider's tissue culture medium (Gibco-BRL, USA).

Method

Salivary glands from CPTI lines were treated with SNAP. 1µl 20mM SNAP was added into 95ul of Schneider's tissue culture medium to achieve an ultimate SNAP concentration of 200µM, which is optimum to stop cell proliferation and growth but not affect viability (Kimber, 2005). Salivary glands were incubated in this mixture for 16-17 hours or 4 hours. In all incubations one of a pair of salivary gland from a larva was treated with SNAP, whereas, the other of the same pair of gland, from the same larva was treated with DMSO (1µl DMSO in 95µl of Schneider's tissue culture medium) as control. Images of both the SNAP treated and DMSO treated) glands were collected by using a Zeiss LSM 510 Meta Laser scanning Confocal microscope at 488nm, modifying the excitation levels to avoid fluorescence saturation.

The CPTI lines which consistently showed changes in expression after SNAP exposure were chosen for shorter treatment with SNAP. Two pairs of salivary glands were taken from two different larvae of a particular CPTI line. One of a pair of salivary gland was incubated in a mixture of 1µl SNAP + 95ul of Schneider's tissue culture medium for

0.5hrs minutes and subsequently for 3.5 hours in 1µl DMSO + 95ul of Schneider's tissue culture medium. The other of the same pair of salivary gland was incubated in the similar mixture of SNAP (1µl SNAP + 95ul of Schneider's tissue culture medium) for 4 hrs. One of the another pair of salivary gland from the same CPTI line was incubated in 1µl SNAP+ 95ul of Schneider's tissue culture medium for 0.5hrs and subsequently for 3.5 hours in 1µl DMSO + 95ul of Schneider's tissue culture medium. The other of the same pair was incubated in 1µl DMSO + 95ul of Schneider's tissue culture medium for 4hrs. After incubation images of the four different salivary glands given different treatments images were collected as above.

2.2. Immunohistochemistry

2.2.1. Antibody staining

Materials

1xPBS (10xPBS: 1.37M NaCl, 0.1M Na_2HPO_4, 0.01M NaH_2PO_4; pH7.4).
4% Paraformaldehyde in 1xPBS.
100% Methanol.
PBT (1xPBS, 0.1% Triton X-100, 0.2% BSA).
Appropriate primary and secondary antibodies (Section 2.2.2.).
Normal Goat and Horse sera (Sigma) (Section 2.2.2.)
DAPI 1:20,000 in 1x PBS with 0.1% Triton X-100.
Aquamount (Polyscience).

Method

Wandering third instar larvae were dissected by inversion and fixed in 4% paraformaldehyde for 20 minutes at room temperature. Tissue was then washed 2x 5min in 1xPBS. If the tissue was to be stored it was washed twice in Methanol and stored at –20^{o}C in Methanol. The tissue was then washed in 1xPBS before making it permeable in PBT for 2 x 30 minutes. The tissue was then incubated in primary antibody overnight at 4^{o}C. Primary antibody was removed and stored, and the tissue was washed 4 x 20 minutes in PBT at room temperature. The tissue was rinsed x 2 in PBT containing 2% animal sera compatible for the respective secondary antibody (Section 2.2.2) then

incubated with secondary antibody in PBT with 2% animal sera (suitable with the secondary antibody being used) at room temperature for 2 hours. The tissue was then washed 4 x 15 minutes in PBT at room tem
perature. DAPI staining of tissue was performed for 15 min. Tissue was then washed 2x 5minutes in 1xPBS before dissection. The required tissues were mounted on a glass slide in Aquamount and examined on a LSM Zeiss inverted-LSM 510 META COMBI Confocal Microscope with Coherent Enterprise UV laser using 40x water lens.

2.2.2. Primary and Secondary antibodies with their respective animal sera

Mi-2 antibody:

Both N-terminus and C-terminus rabbit anti-dMi-2 (Brehm et al., 2000) were gifts from Alexander Brehm, used at 1:1000.

Secondary antibody: goat anti-rabbit Cy5 IgG (Jackson ImmunoResearch Laboratories, Inc.) used at 1:100 in 2% goat sera.

Dref antibody:

Mouse anti-Dref (Hirose et al., 2002) was a gift from Fumiko Hirose, was used at 1:100.

Secondary antibody: horse anti-mouse Cy5 IgG (Jackson ImmunoResearch Laboratories, Inc.) used at 1:100 in 2% horse sera.

Goat anti-mouse Alexa fluor 555 IgG (Invitrogen, Molecular Probe) used at 1: 200 in 2% goat sera.

2.3. Nuclei Staining and Measurement

Materials

1xPBS (10xPBS: 1.37M NaCl, 0.1M Na_2HPO_4, 0.01M NaH_2PO_4; pH7.4)

4% Paraformaldehyde in 1xPBS

DAPI: 1:20,000 in 1x PBS with 0.1% Triton X-100

Aquamount (Polysciences)

Method

Wandering third instar larvae were dissected by inversion and fixed in 4% paraformaldehyde for 20 minutes. Tissue was then washed 2x 5min in 1xPBS. The

tissue was then incubated in diluted DAPI solution of for 15 min. Tissue was then washed 2x 5 minutes in 1xPBS before dissection. Tissues were mounted on a slide in Aquamount and examined on a Zeiss AxioPhot Microscope at 40x.

2.4. Image Analysis on Velocity

Confocal images were analysed using quantitative software package from velocity (Improvision / Perkin Elmer) (http://www.cellularimaging.com/products/Volocity). which generates 3D image of the acquired stacks.

Method

2.4.1. Quantitative analysis of YFP tagged protein localization in the nuclei

Nuclei from 5 pairs of salivary gland images (5 experimental and 5 control genotypes) were captured on velocity through the Z axis to cover the YFP fluorescence in whole section thickness. YFP fluorescence of those nuclei which were available up to 10 μm depth of image Z stack were measured. Sensitivity settings of confocal microscope were kept constant between a control and experimental pair but not necessarily between different pair of comparators. Hence, the threshold point in velocity was kept constant for all the nuclei of a particular pair of control and experimental comparators. Additional analysis and data presentations were performed by exporting velocity acquired datasets into Microsoft Excel.

2.4.2. Quantitative analysis of the volume of nuclei

DAPI staining was performed following the same method mentioned in section 2.3. Using velocity, xy, xz and yz dimensions of nuclei were constructed from Z section series of stacks from salivary gland images of different genotypes to cover the entire volume of nuclei. The threshold point was kept constant for all the nuclei of a particular salivary gland image. Additional analysis and data presentations were performed by exporting velocity acquired datasets into Microsoft Excel.

2.4.3 Estimation of protein accumulation in the nuclei of clone images

Using velocity, xy, xz and yz dimensions of nuclei were constructed from Z stacked image planes of both the clone cell and the non adjacent wild type cells of a particular image to encompass the protein accumulation in the whole section. In this case,

intensity of protein localization in the nuclei of clone cell was compared with that of the non adjacent wild type cells of that particular salivary gland. Hence, sensitivity settings of confocal images differed for every image. Therefore, the threshold point in velocity was kept constant for all the nuclei of a particular salivary gland image. Additional analysis and data presentations were performed by exporting velocity acquired datasets into Microsoft Excel.

2.5. Statistical Analysis on ANOVA

Method

Statistical comparison of nuclear size between genotypes was made using one way ANOVA on MINI tab statistical software package. During the analysis $p < 0.05$ was taken for indicating statistically significant difference across the comparative genotypes. A post hoc Tukey analysis was undertaken on MINI tab for further accurate analysis of nuclear size among the experimental and control genotypes.

Chapter 3: Annotation and Screening of CPTI lines

3.1. Introduction

3.1.1. Brief introduction about protein trapping in *Drosophila*

Protein traps were first used as "CD tagging" in *Chlamydomonas* and later in mammalian cells (Jarvik et al., 1996). In CD tagging the gene is tagged by sequence specific nucleotides and the protein is tagged by sequence specific peptide. As these tags are unique, use of sequence specific nucleotide or antibody probes facilitates the identification and analysis of the functional properties of the gene at the protein level (Jarvik et al., 1996).

CD tagging has been applied to develop a protein trap system which makes use of the P element transposon to carry green fluorescent protein (GFP) as a mobile exon. These GFP fusions facilitate the study of sub-cellular and cellular distribution of the fusion proteins in live tissues (Xavier Morin et al., 2001). GFP was originally cloned from the jellyfish *Aequorea Victoria* (Tsien, 1998). The biggest advantage of using GFP as a reporter is, it has made possible the study of subcellular localisation of proteins in living cells. Hence the investigation of the movement of proteins and their interaction with cellular components are possible by live cell imaging (Lippincott-Schwartz et al., 2001).

3.1.2. Use of yellow fluorescent protein as a reporter in protein trap strategy

Yellow fluorescent protein (YFP) is a variant of GFP and has found to be more useful in biological systems because of its intense fluorescence, brightness and reduced sensitivity to environmental factors such as pH and ionic strength (Rekas et al., 2002). Moreover, the use of YFP as a reporter has overcome the problem of the slow maturation shown by GFP (Nagai et al., 2002). Therefore, a protein trap strategy using YFP as a reporter gene was developed. A network of *Drosophila* researchers in the UK of thirty different universities, co-ordinated by the Department of Genetics, University of Cambridge, has established the Cambridge Protein Trap insertion (CPTI) Project. The scientists of CPTI project make use of hybrid vectors combining Piggy Bac and P-elements.

These vectors contain the following features:

- The mini white gene to track the element in stocks.
- Affinity purification tags: StrepII and FLAG.
- YFP exon.
- Splice accepter and splice donor site.

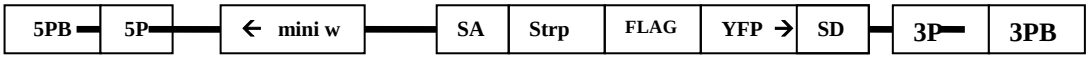

Figure 3.1. PiggyBac construct
Figure adapted from (E. Ryder et al.)
PB = Piggybac ends
P = P element ends

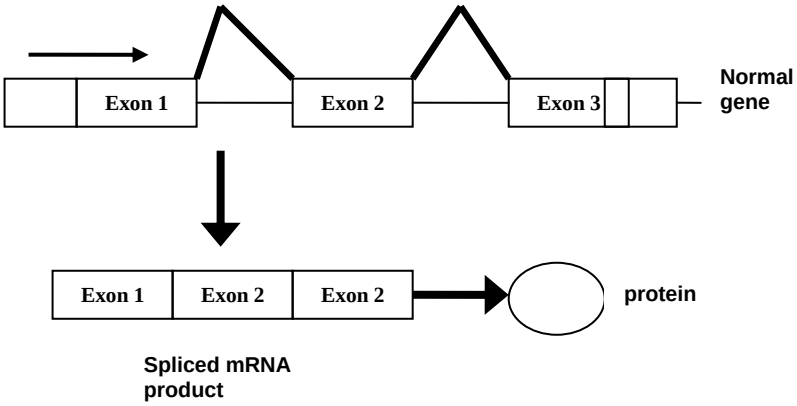

Figure 3.2. Diagrammatic representation of mRNA and protein production from an endogenous gene.
After transcription of mRNA the introns are spliced out. The spliced mRNA product is translated to protein.
Figure adapted from (E. Ryder et al.)

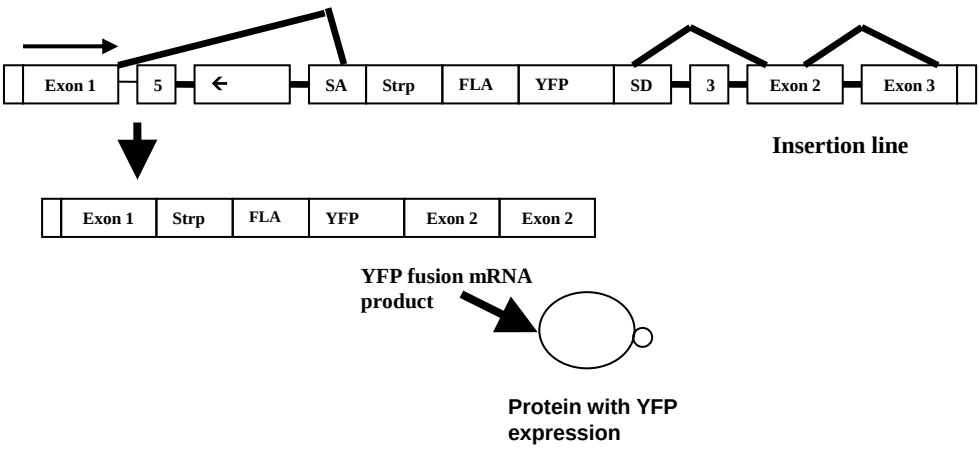

Figure 3.3. Diagrammatic representation of transcription and translation of a fluorescent tagged protein in YFP protein trap

The YFP construct contains splice acceptor (SA) and splice donor (SD) sites. Transcription results in incorporation of SA and SD sites into the YFP fused spliced mRNA. If the PiggyBac element transposes into the intron of a gene in the correct orientation and frame, a functional YFP fusion protein will be expressed (E. Ryder et al.)**.**

In the Piggy Bac and P-element hybrid vector, YFP reporter, devoid of initiation and stop codons, flanked by SA (splice accepter) and SD (splice donor), is used as a mobile artificial exon. If the PiggyBac transposes into the intron in a correct orientation, then the splicing will take place at the SA and SD sites and the remaining YFP exon is inserted into the spliced mRNA product. If the YFP exon is inserted in the correct frame, the protein will be translated from the YFP fused mRNA resulting in a YFP expressing fusion protein (E. Ryder et al.). The researchers of CPTI project have created a new *Drosophila* database termed "The Flannotator" which allows annotation and characterization of the expression patterns of YFP tagged protein trap lines at all stages of development and all tissue types. "The Flannotaor" acts as a software package for the storage of annotated gene expression patterns in *Drosophila melanogaster* (E. Ryder et al., 2009).

Experiments of this chapter were designed for annotation of several YFP tagged protein trap transgenic *Drosophila* lines created and supplied by the coordinating team of Cambridge Protein Trap Insertion Project (CPTI). Another aspect of this chapter was to undertake a genetic screen to search for molecular targets of NO action by examining the effect of NO on YFP tagged proteins of the CPTI lines.

3.1.3. A brief introduction about NO donors

NO is poorly soluble in water (only 2-3mM) and being a free radical gas, having a lone pair of electron NO is unstable in the existence of numerous oxidants Hence, the practical aspect of study of the antiproliferative effect of NO on normal cells of different tissue origin requires the use of chemical NO donors (Tingwei Bill Cai, 2005). A comparative study of the antiproliferative effect between five different NO donors (DEA/NO•, PAPA/NO•, SPER/NO•, DPTA/NO•, DETA/NO•) was performed after exposing rat aortic smooth muscle cells (RA-SMC) to the NO donors for different time periods. The most antiproliferative effect was shown by 500 µm concentration of DETA/NO as cell growth was completely inhibited on 1^{st}, 3^{rd}, and 5^{th} days as confirmed by a 7 days measurement study of the cell numbers (Daniel L. Mooradian et al., 1995). A concentration of 10^{-4} M to 10^{-3} M, of a chemical NO donor PAPA NONOate (pNO) was reported to impart cytostatic effects by inhibiting ribonucleotide reductase, within 24-48hrs, which is similar to the cytostatic effect of NO (Jarry et al., 2004).

3.1.4. SNAP (S-Nitroso-N-acetylpenicillamine)

An advantage of SNAP (S-Nitroso-N-acetylpenicillamine) is, it can release NO within 30 minutes which is much shorter time period compared to that of the other NO donors. The antiproliferative action of NO in fibroblasts acts through the p53 signaling pathway. Cell lines lacking p53 are unable to accomplish growth arrest when given a 30mins exposure to SNAP. It has been shown that, a 30mins exposure of NIH3T3 cell lines to SNAP induces the phosphorylation of Ser18 and Ser373 residues in the active sites of p53, leading to increased cellular level of p53 (Nakaya et al., 2000).

Chemical structure of SNAP (S-Nitroso-N-acetylpenicillamine) (Butler and Rhodes, 1997)

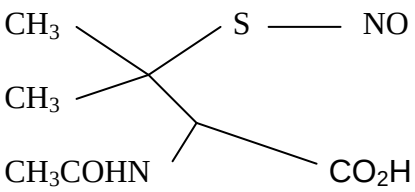

SNAP and other S- nitrosothiol compounds are generated by a reaction between thiols and NO^+ generating nitrous acid, N_2O_3 or an alkyl nitrite (Butler and Rhodes, 1997).

$$RSH + NO^+ \longrightarrow RSNO + H^+$$

$$RS^- + RONO \longrightarrow RSNO + RO^-$$

S- nitrosothiol compounds decompose to produce corresponding disulphide and NO (Butler and Rhodes, 1997).

$$RSNO \longrightarrow NO + \tfrac{1}{2}\ RSSR$$

Three structurally and chemically dissimilar vasodilator drugs: sodium nitroprusside, S-nitroso-N-acetylpenicillamine (SNAP) and isosorbide dinitrate along with 8-bromo-cGMP dose dependently inhibit the mitogenesis and proliferation of rat vascular smooth muscle cells. This inhibitory effect is repressed by the NO scavenger haemoglobin but is strengthened by superoxide dismutase, which implies that NO has been formed by theses drugs and acts as the eventual effector (Garg and Hassid, 1989).

The experiments of this chapter principally focus on the annotations of CPTI lines and on the screening of CPTI lines which respond to *ex vivo* application of NO.

3.2. Results

3.2.1. Visualization of protein expression

The coordinating team of Department of Genetics, University of Cambridge, have generated CPTI-YFP transgenic *Drosophila* lines. As discussed above (Section 3.1.2), in each transgenic *Drosophila* line a particular gene is tagged with YFP to study the expression of the YFP tagged protein. 100 CPTI lines (listed in Appendix C.1) were examined to study the expression of YFP tagged proteins in different tissues. The expression patterns of the CPTI lines were annotated by using standard *Drosophila* anatomy ontology and corresponding controlled vocabulary (CV) terms mentioned in Flybase (http://flybase.org/).

Third instar larvae of the CPTI lines were used as sources of three sample tissues (brain, imaginal discs, and salivary glands) to examine the expression of the tagged gene. Images of the tissues were collected using a Zeiss LSM 510 Meta Laser scanning Confocal microscope at 488nm, by modifying the excitation levels to avoid fluorescence saturation (Fig 3.4, 3.5, 3.6 and 3.7). Images of the tissues of 75 CPTI lines were uploaded to the Flannotator database **(**http://www.flyprot.org).

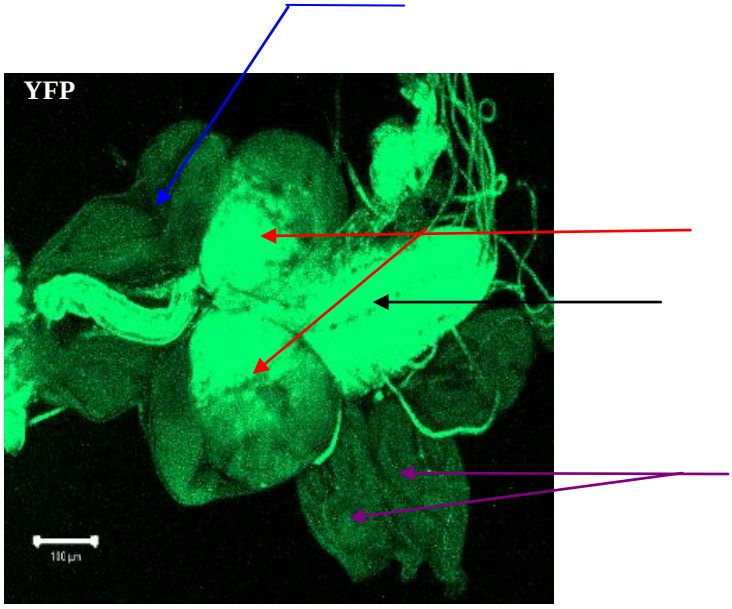

Figure 3.4 Examples of protein trap insertions showing expression of YFP in cerebral hemisphere, ventral ganglion, leg discs and eye antennal discs of third instar larvae of CPTI-000944 transgenic *Drosophila.*
CPTI-000944 image undertaken at 6% laser excitation (Zoom 1)
Black arrow - Ventral ganglion.
Red arrows - Cerebral hemisphere.
Blue arrow - Antenna disc.
Purple arrows - Leg discs.
Scale bar = 100 um.

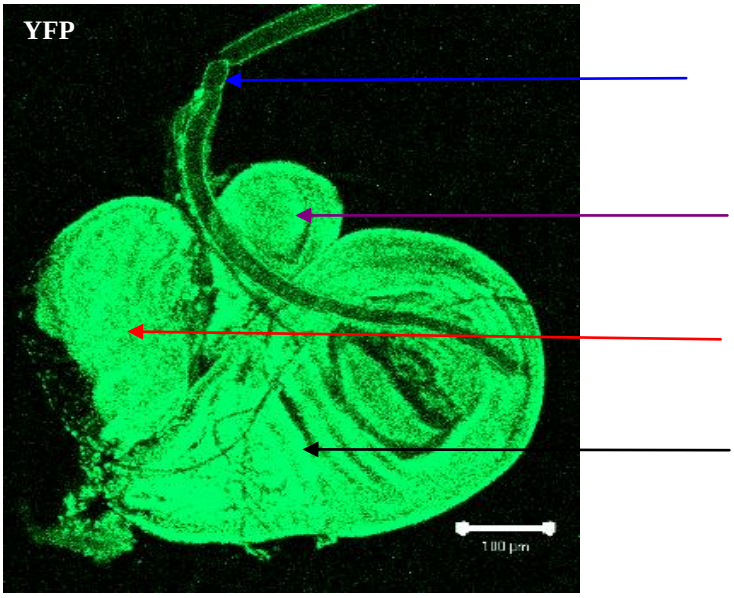

Figure 3.5 Protein trap insertion showing the expression of YFP tagged genes in wing discs, haltere discs, and in leg discs of third instar larvae of CPTI-000239 line.

Image undertaken at 3% laser excitation (zoom 1.4)

Black arrow - Wing disc.

Red arrow - Haltere disc.

Purple arrow - III Leg disc.

Blue arrow - Trachea.

Scale bar = 100 µm.

LOW POWER (10X) HIGH POWER (63X)

A CPTI-000239

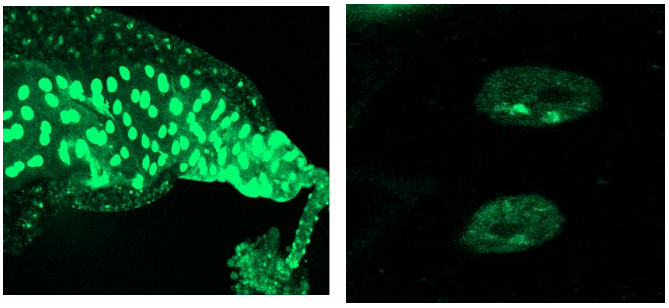

B CPTI-001488

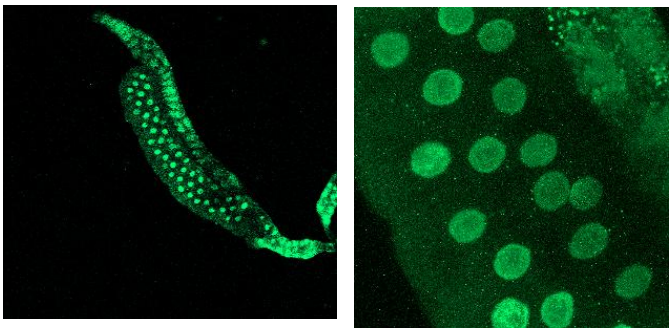

C CPTI-002035

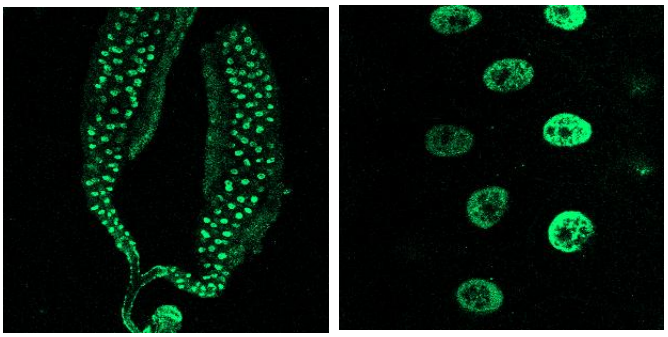

D CPTI-001735

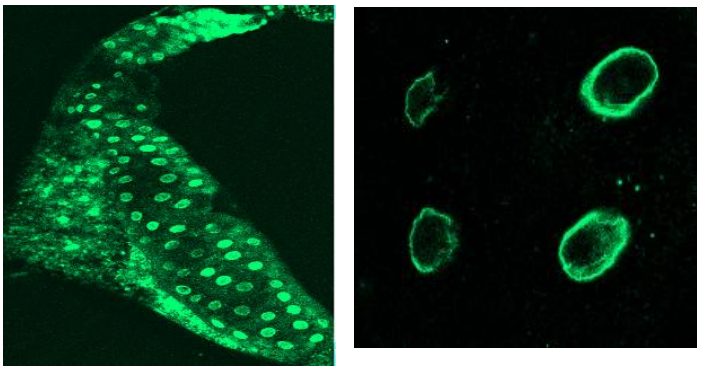

		LOW POWER (10X)	HIGH POWER (63X)
E	**CPTI-001403**	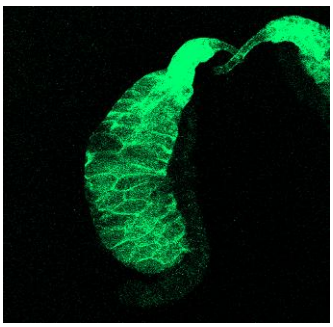	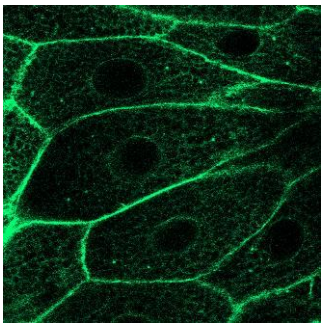
F	**CPTI-100038**	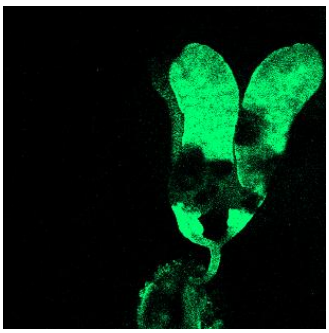	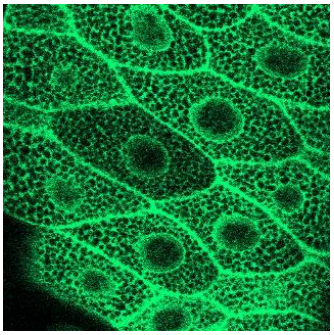
G	**CPTI-002264**	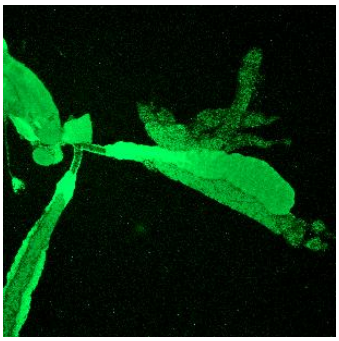	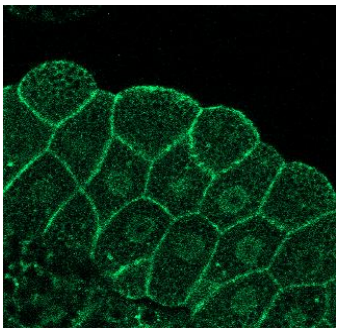

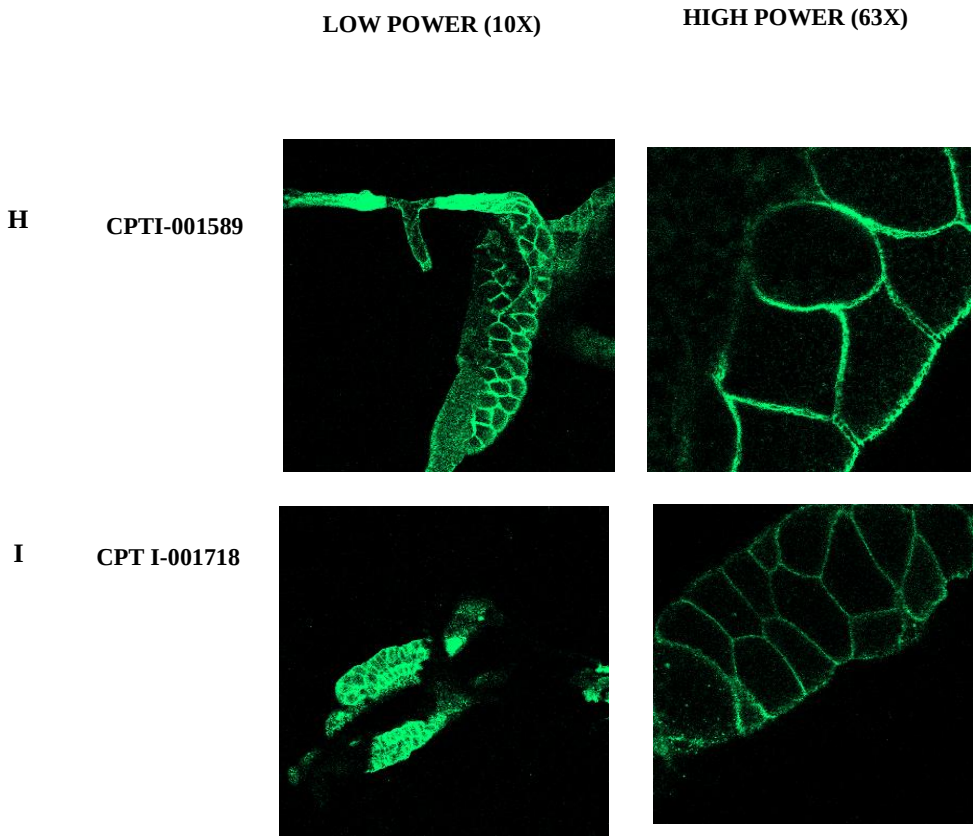

Figure 3.6 Examples of YFP expression in salivary glands of third instar larvae from 9 different CPTI lines.

A) Subcellular localisation of YFP was observed in the nucleus, but no expression was seen in the nucleolus of mature larval salivary gland cells of CPTI-000239.

B) Uniform expression of the YFP tagged protein was seen throughout the nucleus of salivary gland cells of CPTI-001488.

C) The nuclear expression of YFP in CPTI-002035 was not found to be uniform. The nucleolus was not expressing the YFP tagged protein.

D) Localisation of the YFP tagged protein was observed to be distinctly nuclear membrane associated in the larval salivary gland cells of CPTI-001735.

E) In CPTI-001403 the expression of YFP in salivary gland cells was predominantly cell membrane-associated and not nuclear.

F) Salivary gland of CPTI-100038 showed a cytoplasmic, cell membrane bound and perinuclear distribution of the YFP tagged protein.

G) Although some traces of cytoplasmic expression was found, the YFP tagged protein was predominantly cell membrane and nuclear membrane associated in CPTI-002264.

H) & I) subcellular localisation of the YFP tagged protein was exclusively cell membrane associated in case of the salivary gland cells of CPTI-001589 and CPTI-001718.

i)

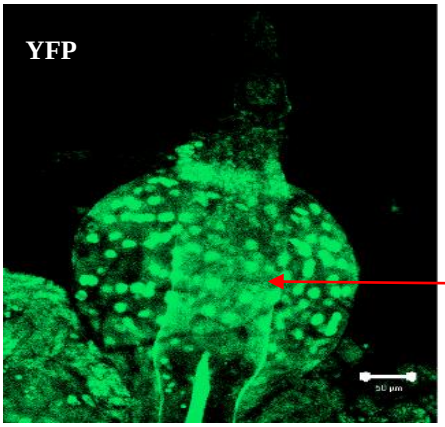

ii)

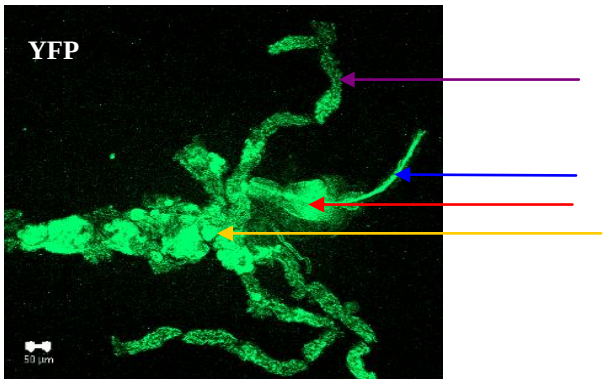

iii)

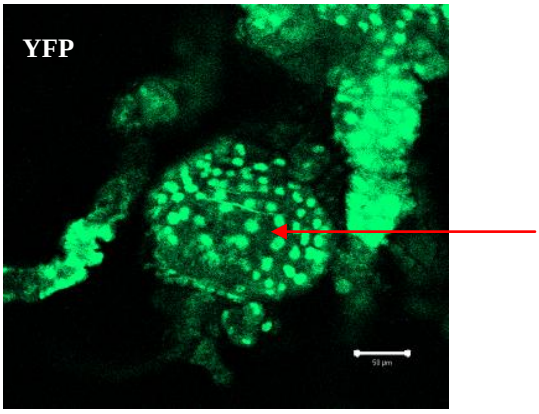

Figure 3.7 Examples of expression of YFP in the proventriculus of third instar larvae of 3 different CPTI lines.
i) Subcellular localisation of YFP tagged protein was observed in the nucleus, of mature proventricular cells of CPTI-000239.
ii) Uniform expression of YFP tagged protein was observed throughout the proventriculus, mid-intestine, esophagus and gastric caecum of CPTI-001137.
iii) Expression of YFP tagged protein was observed in the nucleus of mature proventricular cells of CPTI-001569.
Red arrows - Proventriculus.
Yellow arrow - Mid-intestine.
Blue arrow - Oesophagus.
Purple arrow - Gastric caeca.
Scale bars = 50µm

3.2.2. *Ex vivo* NO treatment

Ex vivo culture was employed to determine the effect of NO on the expression of a randomly selected subset of 75 YFP tagged proteins of the CPTI lines. Salivary glands from CPTI lines (listed in Appendix C.2) were treated with the NO donor, S-Nitroso-N-acetylpenicillamine (SNAP).One of the pair of salivary glands was added into a mixture of SNAP (dissolved in DMSO) and Schneider's tissue culture media. The other salivary gland of the pair was treated with the same quantity of DMSO and tissue culture media. After incubation images of both the SNAP treated (experimental) and DMSO treated (control) glands were collected on meta laser Confocal microscope.75 CPTI-YFP lines were treated with SNAP. All images were taken under 63X objective (high power) of the Confocal microscope for detailed visualization of any change in protein localisation or expression level as a result of SNAP treatment. The majority (71) of CPTI lines showed no alteration in the level or localisation of the tagged proteins after exposure to SNAP (data not shown). However, four lines exhibited differences in the sub cellular localisation of the YFP tagged protein following SNAP treatment. A decrease in the YFP tagged protein expression was observed in the salivary glands of CPTI-000106 after 16 hrs exposures in SNAP compared with the controls (Fig 3.8 A). A different localisation pattern of YFP tagged protein was observed in the salivary gland of CPTI-000847 after 16 hrs exposure in SNAP. Both the control and experimental salivary gland showed traces of membrane associated YFP tagged protein. The localisation of the protein was cytoplasmic and cell membrane associated but was non nuclear in the control salivary gland whereas, after treatment with SNAP the protein was mostly found uniformly distributed in the cytoplasm and in the nucleus as well (Fig 3.8 B). An increase in the nuclear and cytoplasmic localisation of the YFP tagged protein was observed in CPTI-000239 after 16 hrs exposure in SNAP (Fig 3.8 C). The nuclear accumulation of YFP tagged protein was found to be enhanced in CPTI-000232 after treating the salivary gland in SNAP for 16 hrs (Fig 3.8 D). Unfortunately the changes shown by CPTI-000106, CPTI-000847 and CPTI-000239 after giving SNAP exposure were not consistent. Only CPTI-000232 showed a consistent increase in YFP tagged protein localisation with SNAP exposure. It was therefore decided to use this particular CPTI stock for shorter SNAP exposure and further experiments.

Figure 3.8 CPTI lines which showed modification in YFP tagged protein localisation after 16 hrs of SNAP treatment.

A) Salivary glands of CPTI-000106 showed weaker YFP expression compared to the control after 16hrs treatment of SNAP.

B) Traces of membrane associated YFP tagged protein was observed in both DMSO

Figure 3.8 CPTI lines which showed modification in YFP tagged protein localisation after 16 hrs of SNAP treatment.

A) Salivary glands of CPTI-000106 showed weaker YFP expression compared to the control after 16hrs treatment of SNAP.

B) Traces of membrane associated YFP tagged protein was observed in both DMSO treated and SNAP treated salivary glands of CPTI-000847 line. However the DMSO treated salivary gland showed a cytoplasmic but non nuclear distribution of the YFP tagged protein whereas uniformly distributed YFP tagged protein was found throughout the cytoplasm and in the nucleus of the SNAP treated salivary gland.

C) The salivary gland cells of CPTI-000239 showed higher YFP tagged protein expression both in the nucleus and cytoplasm after 16hrs treatment with SNAP.

D) The nuclear expression of YFP tagged protein in the salivary gland cells of CPTI-000232 was observed to be raised after 16 hrs incubation in SNAP.

Scale Bar = 50μm

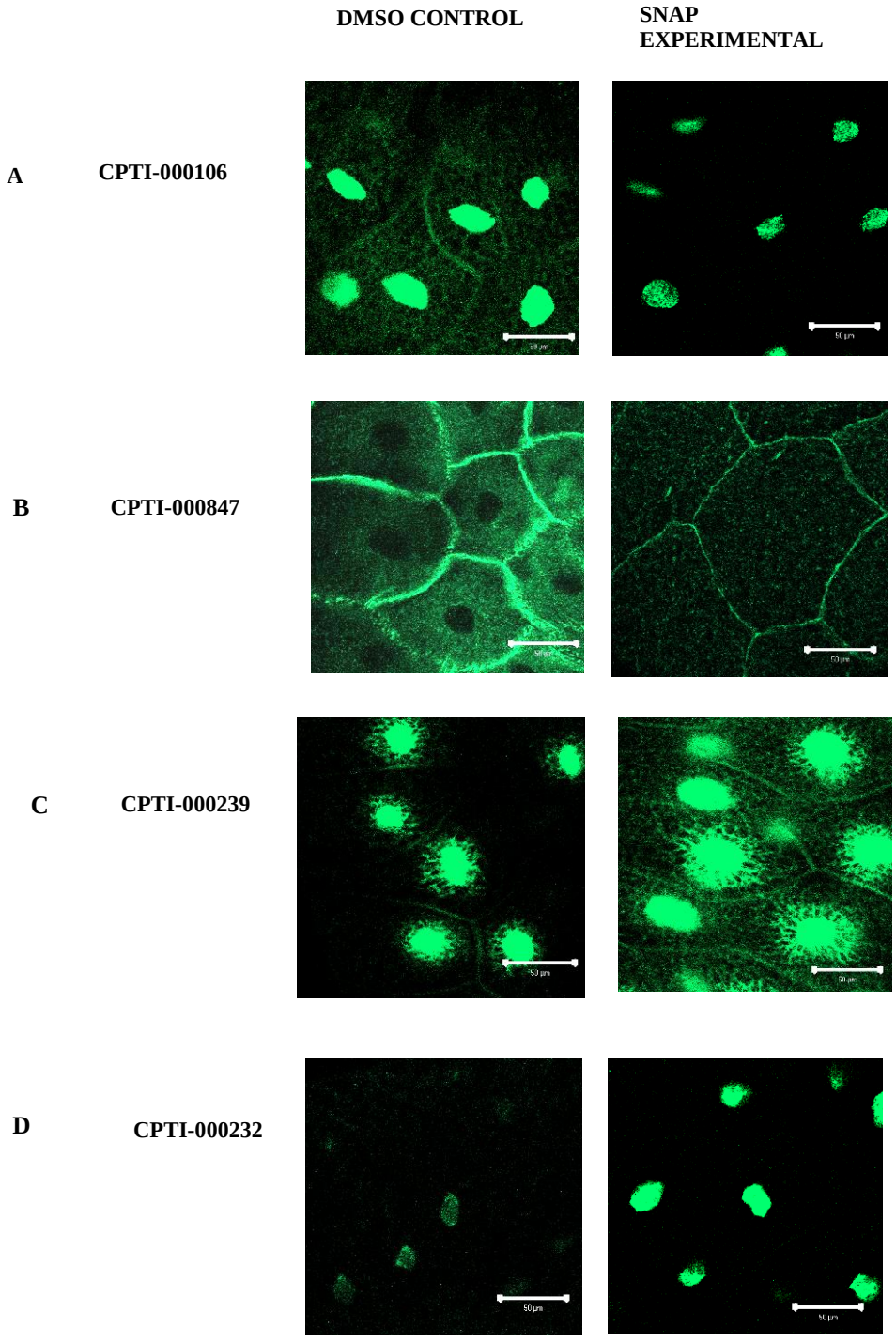

3.2.3. Shorter SNAP exposure of CPTI-000232 larvae

Salivary glands of wandering third instar CPTI-000232 larvae were given a shorter SNAP exposure of 0.5 hours followed by a 3.5 hour incubation in tissue culture media, to determine whether a short exposure to SNAP caused any changes in the YFP tagged protein localisation. Two pairs of salivary glands were taken from two different larvae of CPTI-000232 line. One of a pair of salivary gland was incubated in a mixture of SNAP and tissue culture media for 0.5 hours. The other of the same pair of salivary gland was also incubated in the similar mixture of SNAP and tissue culture media but for 4 hrs. After 0.5 hours the first gland of this pair was taken from SNAP and was incubated in a mixture containing DMSO and tissue culture media for further 3.5hrs. Therefore, the first gland of the pair was incubated in two different mixtures: initially for 0.5 hours in SNAP and then for 3.5 hrs in DMSO (total 0.5 hours + 3.5hours = 4hours) whereas the other gland of the same pair was incubated in SNAP only continuously for 4hours. After 4 hrs of incubation confocal images were acquired and compared.

One of the second pair of salivary glands from another animal of the same line (CPTI-000232) was incubated in SNAP and tissue culture media for 0.5 hours and other of the same pair was incubated in a mixture of DMSO and tissue culture media for 4hours. After 0.5 hours the first gland of this pair was taken out from the SNAP mixture and was further incubated in DMSO and tissue culture media for another 3.5hrs. Therefore, in this case also the first gland of this pair was incubated two times in two different mixtures: 0.5 hours in SNAP and 3.5hrs in DMSO, thus total incubation of 4hrs was achieved. After 4 hours incubation, confocal images were acquired and compared. This experiment was designed to compare and analyse the effect of 0.5 hours exposure to SNAP with no exposure to SNAP (DMSO control) on the expression of the tagged protein in salivary glands.

The salivary gland which was given 0.5 hours exposure to SNAP and then further cultured in DMSO and tissue culture media for 3.5 hrs showed highest increase in YFP tagged protein expression (Fig 3.9, Ci and Cii). The expression of YFP in the salivary gland which was incubated in SNAP for 4hrs (Fig 3.9, Bi and Bii) was lower than one treated in SNAP for 0.5 hours (Fig 3.9, Ci and Cii). The control salivary gland which was incubated in DMSO for 4 hrs showed the weakest expression (Fig 3.9, Ai and Aii).

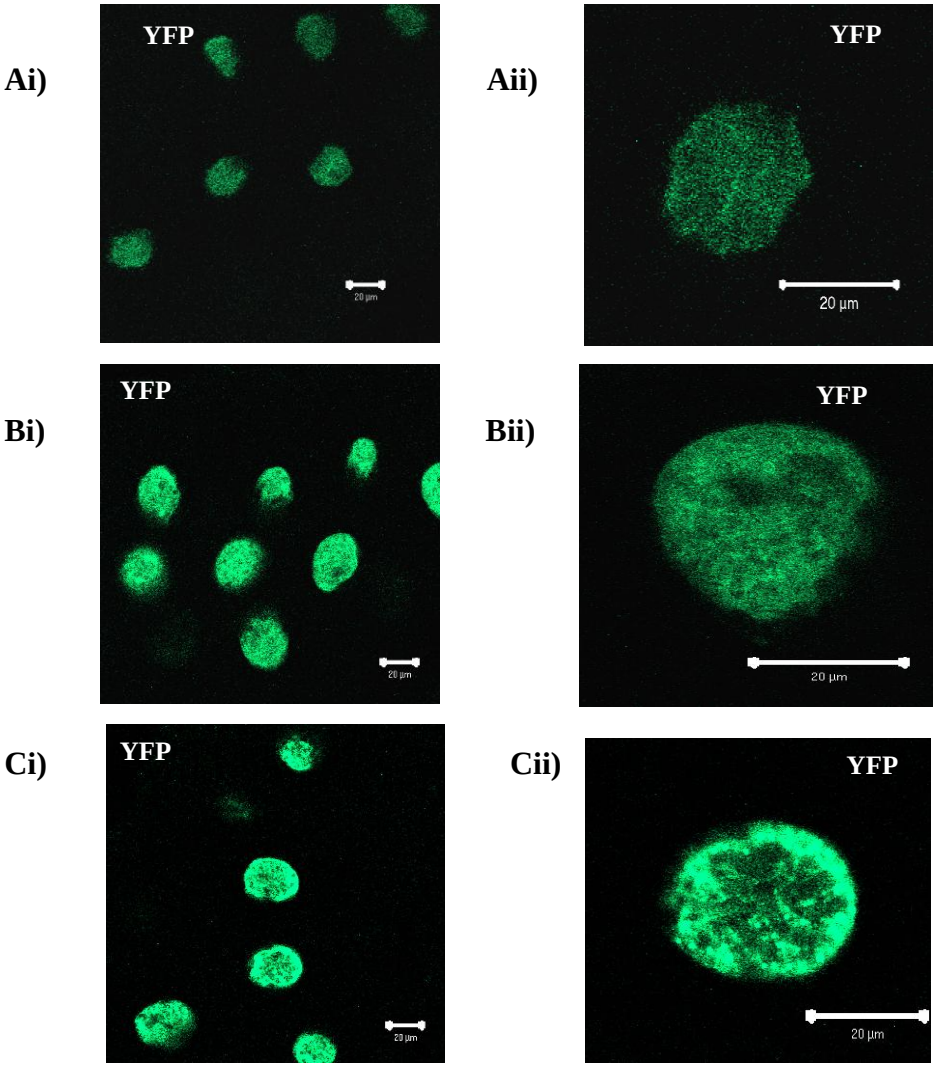

Figure 3.9. Shorter exposure to SNAP

Ai) Salivary gland of CPTI-000232 third instar larva incubated in a mixture of DMSO and tissue culture media for 4 hrs.
Aii) High magnification image of a nucleus shown in Fig (Ai).
Bi) Salivary gland of CPTI-000232 third instar larva incubated with a mixture of SNAP and tissue culture media for 4 hrs showed an increase in YFP tagged protein expression compared to Fig Ai.
Bii) High magnification image of a nucleus shown in Fig (Bi).
Ci) Salivary gland of CPTI-000232 third instar larva incubated with SNAP for 0.5 hours showed maximum accumulation of YFP tagged protein in the nucleus compared to Fig (Ai) and Fig (Bi).
Cii) High magnification image of a nucleus shown in Fig (Ci).
Images acquired and processed using identical settings.
Scale bar = 20 µm.

3.3. Discussion

3.3.1. Visualization of YFP tagged protein expression in CPTI lines

The localisation pattern of YFP tagged proteins was different in all CPTI lines (listed in appendix C.1). Images of the tissues of 75 CPTI lines were uploaded to the *Drosophila* genome database Flannotator **(**http://www.flyprot.org**).**

3.3.2. The protein trapped in CPTI-000232 is a probable target of NO action

The changes in the YFP tagged protein expression shown by CPTI-000106, CPTI-000847 and CPTI-000239 after 16 hrs of SNAP treatment (Fig 3.8 A, B, C) were not consistently repeated in subsequent SNAP exposures. This variation may be caused by small differences in developmental stages of the larvae or by other environmental factors. CPTI-000232 showed a consistent increase in the YFP fluorescence after 16hrs (Fig 3.8 D) and 0.5 hours exposure to SNAP (Fig 3.9 Ci and Cii). This shows even 0.5 hours exposure to SNAP is sufficient to cause changes in protein accumulation.

The CPTI-000232 line traps the gene *Mi-2*, which spans from 19875145 to 19903309 on chromosome 3L. This YFP tagged allele of *Mi-2* will be referred to as *Mi-2*$^{CPTI\text{-}000232}$. The localisation of Mi-2$^{CPTI\text{-}000232}$ protein was exclusively nuclear.

A previous researcher in our laboratory had independently shown an increase in the expression of YFP tagged Mi-2$^{CPTI\text{-}000232}$ in a time course exposure to SNAP (Lasala, 2007)**.** Therefore the results of this chapter confirmed Mi-2$^{CPTI\text{-}000232}$ as a probable target of NO action. Experiments in the following chapters were designed on the basis of the data found in this chapter.

Chapter 4: NO action on Mi-2/NuRD and associated proteins

4.1. Introduction

4.1.1. Mi-2 - A Probable Target of NO

Mi-2 is a component of the nucleosome remodelling and deacetylating (NuRD) complex (Tong et al., 1998). A link between cell proliferation and Mi-2 has also been demonstrated. Dermatomyositis patients producing antibodies against Mi-2 (Seelig HP et al., 1996) are susceptible to malignancy resulting from excessive cell proliferation (Airio et al., 1995).

Nitric Oxide has been reported to act as an antiproliferative agent to down regulate the proliferation of several diverse cell lines (Villalobo, 2006) such as neuronal precursor cells (Contestabile and Ciani, 2004), vascular smooth muscle cells (Nunokawa and Tanaka, 1992) human Caco-2 tumor cells (Buga et al., 1998) leading to cell differentiation.

All these data suggest that cell proliferation can be controlled by both Nitric Oxide and Mi-2. The biochemical pathway of NO action may intersect with that of Mi-2 at a specific point in the process of growth and proliferation arrest. A previous study in the laboratory involving SNAP exposure identified Mi-2 as a possible target of NO (Lasala, 2007). Results of the present study confirmed Mi-2 as a target of NO action (Sections 3.2.2 and 3.2.3). This chapter investigated and extended the *ex vivo* observations (Sections 3.2.2 and 3.2.3) through *in vivo* experiments.

It was hypothesised that the action of NO may be accomplished via Mi-2/NuRD complex. Hence, another important aspect of this chapter was to examine whether the impact of NO on growth regulation is dependent on Mi-2.

4.1.2. NO action on Simj

Simj is reported to function in recruiting the NuRD complex in the induction of methylation mediated gene silencing and hence acts as a regulatory component of NuRD. Simj plays developmental roles through the regulation of ecdysone-responsive genes in *Drosophila* (Kon et al., 2005). Interestingly NO also activates the ecdysone induced protein 75 (E75) and failure in NO production and inactivation of E75 in the ring glands (glands which produce metamorphosis inducing hormone, ecdysone) results into the failure of proper metamorphosis (Aleksandar S. Necakov and (unpublished)). It was therefore hypothesised that some functional links may exist between NO and Simj.

The experiments of this chapter were designed to analyse a functional connection between NO and Simj.

4.1.3. NO action on Dref

Mi-2 genetically and physically interacts with Dref (Hirose et al., 2002). Dref binds with the 8 bp palindromic sequence called the DNA replication related element (DRE) (Fumiko Hirose et al., 1993). This element is present in the promoter region of several cell proliferation related genes and is assumed to be required for their transcription (Matsukage et al., 2008). A gradual decrease in human Dref (hDref) expression was observed in differentiating PC12 cells (Matsukage et al., 2008). In the presence of nerve growth factor (NGF), high levels of three NOS isoforms were identified in PC12 cells during the onset of growth arrest and differentiation (Natalia and Grigori, 1995). The switch of the cell cycle from proliferation to differentiation mediated by differentiation related transcription factors, is probably under the direct control of Dref (Matsukage et al., 2008). Interestingly NO is known to prevent proliferation of rat brown adipocytes during the onset of differentiation (Enzo Nisoli and Carruba, 1998). NO is also reported to mediate the cell cycle switch from proliferation to differentiation during neurogenesis of several nervous system related cells (Gibbs, 2003). As Dref and NO can both influence the switch from proliferation to differentiation, it was hypothesized that the effect of Dref on cell proliferation may be controlled by NO. Hence, the response of the Dref protein to NO expression was also analysed in this chapter.

4.1.4. Study of NO action on Mi-2, Simj and Dref

In order to examine the effect of NO on Mi-2, Simj and Dref, two genetic approaches were used:

In the first approach, the GAL4/UAS binary system (Section 2.1.2) was used to induce *NOS2* expression in the whole salivary glands of YFP tagged *Mi-2* ^{CPTI000232} larvae, as the salivary glands of these larvae showed increased YFP tagged Mi-2 expression when cultured briefly with SNAP (Section 3.3.2).

However, when *NOS2* (Section 1.3) was driven in the whole salivary glands by c147-GAL4 of *Mi-2*$^{CPTI-000232}$ animals, the cells showed reduction in size, as high levels of NO slow down the progression of cell cycle during development (Kuzin et al., 1996). Hence, the approach of expressing NOS in the whole salivary glands did not take into account any physiological affects that the reduced growth of salivary gland may have. It

was not possible to infer if the change in YFP tagged Mi-2$^{CPTI-000232}$ expression was due to the effect of NO signalling or a consequence of the reduced size of the salivary gland resulting from NO expression. Therefore, it was important to monitor whether the expression of Mi-2 was altered when the growth of whole salivary gland was minimally effected in response of NO.

In a second approach, *NOS2* was expressed in single cells of the salivary glands to avoid any physiological changes resulting from reduced growth of the whole salivary gland. To achieve this, expression of NO was induced in single cells by using FLP/FRT technique or Flip out system. In this system random clones are generated via Flp recombinase catalysed recombination between two of it's target sites, FRTs. Flp is a site-specific recombinase encoded by the *S. cerevisiae* 2μm plasmid and efficiently catalyses the recombination between two copies of its 34 bp recognition site termed as Flp recognition target (FRT). A construct containing the Actin5C promoter separated from the Gal4 coding sequence by DNA flanked with FRT sites is used. Hence, there is no expression of Gal4 from this construct in the non clone cells. However in some cells, Flp, under the control of a heat shock promoter (hs-FLP) catalyses the excision of the FRT cassette allowing the expression of Gal4 (Duffy, 2002) (Tuan Rocky. S and Lo W Cecillia, 2000). This system produced single cell clones expressing UAS-GFP/UAS-mRFP as a marker or simultaneously expressing the marker and UAS-NOS (or any other gene of interest) (Fig 4.1).

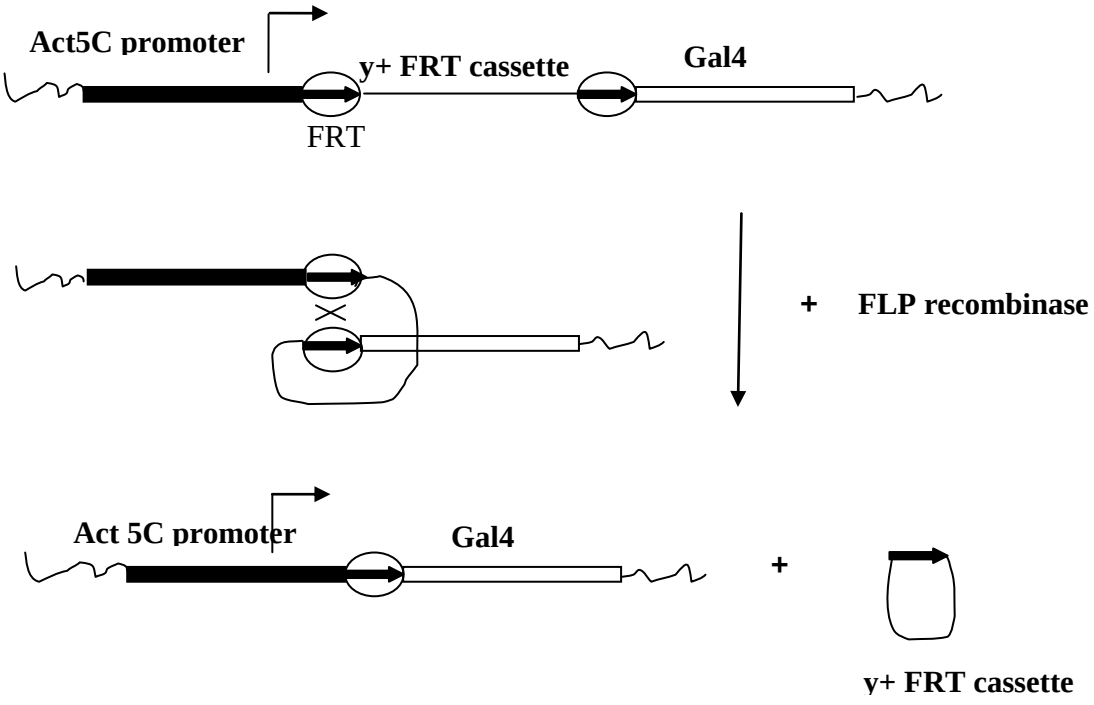

Figure 4.1. The Flip-out system for clonal Gal4 expression:
Flip recombinase (FLP) target sites (FRTs) are arranged as direct repeats flanking the y+ FRT cassette. Flp under the control of a heat shock promoter induces the recombination between the FRT sites resulting into the excision of the y+ FRT cassette. Gal4 is thus juxtaposed next to the Actin5C promoter element leading to the expression of Gal4.
Figure adapted from (Tuan Rocky. S and Lo W Cecillia, 2000).

The single cells expressing *NOS2* produced by this experimental design, could then be used to study the molecular and cellular consequences of high levels of NO production in comparison to the wild type cells which are not affected by Flp mediated recombination.

4.1.5. Does NO signaling and its antiproliferative action require Mi-2?

Although the previous results of the present study have identified Mi-2 as a probable target of NO signaling, it was not known whether the antiproliferative action of NO is dependent on Mi-2. *NOS2* was expressed in Mi-2 down regulated animals to determine whether Mi-2 regulates NO dependent proliferation arrest.

4.1.5.1. RNAi Approach

An efficient way of reducing the expression of proteins is the use of RNA interference (RNAi) which allows a targeted knockdown of proteins. RNAi is a process of genetic interference using dsRNA for physiological gene silencing in an organism (Fire et al., 1998). This particular technique of gene silencing was first exploited in the nematode *Caenorhabditis elegans* (Fire et al., 1991) and proved to be more efficient compared to single stranded RNAs (Fire et al., 1998). A RNase III-type enzyme, Dicer, initiates the process of RNA interference by converting linear, long double stranded RNA or hairpin RNA substrates in to 21-23nt base pair long siRNAs containing 2-nt overhangs at their 3′ ends and phosphate groups at their 5′ ends. The antisense strand of siRNAs, referred as guide strand, is then assembled with the RNA-induced silencing complex (RISC) leading to the formation of a RNA-protein complex known as siRISC. The guide strand containing RISC then cleaves the target mRNA between 10 and 11 nt upstream of the 5′ ends exactly where the perfect complementary region exists resulting in the degradation of mRNA and thus achieving post transcriptional gene silencing (Fig 4.2) (Rana, 2007).

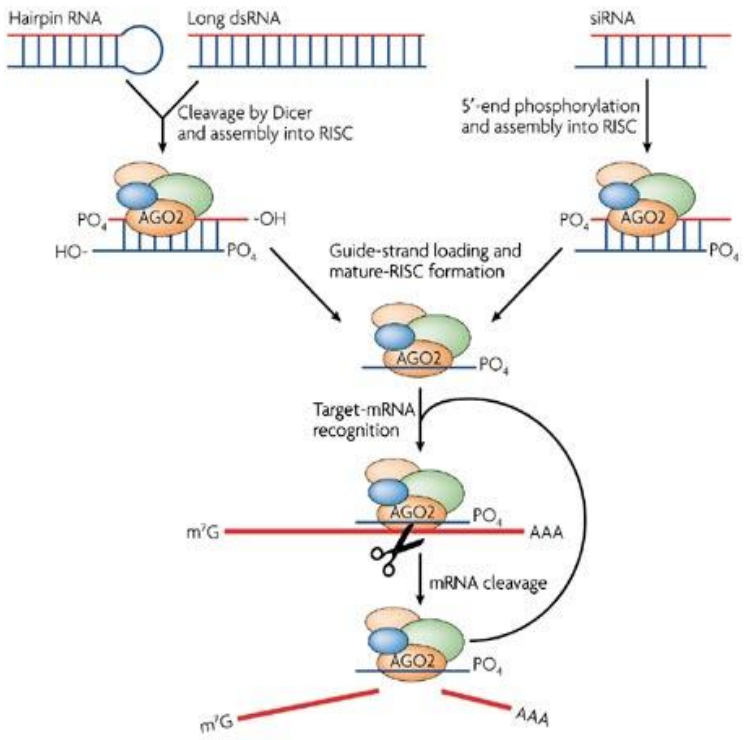

Figure 4.2. An overview of RNAi interference: Long double-stranded (ds)RNA or hairpin RNA substrates are cut by Dicer into smaller (21-nucleotide (nt)) small interfering (si)RNAs with 2-nt overhangs at the 3' ends and phosphate groups at the 5' ends. Alternatively, siRNA duplexes (19–23 nt) can be introduced into cells, where they are phosphorylated at the 5' ends by cellular kinases. These small dsRNAs assemble into the RNA-induced silencing complex (RISC), which contains AGO2, Dicer, and other cellular factors. siRNA then forms activated RISC (siRISC) that contains an antisense (guide) strand. Activated RISC finds its target mRNA and uses the antisense strand to guide the cleavage of the target mRNA. RISC is recycled and could carry out several cleavage events (Rana, 2007).

The first report using RNA interference in *Drosophila* demonstrated the functions of genes acting in the wingless pathway (Kennerdell and Carthew, 1998). The Vienna *Drosophila* RNAi Centre (VDRC) stock centre has generated 22,270 transgenic lines, capable of expressing RNAi corresponding to 88% of the predicted protein-coding genes in the *Drosophila* genome (Dietzl et al., 2007). These lines can be expressed by using tissue specific GAL4 drivers.

To examine whether NO dependent growth regulation requires Mi-2, the size of the salivary gland nuclei of UAS-RNAi-Mi-2 and UAS-NOS2 co-expressed animals would be compared with that of larvae only expressing *NOS2*.

4.1.5.2. *Mi-2* transheterozygous mutants

Another approach to reduce levels of Mi-2 was the use of *Mi-2* alleles that showed reduced levels of Mi-2 expression. The effect of NOS on the salivary gland size of Mi-2 down regulated third instar larvae was determined. Thus *Mi-2* allelic combinations that were viable until the third larval stage were required. The two *Mi-2* alleles used in this study were supplied by Bloomington Stock Centre. One of the mutant lines, *Mi-2[j3D4]*, (Flybase id FB2009_10, Genotype: y[1]w[*];PMi-2[j3D4]Su(Tpl)[j3D4]/TM3;Sb[1]Ser[1]) carries an insertion of P{lacW} at 19900352 location of chromosome 3L situated in the first intron of *Mi-2. Mi-2[j3D4]* homozygotes are reported to be post embryonic lethal (Kehle et al., 1998) and were found to survive till the 2nd larval stage (Khattak et al., 2002).

The other mutant allele used (Flybase id FB2009_10, Genotype y[1] w[67c23];P{w[+mC]y[+mDint2]=EPgy2}Mi-2[EY08138]Su(Tpl)[EY08138]/TM3;Sb[1]Ser[1]) carries an insertion of P{EPgy2} transposable element at 19888742 location of chromosome 3L situated in the first intron of *Mi-2* (Bellen et al., 2004).

4.2. Results

4.2.1. Analysis of YFP tagged Mi-2$^{CPTI-000232}$ expression in whole salivary glands expressing *NOS2*

In order to monitor the effects of long term NOS expression, *NOS2* was over expressed in the whole salivary glands of YFP tagged *Mi-2$^{CPTI-000232}$* larvae, under the control of the salivary gland specific c147-GAL4 driver. The localisation of Mi-2$^{CPTI-000232}$ in *NOS2* expressing larvae was compared with that of the control animals to monitor any change in YFP tagged Mi-2$^{CPTI-000232}$ expression. The nuclei of the salivary glands from the third instar larvae expressing UAS-NOS2 were smaller in size as compared to the controls (Fig 4.3).

Images of salivary glands from five wandering third instar larvae expressing *NOS2* were acquired on the confocal microscope and were compared with five salivary glands from the control animals (Fig 4.3). All salivary glands of the experimental third instar larvae expressing *NOS2* showed an increase in the nuclear expression of the YFP tagged Mi-2$^{CPTI-000232}$ as compared with that of the control larvae. The data from these larvae were analysed using imaging analysis software Velocity (http://www.cellularimaging.com/products/Volocity). The data showed that the mean intensity of brightness of YFP-tagged Mi-2$^{CPTI-000232}$ per volume of the nucleus is higher in the salivary glands of *NOS2* expressing experimental larvae compared to that of the control larvae. Quantification analysis of YFP fluorescent intensities of individual nuclei of each genotype (40 nuclei from five control larvae and 59 nuclei from five UAS-NOS2 expressing larvae) demonstrated a 1.7 fold average increase of YFP tagged Mi-2$^{CPTI-000232}$ expression in UAS-NOS2 expressing animals.

A) **B)**

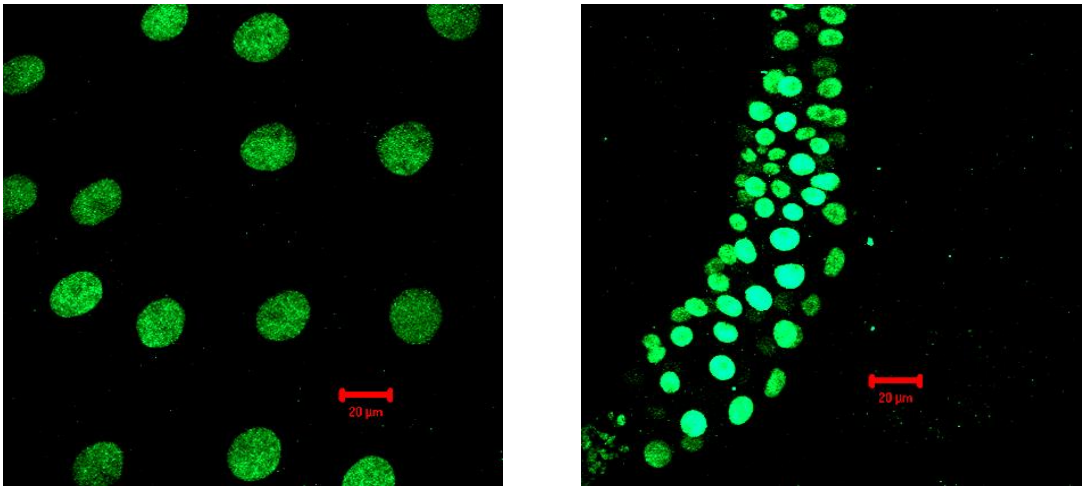

Figure 4.3. Expression of YFP tagged Mi-2 in third instar salivary glands.
A: salivary gland of control larva of genotype c147-GAL4 / +; YFP-Mi-2$^{CPTI-000232}$ / +
B: salivary gland of experimental larva of genotype UAS-NOS2 / +; c147-GAL4 / +; YFP-Mi-2$^{CPTI-000232}$ / + showing a higher expression of YFP tagged Mi-2

(Scale bar = 20 µm)
Images acquired and processed using identical settings.
Raw data is available in Appendix B.1

4.2.2. Analysis of the expression of YFP tagged Mi-2$^{CPTI-000232}$ in *NOS2* expressing single cell clones

The result of previous experiment showed an increase in the nuclear localisation of YFP tagged Mi-2$^{CPTI-000232}$ when *NOS2* was expressed in the whole salivary gland. The increase in the Mi-2$^{CPTI-000232}$ expression could have been a consequence of reduction of salivary gland size caused by *NOS2* expression. Therefore a genetic system where growth of the salivary gland is minimally effected by NOS expression was used. This was achieved by generating Flp/FRT induced, UAS-NOS2 expressing single cell clones in the salivary glands of YFP tagged Mi-2$^{CPTI-000232}$ larvae by 4min heat shock at 38^{o}C between 24- 48hr after egg laying..

NO is known to diffuse between cells (Haley, 1998). Hence, the expression of YFP tagged Mi-2$^{CPTI-000232}$ may be influenced by NO in the cells immediately adjacent to a *NOS2* expressing clone. Thus, the expression of Mi-2$^{CPTI-000232}$ in cells of the immediate neighbours to those expressing *NOS2*, was not considered for the comparison. The intensity of YFP tagged Mi-2$^{CPTI-000232}$ expression in *NOS2* expressing clone cell was compared to that of the wild type cells not adjacent to the clone cell.

NOS2 expressing clone cells showed an increase in the nuclear expression of YFP tagged Mi-2$^{CPTI-000232}$ compared to the non adjacent wild type cells (Fig 4.4).

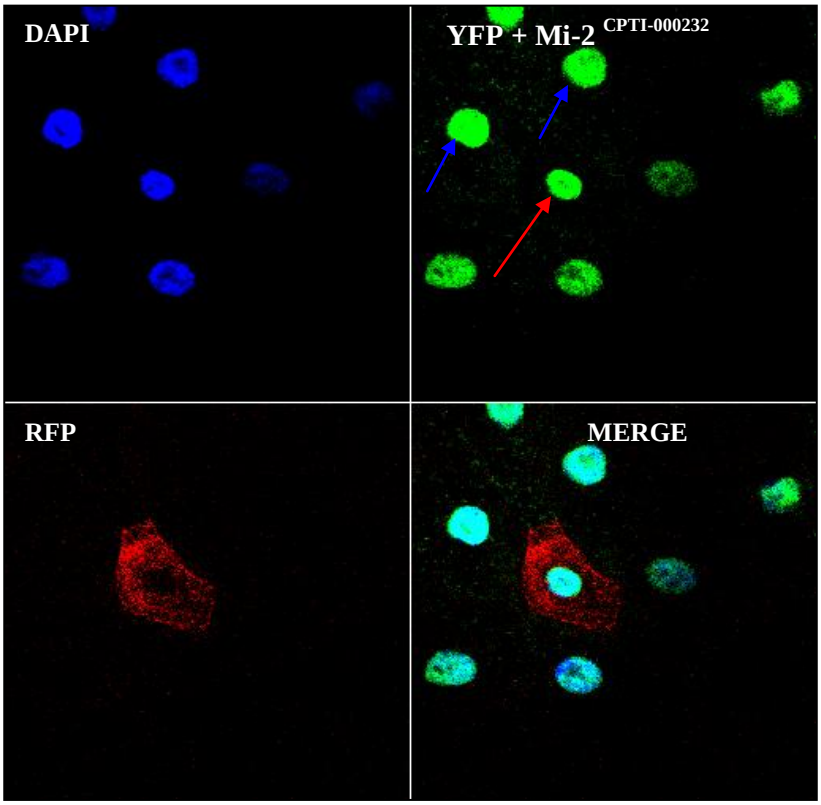

Figure 4.4. Nuclear localisation of YFP tagged Mi-2$^{CPTI-000232}$ in *NOS2* expressing clones.
Clones were generated using a 4min heat shock at 38^{o}C between 24- 48hr AEL, of animals with genotype: UAS-NOS2 / hsFLP; UAS-mRFP / CyO; YFP-Mi-2$^{CPTI-000232}$ / Act5c>y^{+}>Gal4.
Clone is marked with RFP expression.
NOS2 clone shows an increase of YFP tagged Mi-2 expression (red arrow).
An increase in YFP tagged Mi-2 expression was also observed in cells immediately adjacent to the *NOS2* expressing clone (blue arrow).
Blue: DAPI, Green: YFP + Mi-2, Red: RFP.

4.2.3. Visualization of Mi-2 protein in single cell clones expressing NOS

To confirm that the endogenous Mi-2 protein responded in a similar fashion to the YFP tagged protein when NOS was expressed, the localisation of endogenous Mi-2 protein was determined using an anti-Mi-2 antibody. GFP marked clones expressing *NOS2* were generated in a similar way to section 4.2.2.

Rabbit anti-Mi-2 antibody (Brehm et al., 2000) was used in combination with goat anti-rabbit Cy5 secondary antibody to visualize the localisation of Mi-2 protein.

The intensity of nuclear localisation of Mi-2 protein in each *NOS2* expressing clone was compared with that of 10 non adjacent wild type cells of that salivary gland. The *NOS2* expressing clones showed increased nuclear expression of Mi-2 protein when compared with the surrounding wild type cells (Fig 4.5.i. A and B). High magnification of the anti-Mi-2 antibody stained wild type nuclei showed non-nucleolar distribution of Mi-2 protein. Although minor traces of anti-Mi-2 staining was found in the nucleolus of these wild type salivary glands (Fig 4.5.ii. A). In contrast, high magnification of *NOS2* expressing clone cells showed a uniform distribution of Mi-2 protein throughout the nucleus (including the nucleolus) (Fig 4.5.ii. B). However nuclei of both wild type and *NOS2* expressing clone cells also showed a perinuclear localisation of Mi-2 protein (Fig 4.5.ii. A and B). An accurate quantitative analysis of the intensity of Mi-2 localisation in *NOS2* expressing clone cells was performed using the image analysis software velocity. This demonstrated increased Mi-2 levels in the *NOS2* expressing clone cells compared to that of non-adjacent surrounding cells. A 2.074 : 1 (+ 1.199 /- 1.199) ratio of Mi-2 expression in *NOS2* expressing clones versus surrounding wild type cells was recorded (Fig 4.6). In contrast, control GFP marked clones showed no difference in Mi-2 expression compared to surrounding wild type cells; a 0.97:1 (+ 0.371 /- 0.371) ratio of Mi-2 expression in control GFP clones versus surrounding wild type cells was observed (Fig 4.6).

A) **B)**

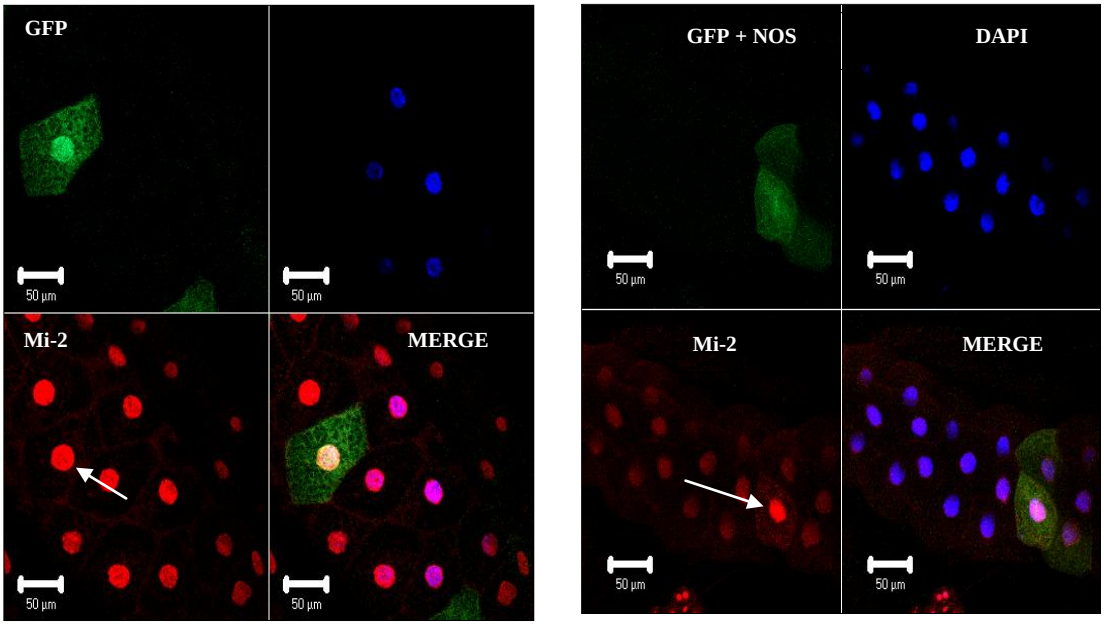

Figure 4.5 (i). Antibody staining of Mi-2 protein expression in wild type and *NOS2* expressing clones of salivary gland cells.

Clones were generated using a 4min heat shock at 38^{o}C between 24- 48hr AEL.

A) GFP marked control clone (white arrow) showing no noticeable change in the intensity or localisation of Mi-2.
Genotype: hsFLP/+; Act5c>y^{+}>Gal4 ;UAS-GFP

B) *NOS2* expressing clone (white arrow) marked with GFP showing an increase in the intensity of nuclear localisation of Mi-2 in the salivary gland of larva.
Genotype: hsFLP/UAS-NOS2; Act5c>y^{+}>Gal4 ; UAS-GFP

Blue: DAPI, Green: GFP, Red: rabbit anti-Mi-2 antibody (Brehm et al, 2000) (Secondary antibody used: goat anti-rabbit Cy5).
Scale Bar = 50 µm

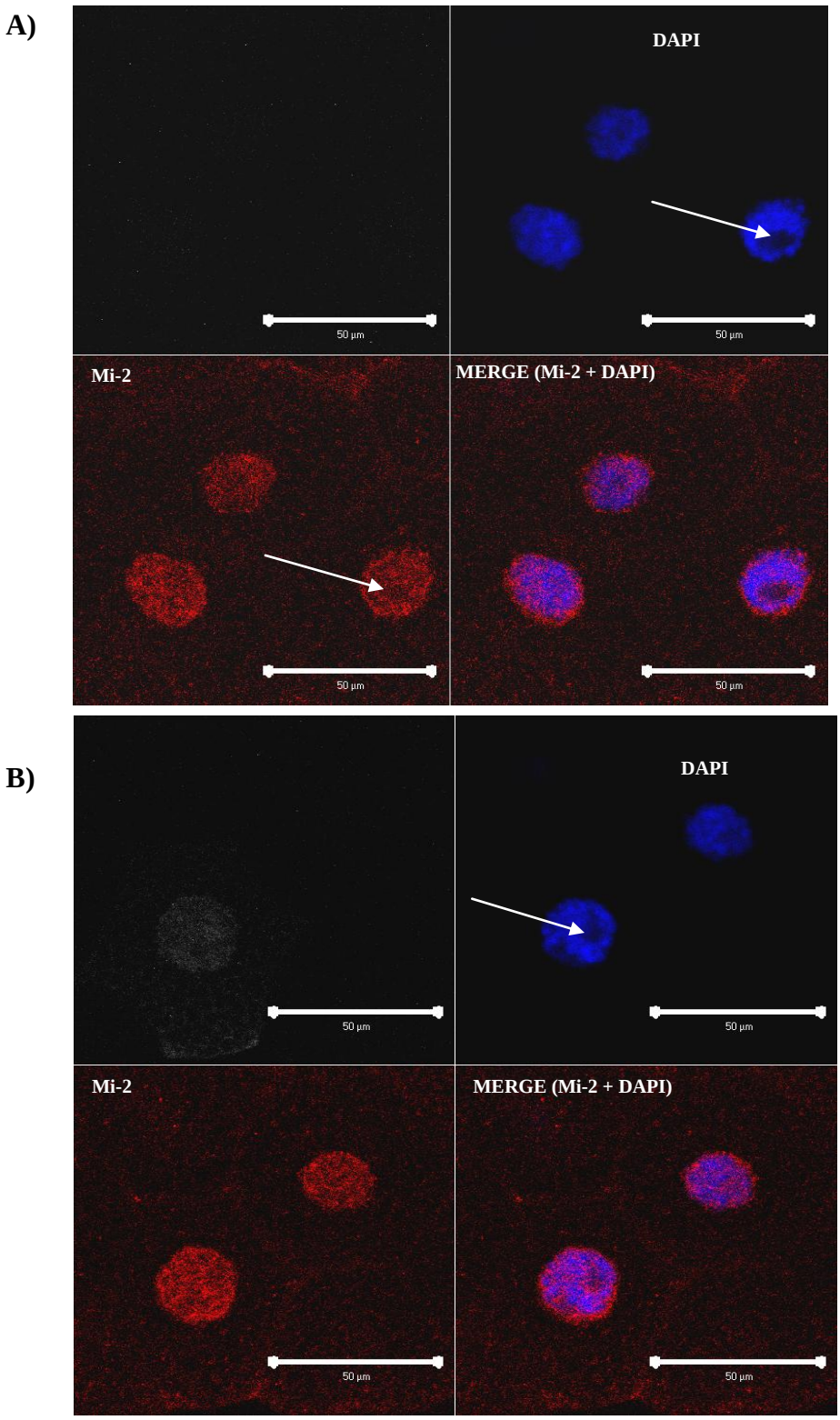

Figure 4.5 (ii) High magnification image of Mi-2 protein expression in wild type and *NOS2* expressing clones in salivary gland cells.

A) Wild type salivary gland. Nucleolus is marked with white arrow.

B) *NOS2* expressing clone cell. Nucleolus is marked with white arrow.
Blue: DAPI, Green: GFP, Red: rabbit anti-Mi-2 antibody (Brehm et al, 2000)
(Secondary antibody used: goat anti-rabbit Cy5). Scale Bar = 50 µm

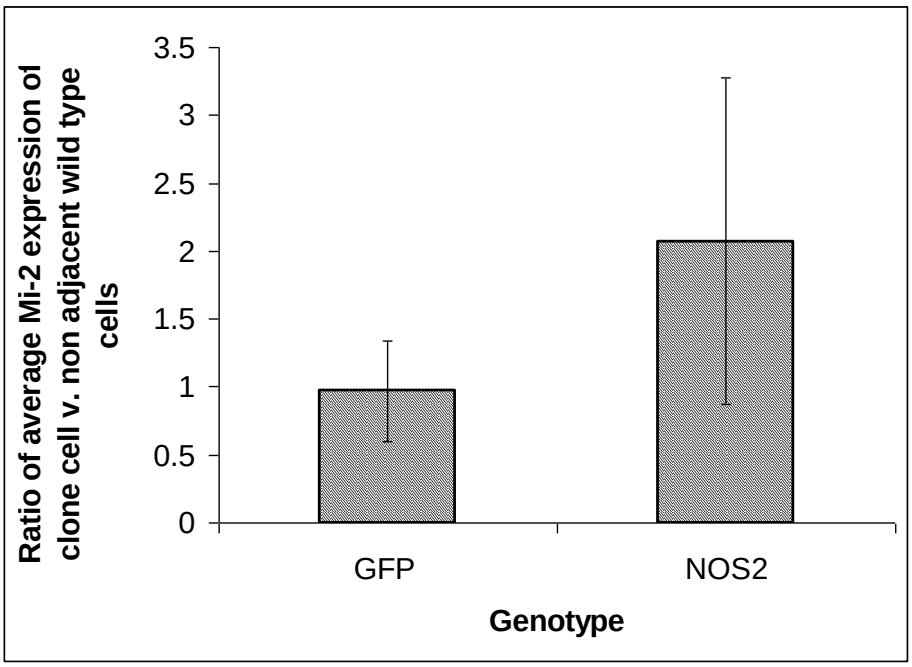

Figure 4.6. Quantification of Mi-2 expression in wild type and *NOS2* expression single cell clones

GFP = Ratio of average intensity of Mi-2 expression in GFP marked control clone cells versus the average intensity of Mi-2 expression in 10 non adjacent wild type cells.
Genotype: hsFLP/+; Act5c>y^+>Gal4 ;UAS-GFP

NOS2 = Ratio of average intensity of Mi-2 in GFP marked clone cells (expressing *NOS2*) verses the same in 10 non adjacent wild type cells.
Genotype: hsFLP/UAS-NOS2; Act5c>y^+>Gal4;UAS-GFP

Data for both genotypes was obtained from 10 salivary glands from 10 animals. Error bars indicate standard deviation. Raw data available in Appendix: B.2 Analysis undertaken using Velocity Image Analysis Software.

4.2.4. Analysis of effect of Simj expression on NOS induced phenotype

As Simj is a regulatory component of the NuRD complex (Discussed in Section 4.1.2), the effect of NOS on Simj expression was determined. Unfortunately immunohistochemistry with an anti-Simj antibody proved unsuccessful (data not shown). Thus a UAS-simj-GFP fusion was used in this purpose.

To analyse the effects of Simj expression on the NOS induced growth phenotype, *NOS2* expression was induced in whole salivary glands of larvae containing GFP tagged UAS-simj-GFP (Kim et al., 2004) under the control of salivary gland specific c147-GAL4 driver. As the simj-GFP was already fused with UAS sequence, using the c147-GAL4 driver would simultaneously up regulate the expression of UAS-NOS2 and UAS-simj-GFP. By co-expressing UAS-NOS2 and UAS-simj-GFP simultaneously in the same salivary gland, it could be determined whether expressing Simj alters the NOS induced phenotype on salivary gland size.

Animals co-expressing UAS-simj-GFP and UAS-NOS2 showed small sized salivary glands, reasonably similar to those expressing UAS-NOS2 only (Figure No 4.7 A and B).

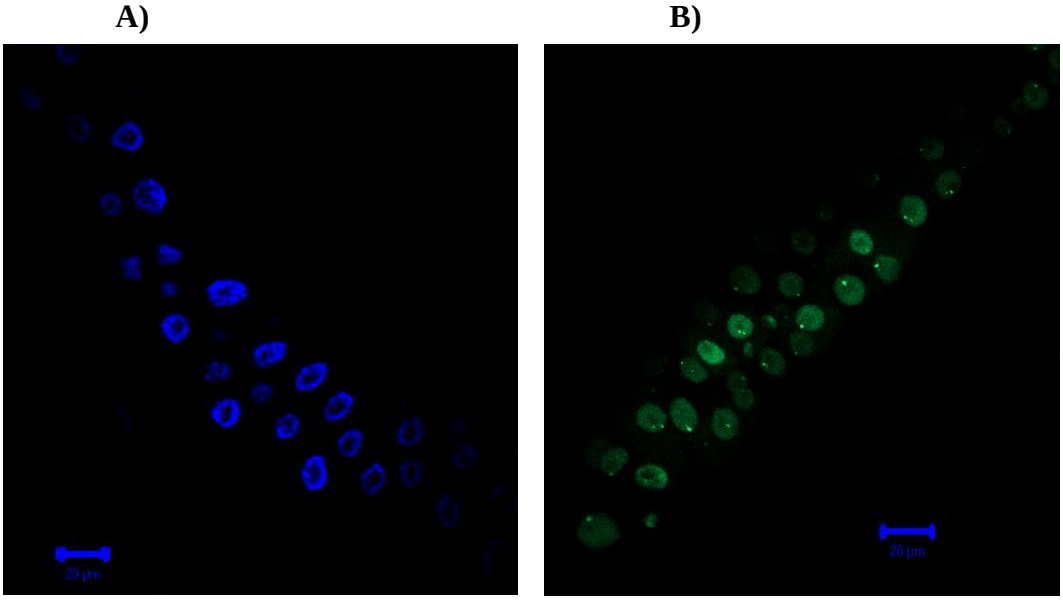

Figure 4.7. Salivary gland of UAS-simj-GFP and UAS-NOS2 co expressed third instar larvae showed small size.
A) DAPI stained Salivary gland of UAS-NOS2 expressed third instar larva.
Genotype: UAS-NOS2 / + ; c147-GAL4 / +.
B) Salivary gland of third instar larva co-expressing GFP tagged UAS-simj and UAS-NOS2.
Genotype: UAS-NOS2 / UAS-simj-GFP ; c147-GAL4 / +.
Scale bar = 20µm

4.2.5. Visualization of Dref protein in single cell clones expressing NOS

To analyse if NO could alter Dref localisation, *NOS2* expressing clones were generated. In this experiment the nuclear localisation of Dref protein was visualized by using a mouse anti-Dref antibody (Hirose et al., 2002) in combination with horse anti mouse Cy5 secondary antibodies. GFP marked clones expressing *NOS2* were generated in a similar way to section 4.2.2.

The intensity of nuclear localisation of Dref protein in the *NOS2* expressing clones was compared with that of non adjoining wild type cells present in the same salivary gland. Similarly the amount of nuclear expression of Dref protein in the GFP marked control clones cells was compared with that of the non adjoining non-clone cells of that particular salivary gland. The intensity of nuclear localisation of Dref protein in the *NOS2* expressing clones was compared to that of 10 non adjacent wild type cells of that salivary gland.

The *NOS2* expressing clones showed no obvious change in the intensity of nuclear accumulation of Dref protein when compared to the surrounding wild type cells (Fig 4.8.i A and B). Localisation pattern of Dref protein was not noticeably altered in *NOS2* expressing clone cells compared to the wild type cells as shown in the high magnification images (Fig 4.8.ii A and B). The perinuclear pattern of localisation of endogenous Mi-2 observed in wild type and *NOS2* expressing clone cells (Section 4.2.3, Fig 4.5.ii A and B) was not shown by Dref protein in anti-Dref antibody stained wild type and *NOS2* expressing clone cells (Fig 4.8.ii A and B).

For a quantitative analysis of the response of Dref protein to NOS expression in single cell clones the image analysis software velocity was used. This demonstrated Dref levels in the *NOS2* expressing clone cells compared to that of non-adjacent surrounding cells. A 0.944333: 1 (+ 0.22356 /- 0.22356) ratio of Dref expression in *NOS2* expressing clones versus surrounding wild type cells was recorded (Fig 4.9). Control GFP marked clones showed no significant difference in Dref expression compared to surrounding wild type cells. A 0.96333:1 (+ 0.48026 / - 0.48026) ratio of Dref expression in control GFP clones versus surrounding wild type cells was observed (Fig 4.9). The ratio of Dref expression in the clone cell verses the non adjacent wild type cells of both the experimental (NOS2) and control (GFP) genotypes was found to be very similar (Fig 4.9).

A)

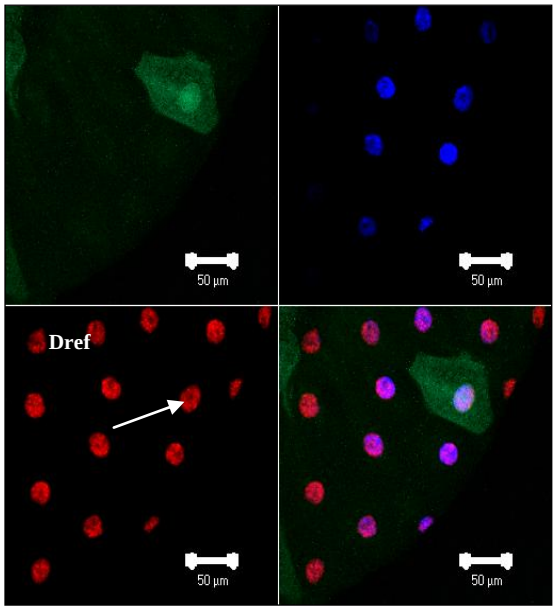

B)

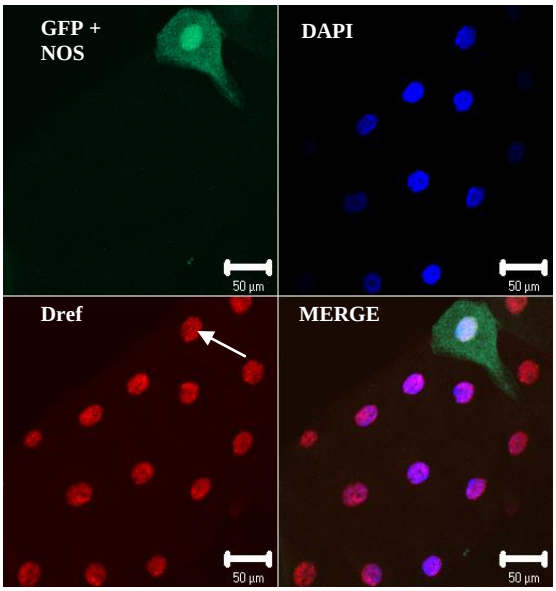

Figure 4.8.(i). Dref protein in *NOS2* expressing clones in salivary glands.
Clones were generated using a 4min heat shock at 38°C between 24- 48hr AEL.

A) GFP marked control clone (white arrow) showing no noticeable change in the intensity of Dref protein expression.
Genotype: hsFLP/+; Act5c>y^+>Gal4 ;UAS-GFP

B) *NOS2* expressing clone marked with GFP (white arrow) showing no noticeable change in the intensity of Dref protein expression.
Genotype: hsFLP / UAS-NOS2; Act5c>y^+>Gal4;UAS-GFP

Blue: DAPI, Green: GFP, Red: mouse anti-Dref antibody (Hirose et al, 2002)
(Secondary antibody used: Horse anti-mouse Cy5).
Scale Bar = 50 µm

A)

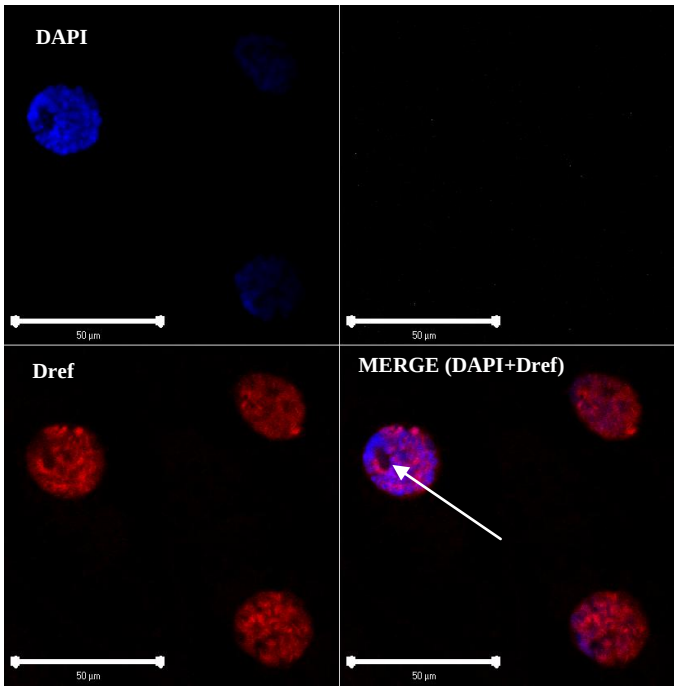

B)

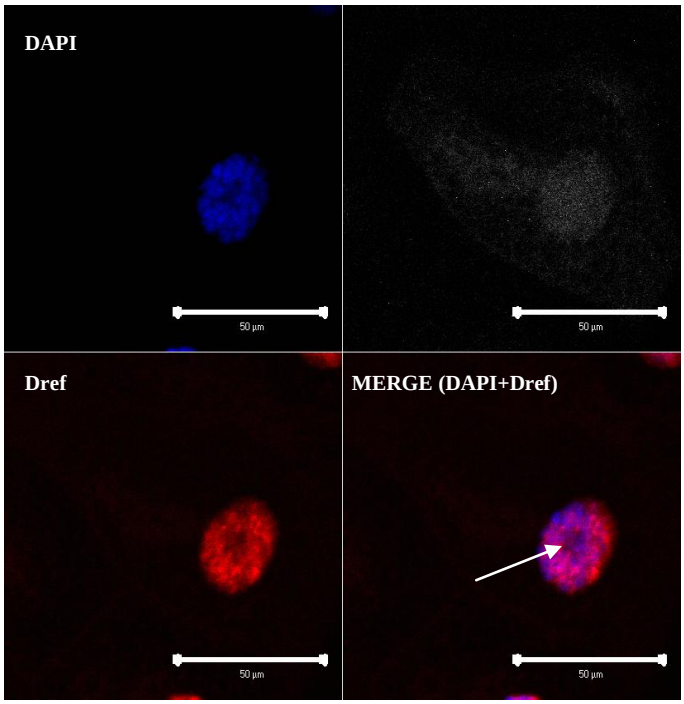

Figure 4.8.(ii). High magnification image of Dref protein expression in wild type and *NOS2* expressing clones in salivary glands.

A) High magnification of anti-Dref stained nuclei from wild type salivary gland. Nucleolus is marked with white arrow.

B) High magnification of anti-Dref stained nuclei of NOS2 expressing clone cell. Nucleolus is marked with white arrow.

Blue: DAPI, Green: GFP, Red: mouse anti-Dref antibody (Hirose et al, 2002) (Secondary antibody used: Horse anti-mouse Cy5).
Scale Bar = 50 µm

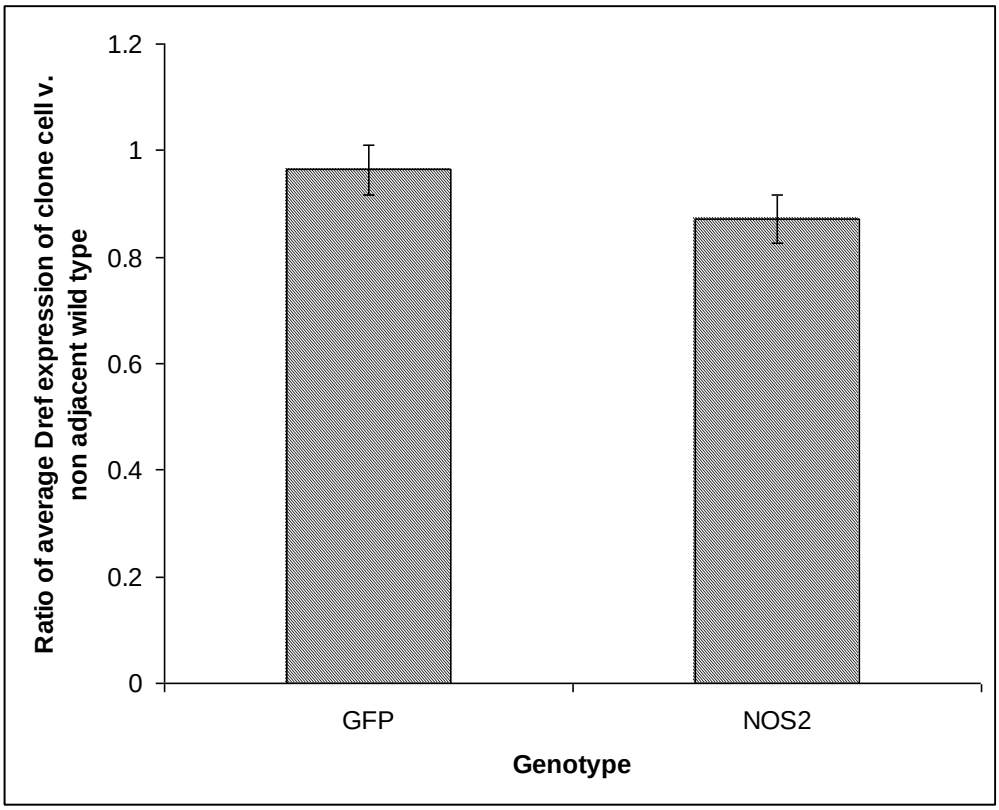

Figure 4.9. Ratio of average Dref expression in GFP and *NOS2* expressing single cell clones compared non adjacent to wild type cells.
GFP = Ratio of average intensity of Dref expression in GFP marked control clone cells versus the average intensity of Dref expression in 10 non adjacent wild type cells.
Genotype: hsFLP/+; Act5c>y^+>Gal4 ;UAS-GFP

NOS2 = Ratio of average intensity of Dref in GFP marked clone cells expressing *NOS2* versus average intensity in 10 non adjacent wild type cells.
Genotype: hsFLP/UAS-NOS2 ; Act5c>y^+>Gal4;UAS-GFP

Data for both genotypes was obtained from 10 salivary glands from 10 animals. Error bars indicate standard deviation. Raw data available in Appendix B.3 Analysis performed using Velocity Image Analysis Software.

4.2.6. Simultaneous visualization of both Mi-2 and Dref proteins in single cell clones expressing NOS

It has been reported that Mi-2 and Dref proteins negatively regulate each others functions and the binding of Mi-2 and Dref to the polytene chromosomes is mutually exclusive (Hirose et al., 2002). Therefore the effect of NOS on the localisation of both the proteins at the same time, in single cell clones was determined. GFP marked clones expressing *NOS2* were generated as in section 4.2.2.

The experimental salivary glands were stained with a combination of rabbit polyclonal anti-Mi-2 and mouse monoclonal anti-Dref antibodies mixed in an appropriate dilution (Described in Section 2.2.2).

Different control samples were used to compare the localisation of both the proteins. Salivary glands from wild type (*y, w*) third instar larvae not expressing *NOS2* were double stained with both the antibodies to use as control samples. The localisation pattern of both the proteins in *NOS2* expressing clones was compared with that of the single stained cells of wild type third instar salivary glands. Several salivary glands from wild type (*y, w)* third instar larvae were singly stained with Mi-2 and Dref antibodies separately and the protein localisation pattern of this individual antibody stained salivary glands was compared to that of the double stained *y, w* salivary glands.

Salivary glands of wild type third instar larva when singly stained with mouse anti-Dref antibody, showed nuclear, cytoplasmic and cell membrane associated Dref protein (Fig 4.10 A), whereas Mi-2 protein was observed to be localised exclusively in the nuclei of the wild type third instar salivary glands when stained with rabbit anti-Mi-2 antibody (Fig 4.10 B). However, no nuclear staining of Dref protein was observed in the wild type third instar larvae when double labelled with both anti-Dref and anti-Mi-2 antibodies simultaneously (Fig 4.11 A). When this double staining procedure was used, anti-Dref staining was observed in the cytoplasm and cell membranes and weakly in the nuclei (Fig 4.11 A). However the nuclei of fat body cells of these double labelled animals did show anti-Dref staining in the nuclei (Fig 4.11 A). The localisation of anti-Dref staining observed in double labelled wild type salivary glands (Fig 4.11 A), was different to that of wild type salivary gland cells singly labelled with anti-Dref antibody (Fig 4.10 A).

The double labelled wild type cells surrounding the *NOS2* expressing clone cells did show prominently cytoplasmic but weak nuclear staining of anti-Dref antibody whereas anti-Mi-2 staining was exclusively nuclear (Fig 4.11 B). This accumulation pattern of

anti-Dref and anti-Mi-2 staining (Fig 4.11 B) was similar to the wild type double labelled salivary gland cells (Fig 4.11 A), whereas, *NOS2* expressing clones of the double stained larvae showed a markedly different pattern of anti-Dref and anti-Mi-2 staining from their surrounding wild type cells (Fig 4.11 B). GFP marked *NOS2* expressing clones, when double stained with anti-Dref and anti-Mi-2 antibodies, showed a novel pattern of Dref staining. The anti-Dref antibody recognized Dref protein in the nuclei of the *NOS2* expressing clone cells (Fig 4.11 B) which was not seen in *NOS2* clone surrounding wild type cells (Fig 4.11 B) and in wild type double stained salivary gland cells (Fig 4.11 A). The anti-Mi-2 staining was predominantly nuclear in *NOS2* expressing clones which was similar to that of the surrounding wild type cells (Fig 4.11 B). However the level of anti-Mi-2 staining was higher in *NOS2* expressing clones compared with the surrounding wild type cells (Fig 4.11 B).

A) **B)**

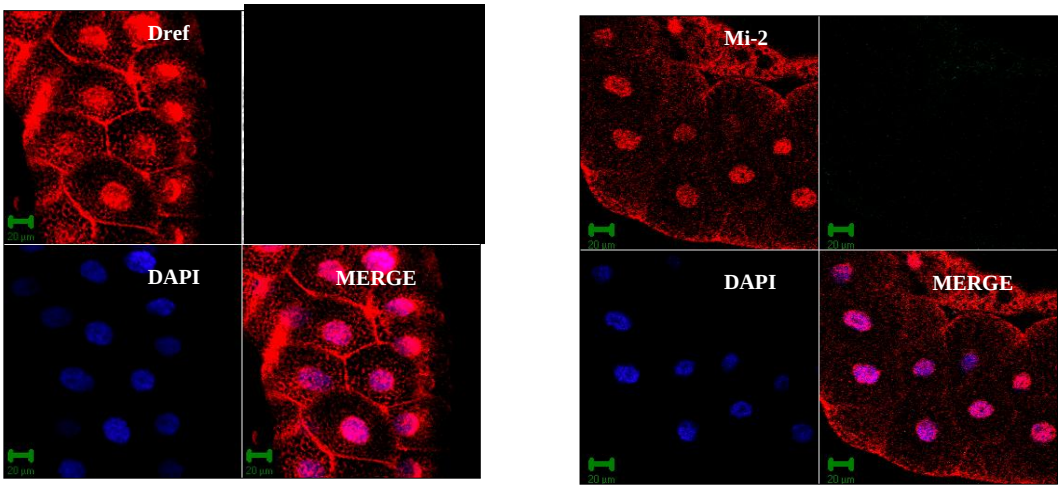

Figure 4.10. Salivary glands of wild type third instar larvae stained with anti-Dref and anti-Mi-2 antibody

A) Dref protein was found in the nucleus, cytoplasm and cell membrane of wild type third instar salivary gland when stained with mouse anti-Dref antibody (Hirose et al, 2002). (Secondary antibody used: horse anti-mouse Cy5)

B) Localisationof Mi-2 protein in wild type third instar salivary gland was predominantly nuclear when stained with rabbit anti-Mi-2 antibody (Brehm et al, 2000). (Secondary antibody used: goat anti-rabbit Cy5).

Blue: DAPI, Red: horse anti-mouse Cy5 (A), goat anti-rabbit Cy5 (B).
Scale Bar = 50µm

Figure 4.11. Double antibody staining of salivary glands with both rabbit anti-Mi-2 and mouse anti-Dref antibodies.

A) Wild type third instar salivary gland stained with anti-Dref and anti-Mi-2 antibodies. In the salivary gland cells anti-Dref staining is localised to the cytoplasm (indicated by yellow Alexa 555 secondary antibody). In the nuclei, the accumulation of anti-Mi-2 is clearly indicated by red Cy5. This nuclear exclusion of anti-Dref staining does not occur in the fat body cells (small white arrows). Genotype: *y,w* ; + /+ ; +/+

B) Third instar salivary gland with GFP marked *NOS2* expressing clone cells (small white arrows). The nuclei of the clone cells show high levels of both anti-Mi-2 and anti-Dref staining whereas the nuclei of the surrounding wild type cells show predominantly anti-Mi-2 staining (Red block arrow). Very low level of anti-Dref staining is observed in the cytoplasm of the wild type cells (red block arrow). Genotype: hsFLP/UAS-NOS2 ; Act5c>y^{+}>Gal4;UAS-GFP

Blue: DAPI, Green: GFP
Yellow: mouse anti-Dref (Hirose et al, 2002), Red: rabbit anti-Mi-2 (Brehm et al, 2000).
Secondary antibodies:
For Mi-2: goat anti rabbit Cy5
For Dref: goat anti mouse Alexa 555
Scale Bar = 20 µm

A)

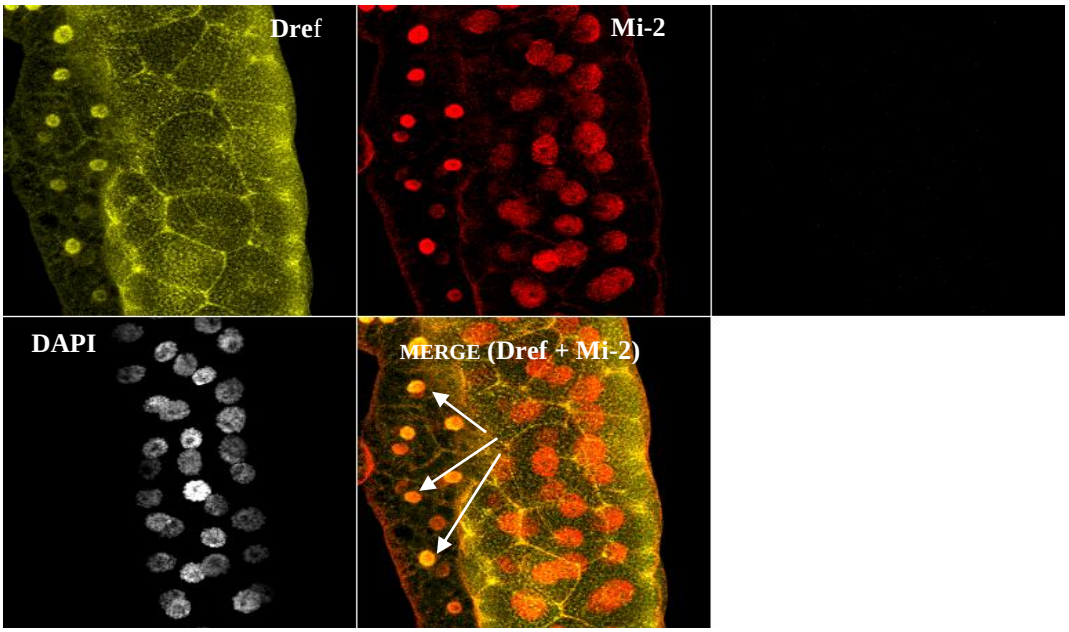
Dref
Mi-2
DAPI
MERGE (Dref + Mi-2)

B)

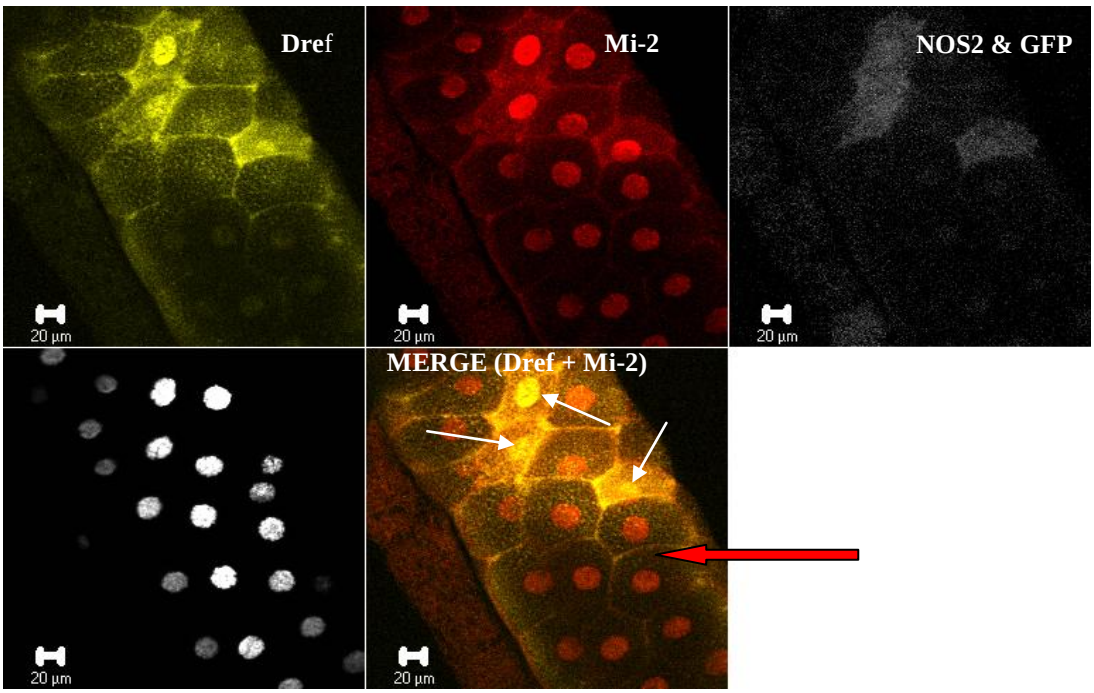
Dref
Mi-2
NOS2 & GFP
20 µm
MERGE (Dref + Mi-2)

4.2.7. Down regulation of Mi-2 expression in YFP tagged Mi-2$^{CPTI-000232}$ using RNAi approach

To determine whether Mi-2 was required for NO signalling to inhibit growth, the levels of Mi-2 were reduced by targeted RNAi. A UAS-RNAi-Mi-2 construct containing stock from VDRC (Vienna drosophila RNAi Center) (Dietzl et al., 2007) was used for this purpose. The efficiency of RNAi dependent reduction of Mi-2 expression was examined by expressing UAS-RNAi-Mi-2 in animals heterozygous for the YFP tagged *Mi-2$^{CPTI-000232}$* allele. RNAi expression was driven in salivary glands with the c147-Gal4 driver. The nuclear expression of the YFP tagged Mi-2$^{CPTI-000232}$ in UAS-RNAi-Mi-2 expressed flies was less than control YFP tagged Mi-2$^{CPTI-000232}$ salivary glands (Fig 4.12 A and B). The expression of RNAi-Mi-2 did not completely eliminate, but did down regulate, the expression of YFP tagged Mi-2$^{CPTI-000232}$ as shown in Figure 4.12.

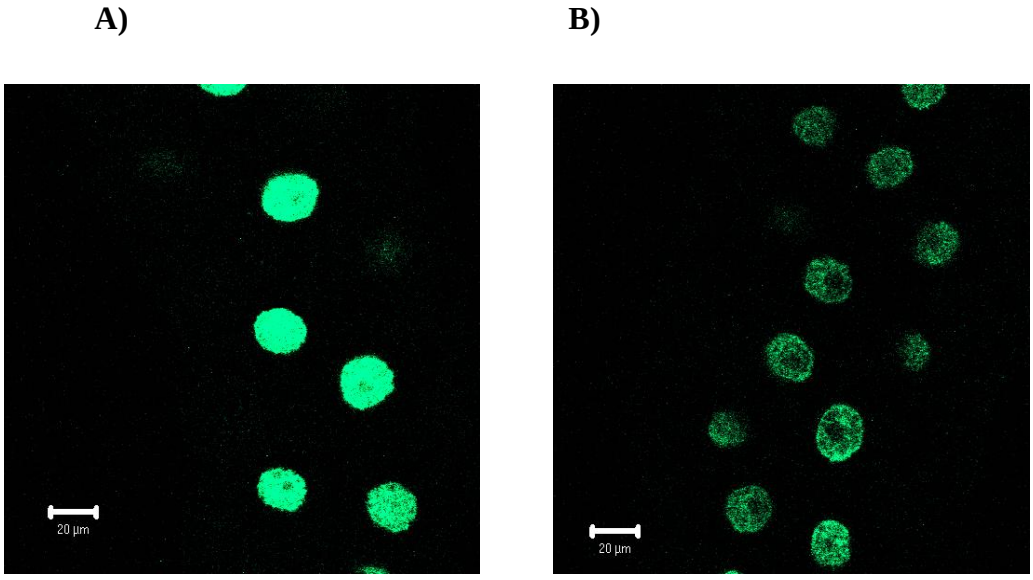

Figure 4.12. RNAi-Mi-2 reduces the expression of YFP tagged Mi-2$^{CPTI-000232}$.

A) Salivary gland of a third instar control larva showing expression of YFP tagged Mi-2$^{CPTI-000232}$
Genotype: c147-GAL4 / + ; YFP-Mi-2$^{CPTI-000232}$/ +

B) Salivary gland of a third instar experimental larva expressing UAS-RNAi-Mi-2 shows reduced expression of YFP tagged Mi-2$^{CPTI-000232}$ as compared with the control animal (A).
Genotype: c147-GAL4 / + ; YFP-Mi-2$^{CPTI-000232}$/ UAS-RNAi-Mi-2.
(Scale bar = 20 µm)
Images acquired and processed using identical settings.

4.2.8. Down regulation of Mi-2 expression by using *Mi-2* transheterozygous mutants

As expression of RNAi-Mi-2 did not eliminate expression of YFP tagged Mi-2, *Mi-2* mutants were used to reduce Mi-2 expression. Stocks carrying two different *Mi-2* alleles (Described in section 4.1.5.2) were used. Each allele was balanced over TM6B to allow identification of non-balancer larvae. When kept as separate stocks no non-Tubby larvae were observed in either of the mutant stocks. However, non-Tubby third instars were recovered when the mutant stocks balanced with TM6B were crossed with each other. In order to test whether this allelic combination reduced the expression of Mi-2 protein in salivary glands of the third instar larvae, the transheterozygous *Mi-2* animals were subjected to immunohistochemistry with rabbit an anti-Mi-2 antibody (Brehm et al., 2000). The expression of Mi-2 protein in these salivary glands was found to be significantly less when compared with that of the wild type third instar larva (Fig 4.13 A and B).

A) **B)**

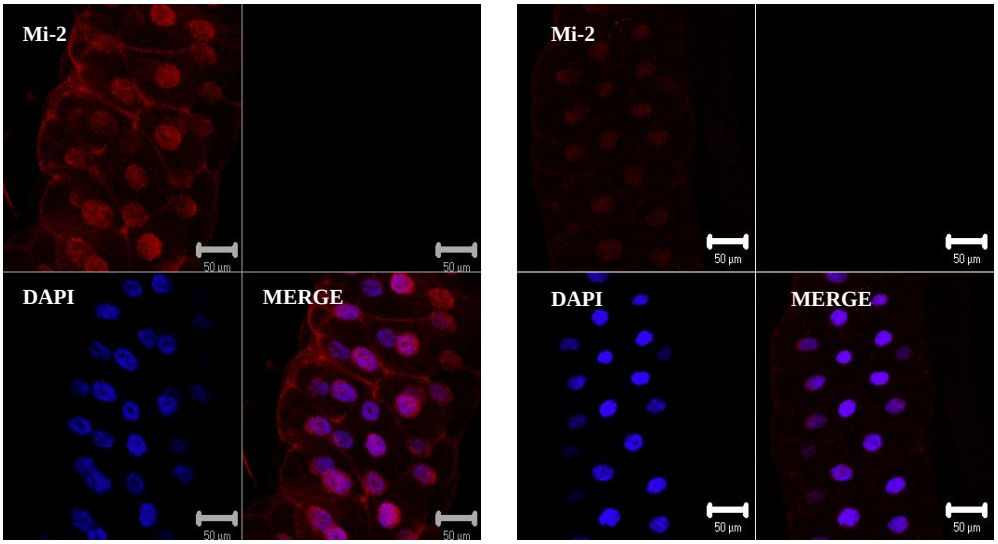

Figure 4.13. Antibody staining of Mi-2 protein in third instar salivary glands.
A) Salivary gland of wild type third instar larva showing nuclear localisation of Mi-2 protein.
B) Salivary gland of third instar *Mi-2* transheterozygote mutant larva showing less Mi-2 protein compared to A
Genotype: P{lacW}*Mi-2*^{j3D4}/ P{EPgy2}*Mi-2*^{EY08138} Su(Tpl)^{EY08138}
Blue: DAPI, Red: rabbit anti-dMi-2 antibody (Brehm et al, 2000)
(Secondary antibody used: goat anti-rabbit Cy5).
Scale Bar = 50 µm.
Images acquired and processed using identical settings.

4.2.9. Study of the phenotype imparted by NOS in a Mi-2 down regulated background

The results of this thesis indicate Mi-2 as a target of NO signalling (Sections 3.2.2, 3.2.3, 4.2.1, 4.2.2 and 4.2.3). NO is known to control organ size (Kuzin et al., 1996). To test whether Mi-2 is required for the NO induced reduced growth phenotype, NOS was expressed in salivary glands expressing reduced levels of Mi-2. As previously shown, Mi-2 levels can be reduced by targeted RNAi or by using transheterozygotes of two *Mi-2* alleles (Section 4.2.7 and 4.2.8). Hence, both RNAi-Mi-2 animals and transheterozygous *Mi-2* mutants were exploited as Mi-2 down regulated systems to examine the Mi-2 dependency of NO induced reduced growth phenotypes.

A functional relationship between Mi-2 and cell proliferation has been discussed above (Section 4.1.1). Another aim of this experiment was to determine whether a decrease of Mi-2 content alters the growth of the salivary glands.

The average volume of DAPI stained nuclei from five different genotypes was calculated (Fig 4.14). Expression of UAS-NOS2 in the salivary glands using the c147-GAL4 driver showed the expected small sized nuclei (Fig 4.14**,** Genotype: NOS2). When UAS-RNAi-Mi-2 and UAS-NOS2 were co-expressed with c147-GAL4, the nuclei of salivary glands again showed a small size phenotype reasonably similar to that when UAS-NOS2 was driven alone (Fig No: 4.14, Genotype NOS2RNAi-Mi-2). Salivary glands of *Mi-2* transheterozygous mutants also exhibited a reduced growth phenotype when UAS-NOS2 was expressed (Fig 4.14, NOS2Mi-2 transheterozygous mutant). The average volume of the salivary gland nuclei of the *Mi-2* transheterozygous mutants (Fig 4.14, Mi-2transheterozygous mutant) was found to be within a close statistical range to that of the wild type salivary gland nuclei (Fig 4.14, WT).

Tub-GAL4 driven expression of the UAS-RNAi-Mi-2 construct was undertaken to determine whether any growth phenotype or lethality would be caused by the reduction in Mi-2 levels in the whole animal. Expression of UAS-RNAi-Mi-2 via Tub-GAL4 neither induced any growth phenotype nor caused any lethality (data not shown). Adult flies carrying UAS-RNAi-Mi-2 driven by Tub-GAL4 showed normal fertility (data not shown).

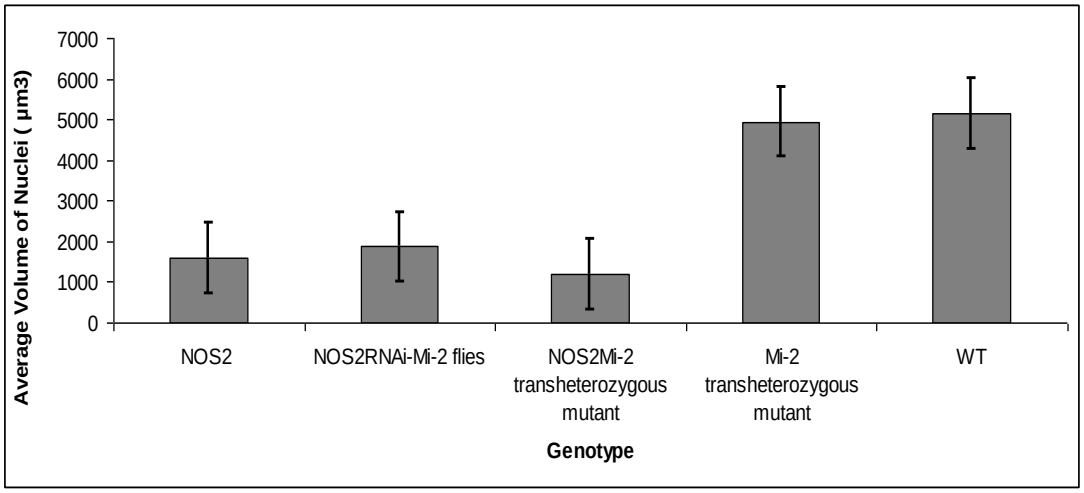

Figure 4.14. Average volume of DAPI stained larval salivary gland nuclei.
WT = Genotype: *y, w* ; **+ / + ; + / +**

NOS2 = Genotype: UAS-NOS2 / + ; c147-GAL4 / +.

NOS2RNAi-Mi-2 = Genotype: UAS-NOS2 / + ; c147-GAL4 / + ; UAS-RNAi-Mi-2 / +.

NOS2Mi-2 transheterozygous mutant = Genotype: UAS-NOS2 / +; c147-GAL4 / + ; P{lacW}*Mi-2*^{j3D4}/ P{EPgy2}*Mi-2*^{EY08138} *Su(Tpl)*^{EY08138}

Mi-2transheterozygous mutant = Genotype: +/+ ; +/+ ; P{lacW}*Mi- 2*^{j3D4}/ P{EPgy2}*Mi-2*^{EY08138} *Su(Tpl)*^{EY08138}

WT = *y, w* **; +/+ ; +/+**

Data derived from 80 DAPI stained nuclei from 8 different salivary glands of 8 different female animals of each of the above genotypes.
Data analysed and processed using Image analysis software Velocity.
Raw data available in Appendix No: B.4.
Error bars indicate standard deviation.

4.3 Discussion

One primary aim of the experiments presented in this chapter was to determine the effects of NO on the Mi-2/NuRD complex and its associated proteins.

As Mi-2 was suspected to be a possible target of the growth control activity of NO (Discussed in Sections 3.2.2 and 3.2.3) and Mi-2/NuRD was itself reported to play an essential role in transcriptional repression and growth control (Discussed in Section 4.1.1), the other important aspect of this chapter was to determine whether the antiproliferative action of NO is through Mi-2/NuRD.

4.3.1. NO alters Mi-2 localisation

The previous *ex vivo* results of SNAP treatment found an increase in the YFP tagged Mi-$2^{CPTI\text{-}000232}$ expression after SNAP exposure (Section 3.2.2 and Section 3.2.3). So by using *Mi-$2^{CPTI\text{-}000232}$* fly stock, a detailed study was undertaken to confirm whether NO alters Mi-2 localisation *in vivo*.

In order to determine this, two different approaches were undertaken:

One approach was to use c147-GAL4 to drive *NOS2* expression in whole salivary glands of YFP tagged Mi-$2^{CPTI\text{-}000232}$ larvae (Section 4.2.1). The size of the *NOS2* expressing experimental salivary gland nuclei were found to be much smaller than that of the control nuclei (Fig 4.3) which is consistent with previous reports (Kuzin et al., 1996), (Kimber, 2005) and (Scott, 2009). Confocal images acquired of five *NOS2* expressing third instar larvae showed a consistent increase in the nuclear localisation of YFP tagged Mi-$2^{CPTI\text{-}000232}$ when compared with the salivary glands of their corresponding control animals (Fig 4.3). Although the size of the salivary gland nuclei were small, the increase of the intensity of YFP tagged Mi-$2^{CPTI\text{-}000232}$ localisation observed in the *NOS2* expressing animals (Fig 4.3) demonstrated that NO modified Mi-2 localisation.

To further investigate the alteration of Mi-2 localisation in response to *NOS2*, the FRT/GAL4 expression system was used. In this approach *NOS2* was expressed in single cells of the salivary glands. mRFP marked single cell clones expressing *NOS2* in the salivary glands of *Mi-$2^{CPTI\text{-}000232}$* animals showed an increase in YFP tagged Mi-2 nuclear localisation when compared with that of the non adjacent wild type cells not expressing *NOS2* (Fig 4.4). The immediate adjoining wild type cells of the mRFP marked *NOS2* expressing clone cell also showed an increase in the YFP tagged Mi-2

(Fig 4.4). The increase in YFP tagged Mi-2$^{CPTI-000232}$ localisation in the immediate adjacent wild type cells is likely to be a result of NO diffusion (Haley, 1998).

Immunohistochemical analysis performed using an anti-Mi-2 antibody showed an increase in Mi-2 expression in *NOS2* expressing single cell clones compared with the non-adjacent wild type cells (Fig 4.5.i B). No increase in the nuclear accumulation of endogenous Mi-2 in cells immediately adjacent to *NOS2* expressing clones may be a result of the very short half life of NO (Haley, 1998) limiting its diffusion to those cells immediately neighboring the source of NO.
Unlike the anti-Mi-2 stained wild type cells (Fig 4.5.ii A), *NOS2* expressing clone cells showed a uniform distribution of Mi-2 protein throughout the nucleus (including the nucleolus) (Fig 4.5.ii B). However, nuclei of both wild type and *NOS2* expressing clone cells also showed perinuclear localisation of Mi-2 protein (Fig 4.5.ii A and B). The ratio of the average intensity of endogenous Mi-2 in the clone cells verses that of the non adjacent wild type cells was found to be higher in *NOS2* expressing cells compared to that of control cells as calculated using image analysis software velocity (Fig 4.6). Although the average ratios were different, there was some overlap in the standard deviations. The range in data may have been minimized by analysing higher number of salivary glands. However, the recovery of *NOS2* expressing clones in the salivary gland is not trivial. *NOS2* expressing clones were only observed in approximately 10% of salivary glands dissected. The very brief heat shock (4-5mins) driving expression of FLP was used as longer heat shocks resulted in the death of the majority of the UAS-NOS2 containing larvae (data not shown). The low recovery of salivary gland clones expressing *NOS2* is presumably due to larval death caused by the expression of *NOS2* in other tissues, as *NOS2* expression, when limited to the salivary gland, has no effect on viability (data not shown). The increase in Mi-2 expression observed by using anti-Mi-2 antibody in response to *NOS2* expression (Fig 4.5) demonstrated that NOS acts to up regulate the nuclear concentration of Mi-2 protein.

4.3.2. Simj does not alter the NOS mediated growth control

Expression of *NOS2* reduces cell proliferation and limb size of *Drosophila* (Kuzin et al., 1996). As Simj has been reported to act as the regulatory component of Mi-2/NuRD (Discussed in 4.1.2) and Mi-2/NuRD was confirmed as a probable target of NO (Sections 4.2.1, 4.2.2 and 4.2.3), it was determined whether animals expressing UAS-

NOS2 or co-expressing UAS-NOS2 and UAS-simj showed any alteration to the reduced growth phenotype that resulted from *NOS2* expression alone (Fig 4.7). Co-expression of UAS-NOS2 and UAS-simj did not noticeably alter the reduced growth observed when compared to *NOS2* expression alone (Fig 4.7). These data suggested that Simj does not alter the growth control activity of NO.

4.3.3. NOS does not noticeably affect the localisation of Dref

As NO had been shown to alter the nuclear localisation of Mi-2 (Sections 4.2.1, 4.2.2 and 4.2.3) and Mi-2 has previously been shown to genetically and physically interact with Dref (Hirose et al., 2002), the localisation of Dref protein in cells expressing high levels of NO was determined. The localisation of Dref in *NOS2* expressing single cell clones did not appear to be noticeably different when compared with the non-adjacent wild type cells (Fig 4.8 i). In addition, the quantitative analysis of the average ratio of Dref localisation in the *NOS2* expressing clone cells verses the corresponding non adjacent wild type cells was similar to that of the control clones (Figure 4.9). These data demonstrate that NOS does not modify Dref expression or localisation. No noticeable alteration in the localisation pattern of Dref protein was observed in *NOS2* expressing clone cells compared to the wild type cells as shown in the high magnification images (Fig 4.8.ii A and B). The perinuclear pattern of localisation of endogenous Mi-2 observed in wild type and *NOS2* expressing clone cells (Section 4.2.3, Fig 4.5.ii A and B) was not mimicked by Dref protein in anti-Dref antibody stained wild type and *NOS2* expressing clone cells (Fig 4.8.ii A and B).

4.3.4. Regulation of growth by NO does not act through Mi-2

Previous data from this thesis showed that Mi-2 is a target of NO (Sections 3.2.2, 3.2.3, 4.2.1, 4.2.2 and 4.2.3). Therefore whether the growth regulating role of NO is dependent on Mi-2 was determined. In order to examine this, the effect of NO was investigated in UAS-NOS2 and UAS-RNAi-Mi-2 co-expressing flies. The salivary gland nuclei of the UAS-NOS2 and UAS-RNAi-Mi-2 co-expressing animals showed a reduced size similar to those expressing only UAS-NOS2 (Fig 4.14). Moreover *NOS2* expression in *Mi-2* transheterozygous mutant larvae also resulted in small salivary gland nuclei (Fig 4.14). These results indicate that NO mediated growth regulation does not act through Mi-2. Mi-2/NuRD plays important role in mediating malignancy caused by extreme cell proliferation as reviewed in (Zhang et al., 1999) and therefore Mi-2/NuRD may be

required for growth or proliferation. Thus it was expected that *Mi-2* transheterozygous mutants, where the amount of Mi-2 protein was very low (Fig 4.13), would show an alteration in the nuclear size compared to those of wild type salivary glands. The quantitative analysis did not show any difference in nuclear size of salivary gland nuclei in *Mi-2* transheterozygous mutants compared to wild types (Fig 4.14). This unpredicted observation coincides with the recent finding that the major portion of *Drosophila* Mi-2 is actually part of a complex termed dMec (dMEP-1 complex). This complex mediates transcriptional repression of proneural genes (Kunert et al., 2009, Kunert N, 2009) however there is no data demonstrating a role for dMec in the control of cell proliferation.

4.3.5. A novel function of NO in the disruption of the *in vivo* Mi-2/Dref protein complex

The localisation pattern of Mi-2 protein both in single stained (Fig 4.10 B) and double stained (with anti-Dref) wild type salivary glands was predominantly nuclear (Fig 4.11 A). In the single stained wild type salivary glands, along with the nuclear localisation some cytoplasmic and cell membrane bound traces of anti-Dref staining were also observed (Fig 4.10 A), whereas in the double stained wild type salivary glands the distribution of anti-Dref staining was found to be exclusively cytoplasmic but weakly nuclear nuclear (Fig 4.11 A).

Interestingly the anti-Dref mouse monoclonal antibody used in this study was raised against bacterially purified recombinant Dref protein consisting of amino acids 16-608 (Hirose et al., 1996). This region overlaps the Mi-2 interacting region of the Dref protein (amino acids 16-145) (Hirose et al., 2002). Therefore, when anti-Mi-2 antibodies interact with Mi-2/Dref to form a Dref /Mi-2/anti-Mi-2 antibody complex, they may mask the epitope sites of the anti-Dref antibody. In double stained wild type salivary glands, it can be suggested that epitope sites of the anti-Dref mouse monoclonal antibody are probably masked in the Dref /Mi-2/anti-Mi-2 antibody complex. Hence, the anti-Dref antibodies can not recognize the epitope sites present on the Dref protein of the nuclear Mi-2 / Dref / anti-Mi-2 antibody complex (Fig 4.11 A). As Mi-2 localisation is higher in the nucleus than the cytoplasm (Fig 4.10 A) it can be speculated that there is insufficient cytoplasmic Mi-2 protein for the formation of Dref /Mi-2 complex in the cytoplasm. Hence in the cytoplasm of the double stained wild type salivary glands the epitope sites of anti-Dref antibody are left unmasked. Consequently

anti-Dref antibody can bind to the epitope sites present on the cytoplasmic Dref protein leading to the visualization of the cytoplasmic Dref protein in the double antibody stained wild type salivary glands (Fig 4.11 A). As the localisation pattern of double labelled Mi-2 and Dref staining observed in wild type cells surrounding *NOS2* expressing clones (Fig 4.11 B) was found to be similar to that of the wild type salivary glands (Fig 4.11 A), it can be inferred that same phenomenon of Mi-2/Dref/anti-Mi-2 antibody interaction was repeated in the wild type cells surrounding the *NOS2* clone (Fig 4.11 B). However, in cells expressing *NOS2* and double labelled with anti-Mi-2 and anti-Dref antibodies, a unique staining pattern was revealed. In these cells nuclear Dref staining can be observed (Fig 4.11B). This indicates that the Mi-2 / Dref / anti-Mi-2-antibody complex has been disrupted allowing access of anti-Dref antibodies to their binding sites.

A search on *Drosophila* genome database revealed that more than 150 cell proliferation related, DRE sequence containing genes, may act as targets of the transcription regulatory activity of Dref (Matsukage et al., 2008). The DNA binding activity of Dref, which acts as the key for the transcriptional control of several DNA proliferation related genes, can be regulated by the intracellular redox state through the active participation of the redox sensitive Cys59 and /or Cys62 amino acids of Dref (Choi et al., 2004). High levels of NO induced by *NOS2*, interact with the thiol groups of proteins leading to the initiation of NO responsive gene expression (Eberhardt and Beck, 2001). NO, which plays fundamental role in cell proliferation (Villalobo, 2006) also functions in altering the transcription factors which are responsive to intracellular redox status to promote cell signalling (Eberhardt and Beck, 2001). All these results suggest that *NOS2* could be involved in the alteration of Dref protein leading to the potential reorganisation of Mi-2/Dref complex in *NOS2* expressing clone cells.

As a consequence of the probable disruption of the Mi-2/Dref complex by NO, Dref epitopes are not masked in Mi-2/Dref complex resulting in the visualization of nuclear Dref by anti-Dref staining in *NOS2* expressing clone cells (Fig 4.11 B). The entirely different pattern of Dref staining in the *NOS2* expressing clones from that of the surrounding wild type cells (Fig 4.11 B) supports the concept of the disruption of Mi-2/Dref complex by NOS. In summary the present study has proposed a novel function of NOS in the reorganisation of Mi-2/Dref protein complex.

Chapter 5: Effect of FOXO on Mi-2/NuRD and associated proteins

5.1. Introduction

5.1.1. FOXO: The forkhead family transcription regulators

FOXO is a member of the forkhead family of transcription factors**.** In humans this family consists of four orthologues: namely FOXO1 (previously known as FKHR), FOXO2, (previously known as AF6q21), FOXO3a (previously known as FKHRL1), and FOXO4 (previously known as AFX) (Jacobs et al., 2003). The only *FOXO* gene in *Drosophila* is a homologue of DAF-16/FOXO family of transcription factors and is closely related with *hFOXO3a* (human *FOXO* gene) and (Junger et al., 2003).

5.1.2. Developmental roles of FOXOs

A sequence of five amino acids present in the DNA binding domain of FOXO (α helix 3) enables sequence specific interaction between FOXO and its DNA binding sites. FOXOs have numerous roles in development such as cell proliferation, apoptosis, metabolism, cell cycle progression and relief from oxidative stress (Andreas Barthel, 2005). FOXOs are targets of protein kinase B (PKB)/Akt, in the repression of cell proliferation leading to growth arrest (Medema, 2003). In cells of the hematopoietic system activation of FOXO factors induce the activation of several proapotopic genes to trigger apoptosis (Medema, 2003). It has been reported that mammalian FOXO4 and DAF-16 inhibit the cell cycle at the G_1 and G_2 phases. FOXO4 and FOXO3a trigger the transcription of GADD45 mRNAs resulting in suppression of cell cycle progression at G_2 phase in mouse (Yoko Furukawa-Hibi et al., 2002). Akt phosphorylates and retains FOXO3a in the cytoplasm, whereas the dephosphorylation of FOXO3a leads to the movement and activation of FOXO3a into the nucleus where it induces expression of several target genes (Fig 5.1). These include Fas ligand genes vital for cell death hence apoptosis or programmed cell death is promoted (Anne Brunet et al., 1999). Under stressful conditions, FOXO family members can induce apoptosis by activating the transcription of numerous pro-apoptopic genes (Dansen and Burgering, 2008). Lethal hyperplasia / germ line tumour in *C. elegans* which is caused by mutations in the tumour suppressor *gld-1* (Francis et al., 1995) is suppressed by a *gld-1* specific proliferation decrease controlled by DAF-16 (Julie M. Pinkston, 2006). Mice carrying null mutations for the FoxO family orthologues, FoxO1, FoxO3a, and FoxO4, show a

mild cancer predisposition indicating that FOXOs act as tumour suppressors (Paik et al., 2007).

Figure 5.1. Insulin signaling pathway in *Drosophila* (taken from (Neufeld, 2003)). The FOXO protein mediates a transcriptional response to insulin signaling. Under conditions of abundant nutrients, FOXO is phosphorylated by Akt and retained in an inactive state in the cytoplasm. When insulin levels fall, FOXO is dephosphorylated and translocates into the nucleus, where it stimulates transcription of *4E-BP* (*Thor*) and presumably other negative regulators of growth. In addition, active FOXO increases expression of the insulin receptor gene, which may result in increased insulin sensitivity under low insulin conditions (Neufeld, 2003).

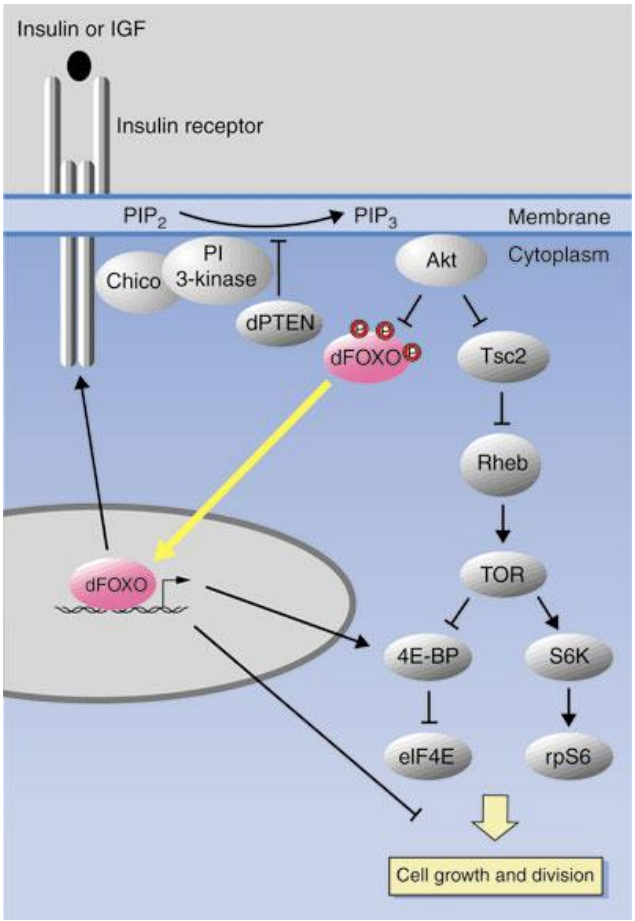

5.1.3. Previous research in the laboratory on FOXO

Previously in our laboratory Affymetrix gene arrays were used to identify transcriptional changes induced in *Drosophila* S2 cells following exposure to NO (Kimber, 2005). These data indicated that many genes which were up regulated by NO are also functional targets of the transcription factor dFOXO. The previous data of our laboratory also showed that *Thor (4E-BP)* which is a member of 4E binding protein *(4E-BP)* family (Bernal and Kimbrell, 2000) is up regulated by NO *in vivo* and is also a transcriptional target of FOXO (Kimber, 2005).When not phosphorylated by Akt, FOXO enters nucleus where it induces the transcription of *Thor* (*4E-BP*) (Puig et al., 2003). Data from our laboratory has indicated that *Thor* transcription is activated by NO in a FOXO dependent manner (Kimber, 2005) (Scott, 2009).

5.1.4. Perspective of the present chapter

During the present study, a genetic screen for targets of NO, using the NO donor SNAP, revealed Mi-2 as a target of NO (Section 3.3.2). An increase in Mi-2 expression was also observed in whole salivary glands and in single cell clones expressing UAS-NOS2 (Section 4.3.1). Thus, as Mi-2 is a probable target of NO, the action of NO on Mi-2 may be regulated by FOXO. Therefore, several experiments were undertaken to determine whether expression of UAS-FOXO changes expression of Mi-2 protein.

Dref activity is known to be negatively regulated by Mi-2 (Hirose et al., 2002) and acts as a transcriptional regulatory factor of several cell proliferation and apoptosis related genes (Matsukage et al., 2008). These two functional properties of Dref indicated that the function of Dref protein may act under the direct control of FOXO signalling. It was therefore decided to study the effect of FOXO expression on the expression and localisation of Dref protein.

As Simj has been demonstrated to be a regulatory subunit for the Mi-2 containing NuRD complex (Kon et al., 2005), the effects of FOXO expression on Simj were also determined.

To achieve these aims, UAS-FOXO was expressed in the whole salivary glands of YFP tagged *Mi-2*$^{CPTI\text{-}000232}$ larvae by using the c147-GAL4 driver. The effect of UAS-FOXO on the localisation of endogenous Mi-2 and Dref proteins was analysed in GFP marked single cell clones by using the FRT-GAL4 system (Described in 4.1.4).

5.2. Results

5.2.1. Analysis of the effect of FOXO expression in the whole salivary glands of YFP tagged Mi-2$^{CPTI-000232.}$

The results of SNAP treatments to salivary glands showed an increase of YFP tagged *Mi-2* $^{CPTI-000232}$ expression (Section 3.3.2). YFP tagged *Mi-2* $^{CPTI-000232}$ larvae also showed an increase in Mi-2 expression when NOS was expressed in the whole salivary glands and also in NOS expressing single cell clones (Section 4.3.1). Therefore it was decided to analyse YFP tagged *Mi-2* $^{CPTI-000232}$ expression in whole salivary glands of animals expressing FOXO under the control of the c147-GAL4 driver.

Five pairs of salivary glands from wandering third instar larvae of experimental (UAS-FOXO expressing) and control animals were imaged on the confocal microscope. The nuclei of the salivary glands from the third instar larvae expressing UAS-FOXO were considerably smaller in size as compared to the control (Fig 5.2). The YFP tagged Mi-2 $^{CPTI-000232}$ expression in these 5 experimental larvae was compared with that of the corresponding control larvae. Two of the five different salivary glands expressing FOXO showed an increase in the nuclear expression of the YFP tagged Mi-2 $^{CPTI-000232}$ (Fig 5.2 Bi). The remaining three larvae did not show any noticeable change as compared to that of the control larvae (Fig 5.2 Bii). The YFP expression from all the larvae was analysed using imaging analysis software Velocity. (http://www.cellularimaging.com/products/Volocity). Quantification analysis of YFP fluorescent intensity of five salivary glands of each genotype (32 control and 33 UAS-FOXO expressing nuclei) demonstrated a 1.3 fold average increase of YFP tagged Mi-2 expression in UAS-FOXO up regulated animals (see appendix B.5. for raw data).

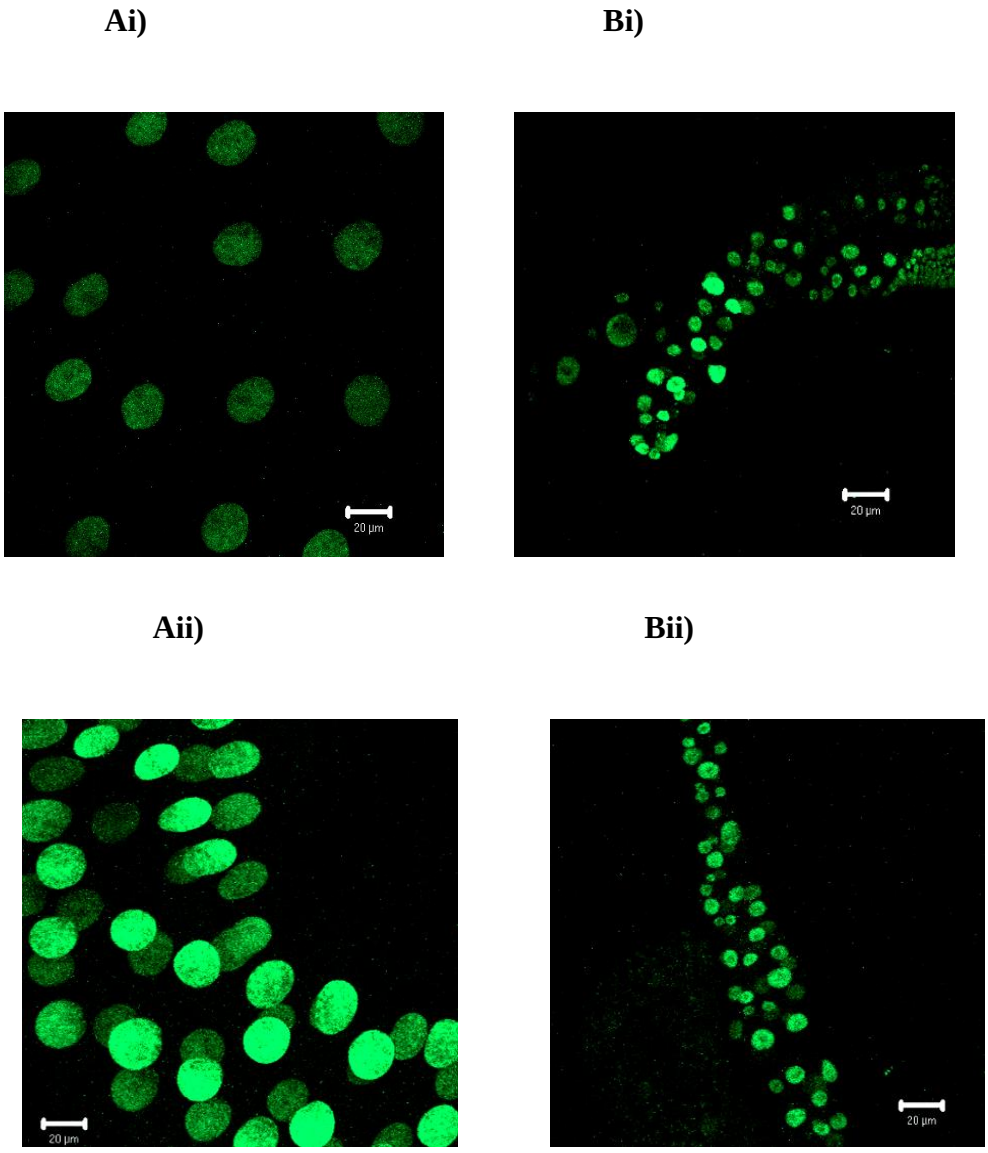

Figure 5.2. Expression of YFP tagged Mi-2$^{CPTI-000232}$ in third instar salivary glands.

Ai and Aii) salivary glands of control larva of genotype c147-GAL4 / +; YFP-Mi-2 $^{CPTI-000232}$ / +

Bi) and Bii) salivary glands of larvae. Genotype c147-GAL4 / UAS-FOXO; YFP-Mi-2 $^{CPTI-000232}$ / +

Bi) salivary gland over expressing FOXO showing higher expression of YFP tagged Mi-2 than the corresponding control Ai)

Bii) Salivary gland over expressing FOXO showing no noticeable change in the expression of YFP tagged Mi-2 compared to the corresponding control Aii).

Scale bars = 20 µm.

Ai and Bi: Images acquired and processed using identical settings.

Aii and Bii: Images acquired and processed using identical settings.

Raw data is available in Appendix B.5.

5.2.2. Visualization of endogenous Mi-2 protein in single cell clones expressing FOXO

Expression of UAS-FOXO in the whole salivary glands of YFP tagged *Mi-2* $^{CPTI\text{-}000232}$ larvae using the c147-GAL4 driver made the salivary glands smaller in size. However, the change in expression of Mi-2 may have been due to the reduced salivary gland size. Therefore the effect of FOXO signalling on endogenous Mi-2 expression, when the size of the salivary gland is minimally affected was determined. In order to undertake this, induction of UAS-FOXO expression was achieved in single cells of salivary glands using the FLP/FRT technique (Discussed in section 4.1.4). UAS-FOXO expressing GFP marked single cell clones were generated using the same hsFLP stock and in a similar protocol as described in section 4.2.3. The hsFLP carrying fly stock was crossed with animals containing UAS-FOXO and thus GFP marked, UAS-FOXO expressing clones could be recovered. Endogenous Mi-2 protein was visualised with a rabbit anti-Mi-2 antibody (Brehm et al., 2000). Control clones expressing only GFP were also generated. 20 salivary glands (10 of the experimental and 10 of control animals) were imaged on the confocal microscope.

The intensity of Mi-2 expression in the clone cells were compared to that of 10 non-adjacent wild type cells in each experimental (FOXO expressing) and control salivary glands. No obvious difference in Mi-2 expression was observed in the confocal images (Fig 5.3). The images were subsequently analysed using the image analysis software velocity. This demonstrated Mi-2 levels in the FOXO expressing clone cells compared to that of non-adjacent surrounding cells. A 0.91: 1 (+ 0.26 /- 0.26) ratio of Mi-2 expression in FOXO expressing clones versus surrounding wild type cells was recorded (Fig 5.4). Control GFP marked clones showed no difference in Mi-2 expression compared to surrounding wild type cells. A 0.97:1 (+ 0.37 /- 0.37) ratio of Mi-2 expression in control GFP clones versus surrounding wild type cells was deduced. This quantitative analysis did not reveal any noticeable change in the nuclear accumulation of Mi-2 in FOXO expressing clone cells (Figure 5.4).

A)

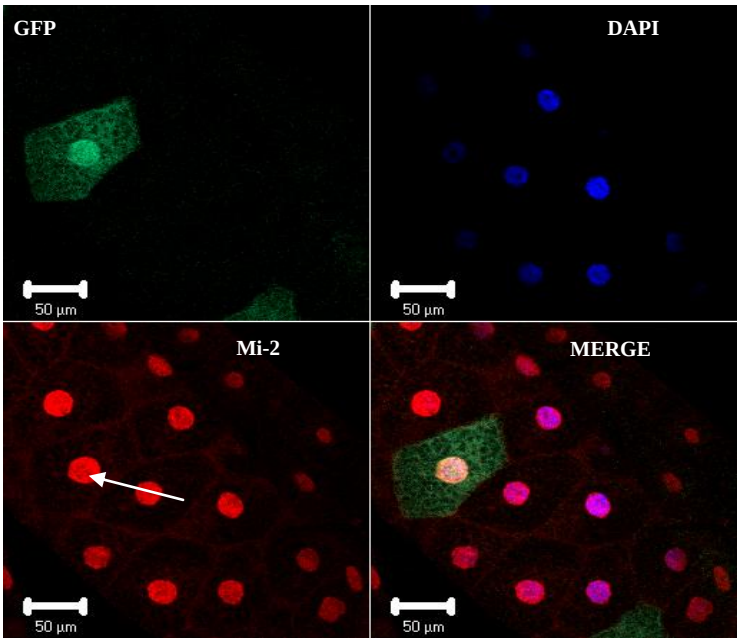

B)

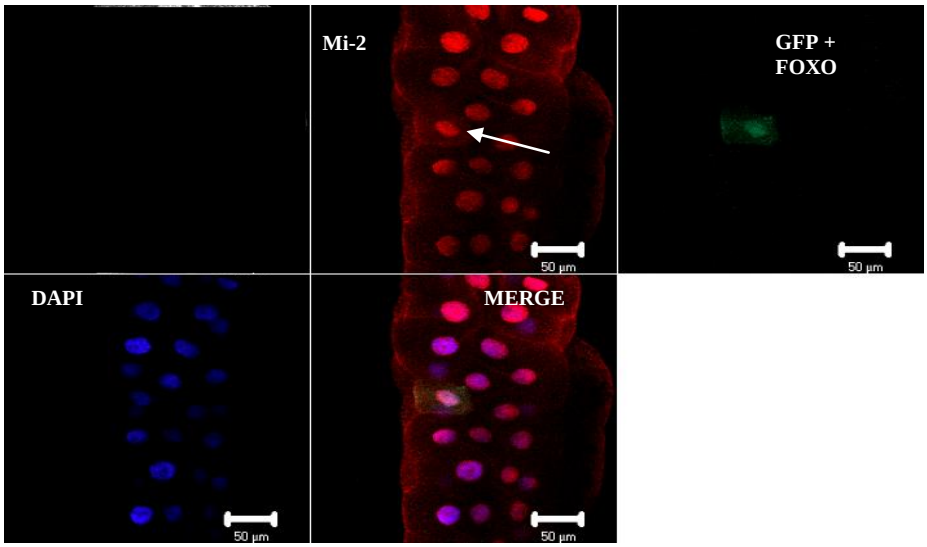

Figure 5.3. Antibody staining of Mi-2 protein expression in wild type and FOXO expressing clones of salivary gland cells.

Clones were generated using a 4min heat shock at 38°C between 24- 48hr AEL.

A) GFP marked control clone (white arrow) showing no noticeable change in the intensity or localisation of Mi-2.
Genotype: hsFLP / + ; Act5c>y^{+}>Gal4;UAS-GFP / +

B) FOXO expressing clone (white arrow) marked with GFP showing no noticeable change in the intensity or localisation of Mi-2.
Genotype: hsFLP / + ; Act5c>y^{+}>Gal4 / UAS-FOXO ;UAS-GFP / +
Blue: DAPI, Green: GFP, Red: Rabbit anti-Mi-2 antibody (Brehm et al 2000)
(Secondary antibody used: goat anti-rabbit Cy5).
Scale Bars = 50 µm

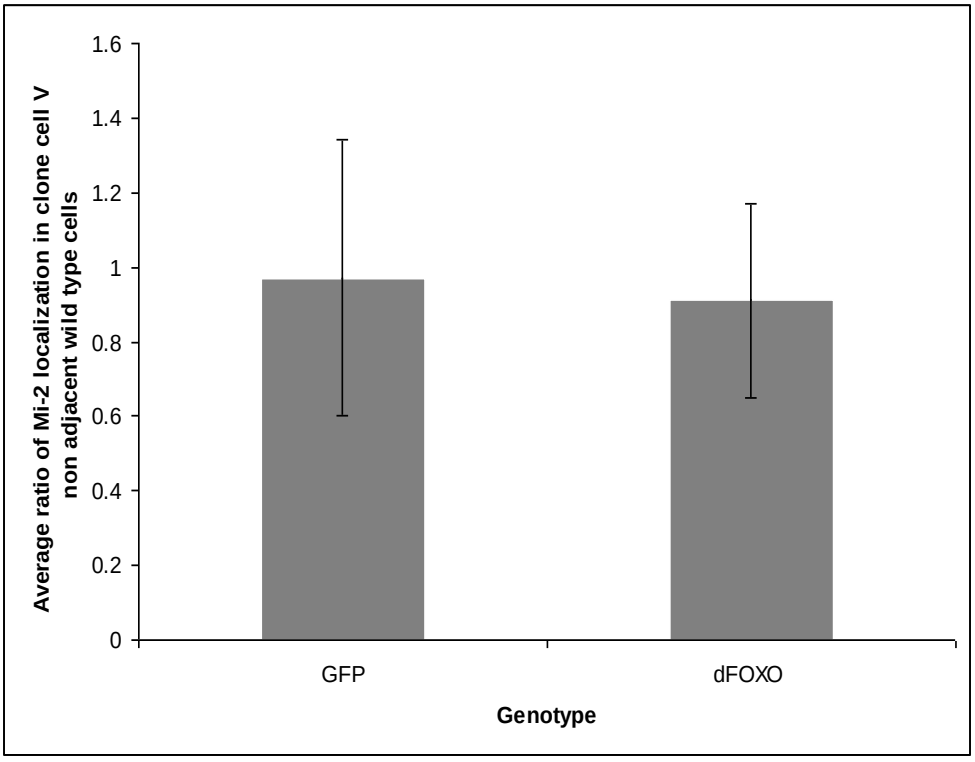

Figure 5.4. Quantification of Mi-2 expression in wild type and FOXO expressing single cell clones.

GFP = Ratio of average intensity of Mi-2 expression in GFP marked control clone cells Versus the average intensity of Mi-2 expression in 10 non adjacent wild type cells.
Genotype: hsFLP / + ; Act5c>y^+>Gal4; UAS-GFP / +

dFOXO = Ratio of average intensity of Mi-2 localisation in GFP marked clone cells over expressing FOXO Versus average intensity of Mi-2 expression in 10 non adjacent wild type cells.
Genotype: hsFLP / + ; Act5c>y^+>Gal4 / UAS-FOXO ;UAS- GFP / +

Data for both genotypes was obtained from 10 salivary glands from 10 animals. Error bars indicate standard deviation.

Raw data available in Appendix B.6.
Analysis undertaken using Velocity Image Analysis Software.

5.2.3. Analysis of the effect of co expression of UAS-FOXO and UAS-simj on salivary gland growth

Whether over expressing Simj could suppress or enhance FOXO induced inhibition of growth of the salivary glands, could be studied by up regulating both UAS-FOXO and UAS-simj at the same time in the same animal.

To determine if over expression of Simj would influence the reduced growth phenotype induced by increased levels of FOXO, both genes were co-expressed in the whole salivary glands using the c147-GAL4 driver.

UAS-simj-GFP (Kim et al., 2004) and UAS-FOXO were driven simultaneously using the c147-GAL4 driver and the phenotypic effect on salivary gland size was determined. Salivary glands of UAS-simj-GFP and UAS-FOXO co-expressed third instar larvae, showed reasonably similar size to that of the flies where UAS-FOXO was driven alone (Fig 5.5).

A) B)

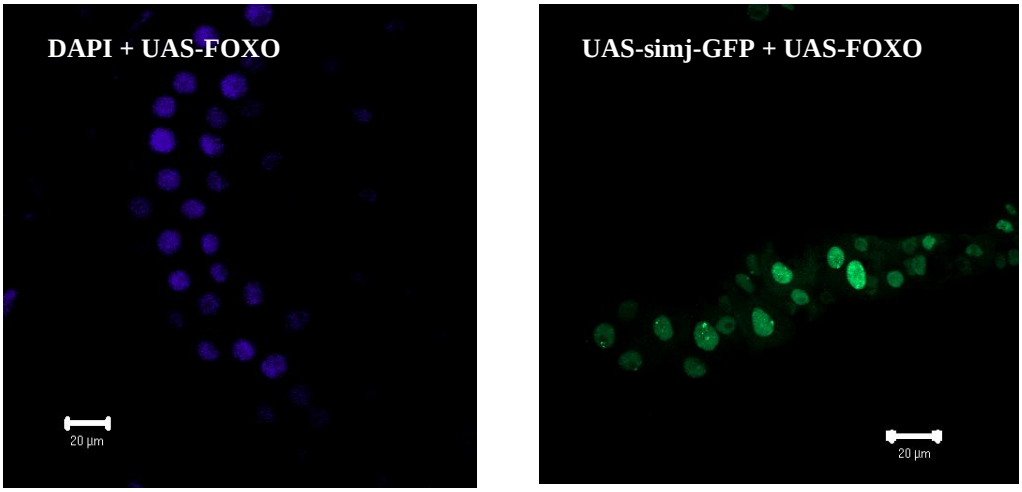

Figure 5.5. Salivary gland of UAS-simj-GFP and UAS-FOXO co expressed third instar larvae showed small size.
A) DAPI stained Salivary gland of FOXO expressed third instar larva.
Genotype: + / + ; c147-GAL4 / UAS-FOXO ; + / +.
B) Salivary gland of GFP tagged UAS-simj and UAS-FOXO co expressed third instar larva.
Genotype: UAS-simj / + ; c147-GAL4 / UAS-FOXO ; + / +.
Scale Bar = 20µm

5.2.4. Visualization of Dref protein in a single cell clones expressing FOXO

The FLP/FRT technique previously described (Section 4.1.4) was used to induce GFP marked FOXO over expressing clones. The control genotypes were generated similarly as in 5.2.2. The nuclear localisation of Dref protein was visualized by using a mouse anti-Dref antibody (Hirose et al., 2002) in combination with goat anti-mouse Alexa 555 secondary antibodies. The intensity of nuclear localisation of Dref protein in the GFP marked FOXO over expressing clones was compared to that of the non-adjacent wild type cells of that particular salivary gland. Similarly the amount of nuclear expression of Dref in the GFP marked control clones cells was compared to that of the non adjacent non-clone cells of that particular salivary gland. 20 confocal images (10 from each of the experimental and control genotypes) of salivary glands were analysed. No obvious change in the expression of Dref protein was found in the images of UAS-FOXO expressing clone cells when visually compared to that of the nonadjacent wild type cells (Fig 5.6 B). However, a minority showed an increase in the expression of Dref protein when compared to non adjacent wild type cells (Fig 5.6 C). To accurately analyse the response of Dref protein to FOXO over expression in single cell clones, the image analysis software velocity was used. This quantitative analysis did demonstrate an increase in Dref protein expression in some FOXO expressing clone cells compared to the non adjoining wild type cells. A 1.35: 1 (+ 1.10 /- 1.10) ratio of Dref expression in FOXO expressing clones versus surrounding wild type cells was recorded (Fig 5.7). Control GFP marked clones showed no significant difference in Dref expression compared to surrounding wild type cells. A 0.38:1 (+1.19 / - 1.19) ratio of Dref expression in control GFP clones versus surrounding wild type cells was observed (Fig 5.7).Although there was a large variation in the levels of Dref expression between clones (Fig 5.7).

Figure 5.6. Antibody staining of Dref protein expression in wild type and FOXO expressing single cell clones in salivary gland cells.

Clones were generated using a 4min heat shock at 38^{o}C between 24- 48hr AEL.

A) GFP marked control clone (white arrow) showing no noticeable change in the intensity or localisation of Dref.
Genotype: hsFLP / + ; Act5c>y^{+}>Gal4;UAS-GFP

B) UAS-FOXO expressing clone (white arrow) marked with GFP showing no noticeable change in the intensity or localisation of Dref.

C) UAS-FOXO expressing clone (white arrow) marked with GFP showing a small increase in the intensity of Dref accumulation
Genotype: hsFLP / +; Act5c>y^{+}>Gal4 / UAS-FOXO; UAS- GFP

Scale Bar = 50 μm

Blue: DAPI, Green: GFP, Yellow: mouse anti-Dref antibody (Hirose et al 2002)
(Secondary antibody used: goat anti-mouse Alexa 555).

91

A)

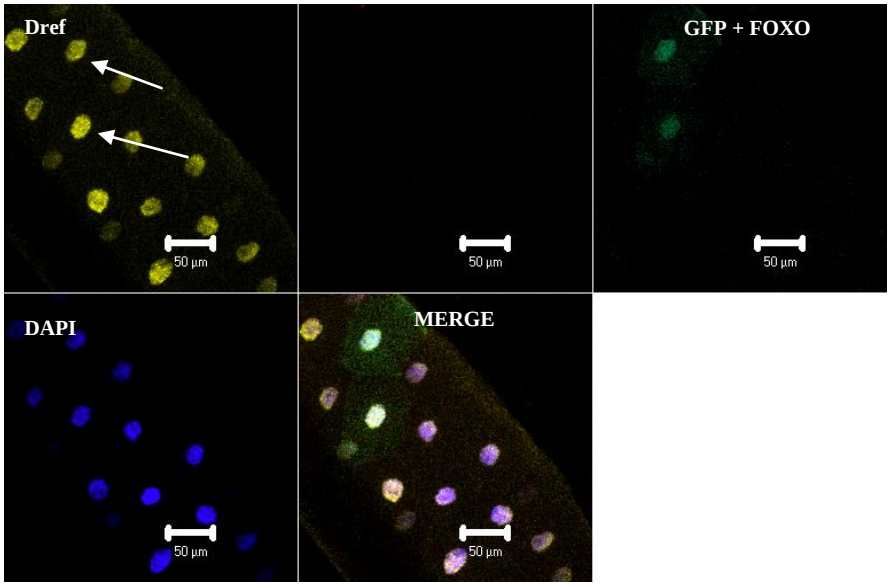
Dref
GFP + FOXO
DAPI
MERGE
50 µm

B)

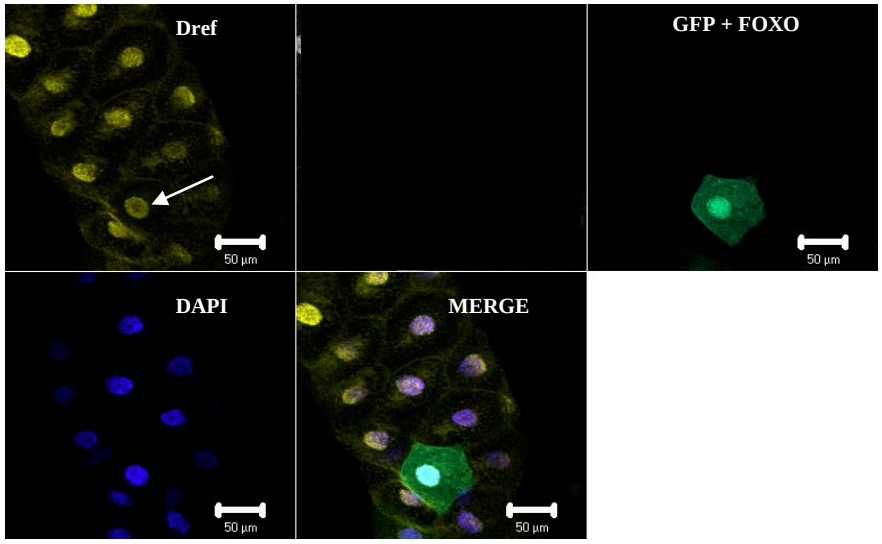
Dref
GFP + FOXO
DAPI
MERGE
50 µm

C)

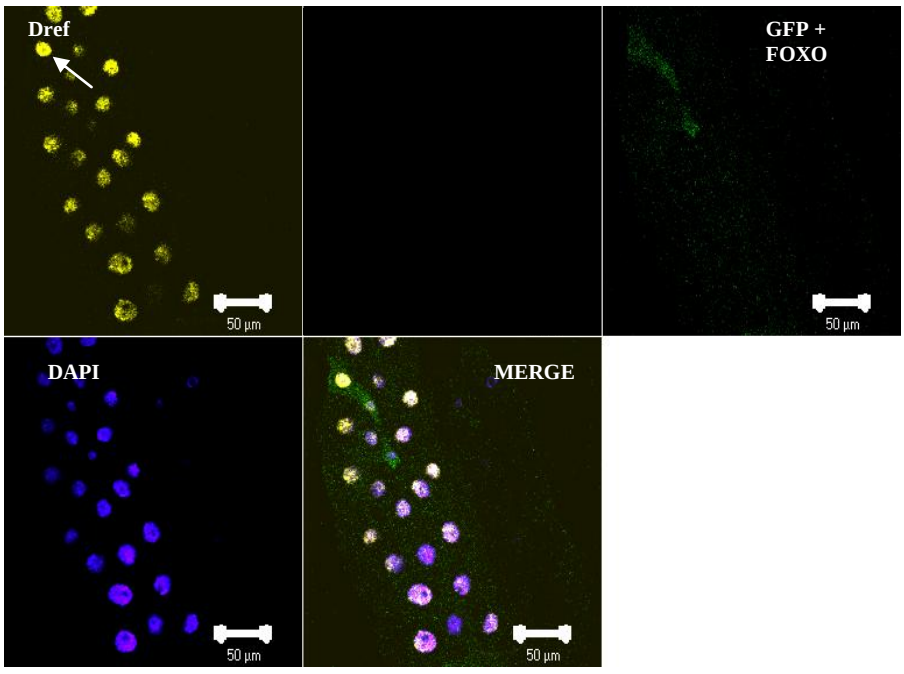
Dref
GFP +
FOXO
DAPI
MERGE
50 µm

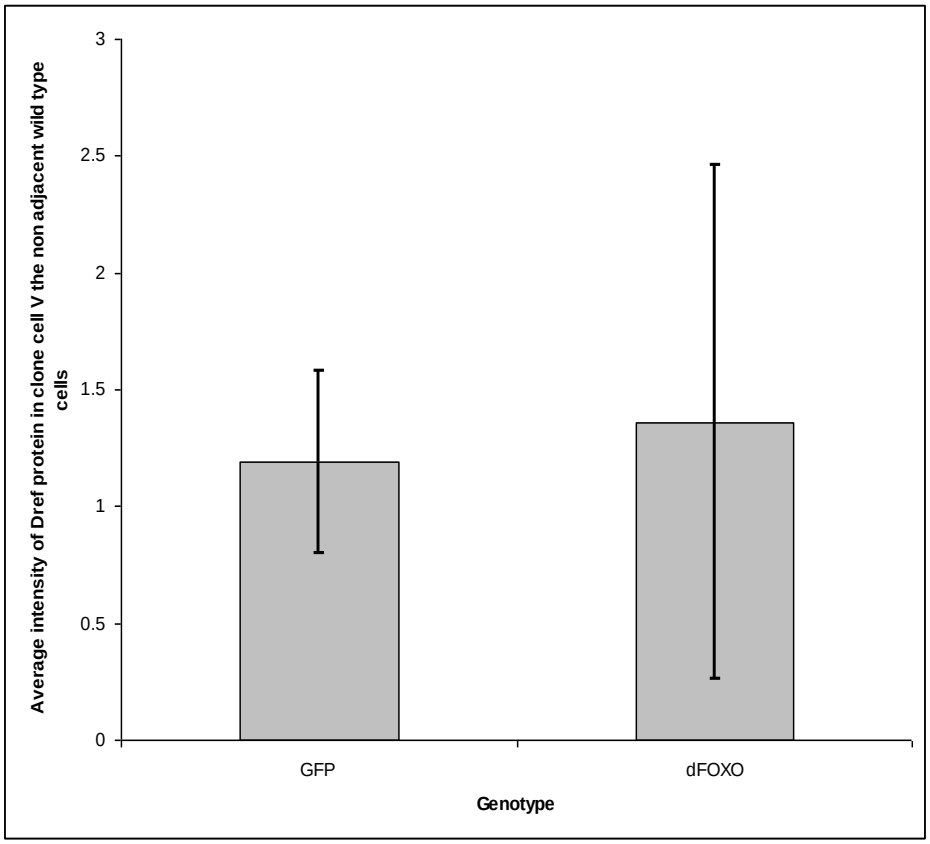

Figure 5.7. Quantification of Dref expression in wild type and UAS-FOXO expressing single cell clones.

GFP = Ratio of average intensity of Dref expression in GFP marked control clone cells Versus the average intensity in 10 non-adjacent wild type cells.
Genotype: hsFLP / + ; Act5c>y^{+}>Gal4 ; UAS-GFP

dFOXO = Ratio of average intensity of Dref expression in GFP marked clone cells over expressing FOXO Versus the average intensity in 10 non-adjacent wild type cells.
Genotype: hsFLP / + ; Act5c>y^{+}>Gal4 / UAS-FOXO ; UAS-GFP.

Data for both genotypes was obtained from 10 salivary glands from 10 animals. Error bars indicate standard deviation. Raw data available in Appendix: B.7 Analysis undertaken using Velocity Image Analysis Software.

5.2.5. Simultaneous visualization of Mi-2 and Dref proteins in single cell clones expressing UAS-FOXO

It has been reported that the anti-Dref antibody can co-immunoprecipitate Mi-2 from *Drosophila* embryos which confirms the existence of an *in vivo* Mi-2/Dref complex (Hirose et al., 2002). The same report also showed that both proteins negatively regulate each others functions and the binding of Mi-2 and Dref to the polytene chromosomes is mutually exclusive (Hirose et al., 2002). Thus the effect of increased FOXO expression on both the proteins at the same time in single cells was determined. GFP marked FOXO expressing clones were generated in an identical way described in section 5.2.2, A mixture of rabbit polyclonal anti-Mi-2 (Brehm et al., 2000) and mouse monoclonal anti-Dref antibodies was prepared following the dilution described in section 2.2.2. The salivary glands of experimental and control animals were stained with this mix of antibodies.

Further control samples were used to compare the localisation of both the proteins. Salivary glands from *y, w* third instar larvae were double stained with both antibodies and with anti-Mi-2 and anti-Dref antibodies separately. The antibody localisation in these single stained *y, w* salivary glands was compared to that of the double stained *y, w* salivary glands.

Salivary gland of wild type third instar larva when stained with anti-Dref antibody alone showed not only nuclear staining but also staining in the cytoplasm and cell membranes (Fig 5.8 A). The accumulation of anti-Mi-2 staining in single stained animals was found to be exclusively in the nuclei of wild type third instar larvae (Fig 5.8 B). However anti-Dref staining was observed only in the cytoplasm and cell membranes of *y, w* larvae double labelled with both anti-Dref and anti-Mi-2 antibodies (Fig 5.9 A). In these double stained larvae, anti-Mi-2 staining was exclusively in the nucleus (Fig 5.9 A). Similar to the double stained wild type cells from *y, w* animals, anti-Dref staining was exclusively cytoplasmic and cell membrane associated and anti-Mi-2 staining was predominantly in the nuclei of the double stained wild type cells surrounding UAS-FOXO expressing clones (Fig 5.9 B and C). Although the non adjacent wild type cells of the double stained larva showed two entirely different localisation patterns of anti-Dref and anti-Mi-2 staining, both the proteins were observed to be simultaneously localised in the nuclei of UAS-FOXO expressing clone cells (Fig 5.9 B and C, Fig 5.10, 5.11, 5.12). An increase in the level of anti-Mi-2 staining was sometimes observed in UAS-FOXO expressing clone cells (Fig 5.9 B and C, 5.10, 5.12). However this increase

of anti-Mi-2 staining was not found in all UAS-FOXO expressing clone cells (Fig 5.11). In UAS-FOXO expressing clone cells, anti-Mi-2 staining showed a perinuclear pattern of distribution (Fig 5.10 vii, 5.11 vii and 5.12 vii), reasonably similar to wild type and *NOS2* expressing clone cells (Section 4.2.3, Fig 4.5. ii A and B). However, the perinuclear localisation of anti-Dref staining observed in UAS-FOXO expressing clone cells (Fig 5.10 v, 5.11 v and 5.12 v) did not mimic the anti-Dref staining in wild type and *NOS2* expressing clone cells (Section 4.2.5, Fig 4.8.ii.A and B).

A) **B)**

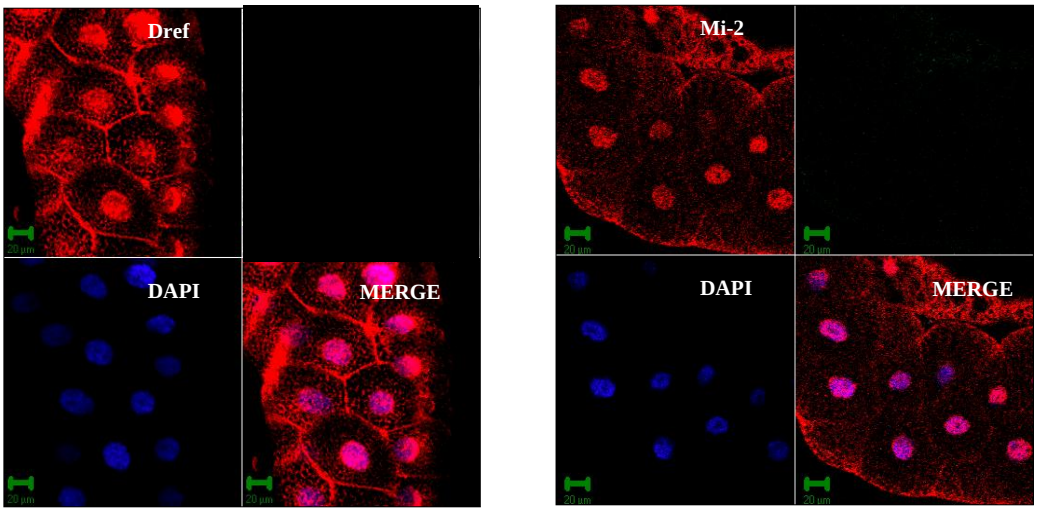

Figure 5.8. Images showing salivary glands of *y, w* wild type third instar larvae singly stained with anti-Dref and dMi-2 antibodies.

A) A noticeable amount of Dref protein was found in the nuclei, cytoplasm and cell membranes of the wild type third instar salivary gland when stained with mouse anti-Dref antibody (Hirose et al, 2002). (Secondary antibody used: horse anti-mouse Cy5).

B) Localisation of Mi-2 protein observed in wild type third instar salivary glands was predominantly nuclear when stained with rabbit anti-Mi-2 antibody (Brehm et al, 2000). (Secondary antibody used: goat anti-rabbit Cy5).

Compared to the Dref stained salivary gland (A) the traces of cytoplasmic and cell membrane bound Mi-2 protein (B) observed was cosiderably less.
Blue: DAPI, Red: goat anti rabbit Cy5 and horse anti-mouse Cy5.
Scale bar = 20µm

Figure 5..9. Localisation of anti-Dref and anti-Mi-2 staining in double labelled third instar salivary glands.

A) Wild type (*y, w*) third instar salivary gland double stained with anti-Dref and anti-Mi-2 antibodies. Dref (yellow) is observed solely in the cytoplasm and cell membranes of the salivary gland cells but is observed in the nuclei of the associated fat body. Accumulation of anti-Mi-2 staining is exclusively nuclear (indicated by red Cy5).

B) Salivary gland with UAS-FOXO expressing clone cell (white arrow) along with non adjacent wild type cells. The nucleus of the UAS-FOXO expressing clone cell shows both anti-Mi-2 and anti-Dref staining. Surrounding wild type cells show anti-Mi-2 staining predominantly in the nuclei (red) with traces of cytoplasmic anti-Dref staining (yellow).A higher level of anti-Mi-2 staining was observed in the UAS-FOXO expressing clone cell compared to the surrounding wild type cells.

C) High magnification of (B). Nuclear accumulation of both anti-Mi-2 and anti-Dref staining is observed in the UAS-FOXO expressing clone cell (white arrow). Surrounding wild type cells show anti-Mi-2 staining predominantly in the nuclei (red) with cytoplasmic and cell membrane associated accumulation of anti-Dref staining (yellow). An increased level of anti-Mi-2 staining was observed in the UAS-FOXO expressing clone cell.

Scale Bar = 50µm
Yellow: mouse anti-Dref (Hirose et al, 2002), Red: rabbit anti-Mi-2 (Brehm et al, 2000).
Secondary antibodies:
For Mi-2: goat anti rabbit Cy5, For Dref: goat anti mouse Alexa 555

97

A)

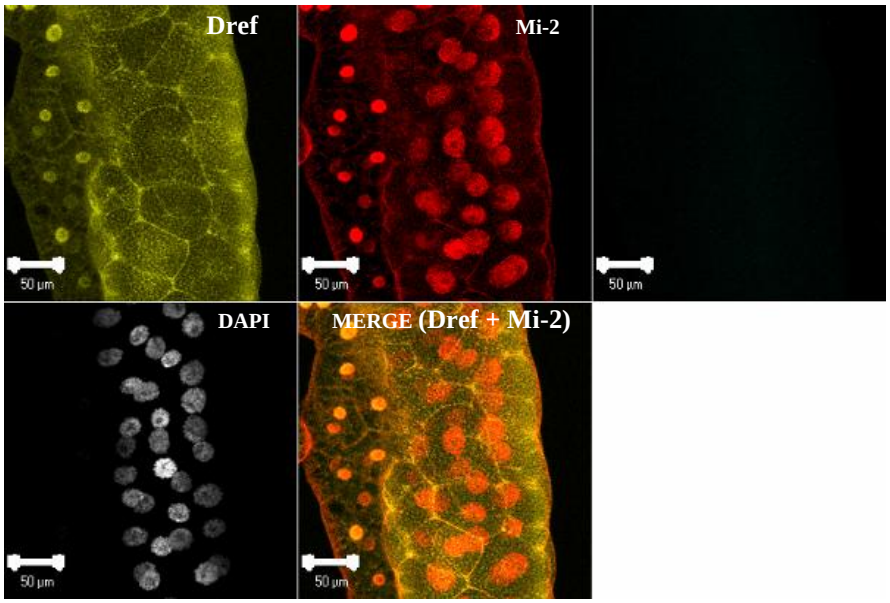
Dref
Mi-2
DAPI
MERGE (Dref + Mi-2)
50 µm

B)

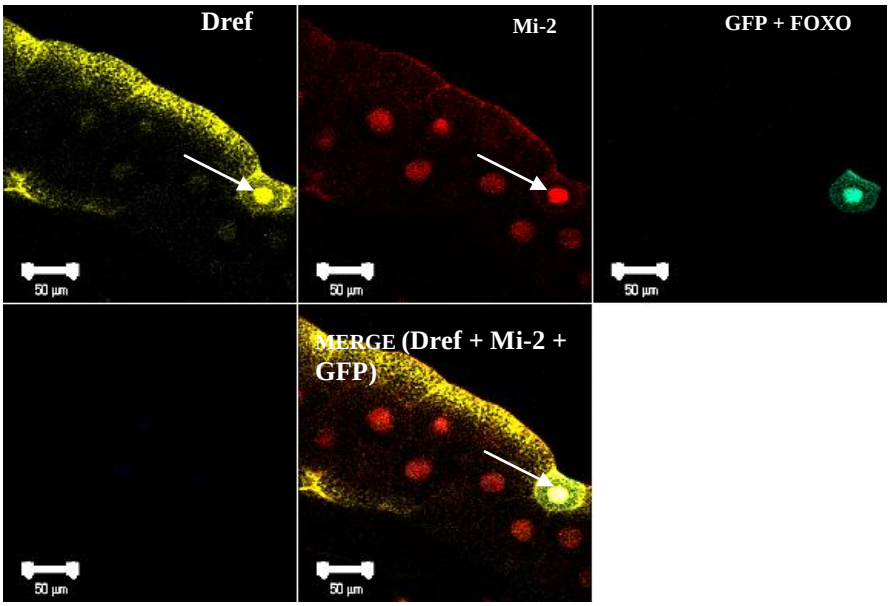
Dref
Mi-2
GFP + FOXO
MERGE (Dref + Mi-2 + GFP)
50 µm

C)

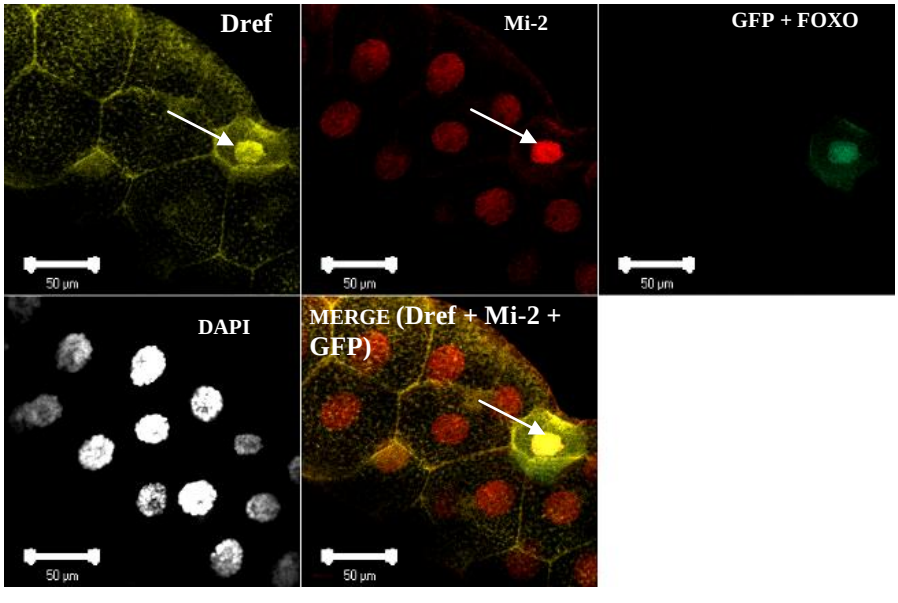
Dref
Mi-2
GFP + FOXO
DAPI
MERGE (Dref + Mi-2 + GFP)
50 µm

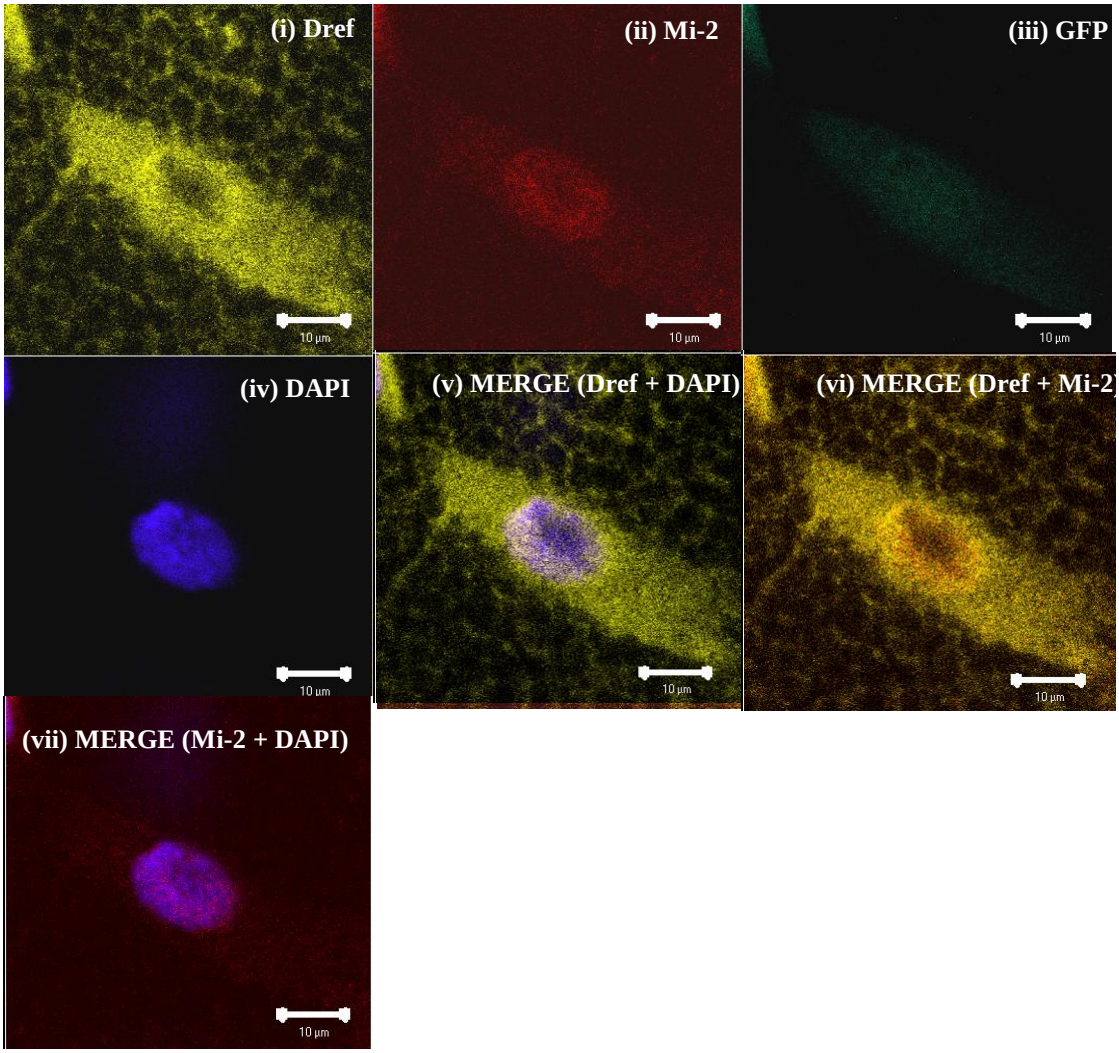

Figure 5.10. High magnification image of single cell clone in salivary gland over expressing FOXO.
marked with iii) GFP (green) and stained with: i) mouse anti-Dref antibody (yellow), ii) rabbit anti-Mi-2 antibody (red), iv) DAPI blue.
Merged images for Dref and DAPI (v), Dref and Mi-2 (vi), and Mi-2 and DAPI (vii).
Secondary antibodies: Alexa 555 goat anti-mouse, Cy5 goat anti-rabbit.
Scale bar = 10µm.

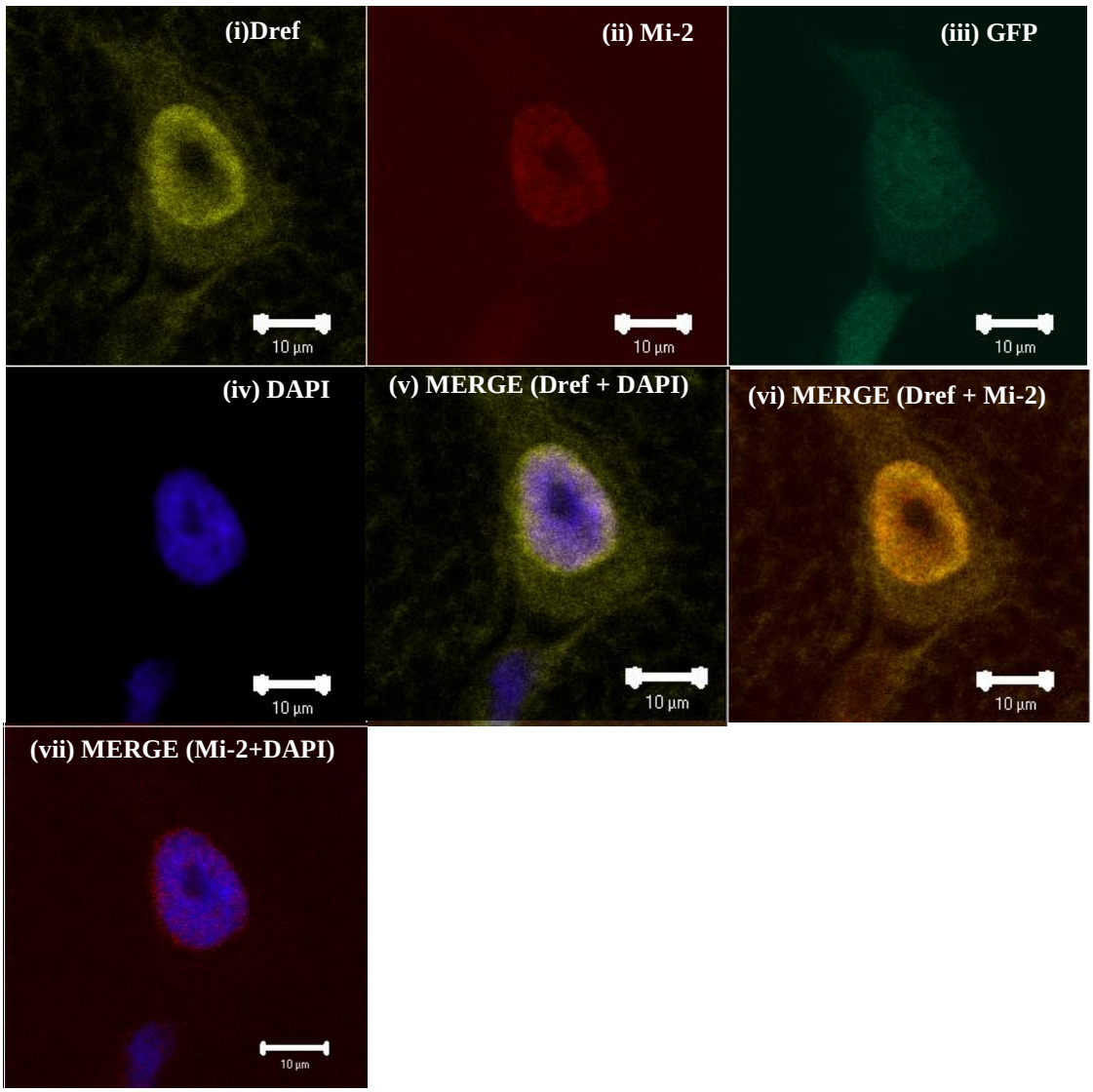

Figure 5.11. High magnification image of single cell clone in salivary gland over expressing FOXO
marked with iii) GFP (green) and stained with: i) mouse anti-Dref antibody (yellow), ii) rabbit anti-Mi-2 antibody (red), iv) DAPI blue.
Merged images for Dref and DAPI (v), Dref and Mi-2 (vi), and Mi-2 and DAPI (vii).
Secondary antibodies: Alexa 555 goat anti-mouse, Cy5 goat anti-rabbit.
Scale bar = 10µm.

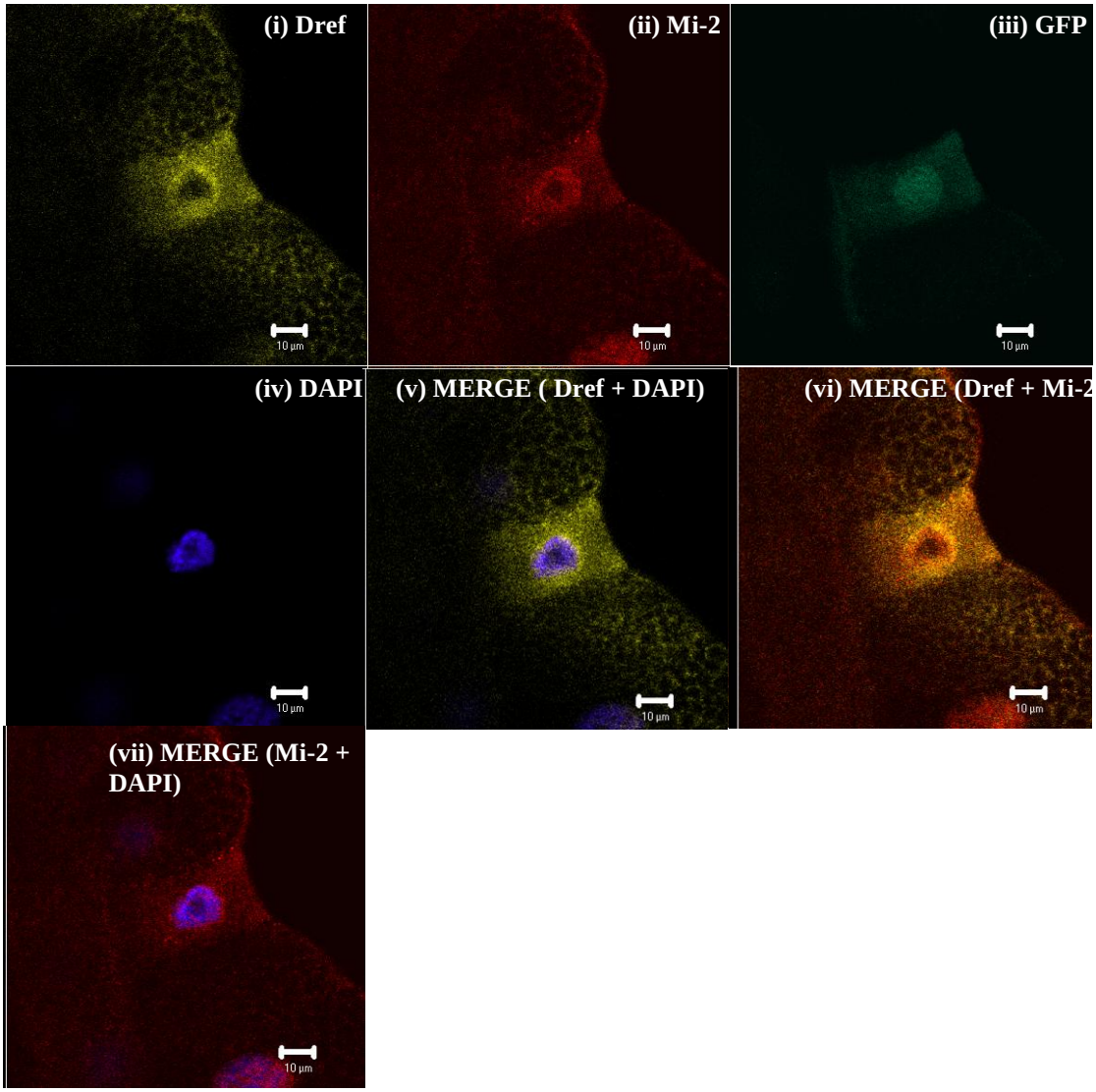

Figure 5.12. High magnification image of single cell clone in salivary gland over expressing FOXO
marked with iii) GFP (green) and stained with: i) mouse anti-Dref antibody (yellow), ii) rabbit anti-Mi-2 antibody (red), iv) DAPI blue.
Merged images for Dref and DAPI (v), Dref and Mi-2 (vi), and Mi-2 and DAPI (vii).
Secondary antibodies: Alexa 555 goat anti-mouse, Cy5 goat anti-rabbit.
Scale bar = 10µm.

5.3. Discussion

5.3.1. FOXO does not noticeably alter Mi-2 localisation

Expression of UAS-FOXO driven by c147-GAL4 in the whole salivary glands of YFP tagged *Mi-2*$^{CPTI-000232}$ animals reduced the size of the salivary glands (Fig 5.2 Bi and Bii). This result coincides with the previous finding that ectopic expression of FOXO and the human FOXO3a results in a reduction of organ size (Junger et al., 2003). The decrease of salivary gland size also agrees with the previous report that FOXO reduces cell size by inhibiting cell proliferation (Kramer et al., 2003). Increased expression of FOXO in the whole salivary glands of YFP tagged Mi-2$^{CPTI-000232}$ does not consistently modify the localisation of the YFP tagged Mi-2 protein (Fig 5.2). However, quantification analysis of these data using the image analysis software velocity, demonstrated a 1.3 fold average increase of YFP tagged Mi-2 expression in UAS-FOXO expressing animals (Section 5.2.1).

No noticeable change in the localisation of Mi-2 protein was observed in the marked UAS-FOXO expressing single cell clones (Fig 5.3). The image analysis software Velocity was used to analyse and calculate the intensity of Mi-2 protein in UAS-FOXO expressing and wild type clone cells compared to Mi-2 levels in surrounding non-clone cells. These data were presented graphically showing the ratio of the average intensity of Mi-2 expression in the clone cell verses that of the non adjoining wild type cells for both the control and experimental genotypes (Fig 5.4). These data reveal that the ratio of the average level of Mi-2 protein in FOXO over expressing clone cells versus the non adjacent wild type does not significantly differ from that of the control genotype (Fig 5.4). Thus, it can be proposed that, the level of Mi-2 protein is not altered by increased levels of FOXO expression. The standard deviations of the data may have been reduced by obtaining data from higher number of salivary glands.

5.3.2. Simj does not alter FOXO mediated reduced sized salivary gland phenotype

It has been reported that expression of FOXO using a hsGAL4 driver results into reduction of body size which was thought to be a consequence of decrease in cell size and cell number (Kramer et al., 2003). Previous findings from the lab also showed that induction of FOXO expression causes a reduction in the size of the salivary gland (Kimber, 2005). Simj, the regulatory component of NuRD complex (Kon et al., 2005) when co-expressed with FOXO, the salivary gland showed a reduced growth phenotype reasonably similar with that of animals expressing only UAS-FOXO (Fig 5.5). These

data suggest that the over expression of Simj cannot enhance or suppress FOXO induced growth arrest.

5.3.3. FOXO does not markedly alter the expression of Dref

The localisation and concentration of Dref protein did not consistently change in FOXO expressing single cell clones as compared with the non adjacent wild type cells (Fig 5.6 B). The intensity of Dref protein these clone cells was analysed using the image analysis software velocity. The ratio of the average amount of Dref protein in clone cells verses that of the non-adjoining wild type cells of was analysed (Fig 5.7). Although the images did not show any consistent change of Dref localisation in FOXO expressing clone cells (Fig 5.6), the quantitative analysis revealed that the ratio of the average intensity of Dref protein in clone cells versus the non adjacent wild type cells of the experimental genotype varied greatly between animals (Fig 5.7). The standard deviation of the data may have been reduced by obtaining data from higher number of salivary glands.

5.3.4. A novel pattern of localisation of Mi-2 and Dref protein was observed in FOXO expressing clone cells

The localisation pattern of anti-Mi-2 staining in both single and double stained wild type salivary glands was observed to be nuclear (Fig 5.8 B and Fig 5.9 A). Along with the nuclear accumulation, some cytoplasmic and cell membrane associated anti-Dref staining was also observed in wild type salivary glands when singly labelled with anti-Dref antibody (Fig 5.8 A). However, wild type salivary glands double stained with anti-Dref and anti-Mi-2 antibodies showed exclusively cytoplasmic anti-Dref staining (without any nuclear labelling) (Fig 5.9 A). Interestingly the anti-Dref mouse monoclonal antibody used in this study was raised against bacterially purified recombinant Dref protein consisting of amino acids 16-608 (Hirose et al., 1996) which overlaps the Mi-2 interacting region of the Dref protein (amino acids 16-145) (Hirose et al., 2002). The existence of an *in vivo* Dref/Mi-2 complex has been reported (Hirose et al., 2002).Therefore, epitope sites of the anti-Dref mouse monoclonal antibody are probably masked in the Dref /Mi-2/anti-Mi-2 antibody complex formed in the double labelled cells. It can be speculated that anti-Dref antibodies can not recognize their own epitope sites on Dref in the Dref /Mi-2/anti-Mi-2 antibody complex formed in the nucleus and hence visualization of Dref protein is not possible in nucleus of the double stained wild type salivary glands (Fig 5.9 A). Unlike the anti-Dref monoclonal antibody,

the anti-Mi-2 polyclonal antibody can recognize its epitope sites and label the nuclear Mi-2 protein. Hence visualization of Mi-2 protein is possible in the nuclei of the double stained wild type salivary glands (Fig 5.9 A). However, as anti-Dref staining was observed in the cytoplasm of the wild type double labelled cells (Fig 5.9 A), it is hypothesized that Mi-2 protein may not form complex with Dref in the cytoplasm or may have a different conformation. This hypothesis does not contradict the evidence showing that localisation of anti-Mi-2 staining is higher in the nucleus than the cytoplasm as shown in singly stained wild type salivary glands (Fig 5.8 B). Hence, in the cytoplasm of the double stained wild type salivary glands, the epitope binding sites of anti-Dref antibody are left unmasked leading to the recognition by anti-Dref antibody (Fig 5.9 A). This same interaction between Mi-2, Dref and anti-Mi-2 antibodies presumably has also occurred in the wild type cells surrounding the UAS-FOXO expressing clones, as the distribution pattern of Dref and Mi-2 staining shown by these cells (Fig 5.9 B and C) is reasonably similar with that of the double stained wild type salivary gland cells (Fig 5.9 A).

Interestingly high levels of both anti-Dref and anti-Mi-2 staining were observed in the nuclei of double stained UAS-FOXO expressing clone cells (Fig 5.9 B and C, Fig 5.10, Fig 5.11, Fig 5.12). The level of anti-Mi-2 staining was increased in some double stained UAS-FOXO expressing clones (Fig 5.9 B and C, Fig 5.10 ii, Fig 5.12 ii). However, this alteration in anti-Mi-2 staining was not consistently observed in all double stained UAS-FOXO expressing clones (Fig 5.11 ii), which supports the previous quantitative analysis data acquired from UAS-FOXO expressing clones singly stained with anti-Mi-2 antibody (Section 5.2.2, Fig 5.4). Anti-Mi-2 staining in double stained UAS-FOXO expressing single cell clones was sometimes, nucleoplasmic (Fig 5.10 vii) but mostly perinuclear (Fig 5.11 vii, 5.12 vii). Some cytoplasmic anti-Dref staining was observed in FOXO expressing clone cells (Fig 5.10 i, Fig 5.11 i, Fig 5.12 i). However, anti-Dref staining was also found to be nuclear membrane associated and perinuclear (Fig 5.10 vi, Fig 5.11 vi, Fig 5.12 vi). The fact that this perinuclear distribution of Dref staining (Fig 5.10 vi, Fig 5.11 vi, Fig 5.12 vi) was not seen in wild type cells and *NOS2* expressing clone cells when singly stained with anti-Dref antibody (Section 4.2.5, Fig 4.8.ii. A and B) suggests, this localisation pattern of Dref protein is uniquely mediated by FOXO. This distinct localisation of anti-Dref staining in UAS-FOXO expressing clone cells (Fig 5.10 vi, Fig 5.11 vi, Fig 5.12 vi) can be analysed from the perspective of the previously reported functional relationships between FOXO, *myc* and Dref.

The presence of a functional Myc binding site (5′-CACGTG canonical E-box) between -78 to -73 nucleotide sequences of the *Dref* promoter suggests that *Dref* is a target of Myc (Dang Thi Phuong Thao, 2007). Myc induces cell growth by promoting G1/S progression (Johnston et al., 1999). The absence of *myc* represses cellular growth and reduces the size of wing cells (Johnston et al., 1999). This growth arrest, coupled with a reduction of organ size, was also observed when a N-terminal Dref fragment (Dref $_{1\text{-}125}$) was expressed in salivary glands. This fragment was shown to inhibit the transcriptional regulatory activity of wild type Dref in a dominant negative manner (Hirose et al., 1999). Dref is known to regulate the transcription of several cell proliferation related genes (Matsukage et al., 2008) and Myc functions in the regulation of normal growth (Johnston et al., 1999).

A decrease in the transcription of *Dref* was found in dm^4/y hemizygous mutants of *myc*, which suggests that Myc is essential for normal *Dref* gene expression (Dang Thi Phuong Thao, 2007). Therefore, Myc may regulate its target genes via the DRE/Dref pathway (Dang Thi Phuong Thao, 2007).

Myc has been identified as a target of FOXO, as *myc* mRNA levels are controlled by FOXO in a tissue specific manner and FOXO can inhibit or increase *myc* expression (Teleman et al., 2008).

All these reports suggest a direct or indirect functional link between FOXO and *myc* and a functional relationship between Myc and *Dref*. These links may explain the unique localisation of Dref protein observed in FOXO expressing clones in the present study (Fig 5.10 vi, Fig 5.11 vi, Fig 5.12 vi). The tendency of Dref protein to localize in the perinuclear space and in the cytoplasm observed in FOXO expressing clones (Fig 5.10 vi, Fig 5.11 vi, Fig 5.12 vi) may be a result of high levels synthesis of Dref protein, induced by FOXO via a Myc dependent pathway.

The perinuclear distribution of anti-Mi-2 staining observed in UAS-FOXO expressing clone cells (Fig 5.11 vii, Fig 5.12 vii) was also observed in wild type cells and *NOS2* expressing clone cells when those were stained with anti-Mi-2 antibody (Section 4.2.3, Fig 4.5.ii. A and B). Therefore, there is no evidence that FOXO induces any change in Mi-2 expression or localisation.

Chapter 6: Interaction between Simj, Mi-2 and Dref

6.1. Introduction

6.1.1. The functional link between Simj and Mi-2/NuRD

Mi-2, a member of Snf2 family of ATPases, promotes chromatin remodelling by ATP hydrolysis (Brehm et al., 2000). The evolutionary conserved, SWI family ATP dependent chromatin remodelling complexes (SWI/SNF, ISWI, CHD and IN080) are reported to be required for the normal development of embryos and play several other developmental roles such as telomere regulation, chromosome segregation, DNA replication during cell division (Crabtree, 2010) and maintenance of higher order X chromosome structure in *Drosophila* (Renate Deuring et al., 2000). ATP dependent chromatin remodelling enzymes control chromatin structure and play several cell specific roles during development (Crabtree, 2010). The ATP hydrolysis driven chromatin regulating activity of Mi-2 is physically linked with the deacetylase enzyme complex in a multi subunit histone deacetylase complex, purified from *Xenopus laevis* (Wade et al., 1998). Therefore, Mi-2 is a part of NuRD (Yi Zhang et al., 1998), NURD (Xue et al., 1998) or NRD (Tong et al., 1998) complex which is known to couple histone decaetylase and chromatin remodelling ATPase activity (Wade, 2007).

A confocal microscopic study reported that the MBD2/3 associated mammalian Simj protein family members (66kDa) are involved in DNA methylation mediated transcriptional repression (Brackertz et al., 2002). Interestingly, Mi-2/NuRD achieves gene silencing through DNA methylation (Zhang et al., 1999). Simj which is a zinc-finger containing protein acts as a functional link between Mi-2/NuRD and methylated DNA binding proteins MBD2 and MBD3, for methylation mediated gene silencing and hence acts as a regulatory component of NuRD (Kon et al., 2005). Therefore, these data suggest that the two core NuRD components Simj and Mi-2 share a common functional sphere of DNA methylation. Considering this relationship between Simj and Mi-2, the experiments of this chapter were designed to determine the effect of Simj on Mi-2 expression. The response of Mi-2 in both Simj up regulated and down regulated third instar larvae would be determined.

6.1.1.1. Use of Simj up regulated system

To achieve high expression of Simj, GFP tagged UAS-simj cDNA containing flies (Kim et al., 2004) were used. These flies were generated by constructing *UAS-simj* vector, containing a 2.7-kb *simj* cDNA fused to the *GFP* coding sequence (Kim et al., 2004). Over expression of GFP tagged UAS-simj would be induced by exploiting the UAS/GAL4 technique (Section 2.1.2). The salivary gland specific c147-GAL4 driver would be used to over express the GFP tagged UAS-simj gene in the whole salivary glands of third instar larvae. UAS-simj-GFP would be over expressed in single cells of salivary glands using FRT/Flp technique (Described in Section 4.1.4) followed by anti-Mi-2 staining of these single cells to determine response of endogenous Mi-2 to the up regulation of Simj levels.

6.1.1.2. Use of Simj down regulated system

Reduction of Simj expression was achieved by generating *simj* transheterozygous mutants. Two different *simj* alleles used in this study, were supplied by Bloomington stock centre.

One of these mutant lines (Flybase id FB2010_02, genotype: P{ry[+t7.2]=PZ}simj[01814] ry[506]/TM3, ry[RK] Sb[1] Ser[1]) carries an insertion of *P{PZ}* (Bellen et al., 2004) in a plus orientation at 10667498 location of 3L chromosome in the first intron of *simj*.

The other mutant line (Flybase id FB2010_02, genotype: w[1118]; P{w[+mGT]=GT1}simj[BG00403]/TM6B, P{w[+mC]=35UZ}DB1, Tb[1]) carries an insertion of P{GT1}(Lukacsovich et al., 2001) in a minus orientation at 10672162 position of 3L chromosome in the first intron of *simj*.

6.1.2. The functional link between Simj, Mi-2 and Dref

Drosophila Dref functions as a transcription regulatory factor (Hirose et al., 1996). A reduction in salivary gland size and endoreplication was observed with the expression of N-terminal Dref fragment (Dref $_{1-125}$). This fragment was shown to inhibit transcriptional regulatory activity of wild type Dref in a dominant negative manner. This suggested the requirement of Dref for DNA replication, cell proliferation, and differentiation leading to proper development (Hirose et al., 1999).

NuRD associated Simj is known to control development through the regulation of ecdysone-responsive genes in *Drosophila* (Kon et al., 2005). These reports suggest that

a common functional link (regulation of development) exists between Simj and Dref. Thus it was decided to determine the effect of Simj on the localisation of Dref.
Mi-2 has been revealed to negatively regulate Dref activity by preventing Dref-DNA binding (Hirose et al., 2002). As Dref function is under the negative control of Mi-2 (Hirose et al., 2002), it would be interesting to find out how Dref would respond both in up and down regulated Mi-2 flies.

6.1.3. How Simj affects either of the proteins when Mi-2/Dref complex is disrupted?

The *in vivo* existence of a Mi-2/Dref complex has been reported (Hirose et al., 2002). The present study has revealed a novel function of NOS in the probable disruption of the *in vivo* Mi-2/Dref complex (discussed in Section 4.3.5). The experiments of this chapter would also focus on the investigation of the effect of Simj on both of the proteins after the potential disruption of the Mi-2/Dref complex by NOS.

6.2. Results

6.2.1. Localisation of Dref protein in the whole salivary glands over expressing Mi-2

The aim of this experiment was to visualize the localisation of Dref protein in larvae expressing high levels of Mi-2. Induction of Mi-2 expression was achieved by crossing UAS-Mi-2 carrying flies (Hirose et al., 2002) with c147-GAL4 containing flies. The salivary glands of these third instar larvae were then stained with mouse monoclonal anti-Dref antibody (Hirose et al., 2002). Control flies were generated by crossing wild type flies with c147-GAL4.

Confocal images of anti-Dref antibody stained salivary glands dissected from 10 different experimental and control animals, were analysed. However, no consistent change in the Dref protein distribution was observed in the experimental salivary glands when compared with their corresponding control samples. Some UAS-Mi-2 expressing flies showed more intense localisation of Dref protein in the nucleus (Fig 6.1 Bi and Bii) whereas others did not show any noticeable changes in Dref localisation (Fig 6.1 Biii) when compared with the corresponding control flies (Fig 6.1 Aiii).

Figure 6.1. Dref localisation in the nuclei of salivary glands from wild type and UAS-Mi-2 expressing larvae

Salivary glands from A) wild type B) UAS-Mi-2 expressing third instar larvae.

Ai) Dref protein associated with the nuclei of salivary glands of a third instar wild type larva.
Bi) Dref protein associated with the nuclei of salivary glands of a third instar larva over expressing Mi-2.
Scale Bar = 20 µm, Images acquired and processed using identical settings.

Aii) High magnification image of the nucleus of control (wild type) salivary gland showing anti-Dref staining within the nucleus.
Bii) High magnification image of the nucleus of Mi-2 expressing salivary gland showing more intense staining of Dref protein in the nucleus and possibly in the polytene chromosomes, as compared to that of control larva.
Scale Bar= 10 µm, Images acquired and processed using identical settings.

Aiii) Dref protein associated with the nuclei of salivary glands from a third instar wild type larva.
Biii) Dref protein associated with the nuclei of salivary glands from a third instar larva over expressing Mi-2. This larva did not show any obvious change in Dref expression as compared with the control sample (Aiii).
Scale Bar= 20 µm.
All images acquired and processed using identical settings.
Red: mouse anti-Dref antibody (Hirose et al, 2002).
Secondary antibody used: Horse anti-mouse Cy5.

Genotype of Ai) Aii) Aiii): *y,w* / + ; c147-GAL4 / + ; + / +
Genotype of Bi) Bii) Biii): UAS-Mi-2 ; c147-GAL4

110

Ai)

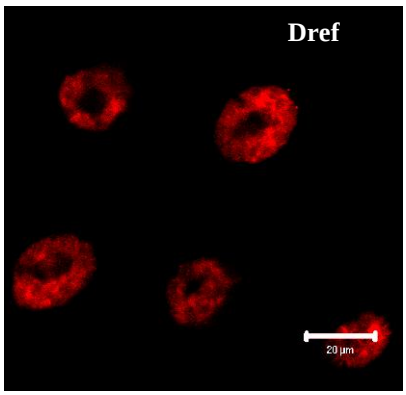

Bi)

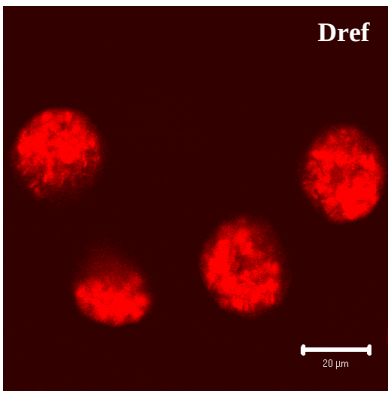

Aii)

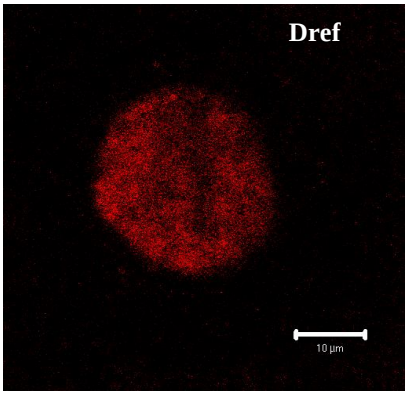

Bii)

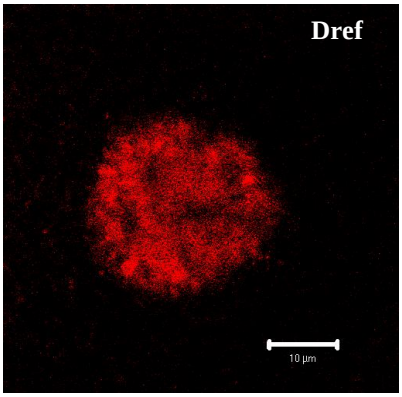

Aiii)

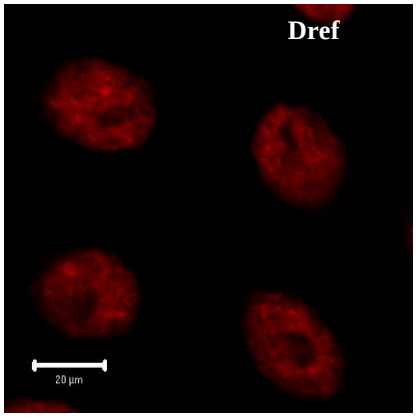

Biii)

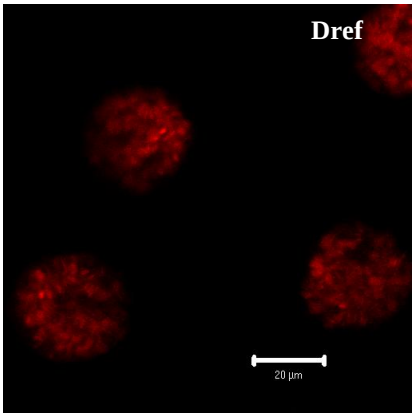

6.2.2. Expression of Dref protein in whole salivary glands of *Mi-2* transheterozygous mutants

Expression of Dref protein in Mi-2 down regulated flies was examined in this experiment.

Salivary glands of *Mi-2* transheterozygous third instar larvae (Discussed in section 4.1.5.2) were stained with anti-Dref antibodies and were used as the experimental samples for this experiment. These larvae showed very low levels of Mi-2 protein (Fig 4.1.3). Control flies were generated as in section 6.2.1, processed and imaged in parallel under identical conditions.

Confocal images of anti-Dref antibody stained salivary glands dissected from 10 different experimental and control animals were analysed. Salivary glands of *Mi-2* transheterozygous third instar larvae showed higher accumulation of nuclear Dref protein (Fig 6.2 B) compared with that of the control larvae (Fig 6.2 A).

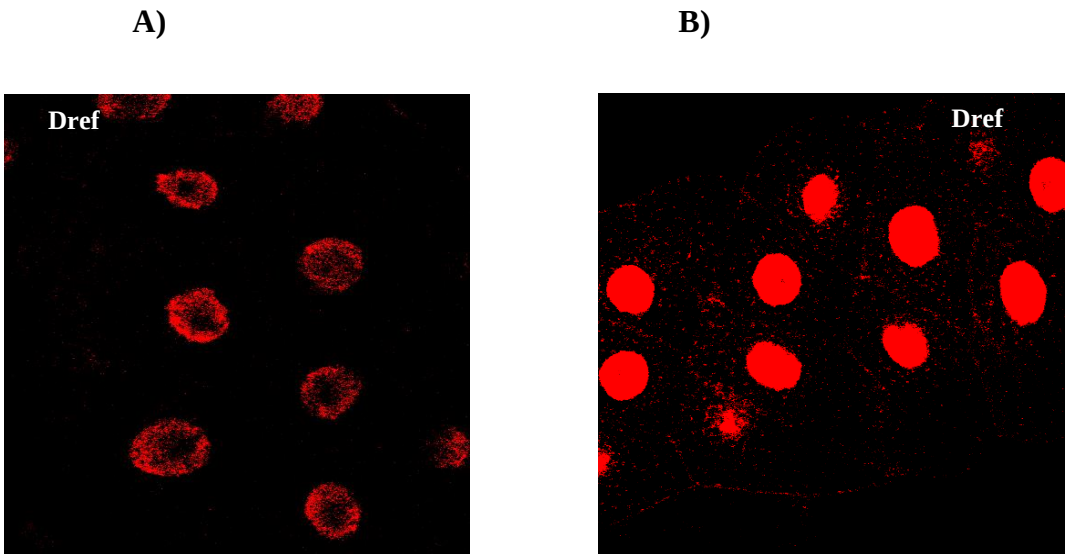

Figure 6.2. Expression of Dref protein in the salivary gland nuclei of wild type and *Mi-2* transheterozygous mutants.

A) Control third instar larvae stained with anti-Dref antibody.
Genotype: *y,w* / + ; c147-GAL4 / + ; + / +

B) Salivary gland of third instar larvae from *Mi-2* transheterozygous mutants showed higher accumulation of Dref in the nucleus compared to that of wild type larvae.
Genotype: $\underline{Mi\text{-}2^{j3D4}}$/ $\underline{Mi\text{-}2^{EY08138}}$ $\underline{Su(Tpl)^{EY08138}}$

Images acquired and processed using identical settings
Red: mouse anti-Dref antibody (Hirose et al, 2002).
Secondary antibody used: Horse anti-mouse Cy5.

6.2.3. Analysis of the phenotypic effect of Simj expression on salivary gland size

simj has been reported to play several developmental roles (discussed in section 6.1.1). Therefore, the phenotypic effect of *simj* over expression on salivary gland size was determined. To achieve this, GFP tagged UAS-simj containing flies (Kim et al., 2004) (described in 6.1.1.1) were used. Induction of GFP tagged UAS-simj expression was accomplished in the whole salivary glands by the c147-GAL4 driver. Two different control samples were used:

Third instar larvae of UAS-simj-GFP animals in which *simj* expression was not induced by GAL4 and third instar larvae of wild type (*y, w*) animals. Surprisingly larvae carrying UAS-simj-GFP showed low levels of GFP (and thus presumably low levels of ectopic Simj expression) in the absence of GAL4 (Fig 6.5 Aii). The experimental and control third instar salivary glands were stained with DAPI and were imaged on Zeiss AxioPhot Microscope at 40x.

The average size of DAPI stained nuclei of c147 driven UAS-*simj* larvae was found to be smaller than that of the larvae where expression of UAS-*simj* was not driven (Fig 6.3, genotype: *simj*). The salivary gland nuclei of wild type larvae were shown to be the largest in size (Fig 6.3, genotype: *WT*). The analysis shows a substantial change in the average nuclei size among these three genotypes. A one-way ANOVA analysis of the three genotypes revealed statistical significant differences among all three genotypes (Fig. 6.3). A post hoc Tukey analysis shows the difference in nuclear size between Simj and wild type, c147 driven Simj and wild type, and Simj and c147 driven Simj animals.

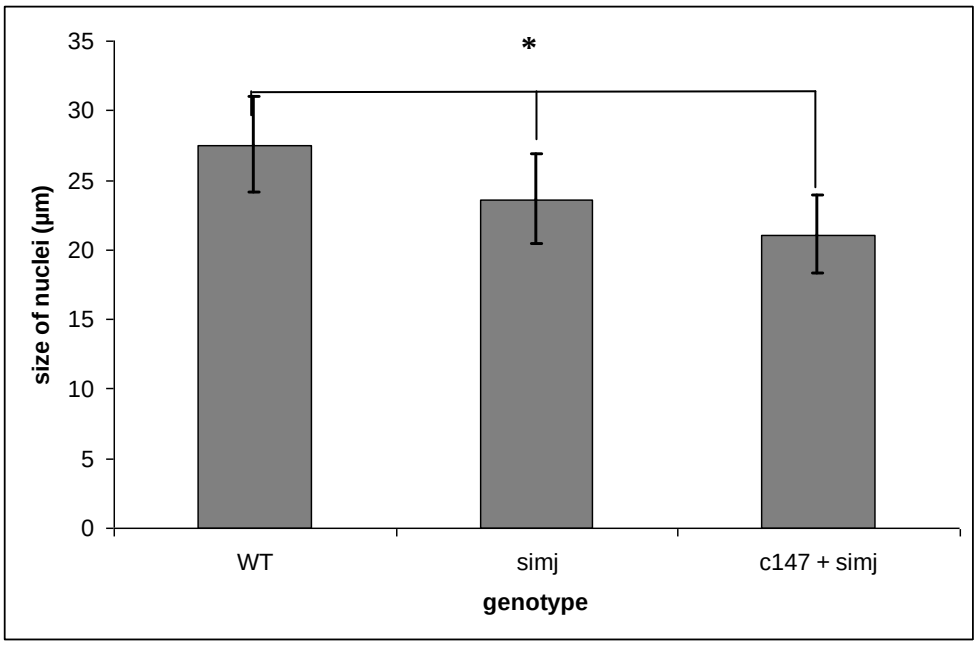

Figure 6.3. Average size of DAPI stained larval salivary gland nuclei

WT* Genotype: y,w* ; **+/+; +/+.**

***Simj*: Genotype:** UAS-simj-GFP / + ; +/+ ; +/+

c147 + *simj*: Genotype: UAS-simj-GFP / + ; c147/+ ; +/+
Data was derived approximately from 120 DAPI stained nuclei from 30 different salivary glands of 30 different female animals of each of the above genotypes. Data from images acquired and processed using Zeiss AxioPhot Microscope with 40x objective. * indicates $P<0.05$, n=90 -144, error bars indicate standard deviation. n represents number of nuclei.
Raw data available in Appendix No: B.8

6.2.4. Analysis of the phenotypic effect of Simj over expression on the whole organism

This experiment was designed to study the effect of inducing *simj* over expression in the whole animal. UAS-simj-GFP expression was induced ubiquitously by the Tub-GAL4 driver. Simultaneously wild type flies were also crossed with Tub-GAL4 driver as controls.

Third instar salivary glands of both the experimental and control progeny were stained with DAPI and were imaged on the confocal microscope. The third instar larvae of Tub-GAL4 driven UAS-simj flies appeared to be sick (data not shown). No adults from these larvae were recovered. The salivary glands of these third instar larvae were radically reduced in size to control larvae (Fig 6.4).

A) **B)**

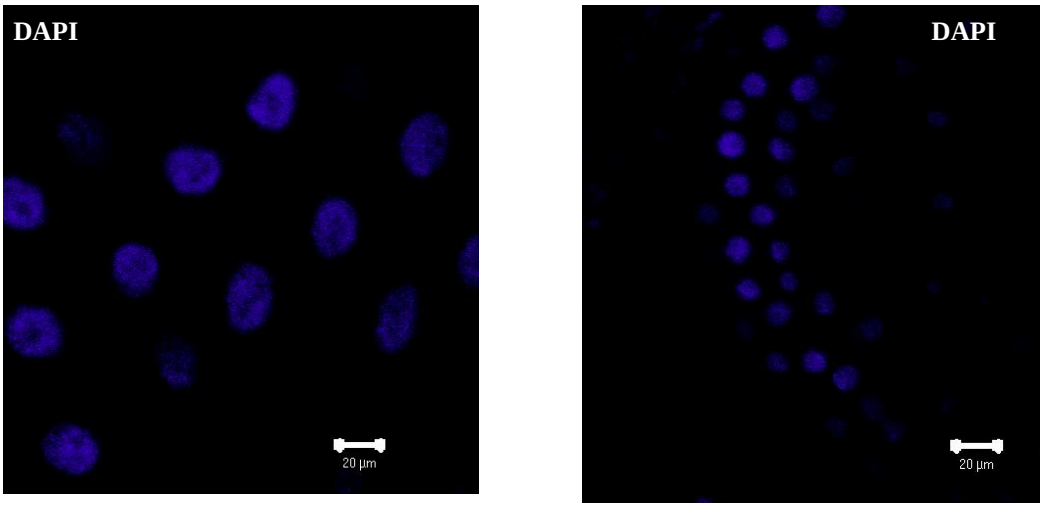

Figure 6.4. DAPI stained nuclei of salivary glands from Tub-GAL4 driven UAS-simj and wild type third instar.
A) DAPI stained salivary gland of wild type third instar larvae.
Genotype: *y*, *w* / +; +/+; Tub-GAL4/+
B) DAPI stained salivary gland nuclei of Tub-GAL4 driven UAS-simj larvae showed a drastic reduction in size.
Genotype: UAS-simj / +; Tub-GAL4/+
Images acquired and processed using identical settings
Blue: DAPI.
Scale bar = 20 µm.

6.2.5. Analysis of expression of Mi-2 protein in the salivary glands of larvae with different levels of Simj expression

The aim of this experiment was to study the response of Mi-2 in third instar salivary glands to different levels of Simj expression. To achieve this, localisation of endogenous Mi-2 protein was examined both in Simj up regulated and Simj down regulated animals.

Up regulation of Simj in whole salivary glands was achieved by inducing GFP tagged UAS-simj expression with the c147-GAL4 driver as described in section 6.2.3.

A reduction in the amount of endogenous Simj was achieved using the allelic combination of *simj* described in 6.1.1.2. It was important to identify the transheterozygous *simj* animals at their larval stage. Each allele was balanced over TM6B to allow identification of non-balancer larvae. Both the mutants carrying TM6B balancer were maintained as two separate stocks. When kept as separate stocks no non-Tubby larvae were observed in either of the mutant stocks. Non-Tubby third instars were recovered when the mutant stocks balanced with TM6B, were crossed with each other. The heteroallelic combination of *simj* alleles used, allowed the recovery of third instar larvae. However third instar larvae containing this allelic combination of *simj* were extremely unhealthy (data not shown).

Third instar larvae of wild type flies were used as one control genotype. Third instar larvae of animals containing UAS-simj but no GAL4 driver were used as another control sample. Surprisingly, these flies carrying UAS-simj-GFP showed some non GAL4 dependent expression of simj-GFP (as judged by GFP expression) (Fig 6.5Aii) and thus presumably have higher levels of Simj than wild type animals. c147-GAL4 driven expression of UAS-simj-GFP produced larvae expressing high levels of Simj in their salivary glands (Fig 6.5Aiii). Therefore, four different genotypes each expressing different levels of Simj were used.

These were: $simj^{01814}$ / $simj^{BG00403}$, wild type, UAS-simj-GFP and UAS-simj-GFP; c147GAL4. Although, immunohistochemistry with an anti-simj antibody in third instar salivary glands of *simj* transheterozygous mutants was unsuccessful (data not shown), it was assumed that this *simj* allelic combination would contain the lowest level of endogenous Simj among these four genotypes.

Salivary glands of all these four genotypes were stained with rabbit anti-Mi-2 antibody (Brehm et al., 2000).

Salivary gland of wild type larvae showed maximal levels of Mi-2 protein (Fig 6.5 Bi). Salivary glands of UAS-simj-GFP containing flies but not driven by GAL4 showed lower levels of GFP tagged *simj* (Fig 6.5 Aii, image taken at 24% laser excitation) compared to c147-GAL4 driven UAS-simj-GFP larva (Fig 6.5 Aiii, image taken at 0.1% laser excitation). The level of Mi-2 expression of UAS-simj-GFP containing larvae (Fig 6.5 Bii) was similar to that of the wild type salivary glands (Fig 6.5 Bi). The amount of Mi-2 protein was noticeably reduced in the salivary glands of c147 driven UAS-simj-GFP larvae (Fig 6.5 Biii) which showed high content of Simj expression (Fig 6.5 Aiii). It was assumed that the transheterozygous *simj* animals (described above) and the c147 driven UAS-simj-GFP expressing larvae would contain the least and highest amount of Simj protein respectively. As the content of Mi-2 protein was observed to decrease with increased levels of Simj (Fig 6.5 Biii), it was expected that the *simj* mutants would show an increase in the level of Mi-2 compared to the c147 driven UAS-simj-GFP larvae. Unexpectedly most *simj* mutants showed lower levels of Mi-2 (Fig, 6.6 Ai and Bi). In some *simj* transheterozygous mutants, the level of Mi-2 was not noticeably different to wild type (Fig 6.6 Aii and Bii).

Figure 6.5. Mi-2 expression in salivary glands of wild type and larvae expressing different levels of simj.

Ai) Salivary gland of wild type third instar larva, did not show any GFP expression (image acquired at 24% laser excitation).
(Bi) wild type salivary gland stained with anti-Mi-2 antibody.
Genotype: *y, w*; +/+; +/+

Aii) Salivary gland of UAS-simj-GFP containing third instar larva (expression not driven by GAL4) showed low levels of GFP tagged simj expression (image acquired at 24% laser excitation).
(Bii) Staining with anti-Mi-2 of this genotype showed no noticeable difference compared to the wild type (compare to Bi).
Genotype: UAS-simj-GFP / +; + / +; + / +

Aiii) Elevated levels of GFP tagged Simj protein was found when UAS-simj-GFP expression was driven by c147-GAL4 (image acquired at 0.1% laser excitation).
(Biii) anti-Mi-2 staining showed lower levels of Mi-2 compared to the other two genotypes (Compare with Bi and Bii).
Genotype: UAS-simj-GFP / + ; c147-GAL4 / + ; + / +

Red: rabbit anti-Mi-2 antibody (Brehm et al 2000), Blue: DAPI, Green: GFP
Scale bar = 50 µm.
Images (Bi), (Bii) and (Biii) were acquired and processed using identical settings.

120

Ai)

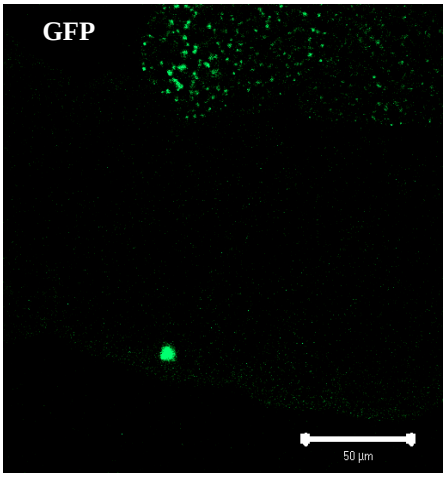

(Bi)

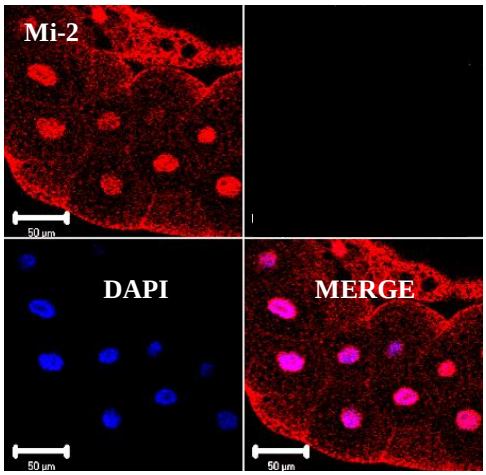

Aii)

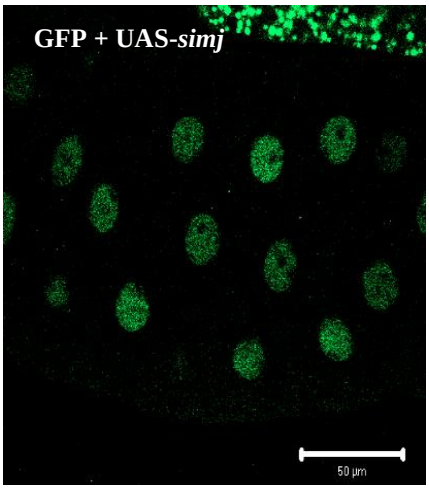

Bii)

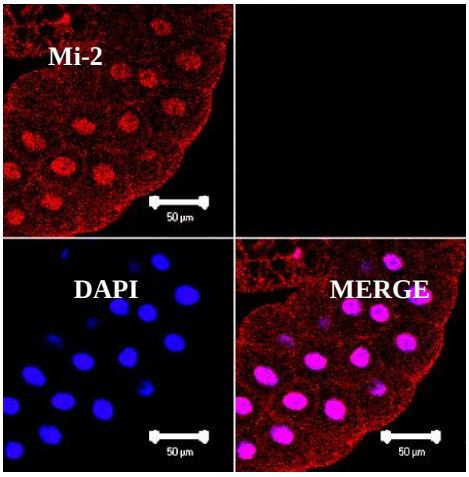

Aiii)

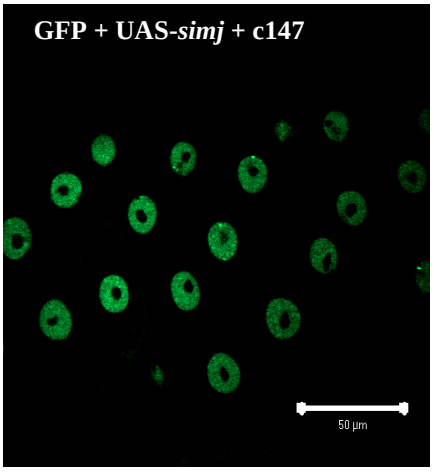

(Biii)

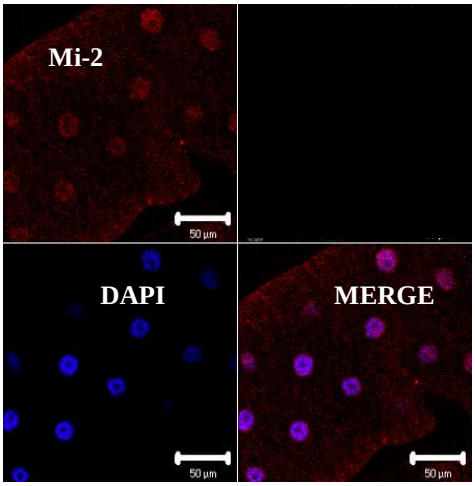

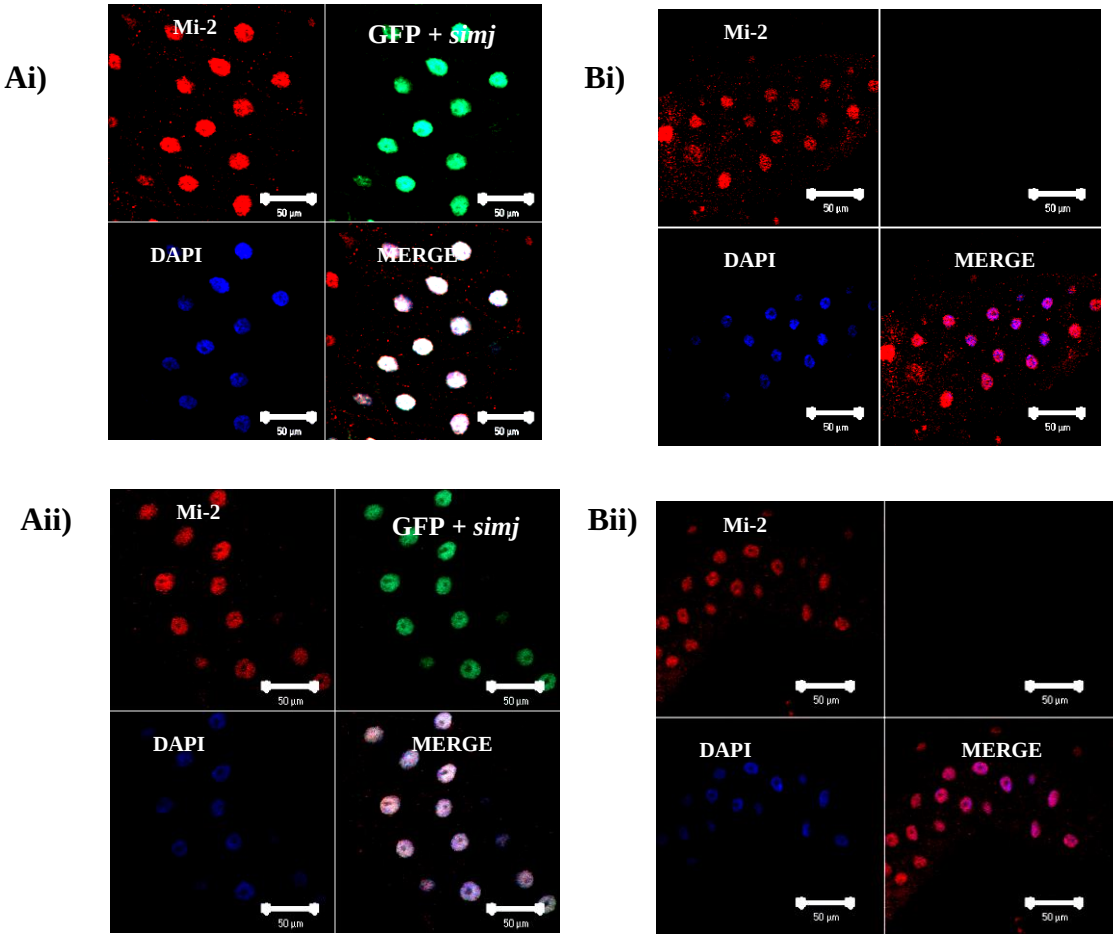

Figure 6.6. Expression of Mi-2 protein in animals expressing high levels of exogenous simj and *simj* transheterozygous mutants

Ai) Mi-2 expression in c147 driven UAS-simj-GFP salivary gland.
Bi) Mi-2 expression in *simj* transheterozygous mutant (showing lower levels of Mi-2 protein compared to Ai).
Images undertaken and processed using identical settings.

Aii) Mi-2 expression in c147 driven UAS-simj-GFP salivary gland.
Bii) Mi-2 expression in *simj* transheterozygous mutant (showing approximately similar levels of Mi-2 protein compared to Aii).
Images undertaken and processed using identical settings.

Genotype of Ai and Aii: UAS-simj-GFP / +; c147-GAL4 / + ; + / +.
Genotype of Bi and Bii: + / +; + / +; *P{PZ}simj*^{01814} *ry*^{506} / *P{GT1}simj*^{BG00403}
Red: rabbit anti-Mi-2 antibody (Brehm et al 2000), Blue: DAPI, Green: GFP
Scale bar = 50 µm.

6.2.6. Effect of Simj expression on Mi-2 localisation in single cell clones

The existence of a Mi-2/Dref complex (Hirose et al., 2002) has been confirmed *in vivo* by the results of this study (Section 4.3.5). The aim of this experiment was to determine the effect of Simj expression on Mi-2/Dref complex. Using the Flp/FRT technique, expression of UAS-simj-GFP was induced in the single cell clones in a similar way as described in Section 4.2.2. These clones were stained with anti-Mi-2 antibody to study the response of Mi- in the Mi-2/Dref complex to Simj expression.

A novel function of NOS in the disruption of Mi-2/Dref complex has been revealed by the present investigation (Section 4.3.5). Therefore it was decided to study the effect of Simj expression on both of the proteins after the disruption of the Mi-2/Dref complex by NOS. Simultaneous expression of UAS-NOS2 and UAS-simj-GFP in single cell clones was achieved using the Flp/FRT technique similar to section 4.2.2, to induce disruption of Mi-2/Dref complex. These clones were stained with anti-Mi-2 antibodies to examine the response of Mi-2 to simj over expression, when the *in vivo* Mi-2/Dref complex is disrupted by NOS.

Cells from salivary glands from four different genotypes were stained with the rabbit anti-Mi-2 antibody: wild type (Fig 6.7 A), UAS-simj-GFP expressing clones (Fig 6.7 C), clones simultaneously expressing UAS-NOS2 and UAS-simj-GFP (Fig 6.7 D) and UAS-NOS2 expressing clones (as in Section 4.2.3) (Fig 6.7 B). Confocal images were acquired of salivary glands from 10 different animals of each genotype.

As described previously (Section 4.2.3) the distribution of Mi-2 in wild type salivary gland cells was found to be mainly nucleoplasmic however low levels of Mi-2 were also found in the nucleolus (Fig 6.7 A). Cells expressing *NOS2* showed a uniform distribution of Mi-2 in the nucleoplasm as well as in the nucleolus (Fig 6.7 B and section 4.2.3). However clone cells expressing either *simj* alone or *simj* and *NOS2* simultaneously showed a markedly non-nucleolar distribution of Mi-2 (Fig 6.7 C and D).

A quantitative examination of the levels of Mi-2 in single cells of all four genotypes was performed using the image analysis software velocity. For the quantitative analysis, wild type GFP marked clone cells, (neither expressing UAS-NOS2 nor UAS-simj-GFP) as described in section 4.2.3 were used as controls. For each genotype the intensity of nuclear staining of Mi-2 protein in the clone cells was compared to that of 10 non adjacent wild type cells of that particular salivary gland (Fig 6.8).

The average ratio of Mi-2 levels in clone cells verses the non adjacent wild type cells was found to be similar in wild type controls, in those expressing *simj* only and in those co expressing *simj* and *NOS2* (Fig 6.8). However the average ratio of Mi-2 expression in *NOS2* only expressing clone cells verses the non adjoining wild type cells was found to be higher (Fig 6.8).

Figure 6.7: Distinctly non-nucleolar localisation of Mi-2 protein in clone cells over expressing *simj* alone or co-expressing *simj* and *NOS2*.

Clones were generated using a 4min heat shock at 38^{o}C between 24- 48hr AEL

A) Salivary gland of wild type third instar larva stained with anti-Mi-2 antibody. Image shows nucleoplasmic distribution of Mi-2 protein. Low levels of Mi-2 protein can be seen in the nucleolus (marked with white arrow).
Genotype: *y,w* ; + / + ; + / +

B) *NOS2* only expressing clone cell stained with anti-Mi-2 antibody shows uniform distribution of Mi-2 protein both in nucleoplasm and in nucleolus (nucleolus is marked with white arrow)
Genotype: hsFLP / UAS-NOS2; Act5c>y^{+}>Gal4; UAS-GFP.

C) Mi-2 is absent from the nucleolus in UAS-simj-GFP expressing clone cell (nucleolus is marked with white arrow).
Genotype: UAS-simj / +; UAS-mRFP / + ; MKRS, hsFLP / Act5c>y^{+}>Gal4

D) Mi-2 protein in a UAS-simj-GFP and UAS-NOS2 co-expressing clone cell is absent from the nucleolus (white arrow).
Genotype: UAS-simj-GFP / UAS-NOS2; UAS-mRFP / + ; MKRS, hsFLP / Act5c>y^{+}>Gal4

Blue: DAPI, Green: GFP, Red: rabbit anti-Mi-2 antibody (Brehm et al, 2000) (Secondary antibody used: goat anti-rabbit Cy5).
Scale Bar = 50 µm.

125

A)

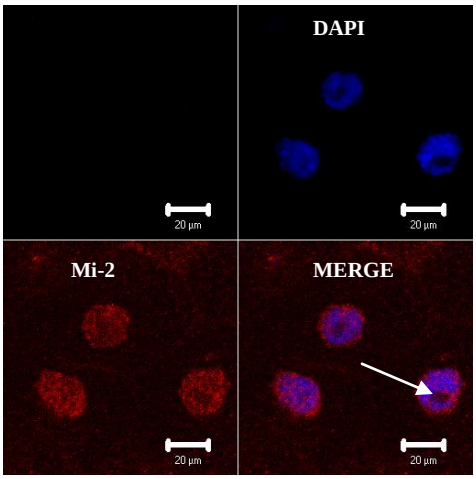
DAPI
Mi-2
MERGE
20 µm

B)

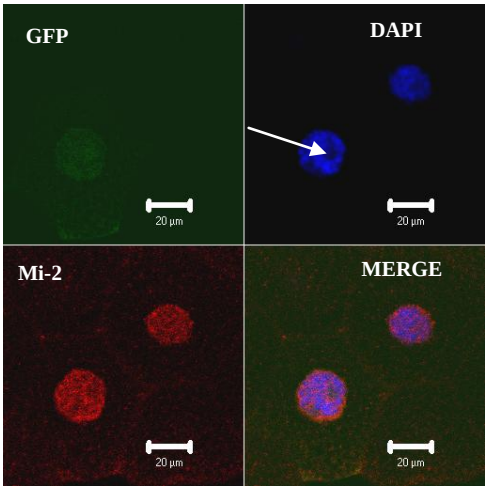
GFP
DAPI
Mi-2
MERGE
20 µm

C)

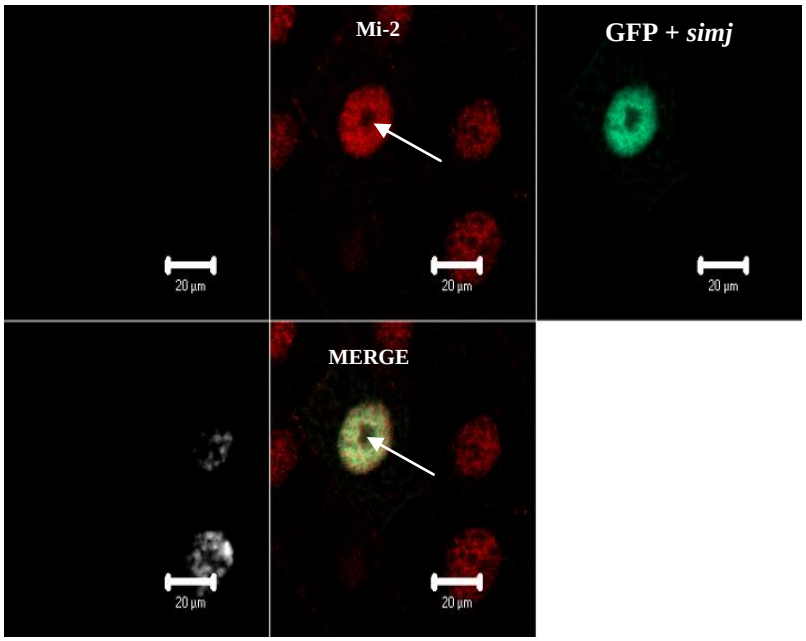
Mi-2
GFP + simj
MERGE
20 µm

D)

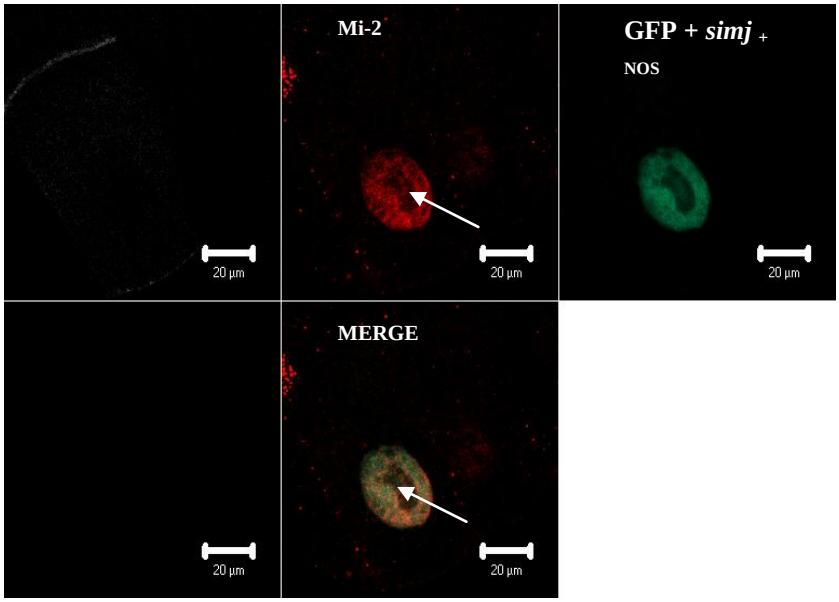
Mi-2
GFP + simj +
NOS
MERGE
20 µm

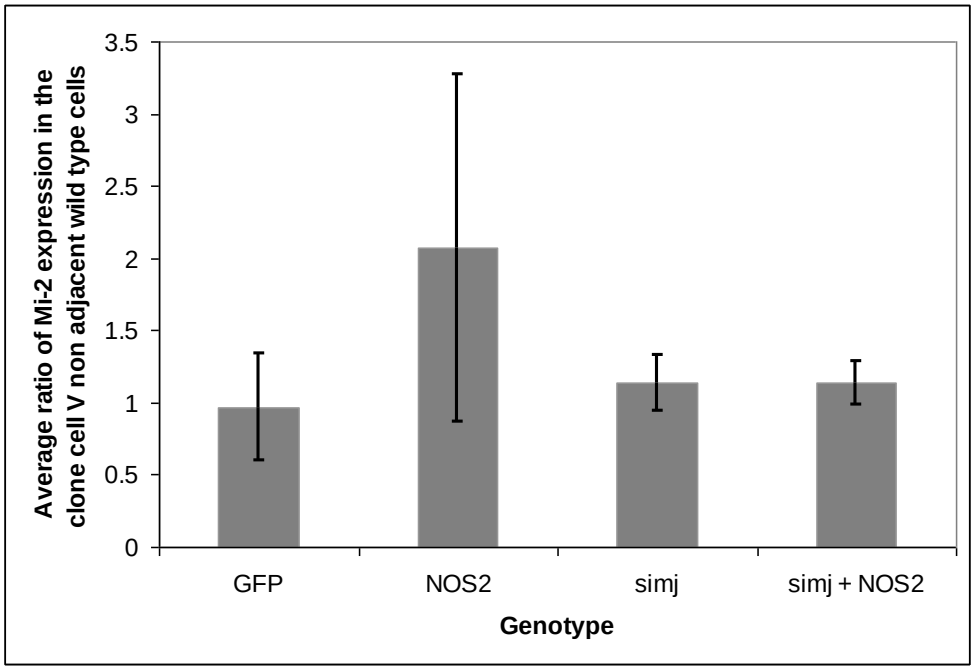

Figure 6.8. Quantification of Mi-2 expression

GFP = Ratio of average intensity of Mi-2 expression in GFP marked control clone cells Versus the average intensity of Mi-2 expression in 10 non adjacent wild type cells.
Genotype: hsFLP / +; Act5c>y^+>Gal4 ; UAS-GFP

NOS2 = Ratio of average intensity of Mi-2 localisation in GFP marked clone cells (expressing *NOS2*) V that in 10 non adjacent wild type cells.
Genotype: hsFLP/ UAS-NOS2; Act5c>y^+>Gal4; UAS- GFP

Simj = Ratio of average intensity of Mi-2 localisation in GFP marked clone cells (expressing *simj*) V that in 10 non adjacent wild type cells.
Genotype: UAS-simj / + ; UAS-mRFP / + ; MKRS, hsFLP / Act5c>y^+>Gal4

Simj + NOS2 = Ratio of average intensity of Mi-2 localisation in GFP marked clone cells (expressing *simj* and *NOS2*) V that in 10 non adjacent wild type cells. Data for both genotypes was obtained from 10 salivary glands from 10 animals.
Genotype: UAS-simj / UAS-NOS2; UAS-mRFP / +; MKRS, hsFLP / Act5c>y^+>Gal4

Error bars indicate standard deviation. Raw data available in Appendix: B.9 Analysis undertaken using Velocity Image Analysis Software.

6.2.7. Effect of Simj expression on Dref localisation

As described in section 4.3.5, *NOS2* expression disrupts the Mi-2 / Dref complex. To determine if over expression of Simj could alter the localisation of Dref in either cells containing the Mi-2 / Dref complex or after this complex had been disrupted, clones of Simj expressing cells were generated in an otherwise wild type background or in cells co-expressing *NOS2* similar to section 6.2.6. To control for the effects of *simj* over expression alone, the localisation of Dref was compared to *NOS2* expressing cells. Salivary glands from animals of genotypes: wild type (Fig 6.9 A), GFP marked UAS-Simj (Fig 6.9 C), clones simultaneously expressing UAS-NOS2 and UAS-simj-GFP (Fig 6.9 D) and clones expressing *NOS2* alone (Fig 6.9 B) were stained with an anti-Dref antibody (Hirose et al., 2002).

Nucleoplasmic but not nucleolar distribution of Dref protein was found both in control (Fig 6.9 A) and in only *NOS2* expressing (Fig 6.9 B) single cell clones. Nuclear membrane associated Dref was observed in *simj* only expressing clone cells (Fig 6.9 C) whereas accumulation of Dref protein was distinctly peri-nuclear in case of clones simultaneously expressing *simj* and *NOS2* (Fig 6.9 D).

I did not attempt to quantify this data as Dref localisation was not confined to a discrete area of cell.

Figure 6.9. Dref localisation in clones expressing *simj* and or *NOS2*

Clones were generated using a 4min heat shock at 38^{o}C between 24- 48hr AEL.

A) Wild type salivary glands. Dref was observed in the nucleoplasm but not in the nucleolus (white arrow).
Genotype: *y*,*w* ; + / + ; + / +

B) *NOS2* expressing clone cell. Dref was observed in the nucleoplasm but not in the nucleolus (white arrow).
Genotype: hsFLP/UAS-NOS2; Act5c>y^{+}>Gal4; UAS- GFP.

C) *simj* expressing clone cell. Dref is associated with the nuclear membrane (white arrow).
Genotype: UAS-simj-GFP / + ; UAS-mRFP / +; MKRS, hsFLP / Act5c>y^{+}>Gal4

D) *simj* and *NOS2* co-expressing clone. Dref localisation is perinuclear (white arrow).
Genotype: UAS-simj-GFP / UAS-NOS2; UAS-mRFP / +; MKRS, hsFLP / Act5c>y^{+}>Gal4

Blue: DAPI, Green: GFP, Red: mouse anti-Dref antibody (Hirose et al, 2002) (Secondary antibody used: horse anti-mouse Cy5). Scale Bar = 50 μm

129

A)

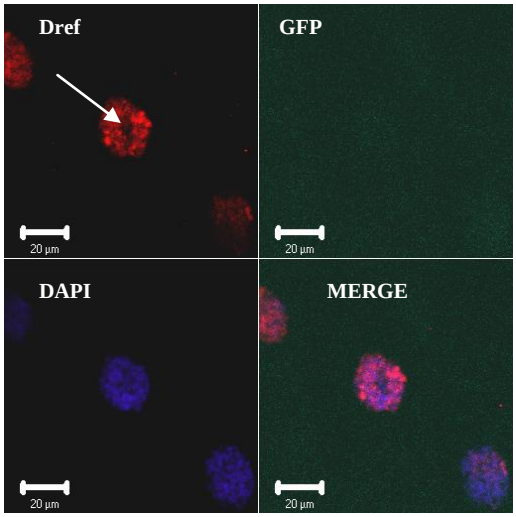
Dref
GFP
DAPI
MERGE
20 µm

B)

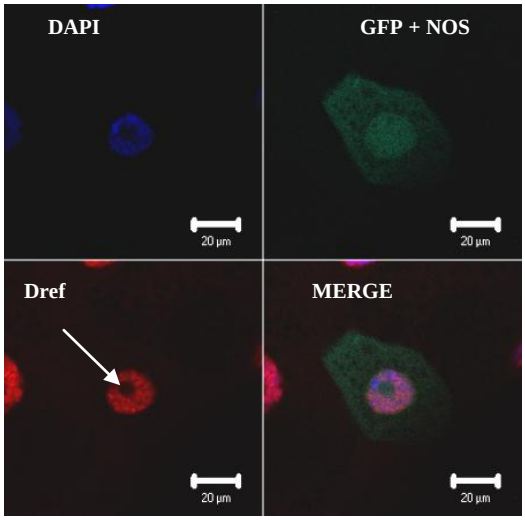
DAPI
GFP + NOS
Dref
MERGE
20 µm

C)

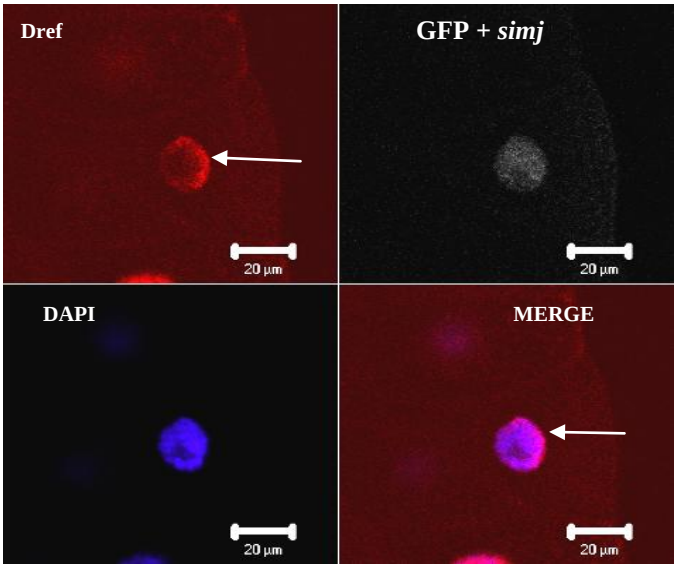
Dref
GFP + simj
DAPI
MERGE
20 µm

D)

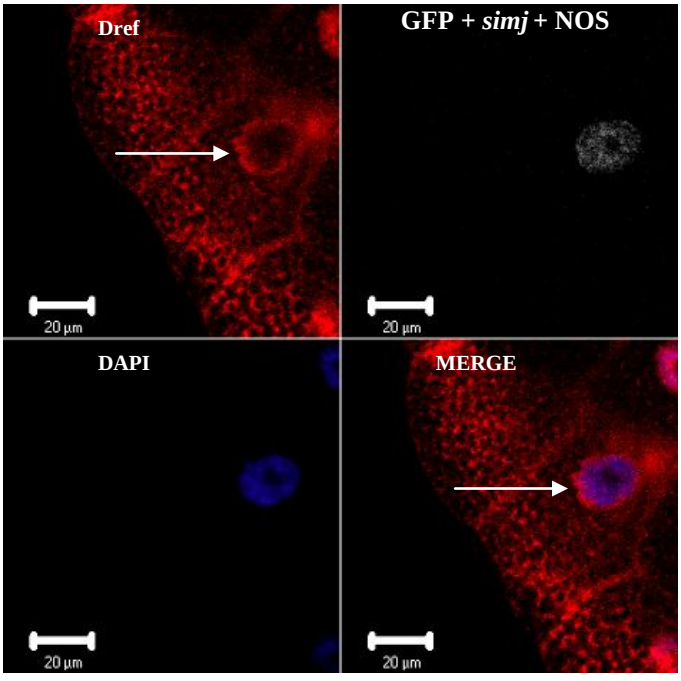
Dref
GFP + simj + NOS
DAPI
MERGE
20 µm

6.3. Discussion

6.3.1. Increased Mi-2 content does not consistently change the localisation of Dref protein

Expression of UAS-Mi-2 in salivary glands did not result in any consistent change in the nuclear localisation of Dref (Fig 6.1). In some cases the nuclear localisation of Dref increased in the Mi-2 over expressing larvae (Fig 6.1 Bi and Bii). However, in some salivary glands, expression of high levels of Mi-2 did not cause any noticeable difference in the nuclear content of Dref (Fig 6.1 Biii). It was expected that an increase in Mi-2 content would increase the probability of Dref / Mi-2 binding and therefore may increase Dref levels in the nucleus. However, as Dref has been reported to bind either with Mi-2 or with DNA (Hirose et al., 2002), it is surprising to occasionally observe higher levels of Dref apparently bound to the polytene chromosomes in Mi-2 over expressing animals(Fig 6.1 Bi and Bii). The apparent difference may be due to small variations in the developmental stages of different animals.

6.3.2. Reduction in Mi-2 content leads to the up regulation of the nuclear accumulation of Dref

Animals transheterozygous for *Mi-2* alleles showed a reduction in the amount of Mi-2 protein (Chapter 4, Fig 4.13). When these larvae were stained with anti-Dref antibodies they showed increased nuclear accumulation of Dref protein (Fig 6.2). This data is consistent with the report that Mi-2 negatively regulates the function of Dref by preventing its binding with DNA (Hirose et al., 2002). It can be speculated that the reduced amount of Mi-2 protein in the mutants was insufficient to inhibit Dref / DNA binding. Consequently, Dref bound to DNA leading to an increase in the nuclear accumulation of Dref (Fig 6.2).

6.3.3. Organ autonomous Simj over expression significantly affects growth and size of salivary glands

The salivary gland size of c147 driven UAS-simj third instar larvae did not appear to be noticeably altered compared to the two control genotypes (Section 6.2.3, Data not shown). However, a one way ANOVA analysis revealed that the average nuclei size of c147 driven UAS-simj larvae is significantly reduced when compared to both the control genotypes used for this experiment (Fig 6.3). Simj has been reported to play developmental roles by regulating expression of ecdysone related genes (Kon et al.,

2005) however there are no reports of proliferation and growth defects in *simj* mutants. Therefore, a novel function of Simj in growth regulation has been demonstrated in this thesis (Section 6.2.3).

Unlike c147 driven UAS-simj animals, the salivary glands of larvae where Tub-GAL4 was driving UAS-simj expression, appeared to be noticeably reduced in size (Fig 6.4 B). However, these animals were sluggish and did not go on to produce pupae (data not shown). This indicates that *simj* expression affects the autonomous growth of salivary glands and ubiquitous expression of Simj affects the viability of the animals.

6.3.4. Up regulation of Simj leads to a reduction in Mi-2 level

Larvae which expressed high levels of Simj protein (c147 driven UAS-simj-GFP) (Fig 6.5 Aiii) showed decreased levels of Mi-2 (Fig 6.5 Biii) compared to the corresponding controls (Fig 6.5 Bi and Bii). These data suggest that an increase in Simj results in the reduction of Mi-2 expression or accumulation. It was therefore expected that UAS-simj-GFP containing larvae, which were not driven by c147 (but do have some ectopic simj-GFP expression) (Fig 6.5 Aii) would show a higher nuclear accumulation of Mi-2 than wild type larvae. Surprisingly the amount of Mi-2 protein found in these (Fig 6.5 Bii) did not differ noticeably from that of wild type larvae (Fig 6.5 Bi). However, the amount of simj-GFP expressed by the UAS-simj-GFP containing larvae which were not driven by c147-GAL4 (Fig 6.5 Aii, image taken at 24% laser excitation) was considerably less than that of the c147-GAL4 driven UAS-simj-GFP larvae (Fig 6.5 Aiii, image taken at 0.1% laser excitation). Therefore, perhaps insufficient extra Simj protein was produced in UAS-simj-GFP containing larvae, when not driven by GAL4 to reach a threshold level sufficient to down regulate Mi-2.

Although immunohistochemistry with an anti-simj antibody was unsuccessful (data not shown), *simj* mutants (Described in 6.1.1.2) were believed to contain less Simj. Considering the difference of Mi-2 levels shown by wild type (6.5 Bi) and c147-GAL4 driven UAS-simj larvae (6.5 Bii) it was assumed that third instar larvae of these *simj* mutants would show high accumulation of nuclear Mi-2. Surprisingly these *simj* mutants did not show any consistent results (Fig 6.6). The third instar larvae of the mutants appeared to be weak (data not shown). Similarly the salivary glands of the mutants were small in size (Fig 6.6). In *simj* null mutant embryos, a subset of pericardial cells are missing (Kim et al., 2004). This evidence suggest that reduction of Simj in the mutants used in the present study may affect their developmental progress.

Therefore translation of Mi-2 protein in these improperly developed and unhealthy third instar larvae may be effected. Thus, these *simj* mutant larvae were not used further to investigate the role of Mi-2 regulation.

6.3.5. Simj affects localisation of both proteins after disruption of the Mi-2/Dref complex

Images of anti-Mi-2 stained wild type cells show that the distribution of Mi-2 is mostly nucleoplasmic, although low levels of nucleolar Mi-2 were also observed (Fig 6.7 A and section 4.2.3). Similarly, the distribution of Dref protein in wild type cells was nucleoplasmic but distinctly non nucleolar (Fig 6.9 A). This suggests that a large proportion of nuclear Mi-2 stays attached in an *in vivo* complex with Dref. This is in agreement with the previous report of a Mi-2/Dref complex (Hirose et al., 2002).
Clone cells expressing *NOS2* showed a uniform distribution of Mi-2 both in nucleoplasm and in nucleolus (Fig 6.7 B and section 4.2.3). However Dref was homogeneously distributed in the nucleoplasm but absent from the nucleolus in *NOS2* expressing clone cells (Fig 6.9 B). These data suggest a reorganisation of the *in vivo* Mi-2/Dref complex by NOS and is further supported by the data of double antibody staining (Section 4.3.5).
Interestingly clone cells over expressing *simj* showed a distinctly non nucleolar distribution of Mi-2 (Fig 6.7 C) unlike the wild type cells (Fig 6.7 A) and the *NOS2* expressing clone cells (Fig 6.7 B). To be more specific, in *simj* expressing clone cells, Mi-2 was found to be distributed in the nuclear area spanning from nucleoplasm to the nuclear membrane, but excluded from the nucleolar space (Fig 6.7 C). Similarly a major change in Dref protein distribution was observed in *simj* expressing clone cells (Fig 6.9 C) compared to that of wild type (Fig 6.9 A) and to *NOS2* expressing clone cells (Fig 6.9 B). The accumulation of Dref protein was exclusively nuclear membrane associated in *simj* expressing clone cells (Fig 6.9 C). The novel localisation of Mi-2 and Dref in *simj* expressing clone cells suggests that when the Mi-2/Dref complex exists, *simj* possibly mediates movement of the complex towards nuclear membrane. In Simj only over expressing clone cells, Mi-2 remained evenly distributed from nucleoplasm to nuclear membrane (Fig 6.7 C) whereas Dref was associated with the nuclear membrane (Fig 6.9 C). This suggests that, compared to Mi-2, Dref is probably more susceptible to the effect of *simj* expression.

The perinuclear distribution of Dref was observed only in *simj* and *NOS2* co-expressing clone cells (Fig 6.9 D). In addition, Mi-2 was observed to be distributed in a distinctly non-nucleolar pattern in these clones simultaneously co-expressing *simj* and *NOS2* (Fig 6.7 D). Considering all these data it can be hypothesized that within *simj* and *NOS2* co-expressing clones, *simj* triggers the movement of Mi-2 and Dref when the Mi-2/Dref complex is disrupted by NOS. The data are consistent with the proposition that the disruption to the Dref / Mi-2 complex results in a perinuclear localisation of Dref in *simj* and *NOS2* co-expressing clones (Fig 6.9 D). However, in clone cells only expressing UAS-simj, the Dref / Mi-2 complex, favours the nuclear membrane associated localisation of Dref (Fig 6.9 C).

The decrease in Mi-2 levels associated with an up regulation of Simj protein content in whole salivary glands (Fig 6.5 Biii) was not observed in the quantitative analysis of Simj over expressing clone cells (Fig 6.8). It was observed that the ratio of Mi-2 concentration in the clone cell verses the non clone cells is similar to that of the control clones (Fig 6.8). The concentration of nuclear Mi-2 in the GAL4 driven UAS-simj and UAS-NOS2 co-expressing clone cells was similar to the non GAL4 expressing cells (Fig 6.8). This may be due to the fact that UAS-simj-GFP is expressed even in the absence of GAL4 as shown in Figure 6.5Aii. Therefore, the surrounding cells of GAL4 driven UAS-simj clones as well as UAS-simj and UAS-NOS2 co-expressing clones also have increased levels of Simj protein. Thus in this experiment, the clone cells and the non-adjacent comparators both express above endogenous levels of Simj, potentially masking any changes to Mi-2.

Chapter 7: General Discussion

7.1. Introduction

The work presented in this thesis has investigated some *in vivo* protein targets of NO. The present study has confirmed Mi-2 as a target of NO. Moreover, the present study has examined NO action on several of its associated proteins.

7.2. NO alters localisation of Mi-2

Previously in our laboratory *ex vivo* experiments, involving treatment with the NO donor SNAP, identified Mi-2 as a probable target of NO (Lasala, 2007). During the present study, SNAP treatment, performed for a shorter time, confirmed an increase in the nuclear localisation of YFP tagged Mi-2$^{CPTI\text{-}000232}$ (Section 3.2.3). Nuclear accumulation of YFP tagged Mi-2 $^{CPTI\text{-}000232}$ was consistently increased when Nitric Oxide levels were up regulated in whole salivary glands via expression of *NOS2* under the control of c147-GAL4 driver (Section 4.2.1). The *NOS2* gene, which was used to control Nitric Oxide levels during the present study, encodes a constitutively active mouse macrophage nitric oxide synthase protein (Section 1.3). The size of the *NOS2* expressing salivary gland nuclei were smaller than that of the control nuclei (Section 4.2.1) which supports previous reports (Kuzin et al., 1996), (Kimber, 2005) and (Scott, 2009).

To avoid any physiological changes resulting from reduced growth of the whole salivary gland, expression of *NOS2* was induced in single cells of salivary glands by exploiting a Flp/FRT technique (Section 4.1.4). Up regulation of NO levels in these single cells resulted in an increase in the nuclear accumulation of YFP tagged Mi-2 $^{CPTI\text{-}000232}$ compared to the non adjoining wild type cells (Section 4.2.2). Increase in the nuclear localisation of Mi-2 $^{CPTI\text{-}000232}$ in the wild type cells immediately adjacent to the *NOS2* expressing clone as shown in figure 4.4 is probably a result of NO diffusion (Haley, 1998).

The wild type Mi-2 protein was shown to behave similarly using a rabbit anti-Mi-2 antibody (Brehm et al., 2000). These data revealed an increase in the endogenous Mi-2 level in *NOS2* expressing single cell clones compared to the non adjacent wild type cells (Section 4.2.3). This finding was confirmed by performing quantitative analysis of nuclear protein levels using image analysis software velocity (Section 4.2.3). However,

in contrast to the wild type cells of the YFP tagged *Mi-2* $^{CPTI-000232}$ larvae (Section 4.2.2), there was no noticeable alteration in the endogenous Mi-2 level of the wild type cells immediately adjacent to *NOS2* expressing clone (Section 4.2.3). Taken together, all these data strongly suggest that nuclear accumulation of Mi-2 is altered by NO, hence Mi-2 is a target of NO.

7.3. Regulation of growth by NO does not act through Mi-2

To examine whether the growth regulatory activity of NO is controlled by Mi-2, the phenotypic effects of NOS expression on animals with reduced levels of Mi-2 was determined. Two different approaches were used to down regulate Mi-2. Levels of Mi-2 were reduced by targeted RNAi (Dietzl et al., 2007) and by using animals transheterozygous for *Mi-2* alleles. The efficiency of RNAi dependent reduction of Mi-2 levels was examined by expressing UAS-RNAi-Mi-2 in the salivary glands of animals heterozygous for the YFP tagged *Mi-2*$^{CPTI-000232}$ allele (Section 4.2.7). The expression of RNAi-Mi-2 under the control of c147-GAL4 driver did not completely eliminate, but did reduce, the expression of YFP tagged Mi-2$^{CPTI-000232}$ (Figure 4.12).

As targeted RNAi did not completely remove the expression of YFP tagged Mi-2$^{CPTI-000232}$, another approach using *Mi-2* transheterozygous mutants was exploited to down regulate the levels of Mi-2. A *Mi-2* allelic combination (Section 4.1.5.2) which showed a reduction in Mi-2 content, as judged by immunohistochemistry with an anti-Mi-2 antibody (Section 4.2.8), was used as a Mi-2 down regulated system. Hence both RNAi-Mi-2 and transheterozygous *Mi-2* mutant animals were used to examine the Mi-2 dependency of NO induced growth phenotypes.

The purpose of these experiments was to examine whether a decrease in Mi-2 content prevented the NOS dependent inhibition of growth and whether it leads to an alteration in salivary gland size.

c147-GAL4 induced expression of UAS-NOS2 was achieved in the salivary glands of UAS-RNAi-Mi-2 and *Mi-2* transheterozygous mutants. The average volume of DAPI stained nuclei of (A) *y,w*; +/+; +/+, (B) UAS-NOS2 / + ; c147-GAL4 / +, (C) UAS-NOS2 / + ; c147-GAL4 / + ; UAS-RNAi-Mi-2 / +, (D) *Mi-2*^{j3D4}/ *Mi-2*^{EY08138} and (E) UAS-NOS2 / + ; c147-GAL4 / + ; *Mi-2*^{j3D4}/ *Mi-2*^{EY08138} animals were calculated using image analysis software velocity (Section 4.2.9). All these NOS expressing genotypes showed a small nuclear size (Section 4.2.9). This evidence suggests that, the NO induced growth phenotype is not controlled by Mi-2. As a functional connection

between Mi-2/NuRD and cell proliferation was reviewed in (Xue et al., 1998), an alteration in the nuclear size in *Mi-2* transheterozygous mutants may have been predicted. However the nuclear size of *Mi-2* transheterozygous mutants did not show any significant difference compared to that of wild type salivary glands (Section 4.2.9). These data are consistent with the recent finding that only a minor portion of *Drosophila* Mi-2 is associated with the NuRD complex, whereas the major fraction is a part of a novel ATP dependent chromatin remodelling complex called *Drosophila* dMec. This complex mediates transcriptional repression of proneural genes however there is no reported data indicating a role for dMec in the control of cell proliferation (Kunert et al., 2009, Kunert N, 2009).

7.4. A novel function of NO in the reorganisation of the *in vivo* Mi-2/Dref complex

Dref and Mi-2 genetically and physically interact with each other. In *Drosophila*, binding of Mi-2 and Dref to polytene chromosomes is mutually exclusive (Hirose et al., 2002). Anti-Dref antibodies coimmunoprecipitate Mi-2 from *Drosophila* embryo, which suggests the existence of an *in vivo* Dref/Mi-2 complex (Hirose et al., 2002). These data indicate that Dref associates with Mi-2 in *Drosophila*.

The cell cycle switch from cell proliferation to differentiation is probably regulated by Dref (Matsukage et al., 2008). NO is also known to control this switch during neurogenesis (Gibbs, 2003). These data suggest that Dref protein localisation may be controlled by NO during the switch of cell cycle from proliferation to differentiation.

To determine an interaction between NO and Dref, visualization of Dref protein was achieved using a mouse anti-Dref antibody (Hirose et al., 2002) in *NOS2* expressing single cell clones. The quantitative analysis of Dref nuclear levels did not reveal any noticeable alteration in *NOS2* expressing clone cells compared to the non adjacent wild type cells (Section 4.2.5). However, *NOS2* expressing clones when double stained with both anti-Dref and anti-Mi-2 antibodies showed an unique nuclear localisation of anti-Dref staining, which was entirely different from that of the surrounding wild type cells (Section 4.2.6). A cytoplasmic and cell membrane bound distribution of anti-Dref staining was found in wild type cells surrounding *NOS2* expressing clones, whereas anti-Mi-2 localisation was distinctly nuclear within them (Fig 4.11 B). As a possible explanation of this, it is hypothesized that the epitope sites for anti-Dref antibody were masked in an *in vivo* Mi-2/Dref/anti-Mi-2 antibody complex (Section 4.3.5). As a consequence of this, anti-Dref antibodies were unable to recognize nuclear Dref protein

(Section 4.3.5). Therefore, formation of an *in vivo* Mi-2/Dref complex was confirmed by the data of double antibody staining shown by wild type cells surrounding *NOS2* expressing clone (Section 4.3.5).

The entirely different pattern of Dref localisation observed in double stained *NOS2* expressing clone cells, compared to surrounding wild type cells, suggests a functional role of NO in the reorganisation of the Mi-2/Dref complex (Section 4.3.5). As the function of Dref is known to be regulated by the intracellular redox state (Choi et al., 2004) and NO is reported to alter transcription factors which are responsive to intracellular redox state (Eberhardt and Beck, 2001), it can be suggested that NO acts in the alteration of Dref by regulating the intracellular redox state, followed by the reorganisation of *in vivo* Mi-2/Dref complex (Section 4.3.5). This disruption of Mi-2/Dref complex ultimately results in growth arrest (section 4.3.5). Therefore, the present study has provided evidence in support of NO mediated reorganisation of Mi-2/Dref complex as a possible growth control mechanism of NO.

7.5. Increased FOXO expression does not markedly alter the expression of Mi-2 or Dref in single cell clones

Previously in our laboratory an Affymetrix gene array analysis on *Drosophila* S2 cells revealed that a common set of genes are targeted both by NO and the transcription factor FOXO (Kimber, 2005). As this present study has confirmed Mi-2 as a probable target of NO (Sections 3.3.2 and 4.3.1), it was hypothesized that the action of NO on Mi-2 may be under the direct control of FOXO transcriptional activity. To determine this, expression of UAS-FOXO was induced under the control of c147-GAL4 driver in the whole salivary gland of YFP tagged *Mi-2*$^{CPTI\text{-}000232}$ animals (Section 5.2.1). The size of the salivary glands expressing UAS-FOXO was reduced compared to the corresponding control salivary glands (Section 5.2.1). This result coincides with the previous finding that ectopic expression of FOXO and human FOXO3a bring about reduction in organ size (Junger et al., 2003). The quantification analysis of this data using the image analysis software velocity, demonstrated a 1.3 fold average increase of YFP tagged Mi-2 $^{CPTI\text{-}000232}$ expression in UAS-FOXO up regulated animals (Section 5.2.1).

To avoid any physiological changes resulting from the reduced growth of the whole salivary gland, nuclear accumulation of endogenous Mi-2 was examined in FOXO expressing single cell clones in salivary glands. An accurate quantitative analysis of

these data showed no noticeable change in nuclear concentration of Mi-2 in response to FOXO expression (Section 5.2.2). Nuclear localisation of Dref was also not noticeably altered in response to FOXO expression in most of the single cell clones (Section 5.2.4). Although some FOXO expressing clone cells showed an increase in nuclear Dref accumulation (Section 5.2.4).

7.6. FOXO mediated growth arrest disrupts the *in vivo* Mi-2/Dref complex

Formation of an *in vivo* Mi-2/Dref complex (Hirose et al., 2002) was confirmed by data acquired from the double anti-Mi2 and anti-Dref antibody staining of *NOS2* over expressing clones (Section 4.3.5). FOXO has been demonstrated to be a probable target of NO (Scott, 2009). Therefore, the response of both Mi-2 and Dref proteins to FOXO was determined by staining FOXO expressing single cell clones simultaneously with anti-Dref and anti-Mi-2 antibodies (Section 5.2.5). The surrounding wild type cells of these FOXO expressing clones showed similar localisation pattern for both the antibodies (Section 5.2.5) as observed in those, surrounding *NOS2* expressing clone cells (Section 4.3.5). As previously observed (Section 4.3.5), the masking of anti-Dref epitope sites in Mi-2/ Dref / anti-Mi-2 antibody complex, prevented the recognition of nuclear Dref protein by anti-Dref antibodies in the double labelled wild type cells surrounding FOXO expressing clone cell (Section 5.3.4).

However clones over expressing FOXO, when double labelled with both anti-Dref and anti-Mi-2 antibodies, showed a perinuclear distribution of both anti-Mi-2 and anti-Dref staining (Section 5.2.5). This perinuclear localisation of anti-Mi-2 staining was also observed in wild type and *NOS2* expressing clone cells when singly stained with anti-Mi-2 antibody (Section 4.2.3). These data suggest that the perinuclear distribution of Mi-2 is not an effect of FOXO up regulation (Section 5.3.4). However, the perinuclear distribution of anti-Dref staining is a result of FOXO signalling (Section 5.2.5), as this was not mimicked either by *NOS2* expressing cells or by wild type cells when singly stained with anti-Dref antibodies (Section 4.2.5). These data support the hypothesis that, the perinuclear distribution pattern of anti-Dref staining is mediated uniquely by FOXO (Section 5.3.4). As well as the perinuclear localisation, a cytoplasmic accumulation of anti-Dref staining was also observed in double labelled FOXO expressing clones (Section 5.2.5). The cytoplasmic anti-Dref staining may be a result of high levels of Dref expression induced by FOXO. As the expression of Dref has been shown to be regulated by *myc* (Dang Thi Phuong Thao et al., 2007) and FOXO has been

demonstrated to control *myc* expression (Teleman et al., 2008), this FOXO induced Dref expression may be through a *myc* dependent pathway (Section 5.3.4). Therefore, the alteration of Dref may be a possible growth control mechanism imparted by FOXO.

7.7. Simj does not alter NO and FOXO mediated reduced sized salivary gland phenotype

Simj is the regulatory component of Mi-2/NuRD (Kon et al., 2005). In *Drosophila*, Simj functions in the regulation of ecdysone responsive genes (Kon et al., 2005). NO affects the ecdysone induced protein 75 (E75) (Section 4.1.2). Therefore, it was hypothesized that a functional link may exist between NO and Simj. Hence, the effect of Simj over expression on NO induced growth arrest was determined by co-expressing UAS-simj (Kim et al., 2004) and UAS-NOS2 in whole salivary glands under the control of c147-GAL4 driver. The salivary glands simultaneously over expressing UAS-simj and UAS-NOS2 showed a reduced size reasonably similar to that of those only expressing UAS-NOS2 (Section 4.2.4).

As FOXO is a probable target of NO (Scott, 2009), the effect of UAS-simj expression on the FOXO induced reduced salivary gland size phenotype was determined (Section 5.2.3). Simultaneous expression of UAS-FOXO and UAS-simj in the whole salivary gland did not result in any noticeable alteration in salivary gland size compared to that of those expressing only UAS-FOXO (section 5.2.3). These data suggest that, Simj does not modify NO or FOXO inhibited growth in salivary glands.

7.8. Simj affects sub cellular distribution of both the proteins after disruption of the Mi-2/Dref complex

The effect of Simj expression on the Mi-2/Dref complex was determined by generating UAS-simj expressing single cell clones and staining them separately with anti-Dref and anti-Mi-2 antibodies (Section 6.2.6 and 6.2.7). This study has provided further evidence in support of a function of NO in the reorganisation of Mi-2/Dref complex (Section 6.3.5). When UAS-NOS2 was co-expressed with UAS-simj, the expression of NOS would cause disruption to the Mi-2/Dref complex and the response of both the proteins to Simj over expression could be examined. To achieve this, UAS-NOS2 and UAS-simj co-expressing clones were stained with anti-Dref and anti-Mi-2 antibodies separately (Section 6.2.6 and 6.2.7).

Clones expressing only UAS-simj showed a distinctly non-nucleolar distribution of anti-Mi-2 staining which was not observed in wild type cells or in those expressing only *NOS2* (Section 6.2.6). UAS-simj expressing clones stained with anti-Dref antibodies also showed a distinctly nuclear membrane associated localisation of Dref. This pattern of Dref expression was not seen in either wild type cells or in clones only expressing *NOS2* (Section 6.2.7). These data demonstrate that, both the non-nucleolar distribution of Mi-2 and nuclear membrane associated localisation of Dref are the unique effects of Simj over expression (Section 6.3.5). UAS-simj and UAS-NOS2 co-expressing clones again showed a non-nucleolar distribution of Mi-2 and a distinctly perinuclear distribution of Dref proteins. Again, this pattern was not observed in wild type cells or clones only expressing *NOS2* (Section 6.2.6 and 6.2.7). This supports the hypothesis that Simj imparts its effect on both the proteins when they exist as a Mi-2/Dref complex as well as after the NO induced disruption of the complex (Section 6.3.5).

7.9. Increased Simj content leads to a reduction in Mi-2 levels

The two core components of NuRD, Simj and Mi-2, function in DNA methylation (Section 6.1.1). Salivary glands expressing high levels of UAS-simj (Kim et al., 2004) under the control of c147-GAL4 driver showed a decrease in Mi-2 content compared to the corresponding control genotypes (section 6.2.5). A transheterozygous allelic combination of *simj* alleles was used as Simj down regulated system to study the response of Mi-2 protein in the salivary glands (Section 6.1.1.2). Unfortunately immunohistochemistry with an anti-Simj antibody was unsuccessful (data not shown). This prevented the study of Simj content in these transheterozygous mutants. However, it was assumed that the mutants would contain less Simj protein. Although up regulation of Simj expression resulted in a reduction in Mi-2 levels (section 6.2.5), anti-Mi-2 staining of *simj* transheterozygous mutants did not result in a consistent alteration of endogenous Mi-2 levels (Section 6.2.5). This may be a result of the apparent weakness observed in the third instar larvae of the mutants (data not shown). The salivary glands of the *simj* mutants were also small (Fig 6.6). In *simj* null mutant embryos, a subset of pericardial cells are missing (Kim et al., 2004). This suggests that the reduction of Simj levels in the transheterozygous mutants may affect their developmental progress followed by a reduction in the expression of Mi-2 (Section 6.3.4). The decrease in Mi-2 levels associated with an up regulation of Simj protein content in whole salivary glands (Section 6.2.5) was not repeated in the quantitative

analysis of UAS-simj expressing clone cells (Section 6.2.6). This may be due to the fact that the UAS-simj is expressed even in the absence of GAL4 (Fig 6.5Aii). Therefore, the non GAL4 expressing cells surrounding either Gal4, UAS-simj or Gal4, UAS-NOS2, and GAL4, UAS-simj co expressing clone cells also have increased levels of Simj protein. Thus in this experiment, the clone cells and the non-adjacent comparators both express above endogenous levels of Simj potentially masking any changes to Mi-2 (Section 6.3.5).

One caveat to these data (discussed in 7.1-7.9) is that some of the variation in the levels of proteins observed in salivary gland cells could be due to differences in the amount of endoreplication in different cells. The process of polytenization in salivary gland cells is achieved by an endo cell cycle in which there is only a synthesis phase (S Phase), a Gap phase (G pahse). Cytokinesis, nuclear division and segregation of chromosomes do not occur (Smith and Orr-Weaver, 1991). Polytene DNA replication or endoreplication in larval salivary gland cells is a discontinuous process and works in a cyclic manner (Pearson, 1974). Differences in the amount of polytenization may cause a variation in the amounts and nuclear accumulation of Mi-2 or other proteins in different salivary gland cells. This may lead to a variation in the quantity of observed proteins found in different salivary glands dissected from different third instar larvae or between cells of different genotypes from the same animal. These differences may explain the relatively large standard deviations observed when the expression data is quantified.

Overexpression of a target gene (*NOS2 / FOXO/ simj*) (discussed in 7.1-7.9) can enhance the normal function of that gene. Another way of studying the function of a particular gene is to generate loss of function cell clones which would be homozygous mutant for the gene of interest. The homozygous mutant cells can be marked by expression of a fluorescent marker (GFP/ YFP). For salivary glands, this method requires the recovery of the mutant clones prior to the end of cell division of the salivary gland primordia which occurs at 8 hours AEL before the beginning of polytenization.

7.10. Organ autonomous Simj over expression significantly affects growth and size of salivary glands

A one-way ANOVA analysis revealed that the nuclear size of cells expressing UAS-simj under the control of c147-GAL4 is significantly reduced compared to both the control genotypes. A post hoc Tukey analysis showed a significant difference between the nuclear size of UAS-simj and wildype, c147 driven UAS-simj and wild type, as well

as UAS-simj and c147 driven UAS-simj animals (Section 6.2.3). Although functional roles for Simj in development have been reported (Kon et al., 2005), no reports of proliferation or growth defects of *simj* mutants have been published. From the evidence of this present study (Section 6.2.3), it can be proposed that Simj does function in growth regulation. Tub-GAL4 driven UAS-simj larvae were noticeably reduced in size (Section 6.2.4). However, these animals were sluggish and did not go on to produce pupae (data not shown). Hence, from the results of this study it can be suggested that Simj expression affects the autonomous growth of salivary glands and ubiquitous expression of Simj affects the viability of the animals.

7.11. Future work

Several other aspects that may be worth investigating are noted below.

The present study has identified a function of NO on the disruption of the Mi-2/Dref complex *in vivo*, possibly through alteration of the transcription factor Dref (Section 4.3.5). Hence, it would be interesting to investigate whether the antiproliferative action of NOS is Dref dependent. To determine this, NOS induced growth inhibition could be studied in *Dref* mutants or in animals expressing RNAi-Dref. This could also be achieved by the simultaneous expression of the dominant negative Dref protein (Dref $_{1\text{-}125}$) (Hirose et al., 1999) and NOS in the same animals.

The present study has also provided evidence in support of alteration of Mi-2 expression by NOS by both *ex vivo* and *in vivo* experiments (Section 4.3.1). It would be revealing to study whether the effect of NOS on Mi-2 is controlled by Dref. To achieve this, animals expressing NOS and RNAi-Dref or dominant negative Dref could be subjected to immunohistochemistry with an anti-Mi-2 antibody.

To further investigate the Mi-2/Dref complex and its disruption by NO, Fluorescence Resonance Energy Transfer (FRET) could be exploited to measure the real time dynamics of the formation and disruption of this complex.

Appendices

A. Fly stock used

A.1. Bloomington stocks, http://flystocks.bio.indiana.edu/

Genotype	Comments
y[1] w[*]; P{w[+mC]=GAL4-Act5C(FRT.CD2).P}S	Ubiquitous expression of GAL4 in FLP-generated clones
w[1118]; P{w[+mW.hs]=GawB}C147	GAL4 expressed in larval brain and salivary glands
w[1118]; P{w[+mC]=UAS-myr-mRFP}1	P{UAS-myr-mRFP} expresses membrane – targeted monomeric RFP
y[1] w[*]; P{w[+mC]=UAS-foxo.P}2	Expresses wild type foxo under UAS control.
P{ry[+t7.2]=PZ}simj[01814] ry[506]/TM3, ry[RK] Sb[1] Ser[1]	Insertional mutant simj[01814], created by Berkeley Drosophila Genome Proj
y[1] w[*]; P{w[+mC]=lacW}Mi-2[j3D4] Su(Tpl)[j3D4]/TM3, Sb[1] Ser[1]	Insertional mutant Mi-2[j3D4] created by Berkeley Drosophila Genome Proj
w[1118]; P{w[+mGT]=GT1}simj[BG00403]/TM6B, P{w[+mC]=35UZ}DB1, Tb[1]	Insertional mutant simj[BG00403], created by Berkeley Drosophila Genome Proj
y[1] w[67c23]; P{w[+mC] y[+mDint2]=EPgy2}Mi-2[EY08138] Su(Tpl)[EY08138]/TM3, Sb[1] Ser[1]	Insertional mutant Mi-2[EY08138] created by Berkeley Drosophila Genome Proj

A.2. Fly stocks from CPTI (Cambridge protein trap insertion project)

Stock	Genotype	Comments
CPTI-000232	+ / + ; + / + ; YFP-Mi-2 / TM3, Sb	Expresses YFP tagged nuclear Mi-2. (Homozygous survives)

A.3. Fly stocks Vienna Drosophila RNAi center (VDRC), http://stockcenter.vdrc.at/control/main

Trans-formant ID	Construct ID	Genotype	Inserted Chromo-some	Comments
10766	4511	+ / +; + /+; UAS-RNAi-Mi-2 / UAS-RNAi-Mi-2	3	Expresses RNAi-Mi-2 under the control of UAS/GAL4 system

A.4. Fly stocks from other sources

Genotype	Chromosome	Comments and Reference
UAS-Mi-2	-	Expresses Mi-2 under the control of UAS/GAL4 system. A kind gift from Prof Fumiko Hirose (Hirose, Ohshima et al. 2002)
UAS-simj-GFP / UAS-simj-GFP; +/+ ; +/+	1	Expresses simj under the control of UAS/GAL4 system. A kind gift from Prof Yongsok Kim (Kim, Park et al. 2004).

B. DATA acquired on image analysis software Velocity

B.1. Analysis of YFP tagged Mi-2$^{CPTI-000232}$ expression in the whole salivary glands expressing *NOS2*

UAS-NOS2 over expression in whole salivary gland of YFP tagged Mi-2 (CPTI-000232)

Cont A

Name	Voxel Count	Centroid Z (µm)	Volume (µm³)	Mean (Ch3-T1)	Sum (Ch3-T1)
Object 24	25286	72.7202	4126.2	58.1848	1.47E+06
Object 23	33842	70.52	5522.38	47.2505	1.60E+06
Object 26	33326	69.127	5438.18	54.5769	1.82E+06
Object 25	34088	68.8204	5562.53	47.8206	1.63E+06

Expt A

Name	Voxel Count	Centroid Z (µm)	Volume (µm³)	Mean (Ch3-T1)	Sum (Ch3-T1)
Object 38	5592	67.5515	912.51	88.4158	494421
Object 39	4356	67.1038	710.818	83.469	363591
Object 35	4732	65.2918	772.174	62.0448	293596
Object 34	4029	62.4629	657.458	87.5791	352856
Object 23	5244	61.398	855.723	65.8837	345494

Cont B

Name	Voxel Count	Centroid Z (オ m)	Volume (オ m ヤ)	Mean (Ch3-T1)	Sum (Ch3-T1)
Object 14	48009	23.6452	7834.17	27.4566	1.32E+06
Object 13	40161	22.212	6553.53	35.6303	1.43E+06
Object 11	34222	20.062	5584.39	30.4014	1.04E+06
Object 8	40384	19.6048	6589.92	33.9002	1.37E+06
Object 12	40755	19.2837	6650.46	32.3408	1.32E+06
Object 6	38822	17.1346	6335.03	32.122	1.25E+06
Object 5	38930	16.7788	6352.65	36.2336	1.41E+06
Object 3	36595	16.5754	5971.62	39.7923	1.46E+06
Object 2	40844	15.1677	6664.98	35.2538	1.44E+06

Expt B

Name	Voxel Count	Centroid Z (µm)	Volume (µm³)	Mean (Ch3-T1)	Sum (Ch3-T1)
Object 75	8682	78.1031	1416.74	99.3401	862471
Object 73	6854	76.7321	1118.45	94.7342	649308
Object 74	10636	75.8938	1735.6	110.449	1.17E+06
Object 70	4972	74.8226	811.338	99.9	496703
Object 71	10885	74.1077	1776.23	108.081	1.18E+06
Object 72	8385	73.2964	1368.28	87.9336	737323
Object 66	4393	72.2864	716.856	77.8318	341915
Object 69	13606	71.9327	2220.25	107.846	1.47E+06
Object 65	6262	71.8764	1021.84	95.0584	595256
Object 68	8828	70.8916	1440.57	95.5185	843237
Object 67	10428	68.8899	1701.66	90.0054	938576

Cont D

Name	Voxel Count	Centroid Z (µm)	Volume (µm³)	Mean (Ch3-T1)	Sum (Ch3-T1)
Object 12	12095	18.4377	1973.68	26.1866	316727
Object 14	16249	17.2592	2651.53	27.0101	438887
Object 18	19626	15.6824	3202.6	28.636	562011
Object 8	29564	13.9267	4824.29	34.3688	1.02E+06
Object 16	24332	13.4331	3970.53	24.7734	602786

Object 9	35545	12.3959	5800.28	34.1995	1.22E+06
Object 6	28760	10.5038	4693.1	29.3227	843322

Exp D

Name	Voxel Count	Centroid Z (μm)	Volume (μm³)	Mean (Ch3-T1)	Sum (Ch3-T1)
Object 87	7111	23.072	1160.38	52.1519	370852
Object 73	6432	21.9123	1049.58	53.6171	344865
Object 84	9515	21.8581	1552.67	54.4465	518058
Object 40	9602	21.8521	1566.87	55.5796	533675
Object 68	10281	21.0288	1677.67	46.7469	480605
Object 49	4421	20.71	721.425	50.4734	223143
Object 81	11427	20.5185	1864.67	61.5428	703250
Object 75	8232	19.9922	1343.31	59.1067	486566
Object 82	9380	19.8525	1530.64	57.6813	541051
Object 56	10172	19.2706	1659.88	41.1826	418909
Object 69	10844	18.375	1769.54	56.9453	617515
Object 25	9173	16.9642	1496.86	50.8822	466742
Object 70	15079	16.8109	2460.61	53.8735	812358
Object 47	10503	16.3195	1713.89	46.0021	483160
Object 31	3905	15.4146	637.223	46.9478	183331
Object 72	23872	15.2709	3895.47	52.5885	1.26E+06
Object 57	18353	15.0972	2994.87	48.5359	890780
Object 83	14298	14.9	2333.17	47.5562	679958
Object 34	12415	14.5551	2025.9	51.4091	638244

Cont C

Name	Voxel Count	Centroid Z (μm)	Volume (μm³)	Mean (Ch3-T1)	Sum (Ch3-T1)
Object 38	24052	69.1717	3924.84	100.58	2.42E+06
Object 37	37702	65.6699	6152.26	72.8587	2.75E+06
Object 33	41509	65.281	6773.5	46.3347	1.92E+06
Object 31	28792	64.1171	4698.32	84.035	2.42E+06
Object 34	46799	63.9385	7636.72	68.5846	3.21E+06
Object 36	37007	63.355	6038.85	82.3135	3.05E+06
Object 32	35243	62.9906	5751	62.3102	2.20E+06
Object 35	38485	62.3911	6280.03	89.4056	3.44E+06
Object 24	44339	61.8734	7235.3	84.0482	3.73E+06
Object 30	37449	61.6228	6110.98	57.2681	2.14E+06
Object 25	38850	60.9841	6339.6	48.0253	1.87E+06
Object 28	34456	60.7114	5622.58	54.4179	1.88E+06

Expt C

Name	Voxel Count	Centroid Z (μm)	Volume (μm³)	Mean (Ch3-T1)	Sum (Ch3-T1)
Object 31	7021	66.6341	1145.7	102.134	717085
Object 25	8763	61.1262	1429.96	108.968	954887
Object 24	8646	56.336	1410.87	77.7735	672430

Cont E

Name	Voxel Count	Centroid Z (μm)	Volume (μm³)	Mean (Ch3-T1)	Sum (Ch3-T1)
Object 17	12077	17.9459	1970.74	40.7311	491910
Object 19	18715	16.7601	3053.94	34.0026	636359
Object 24	37402	12.1436	6103.31	56.443	2.11E+06
Object 23	20998	12.0024	3426.48	38.1291	800635
Object 25	39482	11.0084	6442.73	54.4412	2.15E+06
Object 21	25581	10.7952	4174.34	38.7038	990083

Object 11	27351	10.7	4463.17	51.5613	1.41E+06
Object 18	40722	10.6698	6645.07	48.1523	1.96E+06

ExPt E

Name	Voxel Count	Centroid Z (μm)	Volume (μm³)	Mean (Ch3-T1)	Sum (Ch3-T1)
Object 66	2010	23.1527	327.995	42.6473	85721
Object 99	3154	23.0964	514.674	56.2067	177276
Object 52	2271	23.0828	370.585	44.6579	101418
Object 72	2457	22.9426	400.937	44.5124	109367
Object 67	2004	22.8443	327.015	51.2705	102746
Object 68	1628	22.7942	265.659	41.1886	67055
Object 89	3781	22.6432	616.989	52.5483	198685
Object 95	1797	22.4752	293.237	43.9944	79058
Object 62	2387	22.3498	389.514	52.3293	124910
Object 61	2630	22.1924	429.167	62.7631	165067
Object 39	2966	21.3958	483.996	49.9326	148100
Object 82	2216	21.3542	361.61	54.3466	120432
Object 56	4700	21.0109	766.952	43.4587	204256
Object 87	2376	20.9621	387.719	51.6768	122784
Object 88	2170	20.9567	354.104	52.0802	113014
Object 58	1520	20.6697	248.036	36.2434	55090
Object 78	2864	20.3097	467.351	55.0115	157553
Object 98	6531	19.8352	1065.74	55.2773	361016
Object 37	1989	17.3846	324.568	37.1257	73843
Object 44	4871	16.4584	794.856	45.761	222902
Object 54	4177	16.1415	681.609	33.5154	139994

Ratio of average intensity of YFP tagged Mi-2 in Experimental A/ Control A	**1.49**
Ratio of average intensity of YFP tagged Mi-2 in Experimental B/ Control B	**2.8**
Ratio of average intensity of YFP tagged Mi-2 in Experimental C / Control C	**1.36**
Ratio of average intensity of YFP tagged Mi-2 in Experimental D / Control D	**1.78**
Ratio of average intensity of YFP tagged Mi-2 in Experimental E / Control E	**1.06**

Average value of the ratio of 5 experimental / 5 control salivary glands **1.698**

B.2. Visualization of Mi-2 protein in single cell clones expressing NOS

B.2. (i) Visualization of Mi-2 protein in GFP marked control clone cells

Img No 1	Name	Voxel Count	Volume (μm³)	Mean (Ch3-T1)	Min (Ch2-T2)	Mean (ChS1-T3)	Sum (ChS1-T3)	Centroid X	Centroid Y	Centroid Z
Clone Cell	Object 1	4092	1656.41	34.772	28	72.7454	297674	378.674	314.201	16.6041
Wt 1	Object 1	5458	2209.35	2.60993	28	65.0321	354945	68.382	110.547	12.229
Wt 2	Object 1	8552	3461.78	2.58022	28	72.4279	619403	124.685	256.809	12.7595
Wt 3	Object 1	4474	1811.04	2.57957	28	124.283	556043	154.652	145.929	11.0637
Wt 4	Object 1	6170	2497.57	2.14765	28	69.1929	426920	467.617	183.999	8.26629
Wt 5	Object 1	8758	3545.17	2.58518	28	71.726	628176	124.667	256.836	12.5776
Wt 6	Object 1	1579	639.166	2.51235	28	145.775	230178	58.7809	219.764	9.9658
Wt 7	Object 1	8071	3267.07	1.45979	28	73.6724	594610	401.164	79.4567	21.4443
Wt 8	Object 1	10317	4176.24	1.81749	28	89.5717	924111	220.697	69.515	16.2537
Wt 9	Object 1	7587	3071.16	2.93752	28	135.307	1.03E+06	457.254	305.664	6.50534
Wt 10	Object 1	8820	3570.26	2.56814	28	71.3404	629222	124.665	256.807	12.5022

Img No 2	Name	Voxel Count	Volume (μm³)	Mean (Ch3-T1)	Min (Ch2-T2)	Mean (ChS1-T3)	Sum (ChS1-T3)	Centroid X	Centroid Y	Centroid Z
Clone Cell	Object 1	4044	1636.98	13.3133	24	64.9577	262689	240.738	414.567	15.6681
Wt 1	Object 1	5676	2297.6	0.690803	24	125.473	712182	297.18	108.212	4.34056
Wt 2	Object 1	9346	3783.18	0.598866	24	95.6898	894317	368.616	309.44	10.4607
Wt 3	Object 1	8157	3301.89	0.585142	24	59.862	488294	418.809	396.729	7.59605
Wt 4	Object 1	9095	3681.58	0.540077	24	75.9956	691180	301.144	251.594	11.3282
Wt 5	Object 1	5865	2374.1	0.537084	24	144.682	848558	257.609	54.8382	5.21091
Wt 6	Object 1	9101	3684.01	0.763433	24	79.7734	726018	304.95	364.678	6.56291
Wt 7	Object 1	9808	3970.2	0.743679	24	86.0366	843847	322.587	439.163	7.3023
Wt 8	Object 1	8323	3369.08	0.756218	24	94.7053	788232	360.92	490.65	7.38604
Wt 9	Object 1	2051	830.228	0.592882	24	40.5685	83206	459.175	323.476	23.1853
Wt 10	Object 1	1418	573.995	0.311707	24	68.3709	96950	216.028	118.757	21.1128

Img No 3	Name	Voxel Count	Volume (μm³)	Mean (Ch3-T1)	Min (Ch2-T2)	Mean (ChS1-T3)	Sum (ChS1-T3)	Centroid X	Centroid Y	Centroid Z
Clone Cell	Object 1	10284	4162.88	43.2556	24	74.4185	765320	314.22	383.824	9.33411
Wt 1	Object 1	9714	3932.15	0.328907	24	56.1457	545399	322.867	80.3292	12.8418
Wt 2	Object 1	6234	2523.47	0.281842	24	57.0202	355464	185.006	91.2129	18.5265
Wt 3	Object 1	1360	550.517	0.159559	24	40.5632	55166	220.242	13.1868	20.189
Wt 4	Object 1	9137	3698.58	0.460873	24	90.5354	827222	268.247	126.321	6.98544
Wt 5	Object 1	4018	1626.45	0.486809	24	31.6936	127345	249.026	461.306	11.4278
Wt 6	Object 1	8697	3520.47	0.544441	24	58.912	512358	202.235	376.907	10.9339
Wt 7	Object 1	4685	1896.45	0.528922	24	65.2525	305708	259.702	306.286	9.41067
Wt 8	Object 1	9143	3701.01	0.515476	24	69.233	632997	300.051	233.476	7.43793
Wt 9	Object 1	4271	1728.87	0.46125	24	31.2067	133284	248.817	461.18	11.3409
Wt 10	Object 1	9534	3859.28	0.331026	24	56.676	540349	322.796	80.308	12.9776

Img No 4	Name	Voxel Count	Volume (μm³)	Mean (Ch3-T1)	Min (Ch2-T2)	Mean (ChS1-T3)	Sum (ChS1-T3)	Centroid X	Centroid Y	Centroid Z
Clone Cell	Object 1	2095	848.039	11.3041	28	57.7804	121050	234.395	374.538	22.8449
Wt 1	Object 1	7249	2934.34	0.67361	28	78.8822	571817	355.462	448.744	11.8291
Wt 2	Object 1	5848	2367.22	0.58567	28	129.605	757932	253.172	12.1636	9.83635
Wt 3	Object 1	7362	2980.08	0.559223	28	52.2816	384897	413.646	356.065	12.1254
Wt 4	Object 1	5829	2359.53	0.757934	28	107.897	628934	292.208	66.7854	7.77715
Wt 5	Object 1	10181	4121.18	0.6464	28	70.0202	712876	238.563	142.908	13.1806
Wt 6	Object 1	8124	3288.53	0.50517	28	67.9354	551907	296.176	211.783	15.4978
Wt 7	Object 1	9011	3647.58	0.679836	28	70.9859	639654	299.606	324.61	9.7715
Wt 8	Object 1	8075	3268.69	0.601981	28	79.0031	637950	317.11	397.716	11.3391
Wt 9	Object 1	5043	2041.36	0.543526	28	46.7103	235560	402.853	210.307	22.8057
Wt 10	Object 1	3843	1555.61	0.456154	28	70.7442	271870	322.129	143.14	13.2763

Img No 5	Name	Voxel Count	Volume (μm³)	Mean (Ch3-T1)	Min (Ch2-	Mean (ChS1-	Sum (ChS1-T3)	Centroid X	Centroid Y	Centroid Z

					T2)	T3)				
Clone Cell	Object 1	4448	1800.51	70.8921	22	128.343	570871	116.379	237.168	10.0899
Wt 1	Object 1	9466	3831.76	1.45817	22	80.0567	757817	317.876	436.112	12.9452
Wt 2	Object 1	10312	4174.21	1.43735	22	101.333	1.04E+06	317.113	296.548	13.0702
Wt 3	Object 1	8793	3559.33	1.60696	22	107.226	942834	202.673	276.163	12.0254
Wt 4	Object 1	4404	1782.7	1.32879	22	45.9832	202510	422.568	383.997	19.168
Wt 5	Object 1	1602	648.476	1.68851	22	137.604	220442	80.8533	129.657	8.60924
Wt 6	Object 1	10328	4180.69	1.20149	22	93.1072	961611	247.761	154.328	15.8171
Wt 7	Object 1	1562	632.285	0.652369	22	87.4257	136559	217.456	71.765	23.8566
Wt 8	Object 1	4490	1817.51	0.924722	22	72.3784	324979	133.123	379.306	18.3421
Wt 9	Object 1	1532	620.141	1.04373	22	46.8584	71787	157.152	10.7748	23.3923
Wt 10	Object 1	8710	3525.74	1.28634	22	97.9255	852931	223.001	434.709	13.397

Img No 6	**Name**	**Voxel Count**	**Volume (µm³)**	**Mean (Ch3-T1)**	**Min (Ch2-T2)**	**Mean (ChS1-T3)**	**Sum (ChS1-T3)**	**Centroid X**	**Centroid Y**	**Centroid Z**
Clone Cell	Object 1	1196	484.131	25.3286	20	46.5351	55656	137.286	168.003	12.3428
Wt 1	Object 1	5845	2366.01	1.76185	20	133.855	782384	260.566	329.001	10.3938
Wt 2	Object 1	9208	3727.32	1.8889	20	87.6718	807282	377.286	357.744	16.2217
Wt 3	Object 1	5259	2128.8	2.26868	20	163.816	861508	397.006	314.516	7.95722
Wt 4	Object 1	8189	3314.84	1.74918	20	51.2258	419488	229.999	270.608	11.1508
Wt 5	Object 1	3418	1383.58	1.14716	20	67.1916	229661	56.1987	120.935	10.0506
Wt 6	Object 1	4450	1801.32	2.38517	20	143.404	638148	144.678	227.928	5.59753
Wt 7	Object 2	2703	1094.15	1.15982	20	52.2445	141217	314.991	270.971	11.2105
Wt 8	Object 1	1122	454.176	2.72014	20	89.0624	99928	259.054	204.25	2.92959
Wt 9	Object 1	7981	3230.64	1.75053	20	51.5195	411177	229.924	270.499	11.0107
Wt 10	Object 1	2052	830.633	1.13304	20	2.26657	4651	174.636	329.541	19.2446

Img No 7	**Name**	**Voxel Count**	**Volume (µm³)**	**Mean (Ch3-T1)**	**Min (Ch2-T2)**	**Mean (ChS1-T3)**	**Sum (ChS1-T3)**	**Centroid X**	**Centroid Y**	**Centroid Z**
Clone Cell	Object 1	10653	4312.25	26.2662	27	64.8706	691067	165.19	323.095	14.9699
Wt 1	Object 1	10296	4167.74	0.730963	27	63.4495	653276	268.236	256.218	14.8137
Wt 2	Object 1	11453	4636.08	1.27984	27	63.761	730255	370.229	303.538	13.2058
Wt 3	Object 1	4615	1868.11	0.612351	27	59.7582	275784	312.854	399.133	13.6498
Wt 4	Object 1	11217	4540.55	1.2917	27	121.664	1.36E+06	122.728	94.1002	10.5354
Wt 5	Object 1	6151	2489.87	1.22257	27	124.104	763364	30.9379	226.955	11.6547
Wt 6	Object 1	10965	4438.54	1.38523	27	106.398	1.17E+06	126.074	229.861	9.49375
Wt 7	Object 1	10848	4391.18	1.28844	27	122.905	1.33E+06	122.731	94.0536	10.8046
Wt 8	Object 1	6296	2548.57	1.03161	27	96.4423	607201	464.275	487.661	16.5723
Wt 9	Object 1	9577	3876.69	1.30866	27	89.9552	861501	400.565	410.282	10.543
Wt 10	Object 1	4873	1972.55	3.78617	27	26.7338	130274	454.938	308.635	22.589

Img No 8	**Name**	**Voxel Count**	**Volume (µm³)**	**Mean (Ch3-T1)**	**Min (Ch2-T2)**	**Mean (ChS1-T3)**	**Sum (ChS1-T3)**	**Centroid X**	**Centroid Y**	**Centroid Z**

Clone Cell	Object 1	5038	2039.34	38.6935	30	66.5286	335171	211.32	415.574	23.319
Wt 1	Object 1	9566	3872.24	4.74127	30	92.3503	883423	316.835	360.309	7.07903
Wt 2	Object 1	9895	4005.41	5.01193	30	104.992	1.04E+06	268.334	437.284	9.66741
Wt 3	Object 1	9820	3975.06	3.93697	30	79.2488	778223	230.51	325.717	13.2418
Wt 4	Object 1	8054	3260.19	4.18674	30	74.2208	597774	375.627	319.645	10.0538
Wt 5	Object 1	8553	3462.18	5.11049	30	72.0569	616303	348.917	473.304	7.63627
Wt 6	Object 1	5226	2115.44	2.73421	30	41.3781	216242	415.178	427.291	19.4432
Wt 7	Object 1	8230	3331.44	4.14909	30	99.0128	814875	374.973	147.877	8.8164
Wt 8	Object 1	9337	3779.54	2.93917	30	68.2329	637091	202.764	115.858	16.367
Wt 9	Object 1	8801	3562.57	3.77196	30	69.7973	614286	296.746	99.2607	15.3018
Wt 10	Object 1	8425	3410.37	2.85923	30	52.7828	444695	231.646	182.532	23.1774

Img No 9	**Name**	**Voxel Count**	**Volume (µm³)**	**Mean (Ch3-T1)**	**Min (Ch2-T2)**	**Mean (ChS1-T3)**	**Sum (ChS1-T3)**	**Centroid X**	**Centroid Y**	**Centroid Z**
Clone Cell	Object 1	10729	4343.01	47.4342	24	93.4281	1.00E+06	273.679	194.85	8.24355
Wt 1	Object 1	5033	2037.32	4.52533	24	85.5015	430329	216.591	114.988	9.90145
Wt 2	Object 1	9386	3799.38	3.32506	24	79.4683	745889	258.677	37.2264	8.38547
Wt 3	Object 1	8725	3531.81	4.43381	24	80.6878	704001	155.643	188.08	9.27473
Wt 4	Object 1	9582	3878.71	2.32624	24	59.9517	574457	296.667	277.456	21.971
Wt 5	Object 1	7348	2974.41	2.3997	24	46.5048	341717	137.498	75.7805	18.5558
Wt 6	Object 1	9415	3811.11	2.34041	24	56.0797	527990	332.705	111.069	15.6049
Wt 7	Object 1	4735	1916.69	4.73178	24	51.6644	244631	205.574	274.954	9.50433
Wt 8	Object 1	6823	2761.89	1.55152	24	33.8534	230982	338.473	195.441	32.9963
Wt 9	Object 1	6931	2805.61	1.97288	24	41.7125	289109	146.972	304.105	28.7097
Wt 10	Object 4	1094	442.842	1.64077	24	31.3391	34285	122.561	215.083	32.4378

Img No 10	**Name**	**Voxel Count**	**Volume (µm³)**	**Mean (Ch3-T1)**	**Min (Ch2-T2)**	**Mean (ChS1-T3)**	**Sum (ChS1-T3)**	**Centroid X**	**Centroid Y**	**Centroid Z**
Clone Cell	Object 1	5621	2275.33	13.9448	24	74.8605	420791	114.139	379.704	33.1875
Wt 1	Object 1	8690	3517.64	4.47169	24	82.4487	716479	44.8358	206.962	11.5329
Wt 2	Object 1	9977	4038.61	4.20487	24	101.475	1.01E+06	65.3157	266.602	10.8927
Wt 3	Object 1	9658	3909.48	3.25802	24	110.841	1.07E+06	402.467	380.829	9.74622
Wt 4	Object 3	1708	691.384	1.48888	24	71.6885	122444	88.5082	272.907	38.3226
Wt 5	Object 1	11673	4725.13	3.02467	24	88.0451	1.03E+06	327.923	382.979	13.7417
Wt 6	Object 1	9931	4019.99	1.99325	24	78.6832	781403	214.195	388.646	32.0811
Wt 7	Object 1	6326	2560.71	3.81473	24	110.328	697936	372.008	289.82	8.184
Wt 8	Object 1	7243	2931.91	4.21317	24	119.088	862554	337.183	336.153	8.41419
Wt 9	Object 1	12235	4952.63	4.73813	24	96.6506	1.18E+06	213.501	353.161	8.94508
Wt 10	Object 1	10936	4426.8	4.61924	24	95.2054	1.04E+06	108.008	334.046	9.80907

Average intensity of Mi-2 localization in 10 non adjacent wild type cells of img No 10

Img No 1	**91.832**
Img	**87.115**

Img No 2	
Img No 3	**55.723**
Img No 4	**77.4**
Img No 5	**86.98**
Img No 6	**84.225**
Img No 7	**87.51**
Img No 8	**75.4**
Img No 9	**56.67**
Img No 10	**95.44**

Intensity of Mi-2 localization in clone cell V average intensity of Mi-2 localization in 10 non adjacent wild type cells	
Img No 1	**0.79**
Img No 2	**0.75**
Img No 3	**1.33**
Img No 4	**0.75**
Img No 5	**1.47**
Img No 6	**0.55**
Img No 7	**0.74**
Img No 8	**0.88**
Img No 9	**1.65**
Img No 10	**0.79**

Average value of the ratio Clone cells V wild type cells acquired from Img No 1 to Img No 10	**0.97**
Standared deviation of the average value	**0.371**

B.2. (ii) Visualization of Mi-2 protein in single cell clones expressing *NOS2*

Img No 1	**Voxel Count**	**Volume (μm³)**	**Mean (Ch3-T1)**	**Min (Ch2-T2)**	**Mean (ChS1-T3)**	**Sum (ChS1-T3)**	**Centroid X**	**Centroid Y**	**Centroid Z**
Clone cell	14604	5911.58	15.0083	35	109.514	1.60E+06	388.622	331.901	10.571
Wt 1	13013	5267.56	0.277876	35	81.7953	1.06E+06	91.5113	326.69	10.577
Wt 2	11808	4779.78	0.200119	35	61.8786	730663	126.049	275.419	13.9563
Wt 3	14353	5809.98	0.242179	35	73.2347	1.05E+06	200.526	322.928	12.6651
Wt 4	10953	4433.68	0.219483	35	71.7126	785468	259.34	365.517	29.3118
Wt 5	6531	2643.69	0.261522	35	74.9677	489614	54.0167	373.733	25.46
Wt 6	10606	4293.22	0.142749	35	56.929	603789	255.974	252.923	25.2065
Wt 7	9152	3704.65	0.217767	35	61.8911	566427	76.5605	230.75	21.8563
Wt 8	11809	4780.19	0.405453	35	85.9881	1.02E+06	453.31	282.159	14.2975
Wt 9	4304	1742.22	0.152649	35	42.8483	184419	190.482	232.072	39.6578

Img No 2	**Voxel Count**	**Volume (μm³)**	**Mean (Ch3-T1)**	**Min (Ch2-T2)**	**Mean (ChS1-T3)**	**Sum (ChS1-T3)**	**Centroid X**	**Centroid Y**	**Centroid Z**
Clone cell	12749	5160.69	13.0549	35	87.2923	1.11E+06	384.352	337.584	27.9031
Wt 1	15440	6249.98	0.433873	35	23.0842	356420	63.1302	177.32	15.5132
Wt 2	8334	3373.53	0.314015	35	16.2544	135464	30.2049	224.841	26.2513
Wt 3	12831	5193.88	0.253682	35	17.02	218383	107.526	276.548	25.4352
Wt 4	15877	6426.88	0.309315	35	22.7095	360559	164.767	262.98	17.4217
Wt 5	13597	5503.95	0.26675	35	16.7141	227261	216.497	330.375	27.2523
Wt 6	8550	3460.97	0.477427	35	14.6854	125560	318.703	228.068	34.3013
Wt 7	12344	4996.75	0.260774	35	19.5429	241237	286.56	363.89	38.8339
Wt 8	3497	1415.56	0.373463	35	19.5997	68540	47.3151	108.661	33.9317
Wt 9	10450	4230.07	0.33311	35	17.1344	179054	135.489	143.198	38.2557
Wt 10	14308	5791.76	0.263629	35	16.6615	238393	216.4	330.081	27.5336

Img No 3	Voxel Count	Volume (µm³)	Mean (Ch3-T1)	Min (ChS1-T3)	Mean (ChS1-T3)	Sum (ChS1-T3)	Centroid X	Centroid Y	Centroid Z
Clone cell	9713	3931.74	43.957	26	82.8864	805076	74.0667	362.499	9.42335
Wt 1	14577	5900.65	0.684709	26	86.6768	1.26E+06	476.324	77.7023	11.8076
Wt 2	15524	6283.99	0.505153	26	91.1451	1.41E+06	348.618	150.611	11.4173
Wt 3	15461	6258.49	0.555591	26	94.9919	1.47E+06	213.919	235.506	10.5077
Wt 4	17659	7148.22	0.511977	26	97.138	1.72E+06	96.4015	201.057	10.0208
Wt 5	9231	3736.63	0.479363	26	69.6121	642589	155.105	447.927	30.5911
Wt 6	13415	5430.28	0.549981	26	76.5278	1.03E+06	315.171	265.271	19.3022
Wt 7	15663	6340.25	0.580859	26	92.0846	1.44E+06	15.0774	252.234	10.7504
Wt 8	14949	6051.23	0.557161	26	96.4496	1.44E+06	214.071	235.305	9.98368
Wt 9	15644	6332.56	0.448031	26	85.5269	1.34E+06	179.728	354.157	13.0488
Wt 10	11272	4562.81	0.387243	26	67.912	765504	120.142	474.708	28.3434

Img No 4	Voxel Count	Volume (µm³)	Mean (Ch3-T1)	Min (Ch2-T2)	Mean (ChS1-T3)	Sum (ChS1-T3)	Centroid X	Centroid Y	Centroid Z
Clone cell	727	294.284	10.7909	21	122.993	89416	67.0248	154.905	38.63
Wt 1	11295	4572.12	3.04294	21	58.1656	656981	241.914	214.363	13.255
Wt 2	11062	4477.81	2.93256	21	53.076	587127	373.285	432.568	11.4071
Wt 3	4995	2021.93	1.99339	21	54.1461	270460	337.868	280.066	16.8771
Wt 4	2795	1131.39	2.11521	21	33.9692	94944	487.1	401.273	19.917
Wt 5	3148	1274.28	0.991741	21	26.1185	82221	416.013	485.062	28.2004
Wt 6	6126	2479.75	2.13892	21	61.9993	379808	189.625	165.182	13.0215
Wt 7	10947	4431.26	2.37992	21	46.8976	513388	293.593	412.935	19.3351
Wt 8	3960	1602.98	2.70253	21	51.6929	204704	477.209	482.578	8.53359
Wt 9	10808	4374.99	1.97326	21	40.413	436784	236.15	350.271	22.2197
Wt 10	4469	1809.01	2.23831	21	56.3439	251801	139.318	38.4133	17.2806

Img No 5	Voxel Count	Volume (µm³)	Mean (Ch3-T1)	Min (Ch2-T2)	Mean (ChS1-T3)	Sum (ChS1-T3)	Centroid X	Centroid Y	Centroid Z
Clone cell	2305	933.045	9.51584	34	150.09	345957	418.873	383.629	14.308
Wt 1	7164	2899.93	3.07733	34	107.409	769478	119.171	144.13	15.5197
Wt 2	4616	1868.52	2.21599	34	86.3419	398554	104.826	207.596	26.4892
Wt 3	11121	4501.69	2.46902	34	102.178	1.14E+06	186.737	225.569	18.8666
Wt 4	10000	4047.92	2.1642	34	96.5643	965643	248.932	188.418	17.5805
Wt 5	8133	3292.17	1.5597	34	75.3111	612505	303.439	193.339	25.9203
Wt 6	4515	1827.63	1.73378	34	130.238	588025	359.948	232.992	15.0151
Wt 7	2391	967.857	4.32246	34	139.151	332710	430.93	293.207	10.5491
Wt 8	3679	1489.23	0.915466	34	56.6379	208371	231.796	276.044	35.0106
Wt 9	8345	3377.99	1.54344	34	74.3587	620523	303.499	193.23	25.7584
Wt 10	4590	1857.99	1.72636	34	129.429	594079	359.933	232.923	14.8725

Img No 6	Voxel Count	Volume (µm³)	Mean (Ch3-T1)	Min (Ch2-T2)	Mean (ChS1-T3)	Sum (ChS1-T3)	Centroid X	Centroid Y	Centroid Z
Clone cell	3891	1575.04	7.50938	27	108.935	423868	362.315	327.984	27.2005
Wt 1	7615	3082.49	0.405384	27	109.478	833678	267.77	423.111	29.9326
Wt 2	15103	6113.57	0.537046	27	104.657	1.58E+06	191.953	165.423	16.5025
Wt 3	14416	5835.48	0.616121	27	137.093	1.98E+06	252.638	222.69	12.7725
Wt 4	13189	5338.8	0.342407	27	107.917	1.42E+06	283.423	161.627	28.6243
Wt 5	6312	2555.05	0.125158	27	74.1838	468248	218.26	139.211	52.9053
Wt 6	6406	2593.1	0.823915	27	88.3445	565935	225.078	354.378	37.4243
Wt 7	10209	4132.52	1.2012	27	128.725	1.31E+06	331.765	460.056	13.1615
Wt 8	14221	5756.54	0.519795	27	120.86	1.72E+06	201.248	281.138	16.9596
Wt 9	2955	1196.16	0.111675	27	68.3675	202026	189.482	227.658	50.9411
Wt 10	13769	5573.58	0.631346	27	140.253	1.93E+06	252.778	222.504	12.2768

Img No 7	Voxel Count	Volume (µm³)	Mean (Ch3-T1)	Min (Ch2-T2)	Mean (ChS1-T3)	Sum (ChS1-T3)	Centroid X	Centroid Y	Centroid Z
Clone cell	6978	2824.64	9.682	27	108.015	753732	126.706	71.2154	12.3951
Wt 1	3127	1265.78	1.02047	27	70.2926	219805	441.243	464.01	16.3307
Wt 2	10745	4349.49	1.2966	27	53.1686	571297	259.473	311.824	17.5252
Wt 3	8662	3506.31	1.18737	27	49.6199	429808	358.503	423.675	19.1952
Wt 4	10235	4143.04	1.32702	27	57.4064	587555	327.06	351.838	17.288
Wt 5	12214	4944.13	1.14745	27	44.283	540872	284.17	418.687	19.4485

Wt 6	9760	3950.77	1.1291	27	49.7862	485913	203.725	366.296	19.9442
Wt 7	5656	2289.5	0.766443	27	40.4565	228822	310.768	488.902	26.0483
Wt 8	11559	4678.99	3.07942	27	77.2421	892841	177.364	173.684	13.4064
Wt 9	7461	3020.15	1.12009	27	37.9983	283505	250.085	185.736	27.3605
Wt 10	4237	1715.1	0.707576	27	39.5138	167420	312.635	264.51	34.4397

Img No 8	**Voxel Count**	**Volume (µm³)**	**Mean (Ch3-T1)**	**Min (Ch2-T2)**	**Mean (ChS1-T3)**	**Sum (ChS1-T3)**	**Centroid X**	**Centroid Y**	**Centroid Z**
Clone cell	6584	2665.15	21.4598	27	151.11	994909	298.28	409.585	11.1315
Wt 1	12081	4890.29	3.6372	27	83.3689	1.01E+06	204.17	314.177	14.3757
Wt 2	9646	3904.62	3.00021	27	75.9962	733059	287.268	178.736	22.5122
Wt 3	2769	1120.87	2.64175	27	65.4485	181227	319.649	61.2929	19.333
Wt 4	7302	2955.79	2.13106	27	61.6913	450470	223.472	119.868	32.9984
Wt 5	8749	3541.52	2.99577	27	73.0786	639365	307.337	265.496	24.6226
Wt 6	2641	1069.06	2.11208	27	44.248	116859	338.086	151.421	33.3453
Wt 7	4833	1956.36	1.63915	27	42.66	206176	254.585	16.1235	30.6313
Wt 8	5695	2305.29	2.84039	27	62.7845	357558	179.637	406.727	28.4291
Wt 9	2759	1116.82	2.35774	27	56.9239	157053	326.845	336.399	33.8663
Wt 10	2964	1199.8	1.94872	27	43.8988	130116	183.949	302.899	37.9551

Img No 9	**Voxel Count**	**Volume (µm³)**	**Mean (Ch3-T1)**	**Min (ChS1-T3)**	**Mean (ChS1-T3)**	**Sum (ChS1-T3)**	**Centroid X**	**Centroid Y**	**Centroid Z**
Clone cell	6723	2721.41	13.6903	70	118.427	796185	399.693	306.836	32.221
Wt 1	11361	4598.84	6.18484	70	135.942	1.54E+06	304.203	157.528	15.1175
Wt 2	11241	4550.26	5.45877	70	136.744	1.54E+06	404.655	130.763	12.9722
Wt 3	10068	4075.44	5.4122	70	133.857	1.35E+06	372.911	63.6268	16.8599
Wt 4	10606	4293.22	6.67198	70	134.476	1.43E+06	245.338	378.501	6.56958
Wt 5	10535	4264.48	6.05857	70	128.342	1.35E+06	491.866	97.5585	21.9106
Wt 6	8438	3415.63	6.82259	70	130.373	1.10E+06	30.3668	434.829	7.31785
Wt 7	9630	3898.14	4.95794	70	122.78	1.18E+06	255.281	437.855	20.0157
Wt 8	9978	4039.01	5.3625	70	127.947	1.28E+06	442.811	20.4209	13.4531
Wt 9	9465	3831.35	5.69593	70	130.392	1.23E+06	161.446	409.706	10.0875
Wt 10	9491	3841.88	5.82699	70	139.631	1.33E+06	188.005	481.672	15.6344

Img No 10	**Voxel Count**	**Volume (µm³)**	**Centroid X**	**Centroid Y**	**Centroid Z**	**Mean (ChS2-T2)**	**Sum (ChS2-T2)**	**Mean (Ch3-T3)**	**Min (Ch2-T4)**
Clone cell	12208	4941.7	227.164	65.372	18.3965	112.579	1.37E+06	27.9812	30
Wt 1	7614	3082.08	242.085	350.458	18.2434	28.1027	213974	4.85671	30
Wt 2	11171	4521.93	350.813	448.677	7.20526	30.6185	342039	7.14027	30
Wt 3	7611	3080.87	437.641	417.774	11.0122	27.1084	206322	5.53804	30
Wt 4	14011	5671.54	312.357	343.563	10.2438	33.4028	468007	6.14481	30
Wt 5	13142	5319.77	380.114	270.696	16.9997	41.2019	541476	6.84485	30
Wt 6	5034	2037.72	68.3619	11.1134	8.68733	27.9062	140480	8.47815	30
Wt 7	11361	4598.84	302.521	74.1784	27.9856	69.6052	790785	8.87131	30
Wt 8	12102	4898.79	291.566	176.595	23.9484	50.8028	614815	7.23732	30
Wt 9	11151	4513.83	205.787	239.251	20.9495	30.9032	344602	6.26616	30
Wt 10	1840	744.817	145.205	179.559	26.0353	30.7864	56647	5.93804	30

Average intensity of Mi-2 localization in 10 non adjacent wild type cells

Img No 1	**67.916**
Img No 2	**18.341**
Img No 3	**85.806**
Img No 4	**99.762**
Img No 5	**48.282**
Img No 6	**107.99**
Img No 7	**51.977**
Img No 8	**61.01**
Img No 9	**132.05**
Img No 10	**37.044**

Intensity of Mi-2 localization in clone cell V average intensity of Mi-2 localization in 10 non adjacent wild type cells

Img No 1	**1.61**
Img No 2	**4.8**
Img No 3	**0.97**
Img No 4	**1.5**
Img No 5	**2.5**
Img No 6	**1**
Img No 7	**2**
Img No 8	**2.47**
Img No 9	**0.89**
Img No 10	**3**

Average value of the ratio of the clone cell V wild type cells acquired from Img No 1 to Img No 10	**2.074**
	1.199594
Standard deviation of the average value	**376**

B.3. Visualization of Dref protein in single cell clones expressing *NOS2*

B.3. (i) Visualization of Dref protein in GFP marked control clone cells

Img No 1	**Voxel Count**	**Volume (µm³)**	**Mean (Ch3-T1)**	**Min (Ch2-T2)**	**Mean (ChS1-T3)**	**Sum (ChS1-T3)**	**Centroid X**	**Centroid Y**	**Centroid Z**
Clone cell	10100	4088.4	24.5897	21	29.3016	295946	371.281	252.13	18.9531
Wt 1	12595	5098.35	2.07868	21	46.786	589270	214.03	177.03	17.5405
Wt 2	5066	2050.68	1.76905	21	85.5517	433405	222.544	338.52	15.5914
Wt 3	7061	2858.23	2.61663	21	84.1685	594314	288.309	416.21	9.03711
Wt 4	7295	2952.96	2.27567	21	74.4814	543342	343.797	476.33	8.87361
Wt 5	14946	6050.02	2.35809	21	163.747	2.45E+06	269.889	70.472	13.943
Wt 6	11170	4521.52	1.6701	21	91.5438	1.02E+06	192.808	93.23	22.4355
Wt 7	9654	3907.86	1.93806	21	95.1569	918645	390.351	64.592	20.1717
Wt 8	8349	3379.61	1.64032	21	22.0971	184489	386.266	420.17	21.3259
Wt 9	12396	5017.8	1.99734	21	60.2462	746812	308.241	152.54	18.1158
Wt 10	7093	2871.19	2.47328	21	80.8893	573748	340.135	369.27	10.0925

Img No 2	**Voxel Count**	**Volume (µm³)**	**Mean (Ch3-T1)**	**Min (Ch2-T2)**	**Mean (ChS1-T3)**	**Sum (ChS1-T3)**	**Centroid X**	**Centroid Y**	**Centroid Z**
Clone cell	8583	3474.33	28.0068	21	102.769	882067	226.969	394.36	11.449
Wt 1	13876	5616.89	3.88642	21	40.2023	557847	280.627	365.44	20.4447
Wt 2	8287	3354.51	4.17184	21	72.0115	596759	287.077	54.621	14.8924
Wt 3	12570	5088.23	4.04503	21	42.9156	539449	280.893	365.33	19.3656
Wt 4	2389	967.048	2.23273	21	40.9029	97717	333.625	308.61	34.1168
Wt 5	9228	3735.42	4.42393	21	32.4777	299704	251.97	473.89	13.8808
Wt 6	4587	1856.78	4.34772	21	93.0961	427032	225.109	282.67	21.3056
Wt 7	12401	5019.82	3.41626	21	70.9943	880400	223.214	34.749	28.2733
Wt 8	6597	2670.41	4.05063	21	39.0361	257521	195.338	446.19	18.6382
Wt 9	7394	2993.03	4.40371	21	74.8171	553198	264.299	138.57	13.9145
Wt 10	4317	1747.49	2.91267	21	20.9134	90283	321.005	431.59	27.9657

Img No 3	**Voxel Count**	**Volume (µm³)**	**Mean (Ch3-T1)**	**Min (Ch2-T2)**	**Mean (ChS1-T3)**	**Sum (ChS1-T3)**	**Centroid X**	**Centroid Y**	**Centroid Z**
Clone cell	14975	6061.76	9.62938	21	16.3048	244165	236.487	179.98	28.3275
Wt 1	12144	4915.79	1.78664	21	1.49251	18125	310.228	373.67	34.1846
Wt 2	9671	3914.74	1.82318	21	13.3727	129327	174.523	295	34.5521
Wt 3	24228	9807.29	1.94473	21	45.8214	1.11E+06	116.571	311.43	13.7265
Wt 4	21231	8594.13	2.88705	21	48.7589	1.04E+06	188.523	378.97	12.2754
Wt 5	10525	4260.43	2.35211	21	14.6205	153881	108.672	125.97	38.9587
Wt 6	8275	3349.65	1.29583	21	2.39384	19809	395.4	435.52	34.3932
Wt 7	18812	7614.94	3.34287	21	16.4358	309190	327.715	247.09	11.7219
Wt 8	24906	10081.7	8.53541	21	61.5791	1.53E+06	192.68	114.57	15.2904
Wt 9	9982	4040.63	1.93588	21	11.0224	110026	125.625	219.58	35.1589
Wt 10	8748	3541.12	1.6158	21	5.97062	52231	376.333	319.92	26.6973

Img No 4	**Voxel Count**	**Volume (µm³)**	**Mean (Ch3-T1)**	**Min (Ch2-T2)**	**Mean (ChS1-T3)**	**Sum (ChS1-T3)**	**Centroid X**	**Centroid Y**	**Centroid Z**
Clone cell	10509	4253.96	24.0914	21	41.834	439633	283.312	358.62	10.6986
Wt 1	5095	2062.41	4.75172	21	30.1095	153408	329.4	332.5	25.4471
Wt 2	1558	630.666	2.84403	21	50.2529	78294	216.202	15.135	27.5026
Wt 3	2751	1113.58	2.87096	21	17.5867	48381	249.663	300.16	26.8957
Wt 4	15426	6244.32	4.60755	21	40.3641	622657	215.428	386.74	15.6644
Wt 5	9604	3887.62	3.54425	21	44.4399	426801	72.5614	32.748	15.9109
Wt 6	5536	2240.93	3.07912	21	30.5307	169018	158.256	420.22	25.7607
Wt 7	4736	1917.09	4.78273	21	28.8562	136663	328.663	333.16	25.4419
Wt 8	8686	3516.02	3.43587	21	64.784	562714	236.458	125.97	19.9026

Wt 9	9440	3821.23	4.86578	21	40.3535	380937	329.424	437.93	8.18994
Wt 10	16918	6848.27	5.29885	21	61.767	1.04E+06	188.863	66.022	8.65132

Img No 5	**Voxel Count**	**Volume (μm³)**	**Mean (Ch3-T1)**	**Min (Ch2-T2)**	**Mean (ChS1-T3)**	**Sum (ChS1-T3)**	**Centroid X**	**Centroid Y**	**Centroid Z**
Clone cell	17461	7068.07	17.1294	21	33.0357	576836	333.379	391.89	15.9236
Wt 1	15682	6347.94	4.48992	21	54.3709	852645	138.334	71.042	16.3758
Wt 2	11022	4461.61	4.28171	21	66.2457	730160	226.068	65.968	11.2556
Wt 3	15751	6375.87	5.44372	21	96.1859	1.52E+06	207.588	124.53	8.3709
Wt 4	9513	3850.78	4.13844	21	72.7508	692078	285.647	143.27	11.324
Wt 5	16394	6636.16	4.35434	21	56.6882	929346	240.875	204.4	12.4241
Wt 6	15894	6433.76	3.93545	21	46.4575	738395	286.018	271.53	15.9278
Wt 7	14339	5804.31	3.93821	21	33.1852	475842	423.636	352.68	14.3792
Wt 8	15038	6087.26	4.40371	21	37.0817	557634	354.699	318.67	12.5285
Wt 9	8802	3562.98	3.7354	21	44.6003	392572	379.971	250.66	12.8348
Wt 10	8973	3632.2	2.60493	21	41.5951	373233	301.171	84.714	26.0578

Img No 6	**Voxel Count**	**Volume (μm³)**	**Mean (Ch3-T1)**	**Min (Ch2-T2)**	**Mean (ChS1-T3)**	**Sum (ChS1-T3)**	**Centroid X**	**Centroid Y**	**Centroid Z**
Clone cell	16299	6597.7	20.4275	21	94.7001	1.54E+06	297.438	231.8	19.4014
Wt 1	15456	6256.46	6.44979	21	73.0057	1.13E+06	200.76	421.06	8.60287
Wt 2	7333	2968.34	5.90113	21	69.6506	510748	114.159	403.42	7.12628
Wt 3	9003	3644.34	6.37343	21	62.9328	566584	172.578	336.5	10.1002
Wt 4	16888	6836.12	5.37056	21	54.5131	920617	331.239	123.98	15.3115
Wt 5	14781	5983.23	5.51512	21	88.3513	1.31E+06	240.84	351.68	11.4536
Wt 6	16706	6762.45	6.32617	21	76.3911	1.28E+06	248.406	81.013	12.1808
Wt 7	6682	2704.82	6.23451	21	76.0492	508161	105.635	482.73	5.81562
Wt 8	8575	3471.09	5.43953	21	60.3621	517605	150.585	271.72	12.4609
Wt 9	8242	3336.29	4.31376	21	52.859	435664	91.6744	349.71	24.5901
Wt 10	1549	627.022	3.85539	21	51.5642	79873	190.343	166.88	27.9032

Img No 7	**Voxel Count**	**Volume (μm³)**	**Mean (Ch3-T1)**	**Min (Ch2-T2)**	**Mean (ChS1-T3)**	**Sum (ChS1-T3)**	**Centroid X**	**Centroid Y**	**Centroid Z**
Clone cell	3793	1535.38	24.3201	26	95.4205	361930	228.221	146.73	39.8587
Wt 1	14204	5749.66	8.38658	26	75.9005	1.08E+06	205.605	421.8	18.5348
Wt 2	9065	3669.44	8.20375	26	43.6707	395875	203.432	301.96	29.8202
Wt 3	6481	2623.46	6.18917	26	88.985	576712	348.304	345.37	34.2978
Wt 4	8199	3318.89	6.27869	26	78.6364	644740	364.778	183.15	31.8572
Wt 5	8048	3257.76	6.2459	26	56.5017	454726	343.611	456.09	31.1148
Wt 6	15049	6091.71	10.0706	26	100.521	1.51E+06	261.238	459.13	8.75008
Wt 7	14520	5877.58	9.28733	26	97.8848	1.42E+06	282.646	90.114	16.2149
Wt 8	14549	5889.32	10.0059	26	99.152	1.44E+06	315.805	165.81	11.6897
Wt 9	3462	1401.39	8.5959	26	117.754	407663	375.4	43.009	15.2386
Wt 10	3117	1261.74	6.15656	26	91.6567	285694	347.735	264.66	26.872

Img No 8	**Voxel Count**	**Volume (μm³)**	**Mean (Ch3-T1)**	**Min (Ch2-T2)**	**Mean (ChS1-T3)**	**Sum (ChS1-T3)**	**Centroid X**	**Centroid Y**	**Centroid Z**
Clone cell	8451	3420.9	37.8313	24	51.5898	435985	81.5251	116.1	10.2569
Wt 1	12349	4998.77	3.52231	24	123.722	1.53E+06	258.838	209.53	10.4983
Wt 2	10642	4307.79	3.77382	24	208.041	2.21E+06	148.509	266.48	19.8272
Wt 3	12539	5075.68	3.43863	24	73.126	916927	196.495	23.456	12.1596
Wt 4	8306	3362.2	4.24115	24	36.0211	299191	91.6183	16.678	8.27751
Wt 5	11520	4663.2	3.17543	24	54.8467	631834	249.576	390.37	16.3724
Wt 6	6166	2495.95	3.3495	24	96.8793	597358	102.012	207.21	19.0062
Wt 7	11100	4493.19	2.70865	24	45.3246	503103	311.154	106.51	15.4815
Wt 8	7015	2839.61	3.00613	24	25.9706	182184	419.088	391.36	10.0744
Wt 9	3524	1426.49	2.51703	24	29.6348	104433	368.052	206.22	14.3383
Wt 10	3026	1224.9	2.36682	24	11.0231	33356	444.518	292.61	18.0145

Img No 9	**Voxel Count**	**Volume (μm³)**	**Mean (Ch3-T1)**	**Min (Ch2-T2)**	**Mean (ChS1-T3)**	**Sum (ChS1-T3)**	**Centroid X**	**Centroid Y**	**Centroid Z**
Clone cell	11034	4466.47	56.0247	24	65.4313	721969	397.064	189.49	11.5333
Wt 1	6803	2753.8	2.19756	24	58.8455	400326	157.571	255.41	20.9337
Wt 2	12136	4912.55	3.61149	24	102.993	1.25E+06	130.207	208.92	10.2523
Wt 3	10534	4264.08	4.03332	24	56.8899	599278	301.353	271.16	14.301
Wt 4	8787	3556.91	3.37316	24	61.3249	538862	228.947	254.14	14.8284
Wt 5	7436	3010.03	3.34817	24	78.0258	580200	446.381	332.39	12.0344
Wt 6	3121	1263.36	7.8917	24	47.0119	146724	241.539	87.713	23.71

Average intensity of Mi-2 localization in 10 non adjacent wild type cells

Img No 1	**82.942**
Img No 2	**53.955**
Img No 3	**25.559**

Img No 4	**38.366**
Img No 5	**57.87**
Img No 6	**70.156**
Img No 7	**80.156**
Img No 8	**82.991**
Img No 9	**67.515**

Intensity of Mi-2 localization in clone cell V average intensity of Mi-2 localization in 10 non adjacent wild type cells

Img No 1	**0.35**
Img No 2	**1.9**
Img No 3	**0.64**
Img No 4	**1.08**
Img No 5	**0.57**
Img No 6	**1.35**
Img No 7	**1.19**
Img No 8	**0.62**
Img No 9	**0.97**

Average value of the ratio of the clone cell V wild type cells acquired from Img No 1 to Img No 10 **0.96333**
Std Dev of the avg ratio of clone cell / wild type cell **0.48026**

B.3. (ii) Visualization of Dref protein in single cell clones expressing *NOS2*

Img No 1	**Voxel Count**	**Volume (μm³)**	**Mean (Ch3-T1)**	**Min (Ch2-T2)**	**Mean (ChS1-T3)**	**Sum (ChS1-T3)**	**Centroid X**	**Centroid Y**	**Centroid Z**
Clone cell	3626	1467.77	52.7733	27	88.7921	321960	211.278	406.154	37.4702
Wt 1	9799	3966.55	0.221349	27	100.989	989594	280.865	145.563	14.9135
Wt 2	11017	4459.59	0.248797	27	83.9361	924724	224.906	131.776	15.083
Wt 3	11920	4825.12	1.82508	27	88.6872	1.06E+06	290.347	52.5028	16.4854
Wt 4	9315	3770.64	0.271605	27	97.0998	904485	341.577	110.028	16.748
Wt 5	10358	4192.83	0.234987	27	99.7947	1.03E+06	266.654	239.678	16.2033
Wt 6	11610	4699.63	0.215245	27	80.7769	937820	203.227	254.361	13.7073
Wt 7	9348	3783.99	0.238126	27	80.2221	749916	115.219	295.267	18.0088
Wt 8	10233	4142.23	0.311346	27	76.4842	782663	92.9304	435.065	15.1652
Wt 9	3141	1271.45	0.370901	27	68.9908	216700	21.0729	492.247	13.8695
Wt 10	10489	4245.86	0.260559	27	91.8657	963579	341.066	109.913	17.0923

Img No 2	**Voxel Count**	**Volume (μm³)**	**Mean (Ch3-T1)**	**Min (Ch2-T2)**	**Mean (ChS1-T3)**	**Sum (ChS1-T3)**	**Centroid X**	**Centroid Y**	**Centroid Z**
Clone cell	7079	2865.52	38.2705	27	134.448	951759	162.137	217.752	14.5158
Wt 1	8590	3477.16	0.701746	27	132.28	1.14E+06	364.034	124.077	16.2549
Wt 2	11504	4656.72	1.22827	27	109.556	1.26E+06	294.905	186.818	12.2437
Wt 3	11697	4734.85	0.637599	27	106.184	1.24E+06	282.354	90.1641	14.496
Wt 4	9533	3858.88	1.08161	27	101.002	962855	284.921	246.106	28.8481
Wt 5	11784	4770.07	0.657841	27	93.5411	1.10E+06	222.041	103.322	23.3759
Wt 6	5520	2234.45	6.67355	27	68.8748	380189	79.4187	327.19	15.1049
Wt 7	6372	2579.33	0.77511	27	101.116	644309	181.127	133.68	41.8183
Wt 8	3684	1491.25	0.411509	27	99.813	367711	372.173	182.286	34.8149
Wt 9	5383	2178.99	0.316366	27	73.8148	397345	227.502	21.3974	38.7044
Wt 10	3393	1373.46	0.57707	27	71.7645	243497	248.473	234.055	48.0631

Img No 3	**Voxel Count**	**Volume (μm³)**	**Mean (Ch3-T1)**	**Min (Ch2-T2)**	**Mean (ChS1-T3)**	**Sum (ChS1-T3)**	**Centroid X**	**Centroid Y**	**Centroid Z**
Clone cell	5951	2408.92	33.2437	24	49.5656	294965	407.968	243.998	22.7158
Wt 1	10988	4447.85	1.53722	24	101.557	1.12E+06	106.594	36.709	20.9018
Wt 2	15072	6101.02	1.93305	24	91.7006	1.38E+06	183.121	47.0123	15.4599
Wt 3	13800	5586.13	2.2208	24	107.252	1.48E+06	70.0538	93.0271	6.18065
Wt 4	14703	5951.65	2.44011	24	60.4169	888309	153.869	222.235	6.9949
Wt 5	10909	4415.87	2.32414	24	59.172	645507	243.545	275.975	10.1966
Wt 6	15746	6373.85	2.18068	24	63.2905	996572	250.651	106.739	14.3565
Wt 7	9274	3754.04	1.68191	24	72.4582	671977	133.677	140.967	18.3428

Wt 8	12176	4928.74	1.7909	24	64.9811	791210	203.258	189.859	19.656
Wt 9	2662	1077.56	2.26108	24	12.7926	34054	281.814	121.879	1.32494
Wt 10	16022	6485.57	2.19966	24	63.0753	1.01E+06	250.775	106.477	14.5888

Img No 4	**Voxel Count**	**Volume (µm³)**	**Mean (Ch3-T1)**	**Min (Ch2-T2)**	**Mean (ChS1-T3)**	**Sum (ChS1-T3)**	**Centroid X**	**Centroid Y**	**Centroid Z**
Clone cell	12736	5155.43	20.3642	24	93.3568	1.19E+06	387.162	366.016	16.1611
Wt 1	11992	4854.26	2.99867	24	86.4139	1.04E+06	84.0986	210.525	18.9256
Wt 2	13833	5599.48	3.66464	24	93.05	1.29E+06	71.8269	269.347	14.7801
Wt 3	13624	5514.88	2.86472	24	71.2801	971120	230.258	250.543	20.6847
Wt 4	14197	5746.83	3.02895	24	72.8785	1.03E+06	215.315	310.294	20.2059
Wt 5	9355	3786.83	4.1054	24	105.957	991227	289.179	287.547	10.3844
Wt 6	10057	4070.99	2.36383	24	53.4162	537207	189.602	198.404	30.7734
Wt 7	5860	2372.08	2.33925	24	77.9171	456594	92.7949	167.5	33.3911
Wt 8	8815	3568.24	4.2186	24	70.5612	621997	459.062	307.781	27.6853
Wt 9	6909	2796.71	3.07555	24	81.8987	565838	337.13	264.154	21.7645
Wt 10	6129	2480.97	2.40888	24	78.2211	479417	152.181	244.605	18.5401

Img No 5	**Voxel Count**	**Volume (µm³)**	**Mean (Ch3-T1)**	**Min (Ch2-T2)**	**Mean (ChS1-T3)**	**Sum (ChS1-T3)**	**Centroid X**	**Centroid Y**	**Centroid Z**
Clone cell	7777	3148.07	94.5059	24	88.2321	686181	349.104	56.5303	9.88016
Wt 1	5956	2410.94	0.260745	24	80.8573	481586	143.693	347.979	7.7824
Wt 2	9036	3657.7	0.336653	24	80.3962	726460	260.197	310.275	9.63103
Wt 3	6693	2709.27	0.443747	24	78.0883	522645	174.675	490.083	7.84432
Wt 4	7507	3038.77	0.299454	24	73.2836	550140	285.603	474.779	13.3077
Wt 5	2532	1024.93	0.382306	24	83.7536	212064	442.077	258.901	9.85624
Wt 6	8787	3556.91	0.337544	24	94.5047	830413	164.273	209.366	9.62217
Wt 7	7197	2913.29	0.451855	24	76.1791	548261	174.426	490.026	8.26539
Wt 8	5826	2358.32	0.263646	24	81.7317	476169	143.736	347.937	7.77326

Img No 6	**Voxel Count**	**Volume (µm³)**	**Mean (Ch3-T1)**	**Min (Ch2-T2)**	**Mean (ChS1-T3)**	**Sum (ChS1-T3)**	**Centroid X**	**Centroid Y**	**Centroid Z**
Clone cell	11357	4597.22	32.6142	21	100.826	1.15E+06	345.561	157.249	11.3082
Wt 1	8683	3514.81	1.22101	21	103.873	901929	165.205	377.412	12.0988
Wt 2	3506	1419.2	1.14404	21	123.233	432055	67.6098	318.207	10.8274
Wt 3	5201	2105.32	1.64757	21	99.7641	518873	173.053	43.5485	10.4586
Wt 4	2303	932.235	1.52149	21	128.276	295420	61.2979	174.663	10.7082
Wt 5	5245	2123.13	1.67207	21	99.0766	519657	173.068	43.4463	10.5701
Wt 6	7868	3184.9	1.24428	21	115.677	910149	392.012	43.7262	12.6459
Wt 7	7023	2842.85	1.35441	21	100.501	705819	269.834	21.6046	9.96768
Wt 8	1526	617.712	0.694626	21	92.5714	141264	274.197	371.68	20.5917

Img No 7	**Voxel Count**	**Volume (µm³)**	**Mean (ChS1-T3)**	**Sum (ChS1-T3)**	**Centroid X**	**Centroid Y**	**Centroid Z**	**Min (Ch2-T1)**	**Mean (Ch3-T2)**
Clone cell	3529	1428.51	57.9544	204521	240.852	415.278	20.3961	24	66.5384
Wt 1	8899	3602.24	83.301	741296	301.43	201.784	20.6468	24	1.62187
Wt 2	6672	2700.77	74.4571	496778	193.729	159.2	19.7235	24	0.84967
Wt 3	4949	2003.31	94.5557	467956	128.728	304.521	20.6789	24	1.55789
Wt 4	3838	1553.59	62.3609	239341	387.838	49.4192	21.7939	24	1.1334
Wt 5	3790	1534.16	71.2443	270016	402.341	203.139	21.3541	24	1.22507
Wt 6	3835	1552.38	62.442	239465	387.913	49.4149	21.7718	24	1.13325
Wt 7	8527	3451.66	53.1391	453117	340.801	385.277	12.6475	24	0.40319
Wt 8	8172	3307.96	67.635	552713	326.275	291.646	21.3922	24	1.01199
Wt 9	3241	1311.93	62.8747	203777	255.277	487.528	5.22092	24	0.523604

Img No	**Voxel**	**Volume**	**Mean**	**Sum**	**Centroid X**	**Centroid Y**	**Centroid**	**Min**	**Mean**

8	Count	(µm³)	(ChS1-T3)	(ChS1-T3)			Z	(Ch2-T1)	(Ch3-T2)
Clone cell	8035	3252.5	84.1187	675894	98.1469	200.325	11.7135	21	17.69
Wt 1	12912	5226.67	90.096	1.16E+06	312.575	81.7982	15.0163	21	2.70074
Wt 2	11038	4468.09	91.6124	1.01E+06	376.477	181.518	10.3351	21	3.67992
Wt 3	6196	2508.09	103.359	640414	463.473	230.712	12.4921	21	3.01436
Wt 4	9976	4038.2	109.533	1.09E+06	185.327	76.2812	19.7971	21	3.67622
Wt 5	11955	4839.29	87.5757	1.05E+06	357.072	250.722	10.2494	21	3.35274
Wt 6	1771	716.886	131.58	233029	458.623	101.809	14.5184	21	2.65556
Wt 7	3285	1329.74	100.128	328922	444.549	353.646	19.0061	21	1.70837
Wt 8	12159	4921.86	98.2656	1.19E+06	254.704	311.163	10.7201	21	4.09351
Wt 9	7287	2949.72	111.578	813072	105.476	353.682	10.4304	21	4.39495
Wt 10	10792	4368.51	103.222	1.11E+06	151.934	380.232	14.1374	21	3.2702

Img No 9	Voxel Count	Volume (µm³)	Mean (ChS1-T3)	Sum (ChS1-T3)	Centroid X	Centroid Y	Centroid Z	Min (Ch2-T1)	Mean (Ch3-T2)
Clone cell	2959	1197.78	63.8516	188937	119.635	395.084	19.2068	21	44.2143
Wt 1	8979	3634.63	82.0533	736757	330.342	88.6629	18.2284	21	1.20314
Wt 2	4541	1838.16	63.9176	290250	395.763	278.13	19.1956	21	1.39242
Wt 3	9714	3932.15	113.691	1.10E+06	269.71	200.867	19.4888	21	1.31141
Wt 4	7641	3093.01	77.3464	591004	340.994	344.606	23.8799	21	1.28452
Wt 5	4596	1860.42	93.01	427474	356.205	253.341	30.3734	21	1.16819
Wt 6	6544	2648.96	97.3046	636761	243.536	485.942	28.0254	21	1.24801
Wt 7	7018	2840.83	113.345	795454	322.159	155.405	28.1386	21	1.2666
Wt 8	1278	517.324	81.9116	104683	421.169	39.2199	9.53052	21	1.55634
Wt 9	8085	3272.74	99.3396	803161	384.368	121.232	8.57069	21	2.02474
Wt 10	11461	4639.32	90.9728	1.04E+06	264.649	266.729	9.1177	21	2.24317

Average intensity of Mi-2 localization in 10 non adjacent wild type cells

Img No 1	**88.4987**
Img No 2	**101.546**
Img No 3	**77.6035**
Img No 4	**78.9342**
Img No 5	**81.099**
Img No 6	**107.872**
Img No 7	**71.141**
Img No 8	**101.518**
Img No 9	**90.3224**

Intensity of Mi-2 localization in clone cell V average intensity of Mi-2 localization in 10 non adjacent wild type cells

Img No 1	**1**
Img No 2	**1.32**
Img No 3	**0.639**
Img No 4	**1.18**
Img No 5	**1.08**
Img No 6	**0.93**
Img No 7	**0.82**
Img No 8	**0.83**
Img No 9	**0.7**

Average value of the ratio of the clone cell V wild type cells acquired from Img No 1 to Img No 10	**0.944333**
Std Dev of the average ratio of clone cell / wild type cell	**0.22356**

B.4. Study of the phenotype imparted by NOS in a Mi-2 down regulated background

B.4.(i). Measurements of nuclei volume of third instar salivary glands from wild type larvae

Img No 1	Volume (µm³)	Centroid X	Centroid Y	Centroid Z	Min (Ch2-T2)
N 1	7392.91	184.623	62.4133	13.2324	21
N 2	6476.06	163.611	266.174	14.2848	21
N 3	5903.28	239.937	177.215	13.3151	21
N 4	5236.18	324.832	376.693	10.6902	21
N 5	5079.12	342.004	245.054	15.707	21
N 6	3192.39	292.652	25.3614	19.7381	21
N 7	3516.63	405.742	441.422	10.1335	21
N 8	5390.81	112.81	201.254	21.928	21
N 9	2401.83	307.634	119.887	21.0839	21
N 10	3188.95	174.177	402.736	22.3257	21

Img No 2	Volume (µm³)	Centroid X	Centroid Y	Centroid Z	Min (Ch2-T2)
N 1	5315.32	173.843	97.7574	9.35172	21
N 2	10406.4	141.609	187.206	18.0304	21
N 3	5090.05	272.01	250.705	9.0499	21
N 4	8198.45	195.354	292.501	20.8716	21
N 5	8026.62	307.656	400.657	15.0082	21
N 6	6941.37	361.455	300.488	19.2854	21
N 7	7185.66	279.054	162.921	18.6745	21
N 8	8201.89	420.55	388.435	13.3555	21
N 9	7349.8	426.915	489.146	15.3673	21
N 10	4896.16	278.384	70.0888	26.1336	21

Img No 3	Volume (µm³)	Centroid X	Centroid Y	Centroid Z	Min (Ch2-T2)
N 1	5680.65	348.15	315.296	24.0569	21
N 2	6327.5	51.4387	279.789	21.3139	21
N 3	5811.19	406.219	97.0093	30.7798	21
N 4	6141.91	168.527	387.378	24.6353	21
N 5	5950.44	101.468	476.957	39.4082	21
N 6	5189.63	123.095	169.505	35.8173	21
N 7	3561.97	491.827	311.984	48.9158	21
N 8	6347.54	371.677	203.275	18.1129	21

Img No 4	Volume (µm³)	Centroid X	Centroid Y	Centroid Z	Min (Ch2-T2)
N 1	5466.92	192.708	57.3339	16.0009	21
N 2	4704.09	111.849	157.832	22.7933	21
N 3	5440.2	204.311	193.536	12.411	21
N 4	6172.87	154.848	295.398	14.6124	21
N 5	6384.17	242.095	407.061	11.6266	21
N 6	5367.13	298.77	297.066	13.7222	21
N 7	6701.93	294.665	36.7634	13.0157	21
N 8	5646.64	338.983	135.82	21.5394	21
N 9	4821.07	353.759	220.725	20.8775	21
N 10	1935.11	137.172	400.752	24.9955	21

Img No 5	Volume (µm³)	Min (Ch2-T2)	Centroid X	Centroid Y	Centroid Z
N 1	6934.89	21	253.128	111.448	14.7375

N 2	6394.09	21	362.816	99.4427	14.6919
N 3	7140.12	21	198.271	215.018	16.9155
N 4	3754.65	21	188.006	421.383	12.774
N 5	4260.43	21	251.233	296.355	10.9383
N 6	4223.39	21	133.607	346.366	14.0396
N 7	4740.92	21	437.791	157.504	21.9969
N 8	2815.12	21	48.8673	382.974	21.0347
N 9	4601.27	21	219.32	75.9959	33.7449
N 10	1784.32	21	141.027	178.63	31.9435

Img No 6	**Volume (µm³)**	**Min (Ch2-T2)**	**Centroid X**	**Centroid Y**	**Centroid Z**
N 1	4310.02	21	133.526	335.599	10.8968
N 2	4395.63	21	156.845	145.17	7.59955
N 3	3669.03	21	27.9704	99.8825	9.16119
N 4	3828.52	21	381.691	242.988	7.59817
N 5	4054.6	21	243.573	386.428	12.3903
N 6	4311.44	21	133.202	335.269	10.9962
N 7	3995.5	21	148.984	53.1881	14.3316
N 8	2774.44	21	472.479	213.41	11.9706
N 9	2205.31	21	271.298	161.912	10.8811
N 10	2566.58	21	193.089	257.614	7.62077

Img No 7	**Volume (µm³)**	**Min (Ch2-T2)**	**Centroid X**	**Centroid Y**	**Centroid Z**
N 1	7384.62	21	143.994	395.659	12.1537
N 2	7216.63	21	155.85	247.465	13.3592
N 3	6974.76	21	331.468	313.02	10.6789
N 4	7016.26	21	281.637	462.83	14.2638
N 5	7164.81	21	234.994	107.399	13.4492
N 6	7754.6	21	338.839	187.201	17.9582
N 7	5792.37	21	477.918	289.286	15.0953
N 8	5652.51	21	174.451	458.012	35.3182
N 9	5324.63	21	211.633	206.052	35.0866
N 10	5206.03	21	59.2358	68.0933	34.1458

Img No 8	**Volume (µm³)**	**Min (Ch2-T2)**	**Centroid X**	**Centroid Y**	**Centroid Z**
N 1	6789.17	21	227.709	429.976	27.9552
N 2	4931.78	21	88.9654	345.386	16.1111
N 3	6709.42	21	300.888	156.261	14.2303
N 4	3670.65	21	131.348	169.486	31.2569
N 5	5533.1	21	460.275	236.129	15.2697
N 6	6973.75	21	348.75	351.129	15.5739
N 7	4457.97	21	218.888	266.487	14.2436
N 8	3713.76	21	131.442	169.522	31.3414
N 9	5701.49	21	460.436	236.172	15.2821
N 10	5126.69	21	89.1217	345.293	15.7753

Img No 9	**Volume (µm³)**	**Min (Ch2-T2)**	**Centroid X**	**Centroid Y**	**Centroid Z**
N 1	4568.07	21	382.479	343.711	9.46074
N 2	4191.01	21	220.526	241.191	9.95398
N 3	3746.75	21	292.332	100.682	18.6231
N 4	4443.6	21	286.104	329.871	13.1107
N 5	3856.86	21	412.016	480.994	13.0535
N 6	3920.41	21	338.195	438.299	14.2308
N 7	3085.73	21	132.521	218.755	15.9349

N 8	4081.31	21	130.616	55.4287	7.79494
N 9	4252.94	21	196.13	141.436	8.15095
N 10	2705.02	21	475.44	378.325	18.3009

Average value of the volume of the nuclei	**5159.21225**
Standard deviation of the average value of the volume of nuclei	**1697.29525**

B.4. (ii). Measurement of nuclei volume of third instars salivary glands from larvae where expression of *NOS2* was driven by c147-GAL4.

Img No 1	Volume (µm³)	Min (Ch2-T1)	Centroid X	Centroid Y	Centroid Z
N 1	1522.55	41	244.779	213.433	43.6247
N 2	1329.46	41	185.191	152.753	40.1936
N 3	1711.61	41	137.567	173.921	43.6768
N 4	1984.92	41	213.299	267.936	45.2282
N 5	1834.97	41	137.659	174.177	44.1538
N 6	2031.18	41	263.421	167.165	42.8309
N 7	1560.76	41	143.657	239.146	45.0119
N 8	1800.33	41	36.1984	324.419	48.094
N 9	3553.72	41	46.8244	203.563	42.4571
N 10	3336.5	41	63.3762	163.446	37.3709

Img No 2	Volume (µm³)	Min (Ch2-T1)	Centroid X	Centroid Y	Centroid Z
N 1	1067.99	59	192.075	298.823	14.6717
N 2	2325.94	59	23.3662	409.054	14.5086
N 3	2222.92	59	52.8034	341.861	15.305
N 4	2009.95	59	326.998	220.52	22.4067
N 5	2378.24	59	111.542	294.466	14.5671
N 6	1765.46	59	295.851	180.512	35.9847
N 7	2014.86	59	144.031	247.78	23.286
N 8	1468.46	59	275.005	319.513	15.7987
N 9	1384.66	59	82.9254	389.643	17.7272
N 10	2225.6	59	239.174	346.413	31.4921

Img No 3	Volume (µm³)	Min (Ch2-T1)	Centroid X	Centroid Y	Centroid Z
N 1	2326.17	54	168.53	317.908	21.0677
N 2	2410.86	54	231.58	277.534	25.0113
N 3	1749.37	54	366.311	62.1473	19.4075
N 4	2615.57	54	241.401	187.072	25.3392
N 5	1981.79	54	365.282	107.636	26.5575
N 6	2400.36	54	192.328	252.292	30.8737
N 7	2082.35	54	398.653	30.6933	32.0005
N 8	1817.76	54	310.039	127.23	21.1892
N 9	2365.28	54	291.94	95.8109	21.0841
N 10	2779.82	54	316.614	170.353	25.435

Img No 4	Volume (µm³)	Centroid X	Centroid Y	Centroid Z	Min (Ch2-T2)
N 1	2141.55	221.835	231.965	10.3341	24
N 2	1504.41	265.608	288.811	9.46522	24
N 3	1510.48	310.009	398.346	10.8223	24
N 4	848.444	281.599	355.814	10.1109	24
N 5	1510.68	309.934	398.341	10.8624	24
N 6	1223.48	333.68	336.51	11.736	24
N 7	1778.86	341.873	426.232	24.8752	24
N 8	1632.93	281.773	398.592	24.5212	24

N 9	987.287	281.881	356.435	9.12567	24
N 10	1068.65	211.889	305.849	8.23731	24

Img No 5	**Volume (µm³)**	**Centroid X**	**Centroid Y**	**Centroid Z**	**Min (Ch2-T2)**
N 1	2071.32	167.77	116.476	13.792	21
N 2	1778.25	106.728	191.21	15.4284	21
N 3	1846.26	148.98	199.722	20.0926	21
N 4	1640.01	300.54	252.859	14.25	21
N 5	1686.97	370.935	343.7	9.81188	21
N 6	1596.9	377.391	241.794	10.949	21
N 7	1352	132.154	145.402	6.45404	21
N 8	1081.2	87.977	159.319	6.66323	21
N 9	711.826	129.487	173.868	33.9949	21
N 10	1702.35	370.822	343.89	9.66817	21

Img No 6	**Volume (µm³)**	**Centroid X**	**Centroid Y**	**Centroid Z**	**Min (Ch2-T2)**
N 1	1797.68	251.962	286.808	11.8194	27
N 2	1331.56	297.985	296.409	14.3535	27
N 3	1258.7	244.564	223.723	6.72053	27
N 4	1337.63	289.835	251.012	7.45877	27
N 5	1469.19	298.176	295.931	14.7169	27
N 6	1540.64	379.404	353.367	9.16014	27
N 7	1120.26	85.6596	87.1705	24.0573	27
N 8	1407.26	209.729	244.35	8.97929	27
N 9	1165.6	244.468	223.828	6.3768	27
N 10	931.426	333.076	261.478	9.60083	27

Img No 8	**Volume (µm³)**	**Centroid X**	**Centroid Y**	**Centroid Z**	**Min (Ch2-T2)**
N 1	1586.58	180.663	263.931	29.8227	27
N 2	1047.4	298.323	140.281	24.8696	27
N 3	1309.3	251.569	127.378	27.5137	27
N 4	1672.19	308.502	49.2699	21.6245	27
N 5	1109.74	345.775	20.7137	9.09684	27
N 6	1214.58	390.733	26.1601	22.3088	27
N 7	1568.37	180.853	263.929	29.8022	27
N 8	1009.55	133.978	456.476	17.8998	27
N 9	1095.57	347.992	99.0028	13.9516	27
N 10	749.472	253.244	241.904	18.2039	27

Img No 10	**Volume (µm³)**	**Centroid X**	**Centroid Y**	**Centroid Z**	**Min (Ch2-T2)**
N 1	864.23	247.53	99.9035	10.2581	27
N 2	1303.43	277.212	181.476	10.5137	27
N 3	1219.23	296.33	228.315	11.3315	27
N 4	738.34	215.772	26.2484	8.99644	27
N 5	752.913	207.24	55.7694	7.94462	27
N 6	807.155	298.345	293.387	17.8771	27
N 7	851.682	234.842	11.2548	19.3634	27
N 8	1185.64	192.726	86.1758	10.7835	27
N 9	755.139	260.511	425.365	25.5704	27
N 10	653.941	289.169	332.272	27.2392	27

Average valu of the vol of Nuclei **1582.3458**

SD of the Vol pf nuclei **584. 00291**

B.4. (iii). Measurement of nuclei volume of third instars salivary glands from larvae where UAS-NOS2 and UAS-RNAi-Mi-2 were co expressed

Img No 1	Volume (μm³)	Min (Ch2-T1)	Centroid X	Centroid Y	Centroid Z
N 1	3986.82	61	239.637	265.088	14.0555
N 2	3528.92	61	172.442	192.335	10.8894
N 3	2382.93	61	103.148	155.158	23.7584
N 4	2971.34	61	48.4228	186.801	22.6211
N 5	2698.48	61	122.916	195.66	30.5372
N 6	3557.08	61	335.168	356.703	21.4542
N 7	2114.54	61	350.693	310.198	40.8691
N 8	2118.56	61	37.3095	119.824	25.3175
N 9	2168.62	61	282.156	295.969	23.2276
N 10	1950.5	61	410.449	323.424	37.9448

Img No 2	Volume (μm³)	Min (Ch2-T1)	Centroid X	Centroid Y	Centroid Z
N 1	3033.47	59	277.004	232.537	38.0145
N 2	1411.25	59	190.699	284.481	15.9017
N 3	1791.16	59	208.676	318.957	24.4851
N 4	1446.79	59	141.907	393.89	18.7702
N 5	2671.44	59	252.089	238.4	23.3252
N 6	1672.72	59	319.732	147.136	21.7733
N 7	1598.53	59	277.918	176.804	24.2238
N 8	1643.67	59	367.28	158.518	37.5753
N 9	1256.61	59	183.925	355.491	18.4302
N 10	1409.91	59	95.1	352.391	23.162

Img No 3	Volume (μm³)	Min (Ch2-T1)	Centroid X	Centroid Y	Centroid Z
N 1	1917.21	66	308.656	383.369	34.5863
N 2	1635.4	66	213.142	351.612	33.0872
N 3	2375.78	66	213.603	332.035	16.8159
N 4	2885.98	66	255.16	76.0026	19.1419
N 5	1482.54	66	203.785	228.937	18.5222
N 6	2083.02	66	145.879	234.486	20.6106
N 7	1990.28	66	187.466	273.155	15.6353
N 8	1139.51	66	140.847	110.113	24.109
N 9	1031.79	66	183.594	201.111	34.9251
N 10	1708.25	66	258.673	404.932	17.144

Img No 4	Volume (μm³)	Min (Ch2-T1)	Centroid X	Centroid Y	Centroid Z
N 1	1710.27	58	264.115	286.457	13.7202
N 2	2067.16	58	227.701	223.214	14.4211
N 3	1619.76	58	222.132	296.817	20.9985
N 4	995.141	58	297.569	392.06	32.8439
N 5	1332.59	58	269.166	363.558	29.4496
N 6	1587.8	58	320.02	331.003	14.4662
N 7	1421.09	58	150.168	196.949	19.7691
N 8	1758.54	58	100.157	91.7193	31.9328
N 9	1942.68	58	34.4539	97.4881	14.7017
N 10	1588.92	58	76.3816	27.1707	16.2954

Img No 5	Volume (μm³)	Min (Ch2-T1)	Centroid X	Centroid Y	Centroid Z
N 1	1539.31	41	280.54	271.116	11.848
N 2	2508.08	41	140.376	231.421	12.645

N 3	1338.85	41	332.295	208.409	12.2752
N 4	867.536	41	88.9222	185.98	13.8769
N 5	2453.55	41	269.995	169.129	18.2892
N 6	1097.27	41	339.855	258.532	33.4532
N 7	1586.91	41	362.812	290.057	19.1901
N 8	1049.89	41	151.399	262.969	27.1158
N 9	503.493	41	475.577	207.299	14.5504
N 10	1064.2	41	123.665	168.508	15.5672

Img No 6	**Volume (µm³)**	**Min (Ch2-T1)**	**Centroid X**	**Centroid Y**	**Centroid Z**
N 1	1306.67	41	95.7809	154.518	38.7789
N 2	1337.73	41	280.268	189.135	37.7917
N 3	1004.97	41	50.062	157.284	40.1076
N 4	2831.89	41	213.581	141.543	15.1555
N 5	2656.24	41	460.72	227.784	16.0008
N 6	2497.57	41	433.531	273.287	15.7185
N 7	2031.18	41	213.76	212.449	15.8626
N 8	1914.52	41	13.9623	139.78	39.6229
N 9	1961.68	41	467.096	330.424	17.9294
N 10	3231.92	41	302.628	302.848	23.1456

Img No 8	**Volume (µm³)**	**Min (Ch2-T1)**	**Centroid X**	**Centroid Y**	**Centroid Z**
N 1	1544.45	83	319.141	265.889	16.821
N 2	1294.82	83	259.723	226.155	18.7829
N 3	1045.2	83	327.666	297.269	29.5123
N 4	1838.99	83	206.341	235.953	46.7877
N 5	2060.23	83	279.614	251.311	15.4466
N 6	975.252	83	155.384	214.06	18.0687
N 7	1934.41	83	141.372	185.302	42.1862
N 8	598.023	83	385.888	286.493	38.9638
N 9	1354.71	83	34.0668	131.258	24.1579
N 10	1295.49	83	259.641	226.169	18.7061

Img No 10	**Volume (µm³)**	**Min (Ch2-T1)**	**Centroid X**	**Centroid Y**	**Centroid Z**
N 1	3047.33	58	248.794	94.3459	27.2226
N 2	2319.69	58	203.639	17.7687	28.9678
N 3	2258.9	58	208.572	110.376	27.3783
N 4	2616.02	58	272.332	213.598	24.8275
N 5	2563.05	58	286.542	317.289	29.9609
N 6	1551.6	58	258.568	343.251	21.1383
N 7	2296.22	58	277.879	365.263	39.908
N 8	2478.35	58	248.548	57.6103	42.5077
N 9	1137.27	58	233.393	416.481	34.0586
N 10	958.267	58	219.342	366.63	28.0128

Average value of the volume of the nuclei	**1870.484775**
Standard deviation of the average value of the volume of nuclei	**712.7873072**

B.4. (iv). Measurement of nuclei volume of UAS-NOS2 over expressed third instar salivary glands from Mi-2 transheterozygous mutants

Img No 1	**Volume (µm³)**	**Centroid X**	**Centroid Y**	**Centroid Z**	**Min (Ch2-T2)**
N 1	1264.57	151.398	163.05	11.6759	83
N 2	525.217	98.0204	135.712	16.59	83
N 3	964.416	315.98	213.998	12.1889	83

N 4	501.335	363.956	178.846	14.3242	83
N 5	816.87	269.761	181.878	16.2252	83
N 6	1186.85	53.8404	153.808	24.9072	83
N 7	559.625	123.267	136.279	29.0817	83
N 8	384.957	293.258	165.13	21.0421	83
N 9	947.415	269.236	227.45	16.1938	83
N 10	1140.91	29.8923	123.82	36.9258	83

Img No 2	**Volume (µm³)**	**Min (Ch2-T2)**	**Centroid X**	**Centroid Y**	**Centroid Z**
N 1	1070.88	58	325.784	144.932	10.5381
N 2	671.954	58	331.774	202.451	15.5455
N 3	950.856	58	351.436	166.762	32.1237
N 4	1543.07	58	369.591	184.294	11.8258
N 5	1137.67	58	357.531	150.308	10.9338
N 6	745.829	58	287.203	241.374	12.1251
N 7	1032.42	58	346.684	230.457	11.8996
N 8	1451.18	58	259.238	123.95	20.1165
N 9	752.103	58	332.466	123.673	21.694
N 10	890.137	58	362.439	230.081	25.0705

Img No 5	**Volume (µm³)**	**Min (Ch2-T1)**	**Centroid X**	**Centroid Y**	**Centroid Z**
N 1	2264.93	69	233.306	209.126	15.4465
N 2	1348.68	69	384.339	257.447	16.8437
N 3	1221.08	69	341.115	224.568	20.1746
N 4	3511.49	69	108.96	169.536	40.7226
N 5	3272.81	69	133.979	199.696	28.5379
N 6	467.289	69	430.844	223.549	17.8761
N 7	636.238	69	364.237	211.698	25.0414
N 8	824.628	69	275.111	251.428	13.4702
N 9	1517.63	69	202.523	183.707	32.6501
N 10	1353.6	69	182.15	182.05	19.3107

Img No 6	**Volume (µm³)**	**Centroid X**	**Centroid Y**	**Centroid Z**	**Min (Ch2-T2)**
N 1	716.279	183.903	222.676	10.3815	100
N 2	925.759	275.786	253.109	11.3778	100
N 3	672.562	184.514	246.912	7.88173	100
N 4	695.027	89.9822	211.354	8.79324	100
N 5	1013.19	235.056	265.903	19.8881	100
N 6	817.072	239.165	232.201	16.0037	100
N 7	886.899	289.074	242.599	24.105	100
N 8	651.31	262.325	248.629	25.8434	100
N 9	854.515	335.27	279.541	13.8124	100
N 10	804.119	165.724	259.404	15.9202	100

Img No 7	**Volume (µm³)**	**Centroid X**	**Centroid Y**	**Centroid Z**	**Min (Ch2-T2)**
N 1	583.103	245.501	144.981	21.5588	147
N 2	445.878	181.003	103.956	18.7081	147
N 3	946.606	241.951	247.724	18.5687	147
N 4	891.351	196.074	319.252	19.3122	147
N 5	993.764	159.474	341.37	21.9662	147
N 6	764.854	103.873	347.881	28.4686	147
N 7	775.986	210.309	222.745	13.2287	147
N 8	745.626	231.434	95.9894	8.04425	147

N 9	643.012	206.802	101.03	7.38621	147
N 10	573.995	181.848	86.5628	7.58956	147

Img No 8	**Volume (µm³)**	**Centroid X**	**Centroid Y**	**Centroid Z**	**Min (Ch2-T2)**
N 1	1016.43	165.904	235.754	19.725	65
N 2	1340.06	155.921	159.901	22.9227	65
N 3	1381.35	308.522	303.116	20.5519	65
N 4	1632.53	261.83	223.865	13.7104	65
N 5	1190.09	125.666	179.863	8.41071	65
N 6	2088.32	86.2031	112.925	11.4595	65
N 7	2041.36	268.478	317.905	6.00991	65
N 8	933.45	347.272	377.367	4.70512	65
N 9	831.24	57.4069	129.298	20.3073	65
N 10	1916.69	211.563	164.804	13.2357	65

Img No 9	**Volume (µm³)**	**Min (Ch2-T2)**	**Centroid X**	**Centroid Y**	**Centroid Z**
N 1	1303.23	61	263.096	320.657	24.0311
N 2	1356.86	61	216.733	288.807	25.3082
N 3	1345.12	61	270.31	295.422	12.8562
N 4	868.886	61	244.66	271.792	9.52248
N 5	1413.13	61	233.237	210.828	26.4258
N 6	1385.8	61	195.178	179.957	28.0022
N 7	1381.96	61	180.147	225.401	11.779
N 8	1193.33	61	150.863	215.536	17.5293
N 9	1314.56	61	195.23	179.934	27.9812
N 10	852.087	61	286.283	359.121	19.6059

Img No 10	**Volume (µm³)**	**Min (Ch2-T2)**	**Centroid X**	**Centroid Y**	**Centroid Z**
N 1	1357.67	96	248.413	332.241	33.3904
N 2	2986.55	96	183.341	252.096	26.8399
N 3	2042.38	96	285.452	311.686	37.4758
N 4	2562.33	96	269.043	268.498	17.7375
N 5	1919.52	96	313.812	353.326	23.9146
N 6	1136.66	96	278.72	371.32	40.9801
N 7	2062.21	96	306.255	457.673	34.974
N 8	960.976	96	331.223	435.557	23.007
N 9	1231.58	96	327.372	463.297	25.6687
N 10	2234.45	96	121.456	161.552	14.6901

Average value of the volume of the nuclei	**1195.479438**
Standard deviation of the average value of the volume of nuclei	**621.2223307**

B.4. (v). Measurement of nuclei volume of third instar salivary glands from Mi-2 transheterozygous mutants

Img No 1	**Volume (µm³)**	**Min (Ch2-T2)**	**Centroid X**	**Centroid Y**	**Centroid Z**
N 1	5284.15	46	339.143	342.411	10.6727
N 2	4749.42	46	382.36	107.7	14.7634
N 3	5255.01	46	240.829	397.543	17.1951
N 4	5590.58	46	338.864	342.288	10.994
N 5	6033.83	46	92.3254	480.879	11.0765
N 6	3420.49	46	494.129	32.0604	17.9116
N 7	5166.76	46	138.03	223.444	16.3266
N 8	5684.49	46	254.865	171.762	13.9235
N 9	4882.8	46	408.516	272.056	14.8096
N 10	2300.03	46	450.333	483.4	22.5701

Img No 3	**Volume (µm³)**	**Min (Ch2-T2)**	**Centroid X**	**Centroid Y**	**Centroid Z**

N 1		5831.03	27	347.11	157.802	10.9839
N 2		5145.31	27	36.6176	217.464	11.1124
N 3		5641.18	27	197.054	205.976	10.0017
N 4		5791.76	27	192.117	298.453	10.8653
N 5		4183.12	27	465.67	220.114	7.34198
N 6		4440.16	27	143.412	358.859	17.3444
N 7		4689.51	27	29.0318	311.699	9.1678
N 8		3910.69	27	423.951	70.3383	18.8939
N 9		3556.7	27	288.942	331.97	24.402
N 10		3637.46	27	100.797	170.774	25.9245

Img No 4	**Volume (µm³)**	**Min (Ch2-T2)**	**Centroid X**	**Centroid Y**	**Centroid Z**
N 1	4588.11	24	78.683	207.195	13.6887
N 2	4891.3	24	341.522	233.853	10.1584
N 3	4730.6	24	411.83	163.321	13.8161
N 4	5218.37	24	335.79	440.364	15.9222
N 5	4598.64	24	137.842	109.387	15.0939
N 6	5239.02	24	240.165	287.727	15.4292
N 7	4096.29	24	454.907	377.652	20.3982
N 8	3964.33	24	475.186	119.927	36.143
N 9	2376.53	24	216.954	80.6753	38.5052
N 10	4746.59	24	197.875	478.598	11.7008

Img No 5	**Volume (µm³)**	**Min (Ch2-T2)**	**Centroid X**	**Centroid Y**	**Centroid Z**
N 1	5960.56	24	168.774	397.1	11.3218
N 2	5711.81	24	282.327	329.973	6.58566
N 3	6257.68	24	358.172	174.415	9.58228
N 4	5557.79	24	294.93	49.2474	7.48263
N 5	6167.61	24	276.838	480.986	10.9611
N 6	5113.53	24	411.27	95.9673	15.4703
N 7	4073.82	24	229.791	78.1601	29.4461
N 8	6079.57	24	213.898	146.529	13.9651
N 9	8586.85	24	355.885	370.515	25.5645
N 10	4317.71	24	186.662	349.131	24.7128

Img No 6	**Volume (µm³)**	**Min (Ch2-T2)**	**Centroid X**	**Centroid Y**	**Centroid Z**
N 1	5101.79	24	329.907	274.881	33.1215
N 2	4849.61	24	335.743	108.233	34.2701
N 3	5006.87	24	119.597	236.029	31.0753
N 4	4490.76	24	182.845	330.091	31.8416
N 5	4458.98	24	335.299	108.005	33.9479
N 6	5436.15	24	29.3824	241.579	24.3285
N 7	3336.9	24	171.181	414.014	25.0283
N 8	5866.65	24	266.067	65.4116	23.9173
N 9	6427.49	24	186.582	212.695	12.1873
N 10	3115.48	24	446.786	101.838	11.6269

Img No 7	**Volume (µm³)**	**Min (Ch2-T2)**	**Centroid X**	**Centroid Y**	**Centroid Z**
N 1	5176.27	24	111.124	153.643	11.7426
N 2	4303.54	24	352.363	119.694	20.3326
N 3	4509.18	24	242.531	200.084	14.7969
N 4	5083.37	24	166.161	273.131	11.8575
N 5	4830.99	24	348.61	27.3797	12.1967
N 6	5471.57	24	237.377	386.926	12.1557
N 7	3423.12	24	88.007	359.712	27.994
N 8	2912.27	24	454.945	51.5696	30.513
N 9	4815.4	24	83.9389	472.5	10.4827
N 10	3773.67	24	221.68	485.579	26.2701

Img No 8	**Volume (µm³)**	**Min (Ch2-T2)**	**Centroid X**	**Centroid Y**	**Centroid Z**
N 1	6750.31	24	177.08	65.1586	12.0069
N 2	6299.77	24	189.472	322.661	12.0355

N 3		6185.83		24	121.831	429.633	12.3676
N 4		5779.41		24	312.157	39.4423	11.7621
N 5		5653.73		24	100.419	142.733	21.2535
N 6		3527.96		24	363.988	136.551	13.6011
N 7		5060.3		24	22.6492	310.445	12.2637
N 8		6734.72		24	120.521	229.398	11.9996
N 9		4538.53		24	90.3875	268.31	27.7173
N 10		6062.36		24	304.71	246.137	11.0996
Img No 9	**Volume (µm³)**		**Min (Ch2-T2)**		**Centroid X**	**Centroid Y**	**Centroid Z**
N 1		6777.63		24	210.762	228.464	8.14379
N 2		4240.19		24	302.81	213.304	12.7124
N 3		5709.39		24	330.52	312.057	6.84228
N 4		5096.53		24	57.8488	252.934	22.0597
N 5		4306.17		24	138.081	101.968	9.61722
N 6		4859.12		24	162.511	157.64	28.1226
N 7		3888.63		24	314.969	236.368	22.5831
N 8		4137.98		24	210.887	128.841	15.0736
N 9		4133.33		24	445.687	483.852	9.32005
N 10		4155.59		24	276.422	403.987	8.73183
Average value of the volume of the nuclei						**4921.984125**	
Standard deviation of the average value of the volume of nuclei						**1067.258082**	

B.5. Analysis of the effect of FOXO expression in the whole salivary glands of YFP tagged Mi-2[CPTI-000232.]

Cont A

Name	**Voxel Count**	**Volume (µm³)**	**Centroid Z**	**Mean (Ch3-T1)**	**Sum (Ch3-T1)**
Object 15	31881	5202.38	24.425	36.0363	1.15E+06
Object 13	32314	5273.04	22.5145	41.6159	1.34E+06
Object 12	24634	4019.81	20.5255	38.193	940846
Object 10	31780	5185.9	19.8668	40.1613	1.28E+06
Object 8	31251	5099.58	19.5871	38.9346	1.22E+06
Object 5	29409	4799	17.4124	39.0328	1.15E+06
Object 3	32159	5247.75	16.8994	41.5338	1.34E+06
Object 6	30833	5031.37	16.8562	45.1009	1.39E+06
Object 2	32521	5306.82	15.4246	41.4935	1.35E+06

Expt A

Name	**Voxel Count**	**Volume (µm³)**	**Centroid Z**	**Mean (Ch3-T1)**	**Sum (Ch3-T1)**
Object 61	1913	312.166	75.7156	98.0831	187633
Object 59	2063	336.643	70.5177	66.0388	136238
Object 54	3474	566.892	66.8601	106.03	368348
Object 57	5210	850.175	66.3315	84.7261	441423

ContB

Name	**Voxel Count**	**Volume (µm³)**	**Centroid Z**	**Mean (Ch3-T1)**	**Sum (Ch3-T1)**
Object 48	37761	6161.89	70.0909	104.61	3.95E+06
Object 45	40668	6636.26	70.0565	93.6996	3.81E+06
Object 43	46486	7585.65	69.8131	109.71	5.10E+06
Object 44	44879	7323.42	68.6141	119.723	5.37E+06
Object 41	42676	6963.93	67.9987	94.108	4.02E+06
Object 42	43156	7042.25	66.5385	103.563	4.47E+06
Object 40	46822	7640.48	66.4077	74.1274	3.47E+06
Object 39	40866	6668.57	65.4502	99.4989	4.07E+06
Object 38	59577	9721.86	63.4074	94.5012	5.63E+06
Object 36	29626	4834.41	62.97	84.0115	2.49E+06
Object 35	42979	7013.37	60.8811	75.4185	3.24E+06

Expt B

Name	Voxel Count	Volume (µm³)	Centroid Z	Mean (Ch3-T1)	Sum (Ch3-T1)
Object 48	2174	354.756	76.8878	64.6375	140522
Object 49	7699	1256.33	74.6084	73.5711	566424
Object 44	5631	918.874	71.5212	58.4218	328973
Object 47	5594	912.837	70.5694	70.1144	392220
Object 46	2942	480.08	69.4585	71.9643	211719
Object 45	4654	759.446	69.2293	69.2295	322194
Object 41	1922	313.635	68.6514	64.5812	124125
Object 43	3900	636.407	67.188	69.6141	271495

Cont C

Name	Voxel Count	Volume (µm³)	Centroid Z	Mean (Ch3-T1)	Sum (Ch3-T1)
Object 26	38109	6218.68	70.9409	46.5116	1.77E+06
Object 27	34794	5677.73	70.254	42.448	1.48E+06
Object 25	35241	5750.67	67.1465	36.7517	1.30E+06
Object 24	37213	6072.47	63.5125	28.484	1.06E+06
Object 23	38724	6319.03	60.9162	42.7212	1.65E+06

Expt C

Name	Voxel Count	Volume (µm³)	Centroid Z	Mean (Ch3-T1)	Sum (Ch3-T1)
Object 88	5105	833.041	78.8641	73.7324	376404
Object 95	9783	1596.4	77.8684	91.096	891192
Object 93	2298	374.991	76.2245	59.1131	135842
Object 91	4298	701.353	75.617	91.1519	391771
Object 92	1870	305.149	75.3305	27.9754	52314
Object 86	2746	448.096	71.8245	33.2436	91287
Object 90	4767	777.886	71.0755	87.935	419186
Object 87	7059	1151.9	70.9168	95.5135	674230
Object 83	2286	373.033	70.5717	64.4654	147368
Object 82	1614	263.375	69.6729	35.1846	56788

Cont D

Name	Voxel Count	Volume (µm³)	Centroid Z	Mean (Ch3-T1)	Sum (Ch3-T1)
Object 26	39348	6420.86	67.1587	54.3412	2.14E+06
Object 25	35681	5822.47	66.6211	48.5976	1.73E+06
Object 23	39793	6493.48	58.7591	53.2384	2.12E+06
Object 22	33547	5474.25	57.272	44.3536	1.49E+06

Exp D

Name	Voxel Count	Volume (µm³)	Centroid Z	Mean (Ch3-T1)	Sum (Ch3-T1)
Object 35	6505	1061.49	32.7244	97.5127	634320
Object 29	2694	439.611	31.3486	72.3589	194935
Object 34	2754	449.401	30.7197	66.4942	183125
Object 23	1041	169.872	30.4947	35.2968	36744
Object 14	1470	239.877	29.0156	36.732	53996

Cont E

Name	Voxel Count	Volume (µm³)	Centroid Z	Mean (Ch3-T1)	Sum (Ch3-T1)
Object 33	42655	17266.4	130.502	115.714	4.94E+06
Object 35	43472	17597.1	129.228	128.01	5.56E+06
Object 34	50963	20629.4	128.573	77.4575	3.95E+06

Expt E

Name	Voxel Count	Volume (µm³)	Centroid Z	Mean (Ch3-T1)	Sum (Ch3-T1)
Object 58	4782	1935.71	57.2279	89.8137	429489
Object 59	6375	2580.55	55.3074	87.9973	560983
Object 54	3786	1532.54	53.3761	74.5343	282187
Object 57	5453	2207.33	53.2536	80.0776	436663
Object 55	4457	1804.16	52.188	77.3177	344605
Object 53	6212	2514.57	49.3158	66.9316	415779

Ratio of average intensity of YFP tagged Mi-2 in Experimental A/ Control A	**2.2**
Ratio of average intensity of YFP tagged Mi-2 in Experimental B/ Control B	**0.7**
Ratio of average intensity of YFP tagged Mi-2 in Experimental C / Control C	**1.67**
Ratio of average intensity of YFP tagged Mi-2 in Experimental D / Control D	**1.23**
Ratio of average intensity of YFP tagged Mi-2 in Experimental E / Control E	**0.74**
Average value of the ratio of 5 experimental / 5 control salivary glands	**1.308**

B.6. Visualization of endogenous Mi-2 protein in a single cell clones expressing FOXO

For the data of Visualization of Mi-2 protein in GFP marked control clone cells refer Appendix No B.2 (i)

B.6. (i) Visualization of Mi-2 protein in single cell clones expressing FOXO

Img No 1	Voxel Count	Volume (µm³)	Mean (ChS2-T2)	Sum (ChS2-T2)	Mean (Ch3-T3)	Min (Ch2-T4)	Centroid X	Centroid Y	Centroid Z
Clone cell	5926	2398.8	49.6775	294389	75.1618	26	283.728	279.731	14.5257
Wt 1	12524	5069.61	51.9359	650445	1.75591	26	204.025	453.549	16.7442
Wt 2	11915	4823.09	51.2926	611151	1.8073	26	200.822	373.802	15.6193
Wt 3	5783	2340.91	71.452	413207	4.53761	26	367.516	484.065	16.9395
Wt 4	11616	4702.06	45.6989	530839	1.19249	26	146.313	140.711	19.3238
Wt 5	11405	4616.65	51.7989	590766	1.81482	26	200.966	373.643	15.7554
Wt 6	12158	4921.46	59.2497	720358	1.899	26	244.909	174.154	13.7122
Wt 7	9716	3932.96	49.2633	478642	1.40675	26	320.911	243.523	19.2008
Wt 8	6781	2744.89	86.3367	585449	1.36794	26	256.284	65.1146	16.5195
Wt 9	8147	3297.84	36.0713	293873	1.04812	26	167.601	280.355	25.001
Wt 10	4494	1819.13	44.3981	199525	1.45972	26	347.175	321.852	24.9395

Img No 2	Voxel Count	Volume (µm³)	Mean (ChS2-T2)	Sum (ChS2-T2)	Mean (Ch3-T3)	Min (Ch2-T4)	Centroid X	Centroid Y	Centroid Z
Clone cell	4031	1631.72	56.3659	227211	54.2803	26	411.026	344.151	16.6075
Wt 1	7965	3224.17	162.892	1.30E+06	0.283365	26	57.1547	185.962	9.78293
Wt 2	12462	5044.51	50.2859	626663	0.179024	26	263.574	372.198	14.1944
Wt 3	11982	4850.21	57.0273	683301	0.13345	26	319.826	254.969	12.526
Wt 4	13807	5588.96	96.4381	1.33E+06	0.176505	26	234.058	246.358	9.52937
Wt 5	10972	4441.38	72.4608	795040	0.155031	26	190.322	309.921	13.5886
Wt 6	6730	2724.25	77.8829	524152	0.175632	26	133.884	323.739	18.3195
Wt 7	6233	2523.07	43.3003	269891	0.0657789	26	261.776	223.175	27.1943
Wt 8	2222	899.447	149.495	332178	0.30333	26	23.5603	122.674	10.7259
Wt 9	3811	1542.66	94.7798	361206	0.160588	26	47.8061	309.798	21.6106
Wt 10	5549	2246.19	132.363	734480	0.11876	26	145.192	174.409	19.0674

Img No 3	Voxel Count	Volume (µm³)	Mean (ChS2-T2)	Sum (ChS2-T2)	Mean (Ch3-T3)	Min (Ch2-T4)	Centroid X	Centroid Y	Centroid Z
Clone cell	6309	2553.83	65.1783	411210	33.119	26	228.382	236.142	6.49152
Wt 1	9874	3996.91	31.3227	309280	0.632874	26	228.931	458.284	4.37108
Wt 2	12115	4904.05	32.2943	391246	0.758729	26	265.294	373.192	4.5319
Wt 3	11272	4562.81	43.4707	490002	0.818045	26	222.045	135.728	5.56441
Wt 4	11185	4527.6	93.7366	1.05E+06	0.77139	26	239.796	70.0352	10.0338
Wt 5	11076	4483.47	45.278	501499	0.660437	26	304.409	140.721	5.87306
Wt 6	6704	2713.72	133.328	893830	0.832339	26	373.837	16.761	9.53058

Wt 7	6182	2502.42	55.3874	342405	0.686024	26	355.403	193.393	4.02491
Wt 8	1539	622.975	25.575	39360	0.649123	26	360.851	396.452	1.19883
Wt 9	8229	3331.03	18.2867	150481	0.421801	26	283.387	454.664	8.75987
Wt 10	2639	1068.25	40.0955	105812	0.660856	26	321.793	261.483	9.21448

Img No 4	**Voxel Count**	**Volume (µm³)**	**Min (ChS2-T2)**	**Mean (ChS2-T2)**	**Sum (ChS2-T2)**	**Mean (Ch3-T3)**	**Centroid X**	**Centroid Y**	**Centroid Z**
Clone cell	10468	4237.36	33	106.383	1.11E+06	83.4519	452.46	327.76	45.6859
Wt 1	10131	4100.95	33	72.2375	731838	0.657191	246.275	213.674	42.5127
Wt 2	13212	5348.11	33	78.3427	1.04E+06	0.859824	183.799	155.159	31.8678
Wt 3	14576	5900.24	33	82.0093	1.20E+06	0.79871	331.533	233.046	36.0607
Wt 4	19480	7885.34	33	98.6917	1.92E+06	1.4098	255.995	194.506	12.9562
Wt 5	20915	8466.22	33	95.0971	1.99E+06	1.89716	177.245	213.141	7.78982
Wt 6	12057	4880.57	33	84.9721	1.02E+06	1.63291	375.39	339.631	10.0046
Wt 7	10045	4066.13	33	74.0866	744200	1.60627	471.267	414.628	11.513
Wt 8	15079	6103.85	33	86.6016	1.31E+06	1.66072	119.862	266.294	8.96518
Wt 9	12232	4951.41	33	84.4053	1.03E+06	1.63309	374.928	339.581	9.88645
Wt 10	16867	6827.62	33	94.3196	1.59E+06	1.11282	402.08	278.675	26.2702

Img No 5	**Voxel Count**	**Volume (µm³)**	**Min (ChS2-T2)**	**Mean (ChS2-T2)**	**Sum (ChS2-T2)**	**Mean (Ch3-T3)**	**Centroid X**	**Centroid Y**	**Centroid Z**
Clone cell	12821	5189.84	27	56.7188	727192	111.852	231.773	389.54	8.53288
Wt 1	13638	5520.55	27	59.5908	812700	0.557633	201.071	218.046	13.4928
Wt 2	16085	6511.08	27	80.3816	1.29E+06	0.870314	20.8121	80.8275	7.58781
Wt 3	14627	5920.89	27	56.4721	826017	0.353388	312.262	180.041	16.2528
Wt 4	15047	6090.9	27	66.1061	994698	0.585034	140.411	321.212	11.163
Wt 5	12858	5204.81	27	59.7763	768604	0.449603	305.727	478.685	15.1924
Wt 6	11386	4608.96	27	49.2402	560649	0.259441	354.742	359.779	17.6587
Wt 7	12724	5150.57	27	56.8402	723235	0.541889	101.507	236.225	14.9732
Wt 8	11370	4602.48	27	74.0076	841466	2.08971	201.332	431.815	11.537
Wt 9	13420	5432.31	27	55.9759	751197	0.466841	220.797	102.485	15.3709
Wt 10	1875	758.985	27	45.9237	86107	0.149333	368.123	255.357	30.992

Img No 6	**Voxel Count**	**Volume (µm³)**	**Mean (ChS2-T2)**	**Sum (ChS2-T2)**	**Mean (Ch3-T3)**	**Min (Ch2-T4)**	**Centroid X**	**Centroid Y**	**Centroid Z**
Clone cell	6140	2485.42	68.6511	421518	55.8936	27	234.257	189.536	10.3487
Wt 1	7019	2841.23	133.959	940260	1.24605	27	228.804	369.427	11.5736
Wt 2	9267	3751.21	54.647	506414	0.727959	27	299.465	331.77	15.0627
Wt 3	7951	3218.5	58.8676	468056	1.59401	27	337.06	60.5629	16.0509
Wt 4	7673	3105.97	18.1108	138964	1.01251	27	371.73	211.195	13.9253
Wt 5	5684	2300.84	91.8812	522253	0.937544	27	295.445	499.28	13.1816
Wt 6	5337	2160.37	92.6457	494450	2.3961	27	236.2	14.2147	12.1447
Wt 7	5317	2152.28	22.1896	117982	0.484484	27	293.854	419.962	30.2915
Wt 8	5831	2360.34	26.6892	155625	0.526325	27	174.058	221.053	29.2072
Wt 9	6359	2574.07	121.351	771668	0.980657	27	191.514	460.05	16.1038
Wt 10	4472	1810.23	59.2339	264894	0.58229	27	168.235	330.141	27.0485

Img No 8	**Voxel Count**	**Volume (µm³)**	**Mean (ChS2-T2)**	**Sum (ChS2-T2)**	**Mean (Ch3-T3)**	**Min (Ch2-T4)**	**Centroid X**	**Centroid Y**	**Centroid Z**
Clone cell	1421	525.06	57.3983	81563	134.306	21	355.334	251.882	37.0591
Wt 1	12325	4554.09	63.5747	783558	1.10166	21	186.894	168.546	31.925
Wt 2	13543	5004.14	65.0744	881303	0.594846	21	240.414	264.086	34.618
Wt 3	12054	4453.96	43.7328	527155	0.388087	21	154.396	328.9	29.5766
Wt 4	13875	5126.82	51.9299	720527	1.89477	21	145.61	132.192	20.7063

Wt 5	17071	6307.74	69.2098	1.18E+06	1.63828	21	286.289	236.095	14.8433
Wt 6	11560	4271.42	57.446	664076	1.96765	21	166.577	240.912	16.2061
Wt 7	15473	5717.28	75.304	1.17E+06	0.760551	21	343.064	314.831	14.6899
Wt 8	15948	5892.79	52.7918	841924	0.364623	21	305.497	387.945	22.9689
Wt 9	15229	5627.12	68.4596	1.04E+06	1.12732	21	355.36	217.359	21.9091
Wt 10	12201	4508.27	45.6923	557492	0.304319	21	406.471	262.782	28.7749

Img No 9	**Voxel Count**	**Volume (µm³)**	**Min (ChS2-T2)**	**Mean (ChS2-T2)**	**Sum (ChS2-T2)**	**Mean (Ch3-T3)**	**Centroid X**	**Centroid Y**	**Centroid Z**
Clone cell	1956	791.773	30	56.7459	110995	161.799	370.33	218.358	7.32515
Wt 1	9076	3673.89	30	73.0263	662787	1.43643	61.1887	172.685	12.9802
Wt 2	14497	5868.27	30	63.2197	916496	1.60833	141.671	329.52	8.1143
Wt 3	12837	5196.31	30	63.4625	814668	1.62102	243.821	338.514	11.4434
Wt 4	10809	4375.39	30	71.3652	771386	1.6786	163.418	228.284	11.5409
Wt 5	6680	2704.01	30	49.0921	327935	1.42051	153.951	408.168	14.6097
Wt 6	14115	5713.64	30	98.0985	1.38E+06	1.53688	409.208	131.858	14.9501
Wt 7	12282	4971.65	30	71.975	883997	2.01124	316.695	175.099	12.331
Wt 8	7470	3023.79	30	74.2779	554856	1.06747	347.933	119.697	29.0462
Wt 9	5310	2149.44	30	54.1989	287796	1.40904	35.2719	438.408	26.3774
Wt 10	6647	2690.65	30	49.1405	326637	1.43719	153.926	408.087	14.6597

Img No 10	**Voxel Count**	**Volume (µm³)**	**Mean (ChS2-T2)**	**Sum (ChS2-T2)**	**Mean (Ch3-T3)**	**Min (Ch2-T4)**	**Centroid X**	**Centroid Y**	**Centroid Z**
Clone cell	12652	5121.43	20.3615	257614	24.4991	30	230.162	220.64	12.8897
Wt 1	13263	5368.75	56.0877	743891	2.83314	30	259.755	389.231	11.2082
Wt 2	12012	4862.36	27.1879	326581	1.14311	30	142.511	265.623	12.9088
Wt 3	13311	5388.18	38.6086	513919	2.18894	30	315.96	294.045	13.314
Wt 4	12435	5033.59	21.1697	263245	1.17982	30	268.577	52.6897	15.3642
Wt 5	11803	4777.76	25.4222	300058	1.16242	30	294.699	131.011	18.4865
Wt 6	8203	3320.51	16.8342	138091	1.69657	30	108.99	34.6136	12.7791
Wt 7	12843	5198.74	90.3843	1.16E+06	2.02281	30	307.408	438.677	17.1863
Wt 8	8344	3377.58	71.7765	598903	2.51953	30	431.846	343.675	13.3842
Wt 9	10357	4192.43	38.7801	401645	1.08999	30	148.415	322.919	23.2528
Wt 10	10806	4374.18	52.9699	572393	2.4777	30	217.675	375.933	24.7906

Average intensity of Mi-2 localization in 10 non adjacent wild type cells

	54.749
Img No 1	**74**
	93.692
Img No 2	**51**
	51.877
Img No 3	**49**
	85.076
Img No 4	**35**
	60.431
Img No 5	**45**
	67.957
Img No 6	**5**
	59.321
Img No 8	**53**
	66.785
Img No 9	**66**
	43.922
Img No 10	**11**

Intensity of Mi-2 localization in clone cell V average intensity of Mi-2 localization in 10 non adjacent wild type cells

Img No 1	**0.9**
Img No 2	**0.6**
Img No 3	**1.26**
Img No 4	**1.25**

Img No 5	**0.94**
Img No 6	**1.01**
Img No 8	**0.97**
Img No 9	**0.85**
Img No 10	**0.46**

Average value of the ratio of the clone cell V wild type cells acquired from Img No 1 to Img No 10	**0.91555556**
Std Dev of the average ratio of clone cell / wild type cell	**0.26330169**

B.7.Visualization of Dref protein in a single cell clones expressing FOXO

B.7 (i) Visualization of Dref protein in GFP marked control clone cells

Img No 1 Clone	Voxel Count	Volume (µm³)	Centroid X	Centroid Y	Centroid Z	Mean (ChS1-T1)	Sum (ChS1-T1)	Mean (Ch3-T3)	Min (Ch2-T4)
cell	12537	5074.87	377.334	278.797	17.5966	77.1832	967646	27.3561	28
Wt 1	9483	3838.64	359.095	81.8614	20.5164	54.1479	513485	2.68544	28
Wt 2	11642	4712.59	263.146	193.081	13.9042	63.9853	744917	2.60651	28
Wt 3	12018	4864.79	185.698	393.332	11.9659	35.7308	429413	3.42802	28
Wt 4	12489	5055.44	182.309	274.892	13.9064	30.7777	384383	2.53503	28
Wt 5	11620	4703.68	348.397	462.126	16.0906	52.1121	605543	3.6432	28
Wt 6	10615	4296.86	327.269	152.408	18.7703	91.6864	973251	2.45455	28
Wt 7	4020	1627.26	151.026	189.678	28.4408	5.951	23923	1.17438	28
Wt 8	10639	4306.58	245.377	12.1003	18.4738	64.1035	681997	2.30228	28
Wt 9	10148	4107.83	192.637	104.298	21.6854	46.2587	469433	2.01537	28
Wt 10	10976	4442.99	253.629	500.166	12.9804	39.9289	438260	4.80603	28

Img No 2 Clone	Voxel Count	Volume (µm³)	Centroid X	Centroid Y	Centroid Z	Mean (ChS1-T1)	Sum (ChS1-T1)	Mean (Ch3-T3)	Min (Ch2-T4)
cell	13725	5555.77	189.211	278.667	10.508	110.242	1.51E+06	18.7746	28
Wt 1	8595	3479.19	48.7956	106.63	9.33426	102.433	880409	2.82664	28
Wt 2	12677	5131.55	331.792	442.478	13.3376	43.1782	547370	2.07675	28
Wt 3	10986	4447.04	92.478	210.866	9.60304	26.8934	295451	2.429	28
Wt 4	10355	4191.62	164.653	464.446	13.6862	42.1197	436150	2.14505	28
Wt 5	13742	5562.65	207.951	167.658	13.5564	112.788	1.55E+06	2.53631	28
Wt 6	12488	5055.04	331.826	442.486	13.3804	43.5698	544100	2.09241	28
Wt 7	2683	1086.06	248.127	42.8763	27.1979	38.9307	104451	2.83451	28
Wt 8	7437	3010.44	302.292	228.063	22.551	21.6669	161137	1.53315	28
Wt 9	1598	646.857	99.3811	299.512	27.1658	17.0663	27272	1.38173	28
Wt 10	4257	1723.2	116.315	8.9495	15.1607	83.373	354919	2.74395	28

Img No 3 Clone	Voxel Count	Volume (µm³)	Centroid X	Centroid Y	Centroid Z	Mean (ChS1-T1)	Sum (ChS1-T1)	Mean (Ch3-T3)	Min (Ch2-T4)
cell	13213	5348.51	125.298	81.419	15.3995	48.1247	635872	34.6765	28
Wt 1	13557	5487.76	272.629	473.451	16.8263	59.3622	804773	3.89341	28
Wt 2	12663	5125.88	332.65	285.733	19.6825	36.6146	463651	3.33112	28
Wt 3	10549	4270.15	205.935	138.755	25.9397	28.2233	297728	2.73514	28
Wt 4	9423	3814.35	22.5627	62.1387	11.9434	57.7552	544227	4.76992	28
Wt 5	9954	4029.3	423.482	439.749	17.879	28.3051	281749	3.36528	28
Wt 6	13952	5647.65	352.733	392.638	14.9992	39.9717	557685	3.80275	28
Wt 7	14209	5751.69	255.721	359.249	14.0899	33.7422	479443	3.90647	28
Wt 8	12965	5248.13	223.967	242.7	17.0882	39.3606	510310	3.77817	28
Wt 9	10167	4115.52	52.3317	184.29	16.9343	33.5659	341264	3.49641	28
Wt 10	13705	5547.67	163.323	346.92	15.7745	79.6242	1.09E+06	4.40803	28

Img No 4	Voxel Count	Volume (µm³)	Centroid X	Centroid Y	Centroid Z	Mean (ChS1-T1)	Sum (ChS1-T1)	Mean (Ch3-T3)	Min (Ch2-T4)
Clone	12393	5016.58	108.779	79.0319	15.1173	37.8518	469097	23.1597	28

cell									
Wt 1	14981	6064.19	197.87	193.63	12.981	74.4835	1.12E+06	4.59182	28
Wt 2	12747	5159.88	335.364	247.105	27.2068	24.0705	306827	3.12921	28
Wt 3	11589	4691.13	413.58	369.367	22.9555	36.9629	428363	4.83001	28
Wt 4	13575	5495.05	190.161	94.3954	11.811	62.1421	843579	4.15263	28
Wt 5	11433	4627.98	129.733	165.207	17.2416	52.388	598952	4.05528	28
Wt 6	14141	5724.16	267.585	184.327	15.5676	39.9018	564252	3.84697	28
Wt 7	13774	5575.6	281.987	347.258	34.2766	47.3772	652574	3.67076	28
Wt 8	9289	3760.11	180.812	238.778	35.0764	49.5626	460387	3.08752	28
Wt 9	12298	4978.13	374.037	449.507	28.541	42.649	524498	4.85046	28
Wt 10	6874	2782.54	237.471	116.882	34.1138	6.31001	43375	2.08525	28

Img No 5	**Voxel Count**	**Volume (µm³)**	**Centroid X**	**Centroid Y**	**Centroid Z**	**Mean (ChS1-T1)**	**Sum (ChS1-T1)**	**Mean (Ch3-T3)**	**Min (Ch2-T4)**
Clone cell	12826	5191.86	173.872	81.2192	21.6187	45.5204	583845	19.6176	28
Wt 1	10794	4369.32	78.6402	14.7472	18.6827	45.2675	488617	5.03178	28
Wt 2	11401	4615.03	182.806	363.443	26.6431	36.6784	418171	3.53294	28
Wt 3	14528	5880.81	229.126	178.723	19.6211	36.1043	524523	3.9046	28
Wt 4	12214	4944.13	275.857	287.76	23.5419	56.863	694525	4.09694	28
Wt 5	7398	2994.65	81.1825	241.192	29.8727	28.7931	213011	2.92985	28
Wt 6	3642	1474.25	36.8671	106.013	31.9822	46.1735	168164	3.37534	28
Wt 7	13518	5471.97	125.319	161.095	17.9872	44.2779	598548	4.8866	28
Wt 8	12292	4975.7	272.964	394.309	17.8211	82.228	1.01E+06	4.582	28
Wt 9	3882	1571.4	225.233	463.533	32.5546	21.797	84616	2.21381	28
Wt 10	10309	4173	78.5861	15.5431	18.9176	43.5723	449187	4.97934	28

Img No 6	**Voxel Count**	**Volume (µm³)**	**Mean (ChS1-T1)**	**Sum (ChS1-T1)**	**Mean (Ch3-T3)**	**Min (Ch2-T4)**	**Centroid X**	**Centroid Y**	**Centroid Z**
Clone cell	9718	3933.77	47.8345	464856	21.0777	28	407.54	314.64	32.383
Wt 1	17097	6920.72	87.5692	1.50E+06	6.47851	28	220.61	167.898	16.316
Wt 2	16241	6574.22	49.1439	798146	6.56659	28	215.256	253.571	12.891
Wt 3	16129	6528.89	61.9761	999613	6.64145	28	282.787	333.176	13.368
Wt 4	17725	7174.93	67.6987	1.20E+06	7.78307	28	374.625	404.233	11.282
Wt 5	6514	2636.81	42.6131	277582	4.42247	28	145.116	27.6939	22.498
Wt 6	4268	1727.65	46.8639	200015	3.84372	28	137.837	252.253	24.182
Wt 7	9174	3713.56	30.2893	277874	5.12666	28	301.379	397.25	32.33
Wt 8	7365	2981.29	34.802	256317	4.82811	28	96.6781	173.173	18.242
Wt 9	10700	4331.27	36.9605	395477	3.95178	28	287.512	217.1	32.578

Img No 7	**Voxel Count**	**Volume (µm³)**	**Centroid X**	**Centroid Y**	**Centroid Z**	**Mean (ChS1-T1)**	**Sum (ChS1-T1)**	**Mean (Ch3-T3)**	**Min (Ch2-T4)**
Clone cell	14826	6001.44	347.137	309.923	12.676	51.0206	756432	27.1224	28
Wt 1	13007	5265.13	176.885	245.89	12.1716	55.505	721954	9.55155	28
Wt 2	10132	4101.35	135.929	67.8035	14.0436	65.776	666442	11.5214	28
Wt 3	14354	5810.38	210.721	138.556	11.5438	65.1238	934787	11.2294	28
Wt 4	9144	3701.42	213.131	310.724	26.0844	38.6873	353757	6.4591	28
Wt 5	11801	4776.95	279.501	135.065	23.8101	48.6785	574455	7.79951	28
Wt 6	13859	5610.01	356.079	203.892	12.7502	58.2612	807442	9.22231	28
Wt 7	10164	4114.3	424.537	267.964	12.4464	51.2433	520837	9.59111	28
Wt 8	7314	2960.65	274.263	324.891	14.4835	52.458	383678	8.36164	28
Wt 9	5671	2295.57	369.776	389.47	27.5486	28.6928	162717	5.389	28
Wt 10	11475	4644.99	279.628	134.978	23.6501	49.8126	571600	7.81935	28

Img No 8	Voxel Count	Volume (μm³)	Centroid X	Centroid Y	Centroid Z	Mean (ChS1-T1)	Sum (ChS1-T1)	Mean (Ch3-T3)	Min (Ch2-T4)
Clone cell	15618	6322.04	355.341	235.025	11.2604	44.6134	696772	29.8957	28
Wt 1	15041	6088.47	292.529	172.075	14.4875	42.5186	639522	6.2543	28
Wt 2	11501	4655.51	189.084	456.15	17.9236	45.3553	521631	6.87323	28
Wt 3	12430	5031.56	198.322	330.373	18.4267	35.9471	446823	6.03492	28
Wt 4	14967	6058.52	296.91	474.318	13.3031	34.7166	519604	6.36099	28
Wt 5	12609	5104.02	381.612	409.883	14.8718	27.2877	344070	5.93735	28
Wt 6	10090	4084.35	231.77	237.227	24.1376	27.8793	281302	5.57047	28
Wt 7	6607	2674.46	406.453	167.022	24.6911	43.0506	284435	6.01256	28
Wt 8	8938	3618.03	380.3	495.088	23.6531	31.1232	278179	17.2517	28
Wt 9	17111	6926.39	269.011	292.252	9.96733	29.7325	508753	6.95769	28
Wt 10	5138	2079.82	423.35	12.3854	21.6162	131.713	676739	5.91475	28

Img No 11	Voxel Count	Volume (μm³)	Mean (ChS1-T1)	Sum (ChS1-T1)	Mean (Ch3-T3)	Min (Ch2-T4)	Centroid X	Centroid Y	Centroid Z
Clone cell	6177	2500.4	82.6667	510632	117.508	28	400.127	412.595	8.5242
Wt 1	14232	5761	66.314	943781	4.34444	28	157.131	370.754	11.182
Wt 2	13875	5616.49	74.1209	1.03E+06	4.30941	28	160.762	225.75	14.386
Wt 3	13205	5345.28	75.2273	993376	5.34373	28	158.826	291.771	8.7038
Wt 4	13733	5559.01	53.2673	731520	3.87847	28	279.895	268.383	15.408
Wt 5	13664	5531.07	72.8897	995965	5.32897	28	158.707	291.782	9.0395
Wt 6	12309	4982.58	74.2259	913646	4.52458	28	157.332	370.887	10.29
Wt 7	12352	4999.99	71.6338	884821	5.22579	28	224.97	301.92	9.8881
Wt 8	8663	3506.71	81.2463	703837	4.8332	28	29.0914	304.518	13.889
Wt 9	10430	4221.98	77.3235	806484	3.73873	28	97.7404	201.518	23.078

Average intensity of Dref localization in 10 non adjacent wild type cells

Img No 1	**48.4682**
Img No 2	**53.2019**
Img No 3	**43.6525**
Img No 4	**43.5848**
Img No 5	**44.1755**
Img No 6	**50.8796**
Img No 7	**51.4239**
Img No 8	**44.9324**
Img No 11	**71.8054**

Intensity of Dref localization in clone cell V average intensity of Dref localization in 10 non adjacent wild type cells

Img No 1	**1.59**
Img No 2	**2.07**
Img No 3	**1.1**
Img No 4	**0.87**
Img No 5	**1.03**
Img No 6	**0.94**
Img No 7	**1**

Img No 8	**1**
Img No 11	**1.15**

Average value of the ratio of the clone cell V wild type cells acquired from Img No 1 to Img No 10	**0.388365521**
Std Dev of the average ratio of clone cell / wild type cell	**1.19444444**

B.7. (ii) Visualization of Dref protein in single cell clones expressing FOXO

Img No 1	**Voxel Count**	**Volume (µm³)**	**Centroid X**	**Centroid Y**	**Centroid Z**	**Mean (ChS1-T1)**	**Sum (ChS1-T1)**	**Mean (Ch3-T3)**	**Min (Ch2-T4)**
Clone cell	4897	1982.27	375.6	310.878	14.2473	21.8517	107008	16.0856	28
WT 1	15575	6304.63	224.415	206.745	10.6781	136.941	2.13E+06	5.42324	28
WT 2	11078	4484.28	89.2942	311.583	19.7867	88.1677	976722	2.73948	28
WT 3	13479	5456.19	108.379	226.299	11.448	16.1433	217596	3.19341	28
WT 4	14319	5796.21	195.504	337.59	14.0323	200.847	2.88E+06	3.43292	28
WT 5	11212	4538.53	361.481	166.222	20.1654	49.3318	553108	2.18016	28
WT 6	9469	3832.97	193.071	274.472	6.26296	62.4085	590946	3.37744	28
WT 7	10808	4374.99	424.286	242.217	9.79247	76.0552	822005	2.98788	28
WT 8	13510	5468.74	108.421	226.299	11.4486	16.166	218403	3.18838	28

Img No 2	**Voxel Count**	**Volume (µm³)**	**Centroid X**	**Centroid Y**	**Centroid Z**	**Mean (ChS1-T1)**	**Sum (ChS1-T1)**	**Mean (Ch3-T3)**	**Min (Ch2-T4)**
Clone cell	6049	2448.59	342.108	225.587	20.3715	38.0374	230088	20.8823	28
WT 1	15331	6205.86	199.32	279.764	9.01644	55.5711	851961	6.06444	28
WT 2	15335	6207.48	199.324	279.765	9.01682	55.5605	852021	6.06528	28
WT 3	13747	5564.67	128.1	200.438	9.4721	40.3461	554638	6.69266	28
WT 4	14356	5811.19	349.122	324.05	12.6733	18.8101	270038	5.81081	28
WT 5	5396	2184.26	24.126	222.529	12.7166	90.1638	486524	5.4381	28
WT 6	8868	3589.69	261.217	318.455	29.1053	19.6314	174091	3.39502	28
WT 7	11157	4516.26	88.4358	113.169	12.9671	31.0388	346300	5.38003	28
WT 8	15199	6152.43	241.383	354.481	11.1677	31.1371	473253	5.04744	28

Img No 3	**Voxel Count**	**Volume (µm³)**	**Centroid X**	**Centroid Y**	**Centroid Z**	**Mean (ChS1-T1)**	**Sum (ChS1-T1)**	**Mean (Ch3-T3)**	**Min (Ch2-T4)**
Clone cell	1216	492.227	41.1513	241.415	11.0033	57.6488	70101	27.8865	21
WT 1	11256	4556.34	232.274	186.324	18.3171	16.8251	189383	4.133	21
WT 2	8793	3559.33	369.008	129.241	17.1591	26.4664	232719	3.57125	21
WT 3	10942	4429.23	300.819	200.67	16.772	15.468	169251	4.37224	21
WT 4	8095	3276.79	151.714	132.005	22.157	9.37356	75879	2.8656	21
WT 5	8826	3572.69	330.107	229.223	23.8482	18.4099	162486	3.03988	21
WT 6	8170	3307.15	188.566	251.02	25.0628	4.62876	37817	2.70184	21
WT 7	6949	2812.9	204.129	115.043	31.1917	3.99597	27768	2.09656	21
WT 8	8527	3451.66	303.025	102.961	28.4169	19.1637	163409	2.07928	21

Img No 4	**Voxel Count**	**Volume (µm³)**	**Centroid X**	**Centroid Y**	**Centroid Z**	**Mean (ChS1-T1)**	**Sum (ChS1-T1)**	**Mean (Ch3-T3)**	**Min (Ch2-T4)**
Clone cell	7303	2956.19	363.386	443.577	7.60016	59.8228	436886	22.9521	21
WT 1	14132	5720.52	291.554	249.164	13.6359	46.2291	653309	6.4821	21
WT 2	14354	5810.38	281.576	310.506	18.2718	34.1589	490317	5.37829	21
WT 3	12635	5114.54	240.532	263.373	21.9619	26.9453	340454	4.13613	21
WT 4	12267	4965.58	168.99	124.452	23.8687	59.9623	735558	4.85701	21
WT 5	7981	3230.64	299.287	119.725	23.5886	67.9777	542530	4.04999	21
WT 6	6103	2470.44	399.066	355.092	20.1811	30.9023	188597	3.54039	21
WT 7	12734	5154.62	161.215	47.8902	24.6492	63.2189	805030	3.6836	21

WT 8	8861	3586.86	206.572	148.584	13.0894	79.194	701738	6.11263	21

Img No 6	**Voxel Count**	**Volume (μm³)**	**Centroid X**	**Centroid Y**	**Centroid Z**	**Mean (ChS1-T1)**	**Sum (ChS1-T1)**	**Mean (Ch3-T3)**	**Min (Ch2-T4)**
Clone cell	7098	2873.21	109.303	157.299	9.82065	29.8819	212102	21.2744	21
WT 1	8172	3307.96	177.537	197.043	17.7122	11.0064	89944	4.9836	21
WT 2	11857	4799.62	84.9397	73.8671	14.4626	24.8619	294787	5.42692	21
WT 3	6720	2720.2	187.917	167.141	26.496	9.00863	60538	3.28914	21
WT 4	6263	2535.21	86.7524	287.172	30.0158	8.88424	55642	2.32716	21
WT 5	11596	4693.97	326.727	493.305	15.3965	23.0484	267269	7.31252	21
WT 6	7473	3025.01	269.298	355.555	26.4081	12.2714	91704	6.21584	21
WT 7	11716	4742.54	134.466	391.129	23.2597	9.80889	114921	4.20109	21
WT 8	9167	3710.73	52.4041	207.399	26.4742	13.4633	123418	2.91153	21

Img No 7	**Voxel Count**	**Volume (μm³)**	**Centroid X**	**Centroid Y**	**Centroid Z**	**Mean (ChS1-T1)**	**Sum (ChS1-T1)**	**Mean (Ch3-T3)**	**Min (Ch2-T4)**
Clone cell	1990	805.536	414.375	251.045	9.15327	55.8985	111238	29.5492	21
WT 1	7877	3188.54	152.58	272.38	10.8956	31.1363	245261	8.23715	21
WT 2	8771	3550.43	291.994	345.835	12.9498	21.3459	187225	6.32311	21
WT 3	9096	3681.99	237.207	297.978	12.4757	21.2917	193669	7.35818	21
WT 4	9921	4015.94	224.809	236.512	9.5953	52.1609	517488	7.90586	21
WT 5	7586	3070.75	262.125	213.617	16.6277	7.28091	55233	10.7139	21
WT 6	6072	2457.9	158.028	198.915	21.3613	40.5343	246124	4.55188	21
WT 7	7967	3224.98	356.328	215.213	16.9667	30.1816	240457	4.37128	21
WT 8	5026	2034.48	98.0251	206.822	12.0326	95.0493	477718	6.54318	21

Img No 8	**Voxel Count**	**Volume (μm³)**	**Centroid X**	**Centroid Y**	**Centroid Z**	**Mean (ChS1-T1)**	**Sum (ChS1-T1)**	**Mean (Ch3-T3)**	**Min (Ch2-T4)**
Clone cell	11542	4672.11	286.499	408.29	15.9587	37.7211	435377	72.9244	21
WT 1	12138	4913.36	201.222	373.605	15.6616	48.8208	592587	1.78687	21
WT 2	13174	5332.73	203.953	453.387	16.8026	62.7194	826265	1.72666	21
WT 3	10666	4317.51	320.98	243.583	19.2421	45.7475	487943	1.37943	21
WT 4	7233	2927.86	368.211	484.199	16.6676	105.742	764835	4.51804	21
WT 5	12259	4962.34	244.181	174.201	13.8058	65.4639	802522	1.85578	21
WT 6	8244	3337.1	167.971	280.458	24.5304	17.759	146405	1.06174	21
WT 7	5769	2335.24	347.098	321.55	24.832	44.0579	254170	1.45068	21
WT 8	6319	2557.88	357.765	398.372	20.0392	42.9964	271694	2.04162	21

Img No 9	**Voxel Count**	**Volume (μm³)**	**Centroid X**	**Centroid Y**	**Centroid Z**	**Mean (ChS1-T1)**	**Sum (ChS1-T1)**	**Mean (Ch3-T3)**	**Min (Ch2-T4)**
Clone cell	11905	4819.05	231.138	389.265	9.15691	46.5367	554020	115.238	21
WT 1	10638	4306.17	296.272	279.017	13.4906	26.2712	279473	0.476593	21
WT 2	11720	4744.16	201.702	217.089	13.9402	55.9625	655881	0.544881	21
WT 3	10201	4129.28	222.283	101.375	14.6395	56.4311	575654	0.457504	21
WT 4	10968	4439.76	303.885	479.659	16.1523	20.9043	229278	0.466083	21
WT 5	6199	2509.3	356.197	359.769	16.8495	19.2707	119459	0.27327	21
WT 6	4530	1833.71	91.689	151.512	16.2143	40.9161	185350	0.630243	21
WT 7	7819	3165.07	103.409	234.773	15.7753	36.7053	286999	0.518736	21
WT 8	4115	1665.72	164.33	350.827	27.7618	0.838639	3451	0.277278	21

Img No 10	**Voxel Count**	**Volume (μm³)**	**Centroid X**	**Centroid Y**	**Centroid Z**	**Mean (ChS1-T1)**	**Sum (ChS1-T1)**	**Mean (Ch3-T3)**	**Min (Ch2-T4)**
Clone cell	6568	2658.67	312.575	157.738	8.83085	61.9353	406791	100.419	21
WT 1	11559	4678.99	218.034	271.423	13.515	36.7489	424781	0.967731	21
WT 2	6973	2822.61	228.82	369.204	11.4754	133.994	934340	1.24208	21

WT 3	6915	2799.13	191.89	459.823	16.4315	106.884	739105	0.941287	21
WT 4	11006	4455.14	234.619	88.9119	15.9659	20.0054	220179	33.8953	21
WT 5	9183	3717.2	337.44	60.5975	15.9796	30.5114	280186	1.6304	21
WT 6	6719	2719.8	174.035	221.005	29.2913	4.43146	29775	0.507218	21
WT 7	10410	4213.88	309.405	246.52	17.9939	21.483	223638	1.17839	21
WT 8	4937	1998.46	168.635	3166.86	1713.94	29.4235	145264	0.575248	21

Img No 11	**Voxel Count**	**Volume (µm³)**	**Centroid X**	**Centroid Y**	**Centroid Z**	**Mean (ChS1-T1)**	**Sum (ChS1-T1)**	**Mean (Ch3-T3)**	**Min (Ch2-T4)**
Clone cell	9637	3900.98	238.783	109.481	22.5438	12.1881	117457	53.0554	21
WT 1	9380	3796.95	369.856	296.816	8.20992	82.7686	776369	1.17559	21
WT 2	12345	4997.15	313.687	420.875	16.8358	38.7673	478582	0.701418	21
WT 3	10599	4290.39	370.005	296.718	8.85876	75.5053	800281	1.09124	21
WT 4	11512	4659.96	124.578	223.788	12.3464	83.7859	964543	0.946056	21
WT 5	10073	4077.47	122.759	98.9131	12.4406	49.9169	502813	13.6841	21
WT 6	2232	903.495	443.285	190.723	14.3132	57.1335	127522	0.737455	21
WT 7	1579	639.166	396.669	127.174	27.4471	62.8778	99284	0.535149	21
WT 8	15089	6107.9	267.783	199.961	6.95367	95.2693	1.44E+06	1.11114	21

Average intensity of Dref localization in 10 non adjacent wild type cells

Img No 1	**80.758**
Img No 2	**42.782**
Img No 3	**14.291**
Img No 4	**51.074**
Img No 6	**14.044**
Img No 7	**37.373**
Img No 8	**54.163**
Img No 9	**32.162**
Img No 10	**47.935**
Img No 11	**68.253**

Intensity of Dref localization in clone cell V average intensity of Dref localization in 10 non adjacent wild type cells

Img No 1	**0.27**
Img No 2	**0.89**
Img No 3	**4.03**
Img No 4	**1.17**
Img No 6	**2.12**
Img No 7	**1.5**
Img No 8	**0.7**
Img No 9	**1.44**
Img No 10	**1.29**
Img No 11	**0.18**

Average value of the ratio of the clone cell V wild type cells acquired from Img No 1 to Img No 11	**1.359**
Std Dev of the average ratio of clone cell / wild type cell	**1.10606861**

B.8. <u>Analysis of the phenotypic effect of Simj expression on salivary gland size</u>
B.8. (i) Measurement of DAPI stained nuclei size from yw third instar salivary glands

SG 1	1	Length	Distance	µm	27.61
	2	Length	Distance	µm	27.33
	3	Length	Distance	µm	24.29
	4	Length	Distance	µm	28.5
	5	Length	Distance	µm	25.98
SG 2	1	Length	Distance	µm	25.84
	2	Length	Distance	µm	24.39
	3	Length	Distance	µm	25.83
	4	Length	Distance	µm	27.79
	5	Length	Distance	µm	22.52
SG 3	1	Length	Distance	µm	27.1
	2	Length	Distance	µm	29.81
	3	Length	Distance	µm	25.32
	4	Length	Distance	µm	27.34
SG 4	1	Length	Distance	µm	27.1
	2	Length	Distance	µm	24.17
	3	Length	Distance	µm	25.12
	4	Length	Distance	µm	24.55
	5	Length	Distance	µm	26.31
SG 5	1	Length	Distance	µm	26.18
	2	Length	Distance	µm	27.86
SG 6	1	Length	Distance	µm	24.61
	2	Length	Distance	µm	24.52
	3	Length	Distance	µm	26.99
SG 7	1	Length	Distance	µm	28.54
	2	Length	Distance	µm	27.33
	3	Length	Distance	µm	28.94
	4	Length	Distance	µm	22.4
SG 8	1	Length	Distance	µm	27.76
	2	Length	Distance	µm	26.7
	3	Length	Distance	µm	26.62
SG 9	1	Length	Distance	µm	30.77
	2	Length	Distance	µm	33.9
	3	Length	Distance	µm	29.07
	4	Length	Distance	µm	26.96
	5	Length	Distance	µm	26.03
	6	Length	Distance	µm	29.79
SG 10	1	Length	Distance	µm	30.08
	2	Length	Distance	µm	26.18
	3	Length	Distance	µm	30.41
	4	Length	Distance	µm	26.1
	5	Length	Distance	µm	29.51
	6	Length	Distance	µm	33.22
SG 11	1	Length	Distance	µm	29.63
	2	Length	Distance	µm	30.63
	3	Length	Distance	µm	30.35
	4	Length	Distance	µm	25.68
	5	Length	Distance	µm	25.62
SG 12	1	Length	Distance	µm	34.49
	2	Length	Distance	µm	30.28

	3	Length	Distance	µm	30.38
	4	Length	Distance	µm	30.84
	5	Length	Distance	µm	28.4
SG 13	1	Length	Distance	µm	26.54
	2	Length	Distance	µm	28.14
	3	Length	Distance	µm	29.36
	4	Length	Distance	µm	29.68
	5	Length	Distance	µm	30.99
	6	Length	Distance	µm	24.82
	7	Length	Distance	µm	32.45
SG 14	1	Length	Distance	µm	29.22
	2	Length	Distance	µm	25.61
	3	Length	Distance	µm	27.78
	4	Length	Distance	µm	24.29
	5	Length	Distance	µm	29.97
SG 15	1	Length	Distance	µm	32.91
	2	Length	Distance	µm	28.79
	3	Length	Distance	µm	35.38
	4	Length	Distance	µm	31.87
SG 16	1	Length	Distance	µm	28.36
	2	Length	Distance	µm	28.86
	3	Length	Distance	µm	36.72
SG 17	1	Length	Distance	µm	22.41
	2	Length	Distance	µm	20.22
SG 18	1	Length	Distance	µm	23.88
	2	Length	Distance	µm	19.33
	3	Length	Distance	µm	21.07
	4	Length	Distance	µm	23.85
SG 19	1	Length	Distance	µm	34.37
	2	Length	Distance	µm	31.11
	3	Length	Distance	µm	31.42
	4	Length	Distance	µm	30.3
SG 20	1	Length	Distance	µm	27.6
	2	Length	Distance	µm	23.77
	3	Length	Distance	µm	24.25
SG 21	1	Length	Distance	µm	25.47
	2	Length	Distance	µm	25.73
	3	Length	Distance	µm	22.63
	4	Length	Distance	µm	24.57
	5	Length	Distance	µm	21.02
Average value of nuclei size from 21 salivary glands					**27.53789**
Standard deviation of the average value of nuclei size					**3.424241**

B.8. (ii) Measurement of DAPI stained nuclei size from salivary glands of UAS-simj containing third instar larvae where expression of UAS-simj was not driven by c147-GAL4 driver.

SG 1	1	Length	Distance	µm	26.05
	2	Length	Distance	µm	25.98
	3	Length	Distance	µm	25.53
	4	Length	Distance	µm	24.42
SG 2	1	Length	Distance	µm	24.47
	2	Length	Distance	µm	23.13
	3	Length	Distance	µm	24.87
SG 3	1	Length	Distance	µm	27.51
	2	Length	Distance	µm	29.39

	3	Length	Distance	µm	25.72
	4	Length	Distance	µm	25.69
SG 4	1	Length	Distance	µm	25.51
	2	Length	Distance	µm	19.6
	3	Length	Distance	µm	26.66
	4	Length	Distance	µm	24.13
	5	Length	Distance	µm	20.96
SG 5	1	Length	Distance	µm	28.63
	2	Length	Distance	µm	27.6
	3	Length	Distance	µm	27.7
	4	Length	Distance	µm	26.49
	5	Length	Distance	µm	24.66
SG 6	1	Length	Distance	µm	29.23
	2	Length	Distance	µm	27.7
	3	Length	Distance	µm	30.85
	4	Length	Distance	µm	29.88
SG 7	1	Length	Distance	µm	28.95
	2	Length	Distance	µm	26.33
	3	Length	Distance	µm	26.34
	4	Length	Distance	µm	24.41
	5	Length	Distance	µm	27.67
	6	Length	Distance	µm	29.75
	7	Length	Distance	µm	29.86
SG 8	1	Length	Distance	µm	25.34
	2	Length	Distance	µm	26.99
	3	Length	Distance	µm	23.48
SG 9	1	Length	Distance	µm	27.51
	2	Length	Distance	µm	28.01
	3	Length	Distance	µm	29.43
	4	Length	Distance	µm	26.66
	5	Length	Distance	µm	23.68
	6	Length	Distance	µm	23.93
	7	Length	Distance	µm	29.07
SG 10	1	Length	Distance	µm	23.88
	2	Length	Distance	µm	23.05
	3	Length	Distance	µm	23.53
	4	Length	Distance	µm	27.09
	5	Length	Distance	µm	23.14
SG 11	1	Length	Distance	µm	19.51
	2	Length	Distance	µm	17.61
	3	Length	Distance	µm	16.68
	4	Length	Distance	µm	18.15
	5	Length	Distance	µm	17.86
	6	Length	Distance	µm	19.74
	7	Length	Distance	µm	15.58
SG 12	1	Length	Distance	µm	19.77
	2	Length	Distance	µm	20.41
	3	Length	Distance	µm	21.25
	4	Length	Distance	µm	18.23
	5	Length	Distance	µm	21.27
SG 13	1	Length	Distance	µm	18.83
	2	Length	Distance	µm	21.3
	3	Length	Distance	µm	20.75
	4	Length	Distance	µm	19.95

SG 14	1	Length	Distance	µm	20.71
	2	Length	Distance	µm	19.66
	3	Length	Distance	µm	20.53
	4	Length	Distance	µm	21.98
SG 15	1	Length	Distance	µm	24.02
	2	Length	Distance	µm	23.32
	3	Length	Distance	µm	23.47
	4	Length	Distance	µm	27.84
	5	Length	Distance	µm	23.1
SG 16	1	Length	Distance	µm	25.9
	2	Length	Distance	µm	25.23
	3	Length	Distance	µm	20.77
	4	Length	Distance	µm	24.19
	5	Length	Distance	µm	23.89
	1	Length	Distance	µm	25.18
	2	Length	Distance	µm	23.74
	3	Length	Distance	µm	25.91
	4	Length	Distance	µm	24.98
SG 17	1	Length	Distance	µm	27.77
	2	Length	Distance	µm	27.19
	3	Length	Distance	µm	24.58
	4	Length	Distance	µm	27.03
SG 18	1	Length	Distance	µm	25.04
	2	Length	Distance	µm	20.89
	3	Length	Distance	µm	21.77
	4	Length	Distance	µm	26.81
SG 19	1	Length	Distance	µm	21.51
	2	Length	Distance	µm	21.01
	3	Length	Distance	µm	20.5
	4	Length	Distance	µm	21.41
	5	Length	Distance	µm	19.96
SG 20	1	Length	Distance	µm	25.24
	2	Length	Distance	µm	22.07
	3	Length	Distance	µm	21
	4	Length	Distance	µm	20.75
SG 21	1	Length	Distance	µm	21.1
	2	Length	Distance	µm	26.78
	3	Length	Distance	µm	23.05
	4	Length	Distance	µm	21.88
SG 22	1	Length	Distance	µm	27.16
	2	Length	Distance	µm	24.4
	3	Length	Distance	µm	25.5
	4	Length	Distance	µm	20.86
	5	Length	Distance	µm	26.01
SG 23	1	Length	Distance	µm	19.98
	2	Length	Distance	µm	20.88
	3	Length	Distance	µm	20.54
	4	Length	Distance	µm	18.66
SG 24	1	Length	Distance	µm	22.43
	2	Length	Distance	µm	19.68
	3	Length	Distance	µm	25.41
	4	Length	Distance	µm	21.1
SG 25	1	Length	Distance	µm	30.54
	2	Length	Distance	µm	24.64

	3	Length	Distance	µm	24.4
SG 26	1	Length	Distance	µm	21.99
	2	Length	Distance	µm	20.48
	3	Length	Distance	µm	23.8
SG 27	1	Length	Distance	µm	25.61
	2	Length	Distance	µm	21.96
	3	Length	Distance	µm	22.05
	4	Length	Distance	µm	19.81
SG 28	1	Length	Distance	µm	22.2
	2	Length	Distance	µm	19.93
	3	Length	Distance	µm	21.02
	4	Length	Distance	µm	19.13
	5	Length	Distance	µm	19.47
SG 29	1	Length	Distance	µm	24.09
	2	Length	Distance	µm	21.42
	3	Length	Distance	µm	20.19
	4	Length	Distance	µm	24.32
	5	Length	Distance	µm	20.74
SG 30	1	Length	Distance	µm	25.76
	2	Length	Distance	µm	24.05
	3	Length	Distance	µm	20.73
SG 31	1	Length	Distance	µm	22.83
	2	Length	Distance	µm	22.82
	3	Length	Distance	µm	25.59
SG 32	1	Length	Distance	µm	21.53
	2	Length	Distance	µm	23.82
	3	Length	Distance	µm	24.85

B.8. (iii) Measurement of DAPI stained nuclei size from salivary glands of third instar larvae where expression of UAS-simj was driven by c147-GAL4 driver.

SG 1	1	Length	Distance	µm	21.94
	2	Length	Distance	µm	27.75
	3	Length	Distance	µm	23.26
	4	Length	Distance	µm	23.6
	5	Length	Distance	µm	21.77
SG 2	1	Length	Distance	µm	24.52
	2	Length	Distance	µm	26.2
	3	Length	Distance	µm	22.69
SG 3	1	Length	Distance	µm	19.54
	2	Length	Distance	µm	19.17
	3	Length	Distance	µm	19.77
	4	Length	Distance	µm	20.55
	5	Length	Distance	µm	18.84
SG 4	1	Length	Distance	µm	19.48
	2	Length	Distance	µm	19.32
	3	Length	Distance	µm	21.28
	4	Length	Distance	µm	20.83
	5	Length	Distance	µm	17.33
	6	Length	Distance	µm	18.95
	7	Length	Distance	µm	22.33
SG 5	1	Length	Distance	µm	19.26
	2	Length	Distance	µm	20.36
	3	Length	Distance	µm	20.32
	4	Length	Distance	µm	18.48
SG 6	1	Length	Distance	µm	22.11

	2	Length	Distance	µm	26.07
	3	Length	Distance	µm	17.49
	4	Length	Distance	µm	21.03
	5	Length	Distance	µm	18.33
SG 7	1	Length	Distance	µm	19.53
	2	Length	Distance	µm	20.55
	3	Length	Distance	µm	19.66
	4	Length	Distance	µm	19.4
	5	Length	Distance	µm	18.4
SG 8	1	Length	Distance	µm	17.59
	2	Length	Distance	µm	14.45
	3	Length	Distance	µm	17.26
	4	Length	Distance	µm	15.72
	5	Length	Distance	µm	18.81
SG 9	1	Length	Distance	µm	16
	2	Length	Distance	µm	17.95
	3	Length	Distance	µm	17.33
	4	Length	Distance	µm	17.71
	5	Length	Distance	µm	16.65
	6	Length	Distance	µm	17.11
	7	Length	Distance	µm	17.55
SG 10	1	Length	Distance	µm	16.68
	2	Length	Distance	µm	18.89
	3	Length	Distance	µm	19.03
	4	Length	Distance	µm	19.7
	5	Length	Distance	µm	21.56
	6	Length	Distance	µm	19.4
SG 11	1	Length	Distance	µm	21.66
	2	Length	Distance	µm	21.3
	3	Length	Distance	µm	21.58
	4	Length	Distance	µm	20.87
	5	Length	Distance	µm	18.94
	6	Length	Distance	µm	19.67
SG 12	1	Length	Distance	µm	26.04
	2	Length	Distance	µm	23.58
	3	Length	Distance	µm	20.96
	4	Length	Distance	µm	20.7
	5	Length	Distance	µm	19.88
	6	Length	Distance	µm	23.03
	7	Length	Distance	µm	22.83
SG 13	1	Length	Distance	µm	21.42
	2	Length	Distance	µm	23.52
	3	Length	Distance	µm	22.35
	4	Length	Distance	µm	23.39
SG 14	1	Length	Distance	µm	27.11
	2	Length	Distance	µm	25.36
	3	Length	Distance	µm	24.08
	4	Length	Distance	µm	26.26
	5	Length	Distance	µm	23.65
SG 15	1	Length	Distance	µm	20.75
	2	Length	Distance	µm	26.84
	3	Length	Distance	µm	21.81
	4	Length	Distance	µm	24.9
SG 16	1	Length	Distance	µm	22.66

	2	Length	Distance	µm	22.38
	3	Length	Distance	µm	25.11
	4	Length	Distance	µm	22.63
	5	Length	Distance	µm	21.66
SG 17	1	Length	Distance	µm	21.72
	2	Length	Distance	µm	26.29
	3	Length	Distance	µm	22.7
	4	Length	Distance	µm	23.25
	5	Length	Distance	µm	23.41
	6	Length	Distance	µm	23.5
	7	Length	Distance	µm	22.82
	8	Length	Distance	µm	25.87
SG 18	1	Length	Distance	µm	27.6
	2	Length	Distance	µm	25.59
	3	Length	Distance	µm	25.11
	4	Length	Distance	µm	27.19
SG 19	1	Length	Distance	µm	22.1
	2	Length	Distance	µm	21.63
	3	Length	Distance	µm	22.96
	4	Length	Distance	µm	21.53
	5	Length	Distance	µm	23.4
SG 20	1	Length	Distance	µm	19.99
	2	Length	Distance	µm	21.51
	3	Length	Distance	µm	22.5
	4	Length	Distance	µm	20.94
SG 21	1	Length	Distance	µm	19.37
	2	Length	Distance	µm	25.12
	3	Length	Distance	µm	22.29
	4	Length	Distance	µm	21.81
SG 22	1	Length	Distance	µm	17.89
	2	Length	Distance	µm	17.81
	3	Length	Distance	µm	17.71
	4	Length	Distance	µm	18.77
SG 23	1	Length	Distance	µm	17.81
	2	Length	Distance	µm	17.7
	3	Length	Distance	µm	18.87
	4	Length	Distance	µm	17.87
SG 24	1	Length	Distance	µm	18.15
	2	Length	Distance	µm	17.51
	3	Length	Distance	µm	19.8
	4	Length	Distance	µm	20.09
	5	Length	Distance	µm	21.68
	6	Length	Distance	µm	20.08
	7	Length	Distance	µm	19.7
	8	Length	Distance	µm	18.3
	9	Length	Distance	µm	20.54
SG 25	1	Length	Distance	µm	21.05
	2	Length	Distance	µm	19.77
	3	Length	Distance	µm	19.99
	4	Length	Distance	µm	21.07
	5	Length	Distance	µm	19.19
Average value of nuclei size from 25 salivary glands					**21.061308**
Standard deviation of the average value of nuclei size					**2.8174103**

B.8. (iv) One way ANOVA analysis of the data shown in appendix B.8 (i), B.8 (ii) and B.8 (iii)

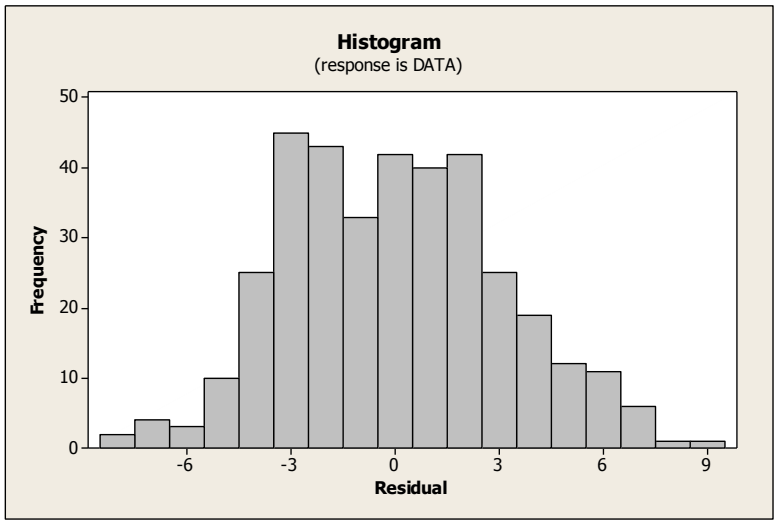

One-way ANOVA: DATA versus GENES

```
Source   DF       SS       MS       F      P
GENES     2  2231.47  1115.73  113.53  0.000
Error   361  3547.93     9.83
Total   363  5779.39

S = 3.135   R-Sq = 38.61%   R-Sq(adj) = 38.27%

                          Individual 95% CIs For Mean Based on
                           Pooled StDev
Level    N    Mean  StDev  -------+---------+---------+---------+--
1       90  27.538  3.424                                  (---*--)
2      144  23.621  3.218               (-*--)
3      130  21.061  2.817  (-*--)
                           -------+---------+---------+---------+--
                               22.0      24.0      26.0      28.0
Pooled StDev = 3.135

Tukey 95% Simultaneous Confidence Intervals
All Pairwise Comparisons among Levels of GENES

Individual confidence level = 98.02%

GENES = 1 subtracted from:

GENES   Lower  Center   Upper  -----+---------+---------+---------+----
2      -4.902  -3.916  -2.930           (--*--)
3      -7.483  -6.477  -5.470  (--*---)
                               -----+---------+---------+---------+----
                                 -6.0      -3.0       0.0       3.0
GENES = 2 subtracted from:

GENES   Lower  Center   Upper  -----+---------+---------+---------+----
3      -3.448  -2.560  -1.672                (-*--)
                               -----+---------+---------+---------+----
                                 -6.0      -3.0       0.0       3.0
```

B.9. Effect of Simj expression on Mi-2 localization in single cell clones
For the data of Visualization of Mi-2 protein in GFP marked control clone cells. refer Appendix B.2. (i)
For the data of Visualization of Mi-2 protein in single cell clones expressing *NOS2* refer Appendix B.2. (ii)
B.9. (i) Visualization of Mi-2 protein in single cell clones expressing *simj*

Img No 1	Voxel Count	Volume (µm³)	Min (ChS2-T2)	Mean (ChS2-T2)	Sum (ChS2-T2)	Mean (Ch3-T3)	Centroid X	Centroid Y	Centroid Z
Clone cell	16360	6622.39	57	141.12	2.31E+06	34.0834	450.376	121.158	6.58191
Wt 1	7803	3158.59	57	134.5	1.05E+06	0.066641	58.9468	231.115	6.39536
Wt 2	6450	2610.91	57	137.121	884431	0.0724031	135.03	228.92	7.17395
Wt 3	6553	2652.6	57	127.699	836809	0.0602777	146.638	318.454	7.77537
Wt 4	6067	2455.87	57	124.882	757657	0.0525795	253.202	287.083	8.43036
Wt 5	7037	2848.52	57	128.13	901654	0.0667898	321.164	297.007	8.19582
Wt 6	11357	4597.22	57	130.938	1.49E+06	0.07185	85.6533	381.751	8.85163
Wt 7	4918	1990.77	57	124.378	611690	0.0518503	37.2056	191.542	16.0702
Wt 8	4313	1745.87	57	120.296	518836	0.0428936	483.09	306.288	14.2054
Wt 9	4564	1847.47	57	128.315	585628	0.0580631	145.961	366.089	17.4189
Wt 10	7057	2856.62	57	127.882	902460	0.0671674	321.05	296.46	8.18591

Img No 2	Voxel Count	Volume (µm³)	Min (ChS2-T2)	Mean (ChS2-T2)	Sum (ChS2-T2)	Mean (Ch3-T3)	Centroid X	Centroid Y	Centroid Z
Clone cell	14667	5937.08	57	147.235	2.16E+06	106.857	111.108	355.654	8.96755
Wt 1	6379	2582.17	57	107.023	682698	0.773632	422.654	171.442	8.37827
Wt 2	2836	1147.99	57	96.3551	273263	0.538082	465.529	91.0815	6.44288
Wt 3	6290	2546.14	57	105.174	661545	0.793323	286.41	127.942	7.10127
Wt 4	4997	2022.74	57	98.9956	494681	0.923154	243.587	206.562	6.3336
Wt 5	3766	1524.45	57	95.427	359378	0.644981	170.429	44.2262	6.25544
Wt 6	4603	1863.26	57	98.6007	453859	1.09841	59.3167	160.709	6.10146
Wt 7	5385	2179.8	57	107.846	580751	0.803528	460.835	324.756	8.42581

Img No 3	Voxel Count	Volume (µm³)	Min (ChS2-T2)	Mean (ChS2-T2)	Sum (ChS2-T2)	Mean (Ch3-T3)	Centroid X	Centroid Y	Centroid Z
Clone cell 1	10897	4411.02	43	105.125	1.15E+06	100.482	69.3808	410.013	9.28421
Wt 1	9418	3812.33	43	100.859	949889	5.40285	167.029	97.5033	14.8709
Wt 2	10938	4427.61	43	116.031	1.27E+06	0.360304	393.396	64.4188	16.2063
Wt 3	10338	4184.74	43	109.234	1.13E+06	0.397079	265.724	60.3963	17.8363
Wt 4	10249	4148.71	43	119.768	1.23E+06	0.465997	369.051	186.718	14.6418
Wt 5	9484	3839.05	43	103.639	982913	0.499578	374.002	395.276	13.7109
Wt 6	7438	3010.84	43	100.523	747693	0.661871	186.82	355.517	13.5144
Wt 7	9304	3766.18	43	100.792	937768	5.42197	166.839	97.4275	14.9012
Wt 8	4113	1664.91	43	83.2815	342537	0.222952	465.848	362.801	13.3744

Img No 4	Voxel Count	Volume (µm³)	Min (ChS2-T2)	Mean (ChS2-T2)	Sum (ChS2-T2)	Mean (Ch3-T3)	Centroid X	Centroid Y	Centroid Z
Clone cell 1	12135	4912.15	46	136.017	1.65E+06	131.048	73.6278	66.9926	6.75731
Wt 1	9413	3810.3	46	104.73	985828	0.232976	299.246	192.522	11.1588
Wt 2	7596	3074.8	46	98.5566	748636	0.180358	366.104	159.209	15.7353
Wt 3	8831	3574.72	46	104.357	921574	0.226362	395.488	228.113	10.5665
Wt 4	6251	2530.35	46	108.921	680867	0.158695	430.473	188.593	18.9736
Wt 5	4965	2009.79	46	83.3398	413782	0.181269	388.245	438.983	12.4427

Img No 5	Voxel Count	Volume (µm³)	Min (ChS2-T2)	Mean (ChS2-T2)	Sum (ChS2-T2)	Mean (Ch3-T3)	Centroid X	Centroid Y	Centroid Z
Clone cell 1	11912	4821.88	46	116.041	1.38E+06	86.7053	262.517	377.754	4.94233
Wt 1	7862	3182.47	46	104.207	819274	1.43933	389.811	237.671	6.54299
Wt 2	8910	3606.69	46	103.984	926498	0.885297	446.283	32.5094	4.98328

Wt 3	8910	3606.69	46	103.984	926498	0.885297	446.283	32.5094	4.98328
Wt 4	14570	5897.82	46	106.463	1.55E+06	1.53974	83.7579	392.986	10.0226
Wt 5	3761	1522.42	46	91.8282	345366	0.711513	483.096	275.215	9.95799
Wt 6	10828	4383.09	46	99.1778	1.07E+06	1.71888	173.078	301.655	7.16236
Wt 7	6918	2800.35	46	92.9818	643248	1.46343	283.103	284.763	6.13544
Wt 8	6202	2510.52	46	92.4595	573434	1.31699	233.008	462.724	12.1098
Wt 9	7090	2869.97	46	100.922	715540	1.1165	468.742	147.919	6.06135
Wt 10	8786	3556.5	46	105.365	925740	1.3402	381.439	334.936	7.32825

Img No 6	**Voxel Count**	**Volume (µm³)**	**Min (ChS2-T2)**	**Mean (ChS2-T2)**	**Sum (ChS2-T2)**	**Mean (Ch3-T3)**	**Centroid X**	**Centroid Y**	**Centroid Z**
Clone cell 1	10737	4346.25	82	144.792	1.55E+06	99.106	382.245	205.242	8.45925
Wt 1	8151	3299.46	82	138.355	1.13E+06	1.2439	190.642	266.164	9.98736
Wt 2	5951	2408.92	82	138.537	824432	1.13325	63.2121	315.229	9.09746
Wt 3	3516	1423.25	82	131.48	462284	0.877986	186.644	376.67	10.1183
Wt 4	5396	2184.26	82	135.979	733744	0.6894	449.377	331.161	10.4459
Wt 5	4025	1629.29	82	141.379	569051	0.693913	225.77	175.476	14.2631
Wt 6	4172	1688.79	82	132.339	552119	0.697987	336.289	373.71	10.8015
Wt 7	5133	2077.8	82	138.425	710534	1.15995	131.847	310.744	10.1773
Wt 8	6482	2623.86	82	144.29	935288	0.695927	362.157	136.408	17.8952
Wt 9	4665	1888.35	82	136.768	638023	0.627653	193.52	295.749	28.0585
Wt 10	4404	1782.7	82	137.188	604178	0.864668	283.085	180.765	22.2007

Img No 7	**Voxel Count**	**Volume (µm³)**	**Min (ChS2-T2)**	**Mean (ChS2-T2)**	**Sum (ChS2-T2)**	**Mean (Ch3-T3)**	**Centroid X**	**Centroid Y**	**Centroid Z**
Clone cell 2	12052	4878.55	48	115.294	1.39E+06	50.3392	446.966	131.514	9.66653
Wt 1	10324	4179.07	48	114.416	1.18E+06	6.90672	206.639	62.141	13.3637
Wt 2	8672	3510.35	48	97.4154	844786	1.07922	241.722	151.791	13.0232
Wt 3	10713	4336.53	48	111.816	1.20E+06	0.782881	310.893	55.49	12.1105
Wt 4	8377	3390.94	48	99.0227	829513	1.06589	49.0674	42.1019	13.7572
Wt 5	6804	2754.2	48	93.1974	634115	1.14947	235.311	272.532	12.8602
Wt 6	8038	3253.72	48	99.6891	801301	0.840134	383.176	82.4943	11.1687
Wt 7	8274	3349.25	48	99.9821	827252	1.09137	117.506	90.594	15.2236
Wt 8	6397	2589.45	48	95.6301	611746	0.849304	136.869	164.634	23.1369
Wt 9	4070	1647.5	48	91.0776	370686	0.746437	441.777	415.365	14.5973
Wt 10	3715	1503.8	48	90.6323	336699	0.474832	492.25	293.276	29.5489

Img No 8	**Voxel Count**	**Volume (µm³)**	**Min (ChS2-T2)**	**Mean (ChS2-T2)**	**Sum (ChS2-T2)**	**Mean (Ch3-T3)**	**Centroid X**	**Centroid Y**	**Centroid Z**
Clone cell 1	6063	2454.25	48	92.7236	562183	71.2057	371.73	188.228	16.8872
Wt 1	10285	4163.28	48	105.176	1.08E+06	0.685853	171.67	152.74	9.84414
Wt 2	8555	3462.99	48	110.321	943799	0.881707	403.47	361.087	28.3517
Wt 3	7818	3164.66	48	112.952	883058	0.46879	161.899	170.223	26.5562
Wt 4	7314	2960.65	48	104.331	763075	0.331146	272.52	168.699	26.5334
Wt 5	7368	2982.51	48	111.402	820808	0.452904	157.032	249.292	27.8422
Wt 6	7900	3197.85	48	102.947	813279	9.6243	75.4914	275.457	20.8491
Wt 7	8657	3504.28	48	111.391	964308	0.354511	289.877	334.798	26.7977
Wt 8	7226	2925.03	48	100.072	723117	0.314282	215.965	89.5086	22.8316
Wt 9	6204	2511.33	48	111.563	692136	0.436331	262.281	381.69	17.829
Wt 10	9198	3723.27	48	113.835	1.05E+06	0.262122	415.942	473.261	27.6655

Average intensity of Mi-2 localization in 10 non adjacent wild type cells

Img No 1	**128.4141**
Img No 2	**101.34591**
Img No 3	**104.26594**
Img No 4	**99.98088**
Img No 5	**100.13723**

Img No 6	**137.474**
Img No 7	**99.28787**
Img No 8	**108.399**

Intensity of Mi-2 localization in clone cell V average intensity of Mi-2 localization in 10 non adjacent wild type cells

Img No 1	**1.09**
Img No 2	**1.45**
Img No 3	**1**
Img No 4	**1.36**
Img No 5	**1.15**
Img No 6	**1.05**
Img No 7	**1.16**
Img No 8	**0.85**

Average value of the ratio of the clone cell V wild type cells acquired from Img No 1 to Img No 10	**1.13875**
Std Dev of the average ratio of clone cell / wild type cell	**0.192460571**

B.9. (ii) Visualization of Mi-2 protein in single cell clones co expressing *simj* and *NOS2*

Img No 1	Voxel Count	Volume (µm³)	Min (ChS2-T2)	Mean (ChS2-T2)	Sum (ChS2-T2)	Mean (Ch3-T3)	Centroid X	Centroid Y	Centroid Z
Clone cell	16172	6546.29	74	123.38	2.00E+06	21.7323	209.454	400.617	17.4676
Wt 1	10776	4362.04	74	107.156	1.15E+06	7.54092	252.024	225.261	8.25965
Wt 2	11466	4641.34	74	108.849	1.25E+06	7.54457	259.279	136.932	10.5404
Wt 3	8045	3256.55	74	107.111	861711	7.5376	433.186	53.2793	10.0894
Wt 4	11732	4749.02	74	109.527	1.28E+06	7.51432	354.609	143.346	9.58302
Wt 5	8333	3373.13	74	106.685	889005	7.52274	433.489	53.6209	10.2934
Wt 6	10327	4180.28	74	110.942	1.15E+06	7.08086	96.8129	224.166	21.5723
Wt 7	10455	4232.1	74	107.647	1.13E+06	7.45806	159.288	197.558	14.5456
Wt 8	8031	3250.88	74	106.099	852080	7.37106	263.567	86.5598	17.6076
Wt 9	11045	4470.92	74	109.702	1.21E+06	7.51299	335.895	229.224	9.92214
Wt 10	14609	5913.6	74	104.654	1.53E+06	7.22411	394.799	249.991	20.6995
Wt 11	12654	5122.23	74	112.387	1.42E+06	7.38897	457.86	211.473	10.6776
Wt 12	10458	4233.31	74	109.68	1.15E+06	7.28772	56.4343	282.082	13.8287

Img No 2	Voxel Count	Volume (µm³)	Min (ChS2-T2)	Mean (ChS2-T2)	Sum (ChS2-T2)	Mean (Ch3-T3)	Centroid X	Centroid Y	Centroid Z
Clone cell	7598	3075.61	20	140.452	1.07E+06	36.667	295.14	160.866	8.2656
Wt 1	2229	902.281	20	120.628	268880	0.0592194	298.851	351.624	10.1534
Wt 2	1839	744.412	20	122.661	225573	0.0598151	358.953	194.269	14.6324
Wt 3	2933	1187.25	20	123.267	361543	0.603478	208.024	283.56	11.4398
Wt 4	6200	2509.71	20	129.018	799912	0.0496774	210.263	109.745	8.24532

Img No 3	Voxel Count	Volume (µm³)	Min (ChS2-T2)	Mean (ChS2-T2)	Sum (ChS2-T2)	Mean (Ch3-T3)	Centroid X	Centroid Y	Centroid Z
Clone cell 2	10518	4257.6	36	113.101	1.19E+06	25.9756	113.54	76.7985	7.80643
Wt 1	5906	2390.7	36	97.1392	573704	0.028615	324.328	187.99	13.5229
Wt 2	5764	2333.22	36	94.2611	543321	0.0294934	398.222	374.03	13.4434
Wt 3	2894	1171.47	36	91.1334	263740	0.0342087	409.428	268.281	15.5746
Wt 4	6295	2548.16	36	96.346	606498	0.029865	323.859	188.042	13.2818
Wt 5	2464	997.407	36	90.9947	224211	0.0434253	287.119	57.7228	15.9123
Wt 6	3128	1266.19	36	92.7986	290274	0.0457161	470.256	465.329	11.4655
Wt 7	4965	2009.79	36	104.999	521320	5.7565	386.103	454.155	10.7984
Wt 8	2797	1132.2	36	92.5359	258823	0.0207365	296.506	432.159	18.6232
Wt 9	4845	1961.22	36	91.9154	445330	0.0276574	306.421	116.699	14.7889
Wt 10	6512	2636	36	96.5951	629027	0.0325553	275.406	337.272	14.601

Img No 4	Voxel Count	Volume (µm³)	Min (ChS2-T2)	Mean (ChS2-T2)	Sum (ChS2-T2)	Mean (Ch3-T3)	Centroid X	Centroid Y	Centroid Z
Clone cell 2	6762	2737.2	21	102.576	693617	40.5945	49.1375	241.077	22.5568
Wt 1	2375	961.38	21	66.3562	157596	0.119158	250.877	195.117	21.968
Wt 2	2585	1046.39	21	66.3749	171579	0.109865	298.417	126.352	18.7911

Wt 3	1409	570.352	21	66.0823	93110	0.106458	499.216	99.1249	18.4592
Wt 4	5402	2186.69	21	68.4304	369661	0.15124	172.493	195.208	16.5041
Wt 5	2597	1051.24	21	67.0316	174081	0.174817	327.301	200.939	19.8552
Wt 6	11364	4600.05	21	92.0505	1.05E+06	0.25308	27.6017	290.467	19.4423
Wt 7	11059	4476.59	21	93.0073	1.03E+06	0.156434	62.9432	335.013	20.1609
Wt 8	2710	1096.99	21	69.5251	188413	0.101107	163.166	355.57	11.7786
Wt 9	6774	2742.06	21	90.1255	610510	0.130794	115.738	341.5	18.6181

Img No 5	**Voxel Count**	**Volume (µm³)**	**Min (ChS2-T2)**	**Mean (ChS2-T2)**	**Sum (ChS2-T2)**	**Mean (Ch3-T3)**	**Centroid X**	**Centroid Y**	**Centroid Z**
Clone cell 3	6347	2569.21	51	110.665	702390	52.8793	325.764	211.777	27.1484
Wt 1	5563	2251.86	51	111.536	620473	0.724609	105.396	266.527	26.1719
Wt 2	6571	2659.89	51	111.541	732938	1.54984	87.9379	289.157	7.86653
Wt 3	6474	2620.62	51	115.156	745523	1.3565	55.7098	389.281	6.10148
Wt 4	6519	2638.84	51	115.015	749780	0.799049	69.1131	436.459	11.7928
Wt 5	6033	2442.11	51	110.87	668876	1.39715	195.29	319.728	7.98989
Wt 6	6903	2794.28	51	102.42	707002	0.97914	146.301	193.111	15.4485
Wt 7	3306	1338.24	51	93.6034	309453	0.805808	415.896	89.7958	11.0266
Wt 8	6236	2524.28	51	99.8161	622453	0.68313	486.299	27.2901	7.37171
Wt 9	3741	1514.33	51	100.294	375201	0.871157	417.927	33.6172	10.3617

Img No 6	**Voxel Count**	**Volume (µm³)**	**Min (ChS2-T2)**	**Mean (ChS2-T2)**	**Sum (ChS2-T2)**	**Mean (Ch3-T3)**	**Centroid X**	**Centroid Y**	**Centroid Z**
Clone cell 1	12381	5011.73	33	118.317	1.46E+06	91.5425	68.9879	186.166	14.4475
Wt 1	7812	3162.23	33	100.612	785979	5.30364	201.783	77.6409	12.6624
Wt 2	5703	2308.53	33	92.2779	526261	0.96686	424.319	119.253	6.47466
Wt 3	4305	1742.63	33	83.4839	359398	0.840186	253.371	411.972	11.1022
Wt 4	3921	1587.19	33	85.8202	336501	0.624586	407.377	308.667	10.9064
Wt 5	4673	1891.59	33	84.6719	395672	1.00492	111.663	439.067	8.6101
Wt 6	3706	1500.16	33	89.8079	332828	0.66082	471.025	240.413	10.629
Wt 7	8022	3247.24	33	99.8736	801186	5.27774	202.405	77.7253	12.4814
Wt 8	7214	2920.17	33	96.9885	699675	0.754921	454.835	191.906	19.2657
Wt 9	4095	1657.62	33	82.8821	339402	1.14701	25.3888	371.083	7.84249
Wt 10	3689	1493.28	33	83.621	308478	0.952833	367.144	31.8336	7.0309

Img No 7	**Voxel Count**	**Volume (µm³)**	**Min (ChS2-T2)**	**Mean (ChS2-T2)**	**Sum (ChS2-T2)**	**Mean (Ch3-T3)**	**Centroid X**	**Centroid Y**	**Centroid Z**
Clone cell	9126	59106.1	46	116.208	1.06E+06	55.5371	86.5536	67.8617	7.99025
Wt 1	1431	9268.11	46	85.8134	122799	0.489867	339.789	367.468	13.6171
Wt 2	2748	17797.9	46	92.321	253698	0.394469	375.177	453.989	15.2682
Wt 3	2103	13620.4	46	84.1555	176979	0.470281	337.789	365.628	14.292
Wt 4	698	4520.71	46	83.894	58558	0.848138	113.301	342.94	15.9943
Wt 5	2014	13044	46	84.1837	169546	0.459782	254.818	400.292	15.2175
Wt 6	1605	10395.1	46	82.5445	132484	0.322118	333.394	248.903	14.4997
Wt 7	511	3309.58	46	95.7358	48921	0.215264	448.374	423.155	8.48532
Wt 8	458	2966.31	46	103.332	47326	0.255459	52.3472	343.98	5.23144

Img No 8	**Voxel Count**	**Volume (µm³)**	**Min (ChS2-T2)**	**Mean (ChS2-T2)**	**Sum (ChS2-T2)**	**Mean (Ch3-T3)**	**Centroid X**	**Centroid Y**	**Centroid Z**
Clone cell 1	5159	2088.32	33	89.4315	461377	12.1022	62.516	184.495	6.93584
Wt 1	2965	1200.21	33	76.6513	227271	4.8543	313.632	191.968	6.60236
Wt 2	3195	1293.31	33	80.713	257878	2.73646	465.044	158.479	8.9011
Wt 3	3847	1557.23	33	83.1339	319816	6.03483	278.747	147.807	11.2132
Wt 4	2165	876.374	33	73.3266	158752	4.67945	222.654	183.005	7.65589
Wt 5	1864	754.532	33	74.9453	139698	3.603	13.4871	105.137	8.57135
Wt 6	4364	1766.51	33	82.2523	358949	3.46746	454.75	212.85	8.04629
Wt 7	1330	538.373	33	73.8128	98171	5.33308	260.156	253.741	6.69624
Wt 8	3140	1271.05	33	77.3914	243009	6.39108	151.116	207.164	6.61911
Wt 9	2481	1004.29	33	80.5917	199948	5.41838	241.277	154.473	18.894
Wt 10	4847	1962.03	33	88.0881	426963	0.736125	468.567	210.101	28.1314
Wt 11	5367	2172.52	33	83.9765	450702	5.50419	318.822	153.324	20.64

Img No 9	Voxel Count	Volume (µm³)	Min (ChS2-T2)	Mean (ChS2-T2)	Sum (ChS2-T2)	Mean (Ch3-T3)	Centroid X	Centroid Y	Centroid Z
Clone cell 1	4906	1985.91	51	126.627	621232	9.57073	190.359	349.251	20.1981
Wt 1	3141	1271.45	51	108.847	341887	1.65266	366.957	200.716	16.7896
Wt 2	5238	2120.3	51	117.063	613176	2.73654	290.002	182.944	12.4519
Wt 3	5754	2329.17	51	123.906	712956	2.40945	35.8479	325.8	17.8203
Wt 4	6808	2755.82	51	124.862	850061	2.17847	59.1281	420.543	17.8685
Wt 5	6808	2755.82	51	124.862	850061	2.17847	59.1281	420.543	17.8685
Wt 6	5504	2227.97	51	119.234	656265	5.80142	333.212	306.852	16.6154
Wt 7	5927	2399.2	51	119.63	709046	3.69226	121.964	429.526	6.25696
Wt 8	4345	1758.82	51	113.008	491020	2.46053	193.529	426.195	8.98067
Wt 9	5179	2096.42	51	117.283	607408	2.50048	265.778	260.33	15.3862
Wt 10	2788	1128.56	51	130.387	363519	3.10976	62.3633	217.58	21.1646

Img No 10	Voxel Count	Volume (µm³)	Min (ChS2-T2)	Mean (ChS2-T2)	Sum (ChS2-T2)	Mean (Ch3-T3)	Centroid X	Centroid Y	Centroid Z
Clone cell 1	8386	3394.58	51	132.969	1.12E+06	24.102	127.356	112.763	8.90651
Wt 1	5141	2081.03	51	115.911	595901	6.94242	212.348	170.187	10.3202
Wt 2	3073	1243.93	51	111.569	342853	3.85421	323.234	273.354	13.7491
Wt 3	4833	1956.36	51	113.276	547463	6.53404	201.155	373.923	8.15622
Wt 4	5064	2049.87	51	113.955	577068	5.85999	166.625	446.863	11.0737
Wt 5	5700	2307.31	51	114.321	651631	7.90053	247.03	234.362	7.06649
Wt 6	5969	2416.2	51	120.682	720348	5.44848	235.86	27.0756	8.97638
Wt 7	4039	1634.95	51	113.083	456744	6.35083	281.482	444.351	9.41025
Wt 8	3700	1497.73	51	112.04	414547	4.34676	108.976	221.151	14.0205
Wt 9	3258	1318.81	51	113.675	370352	4.34254	251.206	80.2769	16.1357
Wt 10	4040	1635.36	51	116.712	471515	3.37673	306.012	43.2859	18.0121
Wt 11	3040	1230.57	51	110.27	335220	3.8727	122.975	374.218	14.6049

Img No 11	Voxel Count	Volume (µm³)	Min (ChS2-T2)	Mean (ChS2-T2)	Sum (ChS2-T2)	Mean (Ch3-T3)	Centroid X	Centroid Y	Centroid Z
Clone cell 1	6420	2598.76	51	132.426	850177	44.7316	204.724	422.07	11.4545
Wt 1	4572	1850.71	51	113.974	521087	3.70516	318.287	307.999	11.2657
Wt 2	7732	3129.85	51	122.111	944165	3.48047	317.877	172.161	8.02742
Wt 3	4525	1831.68	51	111.473	504417	4.02762	268.03	212.661	10.3386
Wt 4	5617	2273.72	51	113.031	634895	3.43493	222.777	270.272	9.98309
Wt 5	4553	1843.02	51	113.834	518285	3.73951	317.936	307.867	11.4707
Wt 6	6451	2611.31	51	119.129	768499	2.86529	424.715	117.475	10.1959
Wt 7	4119	1667.34	51	115.759	476810	1.23258	147.434	257.38	19.4817
Wt 8	7151	2894.67	51	124.812	892530	3.64494	296.389	473.039	9.57013
Wt 9	9874	3996.91	51	134.116	1.32E+06	2.83755	378.877	288.534	12.1791
Wt 10	5249	2124.75	51	117.71	617861	1.83768	369.971	393.477	11.9042

Img No 12	Voxel Count	Volume (µm³)	Min (ChS2-T2)	Mean (ChS2-T2)	Sum (ChS2-T2)	Mean (Ch3-T3)	Centroid X	Centroid Y	Centroid Z
Clone cell 1	1310	530.277	51	91.4618	119815	16.8015	246.427	331.27	11.2359
Wt 1	10693	4328.44	51	128.509	1.37E+06	0.192088	348.976	190.269	9.67446
Wt 2	8180	3311.2	51	121.693	995445	0.162103	459.046	217.906	9.19951
Wt 3	8212	3324.15	51	112.869	926878	0.183999	79.0043	256.897	11.6111
Wt 4	9819	3974.65	51	131.015	1.29E+06	0.217741	67.6166	87.7511	11.1855
Wt 5	8974	3632.6	51	113.611	1.02E+06	0.167818	191.84	138.977	9.7183
Wt 6	8322	3368.68	51	113.014	940506	0.173276	432.103	298.146	9.01754
Wt 7	7475	3025.82	51	111.091	830408	0.146355	445.508	395.162	8.96829
Wt 8	5311	2149.85	51	104.164	553217	0.144229	335.86	409.082	9.62531
Wt 9	7779	3148.88	51	111.224	865209	0.137935	490.169	464.469	9.82311
Wt 10	4368	1768.13	51	102.095	445951	0.466346	283.117	57.8633	8.54006

Average intensity of Mi-2 localization in 10 non adjacent wild type cells

Img No 1	**108.3699**
Img No 2	**123.8935**
Img No 3	**94.87184**
Img No 4	**75.44264**

Img No 5	**106.6946**
Img No 6	**90.0039**
Img No 7	**88.99749**
Img No 8	**79.53481**
Img No 9	**119.9082**
Img No 10	**114.1358**
Img No 11	**118.5949**
Img No 12	**114.9285**

Intensity of Mi-2 localization in clone cell V average intensity of Mi-2 localization in 10 non adjacent wild type cells

Img No 1	**1.3**
Img No 2	**1.13**
Img No 3	**1.13**
Img No 4	**1.19**
Img No 5	**1.36**
Img No 6	**1.03**
Img No 7	**1.31**
Img No 8	**1.12**
Img No 9	**1.05**
Img No 10	**1.16**
Img No 11	**1.11**
Img No 12	**0.79**
Average value of the ratio of the clone cell V wild type cells acquired from Img No 1 to Img No 10	**1.14**
Std Dev of the average ratio of clone cell / wild type cell	**0.15076**

C. List of CPTI lines Annotated and Screened

C.1. List of CPTI lines Annotated

CPTI-000106, CPTI-000110, CPTI 000205, CPTI-000232, CPTI-000239, CPTI-000256, CPTI 000340 , CPTI-000546, CPTI-000703, CPTI-000762, CPTI-000765, CPTI 000774, CPTI-000787, CPTI-000836, CPTI-000847, CPTI-000877, CPTI-000943, CPTI-000944, CPTI 001017, CPTI-001031, CPTI-001137, CPTI-001166, CPTI-001218, CPTI-001223, CPTI-001224, CPTI-001259, CPTI-001261, CPTI-001262, CPTI-001272, CPTI-001279, CPTI-001282, CPTI-001308, CPTI-001309, CPTI-001323, CPTI-001324, CPTI-001328, CPTI-001332, CPTI-001334, CPTI-001341, CPTI-001403, CPTI-001412, CPTI-001414, CPTI-001423, CPTI-001427, CPTI-001455, CPTI-001478, CPTI-001481, CPTI-001488, CPTI-001495, CPTI-001515, CPTI-001516, CPTI-001527, CPTI-001569, CPTI-001586, CPTI-001589, CPTI-001595, CPTI- 001636, CPTI-001654, CPTI-001660, CPTI-001678, CPTI 001685, CPTI-001692, CPTI-001693, CPTI-001695, CPTI-001709, CPTI-001714 , CPTI-001718, CPTI-001735, CPTI-001740, CPTI-001765, CPTI-001769, CPTI-001771, CPTI-001775, CPTI-001796, CPTI-001879, CPTI-001881, CPTI-001883, CPTI-001919, CPTI-001977, CPTI-001987, CPTI-001990, CPTI-002016, CPTI-002032, CPTI-002035, CPTI-002085, CPTI-002102, CPTI-002118, CPTI-002129, CPTI-002256, CPTI-002264, CPTI-002285, CPTI-002292, CPTI-002315, CPTI-002343, CPTI-002401, CPTI-002487, CPTI 002773 , CPTI 002786, CPTI-002805, CPTI-100038.

C.2. List of CPTI lines Screened

CPTI-000847, CPTI-000256, CPTI-001409, CPTI- 000106, CPTI -000199, CPTI -001332, CPTI 000205, CPTI 000232, CPTI 000239, CPTI 000340 CPTI 000472, CPTI 000546, CPTI 000703, CPTI 000762, CPTI 001017, CPTI 000765, CPTI 000774, CPTI 000787, CPTI 000836, CPTI 001224, CPTI 001223 , CPTI 000943, CPTI 001031, CPTI 001166, CPTI 001279, CPTI 001308, CPTI 001198, CPTI 001218, CPTI 001259, CPTI 001262, CPTI 001272, CPTI 001282, CPTI 001309, CPTI 001323, CPTI 001324, CPTI 001328, CPTI 001334, CPTI 001883, CPTI 001455, CPTI 001478., CPTI 001775, CPTI 001802, CPTI 001881, CPTI 001987, CPTI 002118, CPTI 002292, CPTI 002016, CPTI 001998, CPTI 002035, CPTI 002315, CPTI 002292, CPTI 002773, CPTI 002264, CPTI 001919, CPTI 002406, CPTI 002032, CPTI 000877, CPTI 002786, CPTI 002264, CPTI 002129, CPTI 002256, CPTI 002085, CPTI 001569, CPTI 001527,CPTI 001586, CPTI 001660, CPTI 001636, CPTI 001685, CPTI 001714, CPTI 001718, CPTI 001802, CPTI 001692 CPTI 000774, CPTI 001879, CPTI 002805, CPTI 100038.

REFERENCES:

AHRINGER, J. (2000) NuRD and SIN3 histone deacetylase complexes in development. *Trends Genet,* 16**,** 351-6.

AIRIO, A., PUKKALA, E. & ISOMAKI, H. (1995) Elevated cancer incidence in patients with dermatomyositis: a population based study. *J Rheumatol,* 22**,** 1300-3.

ALBERTS, B., JOHNSON, A., LEWIS, J., RAFF, M., ROBERTS, K. A. & WALTER, P. (2002) *Molecular Biology of the Cell.*

ALEKSANDAR S. NECAKOV, L. C., CAROL SCHWARTZ, IAN J. H. ROBERTS AND HENRY M. & (UNPUBLISHED), K. Nitric oxide signaling controls the nuclear receptor-directed transition from growth to metamorphosis.

ALLAND, L., MUHLE, R., HOU, H., JR., POTES, J., CHIN, L., SCHREIBER-AGUS, N. & DEPINHO, R. A. (1997) Role for N-CoR and histone deacetylase in Sin3-mediated transcriptional repression. *Nature,* 387**,** 49-55.

ANDREAS BARTHEL, D. S., TERRY G UNTERMAN (2005) FoxO proteins in insulin action and metabolism *Trends in Endocrinology and Metabolism,* 16**,** 183-189.

ANNE BRUNET, A. B., MICHAEL J. ZIGMOND,K, MICHAEL Z. LIN, P. J., † LINDA S. HU,, MICHAEL J. ANDERSON, K. C. A., JOHN BLENIS, & GREENBERG, A. M. E. (1999) Akt Promotes Cell Survival by Phosphorylating and Inhibiting a Forkhead Transcription Factor. *Cell, Vol,* 96**,** 857–868.

ASADA, K., KUROKAWA, J. & FURUKAWA, T. (2009) Redox- and calmodulin-dependent S-nitrosylation of the KCNQ1 channel. *J Biol Chem,* 284**,** 6014-20.

AYER, D. E. (1999) Histone deacetylases: transcriptional repression with SINers and NuRDs. *Trends in Cell Biology,* 9**,** 193-198.

BELLEN, H. J., LEVIS, R. W., LIAO, G., HE, Y., CARLSON, J. W., TSANG, G., EVANS-HOLM, M., HIESINGER, P. R., SCHULZE, K. L., RUBIN, G. M., HOSKINS, R. A. & SPRADLING, A. C. (2004) The BDGP gene disruption project: single transposon insertions associated with 40% of Drosophila genes. *Genetics,* 167**,** 761-81.

BERNAL, A. & KIMBRELL, D. A. (2000) Drosophila Thor participates in host immune defense and connects a translational regulator with innate immunity. *Proc Natl Acad Sci U S A,* 97**,** 6019-24.

BOUAZOUNE, K., MITTERWEGER, A., LANGST, G., IMHOF, A., AKHTAR, A., BECKER, P. B. & BREHM, A. (2002) The dMi-2 chromodomains are DNA binding modules important for ATP-dependent nucleosome mobilization. *Embo J,* 21**,** 2430-40.

BRACKERTZ, M., BOEKE, J., ZHANG, R. & RENKAWITZ, R. (2002) Two highly related p66 proteins comprise a new family of potent transcriptional repressors interacting with MBD2 and MBD3. *J Biol Chem,* 277**,** 40958-66.

BRAND, A. H. & PERRIMON, N. (1993) Targeted gene expression as a means of altering cell fates and generating dominant phenotypes. *Development,* 118**,** 401-15.

BREDT, D. S. (1999) Endogenous nitric oxide synthesis: biological functions and pathophysiology. *Free Radic Res,* 31**,** 577-96.

BREDT DS & SH., S. (1994) Nitric Oxide: A Physiologic Messenger Molecule. *Annual Review of Biochemistry,* 63**,** 175-195.

BREDT, D. S. & SNYDER, S. H. (1990) Isolation of nitric oxide synthetase, a calmodulin-requiring enzyme. *Proc Natl Acad Sci U S A,* 87**,** 682-5.

BREHM, A., LÄNGST, G., KEHLE, J., CEDRIC R CLAPIER, AXEL IMHOF, ANTON EBERHARTER, MÜLLER, J. & BECKER, P. B. (2000) dMi-2 and ISWI chromatin remodelling factors have distinct nucleosome binding and mobilization properties. *EMBO J,* 19**,** 4332-4341.

BRUCKDORFER, R. (2005) The basics about nitric oxide. *Mol Aspects Med.,* 26**,** 3-31.

BUGA, G. M., WEI, L. H., BAUER, P. M., FUKUTO, J. M. & IGNARRO, L. J. (1998) NG-hydroxy-L-arginine and nitric oxide inhibit Caco-2 tumor cell proliferation by distinct mechanisms. *Am J Physiol,* 275**,** R1256-64.

BUTLER, A. R. & RHODES, P. (1997) Chemistry, analysis, and biological roles of S-nitrosothiols. *Anal Biochem,* 249**,** 1-9.

CA GRUETTER, DY GRUETTER, JE LYON, PJ KADOWITZ & IGNARRO, L. (1981) Relationship between cyclic guanosine 3':5'-monophosphate formation and relaxation of coronary arterial smooth muscle by glyceryl trinitrate, nitroprusside, nitrite and nitric oxide: effects of methylene blue and methemoglobin *The journal of pharmacology and experimental therapeutics.,* 219**,** 181-186.

CHA, M. S., LEE, M. J., JE, G. H. & KWAK, J. Y. (2001) Endogenous production of nitric oxide by vascular endothelial growth factor down-regulates proliferation of choriocarcinoma cells. *Biochem Biophys Res Commun,* 282**,** 1061-6.

CHOI, T. Y., PARK, S. Y., KANG, H. S., CHEONG, J. H., KIM, H. D., LEE, B. L., HIROSE, F., YAMAGUCHI, M. & YOO, M. A. (2004) Redox regulation of DNA binding activity of DREF (DNA replication-related element binding factor) in *Drosophila*. *Biochem J,* 378**,** 833-8.

CIANI, E., SEVERI, S., CONTESTABILE, A., BARTESAGHI, R. & CONTESTABILE, A. (2004) Nitric oxide negatively regulates proliferation and

promotes neuronal differentiation through N-Myc downregulation. *J Cell Sci,* 117**,** 4727-37.

CONTESTABILE, A. & CIANI, E. (2004) Role of nitric oxide in the regulation of neuronal proliferation, survival and differentiation. *Neurochemistry International Nitric Oxide and Cyclic GMP Signal Transduction in Brain,* 45**,** 903-914.

CORTES, M., WONG, E., KOIPALLY, J. & GEORGOPOULOS, K. (1999) Control of lymphocyte development by the lkaros gene family. *Current Opinion in Immunology,* 11**,** 167-171.

CRABTREE, L. H. G. R. (2010) Chromatin remodelling during development. *Nature,* 463**,** 474-484.

CULOTTA, E. & JR., D. E. K. (1992) NO News Is Good News. *Science,* 258**,** 1862-1865.

DANG THI PHUONG THAO, HIROKAZU SETO & YAMAGUCHI, M. (2007) Drosophila Myc is required for normal DREF gene expression. *Experimental Cell Research* 314**,** 1 8 4 – 1 9 2.

DANIEL L. MOORADIAN, THOMAS C HUTSELL & KEEFER, L. K. (1995) Nitric Oxide (NO) Donor MOlecules: Effect of NO Release Rate on Vascular Smooth Muscle Cell Proliferation In Vitro *Journal of Cardiovascular Pharmacology,* 25**,** 674-678.

DANSEN, T. B. & BURGERING, B. M. (2008) Unravelling the tumor-suppressive functions of FOXO proteins. *Trends Cell Biol,* 18**,** 421-9.

DEMEREC, M. (1950) *Biology of Drosophila*.

DENHAM, S. & ROWLAND, I. J. (1992) Inhibition of the reactive proliferation of lymphocytes by activated macrophages: the role of nitric oxide. *Clin Exp Immunol,* 87**,** 157-62.

DIETZL, G., CHEN, D., SCHNORRER, F., SU, K. C., BARINOVA, Y., FELLNER, M., GASSER, B., KINSEY, K., OPPEL, S., SCHEIBLAUER, S., COUTO, A., MARRA, V., KELEMAN, K. & DICKSON, B. J. (2007) A genome-wide transgenic RNAi library for conditional gene inactivation in Drosophila. *Nature,* 448**,** 151-6.

DUFFY, J. B. (2002) GAL4 system in Drosophila: a fly geneticist's Swiss army knife. *Genesis,* 34**,** 1-15.

DUNCAN, A. J. & HEALES, S. J. R. (2005) Nitric oxide and neurological disorders. *Molecular Aspects of Medicine,* 26**,** 67–96.

E. RYDER, H. SPRIGGS, E. DRUMMOND, JOHNSTON, D. S. & RUSSELL, S. (2009) The Flannotator—a gene and protein expression annotation tool for *Drosophila melanogaster*. *Bioinformatics Applications Note,* 25**,** 548–549.

E. RYDER, H. SPRIGGS, G. JOHNSON, E. DRUMMOND, J. DRUMMOND, J. WEBSTER, J. ROOTE, N. LOWE, K. LILLEY, S. HESTER, J. HOWARD, J. REES, S. RUSSELL & JOHNSTON, D. S. mapping and characterisation of protein expression and interaction in *Drosophila melanogaster*, using a hybrid piggyBac/P-element YFP gene trap system with tandem affinity tags.

EBERHARDT, J. P. W. & BECK, K.-F. (2001) Regulation of gene expression by nitric oxide. *Eur J Physiol,* 442**,** 479–486.

ENZO NISOLI, E. C., CRISTINA TONELLO, CLARA SCIORATI, LUCA BRISCINI & & CARRUBA, M. O. (1998) Effects of nitric oxide on proliferation and differentiation of rat brown adipocytes in primary cultures. *British Journal of Pharmacology,* 125**,** 888-894.

ESSAM A. SHETA, KIRK MCMILLAN & MASTERS, B. S. S. (1994) Evidence for a Bidomain Structure of Constitutive Cerebellar NitricOxide Synthase. *The journal of Biological Chemistry,* 269 15147-15153.

FENG, Q., CAO, R., XIA, L., ERDJUMENT-BROMAGE, H., TEMPST, P. & ZHANG, Y. (2002) Identification and functional characterization of the p66/p68 components of the MeCP1 complex. *Mol Cell Biol,* 22**,** 536-46.

FENG, Q. & ZHANG, Y. (2001) The MeCP1 complex represses transcription through preferential binding, remodeling, and deacetylating methylated nucleosomes. *Genes Dev,* 15**,** 827-32.

FIRE, A., ALBERTSON, D., HARRISON, S. W. & MOERMAN, D. G. (1991) Production of antisense RNA leads to effective and specific inhibition of gene expression in C. elegans muscle. *Development,* 113**,** 503-14.

FIRE, A., XU, S., MONTGOMERY, M. K., KOSTAS, S. A., DRIVER, S. E. & MELLO, C. C. (1998) Potent and specific genetic interference by double-stranded RNA in Caenorhabditis elegans. *Nature,* 391**,** 806-11.

FORSTERMANN, U., MUGGE, A., ALHEID, U., HAVERICH, A. & FROLICH, J. C. (1988) Selective attenuation of endothelium-mediated vasodilation in atherosclerotic human coronary arteries. *Circulation Research,* 62**,** 185-90.

FRANCIS, R., BARTON, M. K., KIMBLE, J. & SCHEDL, T. (1995) gld-1, a tumor suppressor gene required for oocyte development in Caenorhabditis elegans. *Genetics,* 139**,** 579-606.

FREEDMAN, J. E., LOSCALZO, J., BARNARD, M. R., ALPERT, C., KEANEY, J. F. & MICHELSON, A. D. (1997) Nitric oxide released from activated platelets inhibits platelet recruitment. *J Clin Invest,* 100**,** 350-6.

FREEDMAN, J. E., TING, B., HANKIN, B., LOSCALZO, J., KEANEY, J. F., JR. & VITA, J. A. (1998) Impaired platelet production of nitric oxide predicts presence of acute coronary syndromes. *Circulation,* 98**,** 1481-6.

FUMIKO HIROSE, MASAMITSU YAMAGUCHI, HIROSHI HANDA, YUKIO INOMATA & MATSUKAGE, A. (1993) Novel 8-Base Pair Sequence (Drosophila DNA Replication-related Element) andS pecific Binding Factor Involved in the Expressiono of Drosophila Genes for DNA Polymerase a! and Proliferating Cell Nuclear Antigen. *The Journal of Biological Chemistry,* 268**,** 2092-2099.

FURCHGOTT, R. (1983) Role of endothelium in responses of vascular smooth muscle. *Circulation Research,* 53**,** 557-573.

FURCHGOTT, R. F. & ZAWADZKI, J. V. (1980) The obligatory role of endothelial cells in the relaxation of arterial smooth muscle by acetylcholine. *Nature,* 288**,** 373-6.

GARG, U. C. & HASSID, A. (1989) Inhibition of rat mesangial cell mitogenesis by nitric oxide-generating vasodilators. *Am J Physiol,* 257**,** F60-6.

GEORGOPOULOS, K., WINANDY, S. & AVITAHL, N. (1997) The role of the Ikaros gene in lymphocyte development and homeostasis. *Annu Rev Immunol,* 15**,** 155-76.

GIBBS, S. M. (2003) Regulation of neuronal proliferation and differentiation by nitric oxide. *Mol Neurobiol,* 27**,** 107-20.

GREENSPAN, R. J. (1997) *Fly Pushing The theory and Practice of Drosophila Genetics*, Cold Spring Harbor Laboratory Press

GRIFFITH OW & DJ., S. (1995) Nitric oxide synthases: properties and catalytic mechanism. *Annu Rev Physiol,* 57**,** 707-36.

HAENLIN, M., STELLER, H., PIRROTTA, V. & MOHIER, E. (1985) A 43 kilobase cosmid P transposon rescues the fs(1)K10 morphogenetic locus and three adjacent Drosophila developmental mutants. *Cell,* 40**,** 827-37.

HALEY, J. E. (1998) Gases as neurotransmitters. *Essays Biochem,* 33**,** 79-91.

HANCOCK, J. T. (1997) *Cell Signalling,* Edinburgh Gate, Harlow, Addition Wesley Longman.

HANS PETER SEELIG , ISABELLE MOOSBRUGGER, HANS EHRFELD, THOMAS FINK, MANFRED RENZ & EKKEHARD GENTH (1995) The major dermatomyositis-specific mi-2 autoantigen is a presumed helicase involved in transcriptional activation. *Arthritis Rheum. ,* 38 1389 - 1399.

HIROSE, F., OHSHIMA, N., KWON, E. J., YOSHIDA, H. & YAMAGUCHI, M. (2002) Drosophila Mi-2 negatively regulates dDREF by inhibiting its DNA-binding activity. *Mol Cell Biol,* 22**,** 5182-93.

HIROSE, F., YAMAGUCHI, M., KURODA, K., OMORI, A., HACHIYA, T., IKEDA, M., NISHIMOTO, Y. & MATSUKAGE, A. (1996) Isolation and Characterization of cDNA for DREF, a Promoteractivating Factor for Drosophila DNA Replication-related Genes. *Biochemistry,* 271**,** 3930 -3937.

HIROSE, F., YAMAGUCHI, M. & MATSUKAGE, A. (1999) Targeted expression of the DNA binding domain of DRE-binding factor, a Drosophila transcription factor, attenuates DNA replication of the salivary gland and eye imaginal disc. *Mol Cell Biol,* 19**,** 6020-8.

HIROSE, F., YAMAGUCHI, M., NISHIDA, Y., MASUTANI, M., MIYAZAWA, H., HANAOKA, F. & MATSUKAGE, A. (1991) Structure and expression during development of Drosophila melanogaster gene for DNA polymerase alpha. *Nucleic Acids Res,* 19**,** 4991-8.

HOLSCHER, C. (1997) Nitric oxide, the enigmatic neuronal messenger: its role in synaptic plasticity. *Trends Neurosci,* 20**,** 298-303.

IGNARRO LJ, BUGA GM, WOOD KS, BYRNS RE & G., C. (1987) Endothelium-derived relaxing factor produced and released from artery and vein is nitric oxide. *Proceedings of National Academy of Sciences USA,* 84**,** 9265-9269,.

IGNARRO, L. J., ADAMS, J. B., HORWITZ, P. M. & WOOD, K. S. (1986) Activation of soluble guanylate cyclase by NO-hemoproteins involves NO-heme exchange. Comparison of heme-containing and heme-deficient enzyme forms. *J Biol Chem,* 261**,** 4997-5002.

JACOBS, F. M., VAN DER HEIDE, L. P., WIJCHERS, P. J., BURBACH, J. P., HOEKMAN, M. F. & SMIDT, M. P. (2003) FoxO6, a novel member of the FoxO class of transcription factors with distinct shuttling dynamics. *J Biol Chem,* 278**,** 35959-67.

JARRY, A., CHARRIER, L., BOU-HANNA, C., DEVILDER, M. C., CRUSSAIRE, V., DENIS, M. G., VALLETTE, G. & LABOISSE, C. L. (2004) Position in cell cycle controls the sensitivity of colon cancer cells to nitric oxide-dependent programmed cell death. *Cancer Res,* 64**,** 4227-34.

JARVIK, J. W., ADLER, S. A., TELMER, C. A., SUBRAMANIAM, V. & LOPEZ, A. J. (1996) CD-tagging: a new approach to gene and protein discovery and analysis. *Biotechniques,* 20**,** 896-904.

JEON, H. K., CHOI, S. U. & JUNG, N. P. (2005) Association of the ERK1/2 and p38 kinase pathways with nitric oxide-induced apoptosis and cell cycle arrest in colon cancer cells. *Cell Biol Toxicol,* 21**,** 115-25.

JOHNSTON, L. A., PROBER, D. A., EDGAR, B. A., EISENMAN, R. N. & GALLANT, P. (1999) Drosophila myc regulates cellular growth during development. *Cell,* 98**,** 779-90.

JULIE M. PINKSTON, D. G., MALENE HANSEN, CYNTHIA KENYON (2006) Mutations That Increase the Life Span of C. elegans Inhibit Tumor Growth. *SCIENCE,* 313.

JUNGER, M., RINTELEN, F., STOCKER, H., WASSERMAN, J., VEGH, M., RADIMERSKI, T., GREENBERG, M. & HAFEN, E. (2003) The Drosophila Forkhead transcription factor FOXO mediates the reduction in cell number associated with reduced insulin signaling. *Journal of Biology,* 2**,** 20.

KEHLE, J., BEUCHLE, D., TREUHEIT, S., CHRISTEN, B., KENNISON, J. A., BIENZ, M. & MULLER, J. (1998) dMi-2, a Hunchback-Interacting Protein That Functions in Polycomb Repression. *Science,* 282**,** 2-6.

KENNERDELL, J. R. & CARTHEW, R. W. (1998) Use of dsRNA-Mediated Genetic Interference to Demonstrate that frizzled and frizzled 2 Act in the Wingless Pathway. *Cell,* 95**,** 1017-1026.

KHATTAK, S., LEE, B. R., CHO, S. H., AHNN, J. & SPOEREL, N. A. (2002) Genetic characterization of Drosophila Mi-2 ATPase. *Gene,* 293**,** 107-14.

KIM, J., SIF, S., JONES, B., JACKSON, A., KOIPALLY, J., HELLER, E., WINANDY, S., VIEL, A., SAWYER, A., IKEDA, T., KINGSTON, R. & GEORGOPOULOS, K. (1999) Ikaros DNA-binding proteins direct formation of chromatin remodeling complexes in lymphocytes. *Immunity,* 10**,** 345-55.

KIM, Y.-O., PARK, S.-J., BALABAN, R. S., NIRENBERG, M. & KIM, Y. (2004) A functional genomic screen for cardiogenic genes using RNA interference in developing Drosophila embryos. *PNAS, Developmental Biology,* 101**,** 159-164.

KIMBER, S. J. (2005) The regulation of Growth by Nitric Oxide Signalling in Drosophila Melanogaster (DPhil). *Department of Biology and Environmental sciences.* Brighton, University of sussex.

KON, C., CADIGAN, K. M., DA SILVA, S. L. & NUSSE, R. (2005) Developmental roles of the Mi-2/NURD-associated protein p66 in Drosophila. *Genetics,* 169**,** 2087-100.

KRAMER, J. M., DAVIDGE, J. T., LOCKYER, J. M. & STAVELEY, B. E. (2003) Expression of Drosophila FOXO regulates growth and can phenocopy starvation. *BMC Developmental Biology,* 3**,** 1-14.

KUNERT N, B. A. (2009) Novel Mi-2 related ATP-dependent chromatin remodelers. *Epigenetics,* 4**,** 209-211.

KUNERT, N., WAGNER, E., MURAWSKA, M., KLINKER, H., KREMMER, E. & BREHM, A. (2009) dMec: a novel Mi-2 chromatin remodelling complex involved in transcriptional repression. *Embo J,* 28**,** 533-44.

KUZIN, B., REGULSKI, M., STASIV, Y., SCHEINKER, V., TULLY, T. & ENIKOLOPOV, G. (2000) Nitric oxide interacts with the retinoblastoma pathway to control eye development in Drosophila. *Current Biology,* 10**,** 459-462.

KUZIN, B., ROBERTS, I., PEUNOVA, N. & ENIKOLOPOV, G. (1996) Nitric Oxide Regulates Cell Proliferation during Drosophila Development. *Cell,* 87**,** 639-649.

KWON, N. S., STUEHR, D. J. & NATHAN, C. F. (1991) Inhibition of tumor cell ribonucleotide reductase by macrophage-derived nitric oxide. *J Exp Med,* 174**,** 761-7.

LASALA, R. A. S. (2007) The Effect of Nitric Oxide on Gene Expression in YFP-Tagged Drosophila melanogaster Protein Trap Insertions (M.Sc). *School of Life Sciences.* Brighton, University Of Sussex.

LAUDANSKI, P., DZIECIOL, J., ANCHIM, T. & WOLCZYNSKI, S. (2001) The influence of glyco-nitric oxide conjugate on proliferation of breast cancer cells in vitro. *Folia Histochem Cytobiol,* 39 Suppl 2**,** 87-8.

LEIPER, J. M., SANTA MARIA, J., CHUBB, A., MACALLISTER, R. J., CHARLES, I. G., WHITLEY, G. S. & VALLANCE, P. (1999) Identification of two human dimethylarginine dimethylaminohydrolases with distinct tissue distributions and homology with microbial arginine deiminases. *Biochem J,* 343 Pt 1**,** 209-14.

LIPPINCOTT-SCHWARTZ, J., SNAPP, E. & KENWORTHY, A. (2001) Studying protein dynamics in living cells. *Nat Rev Mol Cell Biol,* 2**,** 444-56.

LOUIS J. IGNARRO, GEORGETTE M. BUGA, KEITH S. WOOD, RUSSELL E. BYRNS & CHAUDHURI, A. G. (1987) Endothelium-derived relaxing factor produced and released from artery and vein is nitric oxide. *Proceedings of National Academy of Sciences USA,* 84**,** 9265-9269,.

LUKACSOVICH, T., ASZTALOS, Z., AWANO, W., BABA, K., KONDO, S., NIWA, S. & YAMAMOTO, D. (2001) Dual-tagging gene trap of novel genes in Drosophila melanogaster. *Genetics,* 157**,** 727-42.

MALINSKI, T. THE VITAL ROLE OF NITRIC OXIDE. 47-57.

MARK A. SMITH, PEGGY L. RICHEY HARRIS, LAWRENCE M. SAYRE, JOSEPH S. BECKMAN & PERRY, G. (1997) Widespread Peroxynitrite-Mediated Damage in Alzheimer's Disease *The Journal of Neuroscience,* 17 2653–2657.

MATSUKAGE, A., HIROSE, F., YOO, M. A. & YAMAGUCHI, M. (2008) The DRE/DREF transcriptional regulatory system: a master key for cell proliferation. *Biochim Biophys Acta,* 1779**,** 81-9.

MEDEMA, B. M. T. B. A. R. H. (2003) Decisions on life and death: FOXO Forkhead transcription factors are in command when PKB/Akt is off duty. *Journal of Leukocyte Biology,* 73**,** 689-701.

NAGAI, T., IBATA, K., PARK, E. S., KUBOTA, M., MIKOSHIBA, K. & MIYAWAKI, A. (2002) A variant of yellow fluorescent protein with fast and efficient maturation for cell-biological applications. *Nat Biotechnol,* 20**,** 87-90.

NAKAYA N, LOWE SW, TAYA Y, CHENCHIK A & G., E. (2000) Specific pattern of p53 phosphorylation during nitric oxide-induced cell cycle arrest. *Oncogene,* 19**,** 6369-6375.

NAKAYA, N., LOWE, S. W., TAYA, Y., CHENCHIK, A. & ENIKOLOPOV, G. (2000) Specific pattern of p53 phosphorylation during nitric oxide-induced cell cycle arrest. *Oncogene,* 19**,** 6369-75.

NAN, X., NG, H. H., JOHNSON, C. A., LAHERTY, C. D., TURNER, B. M., EISENMAN, R. N. & BIRD, A. (1998) Transcriptional repression by the methyl-CpG-binding protein MeCP2 involves a histone deacetylase complex. *Nature,* 393**,** 386-9.

NASEEM, K. M. (2005) The role of nitric oxide in cardiovascular diseases. *Molecular Aspects of Medicine,* 26**,** 33–65.

NATALIA, P. & GRIGORI, E. (1995) Nitric oxide triggers a switch to growth arrest during differentiation of neuronal cells. 375**,** 68-73.

NEUFELD, T. (2003) Shrinkage control: regulation of insulin-mediated growth by FOXO transcription factors. *Journal of Biology,* 2**,** 18.

NG, H. H. & BIRD, A. (2000) Histone deacetylases: silencers for hire. *Trends Biochem Sci,* 25**,** 121-6.

NUNOKAWA, Y. & TANAKA, S. (1992) INTERFERON-y INHIBITS PROLIFERATION OF RAT VASCULAR SMOOTH MUSCLE CELLS BY NITRIC OXIDE GENERATION. *Biochemical and Biophysical Research Communications,* 188,**,** 409-415.

O'KANE, C. J. & GEHRING, W. J. (1987) Detection in situ of genomic regulatory elements in Drosophila. *Proc Natl Acad Sci U S A,* 84**,** 9123-7.

OHSHIMA, N., TAKAHASHI, M. & HIROSE, F. (2003) Identification of a human homologue of the DREF transcription factor with a potential role in regulation of the histone H1 gene. *J Biol Chem,* 278**,** 22928-38.

ORNITZ, D. M., MOREADITH, R. W. & LEDER, P. (1991) Binary system for regulating transgene expression in mice: targeting int-2 gene expression with yeast GAL4/UAS control elements. *Proc Natl Acad Sci U S A,* 88**,** 698-702.

PAIK, J. H., KOLLIPARA, R., CHU, G., JI, H., XIAO, Y., DING, Z., MIAO, L., TOTHOVA, Z., HORNER, J. W., CARRASCO, D. R., JIANG, S., GILLILAND, D. G., CHIN, L., WONG, W. H., CASTRILLON, D. H. & DEPINHO, R. A. (2007) FoxOs are lineage-restricted redundant tumor suppressors and regulate endothelial cell homeostasis. *Cell,* 128**,** 309-23.

PAZIN, M. J. & KADONAGA, J. T. (1997) SWI2/SNF2 and Related Proteins: Minireview ATP-Driven Motors That Disrupt Protein–DNA Interactions? *Cell,* 88**,** 737–740.

PEARSON, M. J. (1974) Polyteny and the functional significance of the polytene cell cycle. *J Cell Sci,* 15**,** 457-79.

PIRROTTA, V. (1997) PcG complexes and chromatin silencing. *Current Opinion in Genetics & Development* 7**,** 249-258.

POLLOCK, J. S., FORSTERMANN, U., MITCHELL, J. A., WARNER, T. D., SCHMIDT, H. H., NAKANE, M. & MURAD, F. (1991) Purification and characterization of particulate endothelium-derived relaxing factor synthase from cultured and native bovine aortic endothelial cells. *Proc Natl Acad Sci U S A,* 88**,** 10480-4.

POLYSCIENCES, I. Warrington, PA PUIG, O., MARR, M. T., RUHF, M. L. & TJIAN, R. (2003) Control of cell number by Drosophila FOXO: downstream and feedback regulation of the insulin receptor pathway 10.1101/gad.1098703. *Genes Dev.,* 17**,** 2006-2020.

R. TIMOTHY MILLER, PAVEL MARTA´SEK, TSUNEO OMURA & MASTERS, B. S. S. (1999) Rapid Kinetic Studies of Electron Transfer in the Three Isoforms of Nitric Oxide Synthase1. *Biochemical and Biophysical Research Communications,* 265**,** 184–188

RANA, T. M. (2007) Illuminating the silence: understanding the structure and function of small RNAs. *Nat Rev Mol Cell Biol,* 8**,** 23-36.

REGULSKI, M. & TULLY, T. (1995) Molecular and Biochemical Characterization of dNOS: A Drosophila Ca2+/ Calmodulin-Dependent Nitric Oxide Synthase. *PNAS,* 92**,** 9072-9076.

REKAS, A., ALATTIA, J. R., NAGAI, T., MIYAWAKI, A. & IKURA, M. (2002) Crystal structure of venus, a yellow fluorescent protein with improved maturation and reduced environmental sensitivity. *J Biol Chem,* 277**,** 50573-8.

RENATE DEURING, L. F., JENNIFER A. ARMSTRONG, M. S., OPHELIA PAPOULAS, M. P., GARY DAUBRESSE, M. V., SARAH L. MOSELEY,, MARIA BERLOCO, T. T., CARL WU, & SERGIO PIMPINELLI, A. J. W. T. (2000) The ISWI chromatin-remodeling protein is required for gene expression and the maintenance of higher order chromatin structure in Vivo. *Molecular Cell,* 5**,** 355–365.

SALVADOR MONCADA, ANNIE HIGGS & FURCHGOTT, R. (1997) XIV. International Union of Pharmacology Nomenclature in Nitric Oxide Researcha. *PHARMACOLOGICAL REVIEWS,* 49**,** 137-142.

SCHMIDT, H. H., POLLOCK, J. S., NAKANE, M., GORSKY, L. D., FORSTERMANN, U. & MURAD, F. (1991) Purification of a soluble isoform of guanylyl cyclase-activating-factor synthase. *Proc Natl Acad Sci U S A,* 88**,** 365-9.

SCOTT, A. (2009) Characterisation of the Regulation of Growth by Nitric Oxide Signalling in *Drosophila melanogaster (DPhil)Biology and Environmental Sciences.* Brighton, Sussex.

SEELIG HP, RENZ M, T., ARGOFF IN, GE Q & MB., F. (1996) Two forms of the major antigenic protein of the dermatomyositis-specific Mi-2 autoantigen. *Arthritis Rheum,* 39**,** 1769-71.

SMITH, A. V. & ORR-WEAVER, T. L. (1991) The regulation of the cell cycle during Drosophila embryogenesis: the transition to polyteny. *Development,* 112**,** 997-1008.

SPRADLING, A. C. & RUBIN, G. M. (1982) Transposition of Cloned P Elements into Drosophila Germ Line Chromosomes. *Science,* 218**,** 341-347.

STAMLER, J. S., LAMAS, S. & FANG, F. C. (2001) Nitrosylation. the prototypic redox-based signaling mechanism. *Cell,* 106**,** 675-83.

STEPHEN E. RUNDLETT, ANDREW A. CARMEN, NORIYUKI SUKA, &, B. M. T. & GRUNSTEIN, M. (1998) Transcriptional repression byUME6 involves deacetylation of lysine 5 of histoneH4 by RPD3. *Nature,* 392**,** 831-835.

STRUHL, K. (1998) Histone acetylation and transcriptional regulatory mechanisms. *Genes Dev,* 12**,** 599-606.

STUEHR, D. J. (1997) STRUCTURE-FUNCTION ASPECTS IN THE NITRIC OXIDE SYNTHASES. *Annu. Rev. Pharmacol. Toxicol. ,* 37**,** 339–59.

STUEHR, D. J. & IKEDA-SAITO, M. (1992) Spectral characterization of brain and macrophage nitric oxide synthases. Cytochrome P-450-like hemeproteins that contain a flavin semiquinone radical. *J Biol Chem,* 267**,** 20547-50.

TAUNTON, J., HASSIG, C. A. & SCHREIBER, S. L. (1996) A mammalian histone deacetylase related to the yeast transcriptional regulator Rpd3p. *Science,* 272**,** 408-11.

TELEMAN, A. A., HIETAKANGAS, V., SAYADIAN, A. C. & COHEN, S. M. (2008) Nutritional control of protein biosynthetic capacity by insulin via Myc in Drosophila. *Cell Metab,* 7**,** 21-32.

TINGWEI BILL CAI, P. G. W., AND ALVIN A. HOLDER Part 1 Chemistry of NO Donors.

TINGWEI BILL CAI, P. G. W., AND ALVIN A. HOLDER (2005) NO and NO Donors.

TOH, Y., PENCIL, S. D. & NICOLSON, G. L. (1994) A novel candidate metastasis-associated gene, mta1, differentially expressed in highly metastatic mammary adenocarcinoma cell lines. cDNA cloning, expression, and protein analyses. *J Biol Chem,* 269**,** 22958-63.

TONG JK, HASSIG CA, SCHNITZLER GR, KINGSTON RE & SL., S. (1998) Chromatin deacetylation by an ATP-dependent nucleosome remodelling complex. *Nature,* 395**,** 917-21.

TONG, J. K., HASSIG, C. A., SCHNITZLER, G. R., KINGSTON, R. E. & SCHREIBER, S. L. (1998) Chromatin deacetylation by an ATP-dependent nucleosome remodelling complex. *Nature,* 395**,** 917-21.

TSIEN, R. Y. (1998) THE GREEN FLUORESCENT PROTEIN. *Annu. Rev. Biochem.,* 67**,** 509–44.

TSUKIYAMA, T. & WU, C. (1997) Chromatin remodeling and transcription. *Current Opinion in Genetics & Development,* 7**,** 182-191.

TUAN ROCKY. S & LO W CECILLIA (2000) *Developmental Biology Protocols, Vol III,*, Humana Press, Totowa, New Jersey.

VENKEN, K. J. & BELLEN, H. J. (2005) Emerging technologies for gene manipulation in Drosophila melanogaster. *Nat Rev Genet,* 6**,** 167-78.

VILLALOBO, A. (2006) Nitric oxide and cell proliferation. *FEBS J.,* 273**,** 2329-2344.

WADE, P. A., GEGONNE, A., JONES, P. L., BALLESTAR, E., AUBRY, F. & WOLFFE, A. P. (1999) Mi-2 complex couples DNA methylation to chromatin remodelling and histone deacetylation. *Nat Genet,* 23**,** 62-6.

WADE, P. A., JONES, P. L., VERMAAK, D. & WOLFFE, A. P. (1998) A multiple subunit Mi-2 histone deacetylase from Xenopus laevis cofractionates with an associated Snf2 superfamily ATPase. *Curr Biol,* 8**,** 843-6.

WADE, S. A. D. P. A. (2007) The human Mi-2|[sol]|NuRD complex and gene regulation. *Oncogene* 26**,** 5433–5438.

XAVIER MORIN, RICHARD DANEMAN, MICHAEL ZAVORTINK & CHIA, W. (2001) A protein trap strategy to detect GFP-tagged proteins expressed from their endogenous loci in Drosophila. *PNAS,* 98**,** 15050–15055.

XUE, Y., IEMIN WONG, G., MORENO, T., MARY K. YOUNG, J. C. T. & WANG*K, A. W. (1998) NURD, a Novel Complex with Both ATP-Dependent

Chromatin-Remodeling and Histone Deacetylase Activities. *Molecular Cell,* 2**,** 851–861.

YAMAGUCHI, M., NISHIDA, Y., MORIUCHI, T., HIROSE, F., HUI, C. C., SUZUKI, Y. & MATSUKAGE, A. (1990) Drosophila proliferating cell nuclear antigen (cyclin) gene: structure, expression during development, and specific binding of homeodomain proteins to its 5'-flanking region. *Mol Cell Biol,* 10**,** 872-9.

YI ZHANG, GARY LEROY, HANS-PETER SEELIG, WILLIAM S. LANE & REINBERG, D. (1998) The Dermatomyositis-Specific Autoantigen Mi2 Is a Component of a Complex Containing Histone Deacetylase and Nucleosome Remodeling Activities. *Cell,* 95**,** 279–289.

YOKO FURUKAWA-HIBI, KIYOMI YOSHIDA-ARAKI, TSUTOMU OHTA, KYOJI IKEDA & MOTOYAMA, N. (2002) FOXO Forkhead Transcription Factors Induce G2-M Checkpoint in Response to Oxidative Stress. *The journal of Biological Chemistry,* 30**,** 26729–26732.

YU, S. M., HUNG, L. M. & LIN, C. C. (1997) cGMP-elevating agents suppress proliferation of vascular smooth muscle cells by inhibiting the activation of epidermal growth factor signaling pathway. *Circulation,* 95**,** 1269-77.

YUI, Y., HATTORI, R., KOSUGA, K., EIZAWA, H., HIKI, K. & KAWAI, C. (1991) Purification of nitric oxide synthase from rat macrophages. *J Biol Chem,* 266**,** 12544-7.

ZHANG, Y., NG, H. H., ERDJUMENT-BROMAGE, H., TEMPST, P., BIRD, A. & REINBERG, D. (1999) Analysis of the NuRD subunits reveals a histone deacetylase core complex and a connection with DNA methylation. *Genes Dev,* 13**,** 1924-35.

COMPONENTS OF NURD COMPLEX

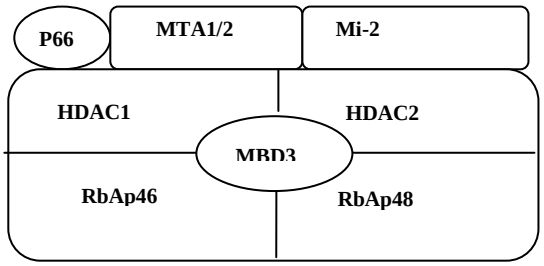

Schematic diagram of 2MDa NuRD complex consisting of eight polypeptides: MTA1/2, HDAC1, HDAC2, RbAp46, RbAp48, MBD3, p66 and Mi-2. Figure adopted from (Ahringer, 2000).

NuRD component	Organism	Developmental Roles
HDAC1/2		
i) *Rpd3*	*D. melanogaster*	Groucho-mediated transcriptional repression. (Mannervik M, 1999).
ii) *Hda-1*	*C. elegans*	Embryonic viability.(Solari and Ahringer, 2000).
iii) *Hdac1/2*	*M. musculus*	Control of proliferation.(Montgomery et al., 2007)
RbAp46/48		
i) *Rba-1*	*C. elegans*	Embryonic viability. (Solari and Ahringer, 2000)
ii) RbAp46/48	*D. melanogaster*	Histone binding. (Ahringer, 2000)
Mi-2		
i) *dMi-2*	*D. melanogaster*	Hox repression, larval and germ cell viability. (Kehle et al., 1998).
ii) *let-418*	*C. elegans.*	Larval viability, vulval development, maintenance. (Solari and Ahringer, 2000).
iii) *Chd4*	*M. musculus*	Haematopoiesis, epidermal development, peri-implantation development. (Kashiwagi M, 2007).
MTA1/2		.
i) *mta1/2*	*D. melanogaster*	Interaction with hunchback, polycomb repression (Kehle et al., 1998).
ii) *Egr-1*	*C. elegans.*	Embryonic patterning, Hox regulation. (Solari and Ahringer, 2000).
iii) *Mta2*	*M. musculus*	Metastasis. (Toh et al., 1995).
Mbd3		
i) *dMbd2/3*	*D. melanogaster*	Methylation mediated gene silencing (Feng and Zhang, 2001).
ii) *Mbd2/3*	*C. elegans.*	Morphological defects. (Gutierrez and Sommer, 2004)
iii) *Mbd3*	*M. musculus*	Silencing of pre-implanation genes. (Keisuke Kaji, 2007)
P66		
i) *Simj*	*D. melanogaster*	Wnt signalling, activation of ecdysone responsive genes. (Kon et al., 2005)
ii) *p66*	*M. musculus*	Pleiotrophic effects post-gastrulation, silencing of a few TE genes. (Marino and Nusse, 2007).